Caveolae allow smooth muscles cells to adapt to stress through the Gαq/PLCβ pathway

by

Androniqi Qifti

A Dissertation Submitted to the Faculty of

WORCESTER POLYTECHNIC INSTITUTE

In Partial Fulfillment of the Requirements for the Degree of

DOCTOR OF PHILOSOPHY

in Biochemistry

April 25, 2022

Approved by:

Suzanne Scarlata, PhD
Dissertation Advisor
Professor
Chemistry & Biochemistry
Worcester Polytechnic Institute

Kristen Billiar, PhD
Chairperson of Defense
Professor & Department Head
Biomedical Engineering
Worcester Polytechnic Institute

Mary Munson, PhD
Professor
Biochemistry & Molecular Biotechnology
University of Massachusetts Medical School

Carissa Lynn Olsen, PhD
Assistant Professor
Chemistry & Biochemistry
Worcester Polytechnic Institute

ACKNOWLEDGEMENTS

The completion of this dissertation work and all the other projects I have been involved with, would not be possible without the help from many people who have supported me throughout the last five years. First and foremost, I would like to thank my advisor Dr. Suzanne Scarlata for her invaluable guidance and mentorship. Thank you for believing in me when not many people did, for giving me the opportunity to work on this exciting project and for the encouragement through successes and failures. I feel lucky and blessed that I had the opportunity to learn so much from such an outstanding mentor. I would also like to extend my gratitude to the rest of my dissertation committee: Dr. Kristen Billiar, Dr. Mary Munson and Dr. Carissa Olsen for the insights and valuable expertise they have shared with me during my time in graduate school.

In addition to that, I would like to thank the current and previous members of the Scarlata lab who have worked with me to design new experiments and techniques, troubleshoot issues, image cells in the dark room for hours at a time, complete data analysis, and publish papers. Special thanks to Dr. Osama Garwain who initially welcomed me in the lab as an undergraduate student and trained me in lab techniques; setting the foundation of the scientist I was yet to become. Thank you to Lela Jackson who has been my partner in crime and my shoulder to cry on through the good and the bad days of graduate school. I couldn't have asked for a more down-to-earth and collaborative, bright individual to share this learning journey with. An additional thank you goes to all the undergraduate students that I have had the honor to mentor through the years. Even though it was my job to teach you how to be successful scientists in the future, I learned so much from you at the same time. I also want to thank my amazing friends and colleagues I have made at WPI over the years, especially the Gateway basement crew. Spending nine years in Worcester was certainly a stretch, however, you all made it worth it, and you have given me a lifetime of memories that I will cherish forever.

Last but certainly not least, I would like to thank my family for their unconditional love, support, and patience. Sending me to the United States at the age of nineteen to continue my education and pursue my dreams was an emotional and financial sacrifice from your end. As a first-generation college graduate in the family who also received a PhD, I hope I made you proud. Thank you to my brother Niko for always challenging me to be better than average and think outside of the box.

And of course, thank you to my husband Abdullah Al-Shawk who has been with me throughout this journey supporting me unconditionally and always believing in me.

TABLE OF CONTENTS

LIST OF FIGURES

LIST OF TABLES

LIST OF ABBREVIATIONS

afap1l2	Actin Filament Associated Protein 1 Like 2
Ago2	Argonaute 2
ALS	Amyotrophic lateral sclerosis
ASD	Autism spectrum disorder
BMAL1	Brain and Muscle Arnt1-like-1
Cav-1	Caveolin-1
C3PO	Component 3 promoter of RISC
CLOCK	Circadian Locomotor Output Cycles Kaput
Cry	Cryptochrome
DAG	Diacylglycerol
DLS	Dynamic Light Scattering
dsRNA	Double stranded RNA
E-boxes	Enhancer boxes
eIF	Eukaryotic initiation factor proteins
ER	Endoplasmic Reticulum
fat3	FAT Atypical Cadherin 3
FLIM	Fluorescence-lifetime Imaging Microscopy
fos	Fos Proto-Oncogene Ap-1 Transcription Factor Subunit
FRET	Förster resonance energy transfer
G3BP1	Ras GTPase activating protein-binding Protein 1
GPCR	G-protein coupled receptor
gja5	Gap Junction Protein Alpha 5
Gαq	Gq protein alpha subunit
G$\beta\gamma$	Gq protein beta gamma subunit
Hz	Hertz
IDR	Intrinsically disordered region
IP$_3$	Inositol trisphosphate
miRNA or miR	Micro RNA

N&B	Number and Brightness
NGF	Nerve growth factor
PABPC1	Polyadenylate binding protein 1
PA	Particle Analysis
P-bodies	Processing bodies
PCP	Planar cell polarity
Per	Period
PIP_2	Phosphatidylinositol 4,5-bisphosphate
PLCβ1	Phospholipase C β1
PTRF-1	Polymerase Transcript Release Factor 1
RISC	RNA induced silencing complex
RNAi	Ribonucleic acid interference
SG	Stress granule
siRNA	Small interfering RNA
SV40	Simian virus 40
TRAX	Translin-associated factor X

ABSTRACT

Phospholipase Cβ1 (PLCβ1) is a multifunctional protein localized mainly on the plasma membrane that also binds to stress granule (SG) proteins in the cytoplasm. While activation of Gαq, the membrane bound subunit of the GPCR, leads to the activation of PLCβ1 on the membrane, Gαq also binds to Caveolin-1 (Cav-1) at a different binding site. Cav-1, a fundamental component of the formation and maintenance of caveolae domains, stabilizes the activated state of Gαq enhancing the activation of PLCβ1 and prolonging the intracellular calcium efflux. Caveolae disruption and irregular stress granule assembly and disassembly have been implicated in several diseases including spontaneous hypertrophy (muscle enlargement of cardiac cells), ALS and autism spectrum disorder. Here we provide valuable insight into the ways cells adapt to different environmental stresses including hypo-osmotic stress, heat shock, cold shock, carbachol and arsenite treatment.

This dissertation examines the effects of various environmental stresses in smooth muscle cells and their ability to adapt to them through the Gαq/PLCβ1 signaling. We found that all environmental stresses increase the number and size of PABPC1 and Ago2 related particles suggesting the increased incorporation of stress granules. We also found that loss of PLCβ1 from the cytoplasm promotes stress granule oligomerization. We next identified the caveolae involvement in this process and we were mainly interested in the role of Cav-1 and cavin-1. We discovered that caveolae deformation through mechanical stretch or Gαq activation promotes cavin-1 relocalization from the plasma membrane to the nucleus to impact transcription and translation. With that in mind, we wanted to understand the series of events taking place in the nucleus and identify genes whose production is severely affected due to the caveolae deformation. Overall, we found several anti-viral genes being upregulated when caveolae were deformed, leading to a novel discovery.

CHAPTER 1 – GENERAL INTRODUCTION

1.1 PHOSPHOLIPASE C B1 SIGNALING PATHWAY

The large family of guanine nucleotide-binding proteins (G proteins) receptors consist of seven transmembrane proteins that serve as membrane-bound transducers of chemically and physically coded information[1]. A diverse array of ligands such as hormones, neurotransmitters, vasodilators and many pharmaceutical agents elicit different cell responses causing changes such as movement or cell morphology. Over the past few decades, G proteins have been the main subject of several studies that revealed their role as intermediates in transmembrane signaling pathways that consist of three types of proteins: receptors, G proteins, and effectors[2; 3; 4].
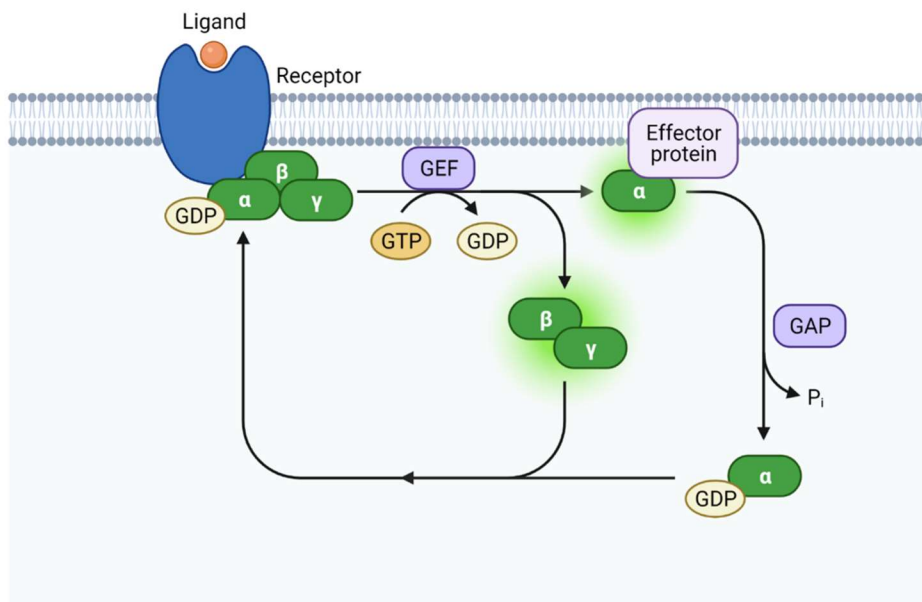
Figure 1. 1: Heterotrimeric G-proteins activation and de-activation signaling events.

G-proteins can be monomeric or heteromeric. Heterotrimers have subunits designated as α, β and γ in order of decreasing mass. When the G-protein coupled receptors (GPCR) are activated by hormones or neurotransmitters, they in turn activate the membrane-bound Gα subunit by catalyzing the exchange of GDP to GTP. In the GTP-bound state, Gα has a ~50-fold weaker affinity to Gβγ subunits, which destabilizes the heterotrimer leaving the Gα and Gβγ to separately

bind to and activate specific proteins such as second messengers[5]. This conformational change is mediated by the Guanine Nucleotide Exchange Factor (GEF). This active state of GPCR can go back to its inactive state with the help of the GTPase Activating Protein also known as GAP which hydrolyzes GTP removing its dominal phosphate and promoting the re-association of the heterotrimeric proteins back on the plasma membrane (**Fig 1.1**).

G protein α subunit is also divided into four subfamilies, Gαs, Gαi, Gαq, and Gα12, and these subunits bind to only β isoforms of PLC. Depending on the Gα subunit family, Gα will act to stimulate or inhibit adenylyl cyclase (AC), activate phosphoinositide-specific phospholipase C (PI-PLC), or regulate RhoA proteins. On the other hand, Gβγ subunits are thought to play a role in calcium channel activity, and regulate protein kinases and small G-proteins, such as ERK1/2, JNK, phosphoinositide-3 kinase (PI3K), and mitogen-activated protein kinases (MAPKs). The Gαq family is activated by acetylcholine, dopamine, serotonin, histamine, bradykinin, endothelial I and angiotensin II, and activates phospholipase Cβ (PLCβ)[6].

While on the membrane PLCβ is soluble but binds to membranes, catalyzing the hydrolysis of the signaling lipid phosphatidylinositol (4, 5) bisphosphate (PIP2). PIP_2 hydrolysis leads to the release of inositol 1,4,5-triphosphate (IP3) that diffuses to the endoplasmic reticulum (ER) to bind to IP3 channels, along with diacylglycerol (DAG) which is involved and several signaling pathways originating by the activation of Protein Kinase C. The hydrolysis of PIP_2 and the binding of IP_3 to its appropriate receptors, is the first of many events that occur to lead to an increase in intracellular calcium mediated by PLCβ1[7]. These events are critical for gene expression, cell growth, development, survival, and cell death (**Fig. 1.2**)

1.2 CAVEOLAE PROVIDE MECHANICAL STRENGTH TO CELLS

One of the most distinct features of the lipid membrane is the presence of caveolae. Caveolae are flask-shaped membrane invaginations with 50-100nm size that provide mechanical strength to cells and impact calcium signals initiated through the Gαq signaling pathway[8]. Caveolae are found in many types of mammalian cells and can provide almost a 2-fold increase in the surface area of the membrane. The "U" shape of these proteins results in the occupation of only the inner leaflet of the plasma membrane. The proteins contain multiple palmitoylation sites, which together

with cholesterol and other lipids, promote the formation of tightly packed domains that can phase separate from other membrane lipids. This separation is caused by the aggregation of ~144 Cav1 or Cav3 molecules, and because of their shape, an inward curvature of the membrane is induced[9].

Caveolae are known to play an important role in mechanosensation, endocytosis, scaffolding and cell signaling[10]. Structurally, caveolae are composed of caveolae specific proteins such as Cav1 comprising 178 amino acids and caveolin-3 (Cav-3), where Cav-3 is muscle specific as well as cavin and other proteins. It is important to mention that cells lacking the Cav1 gene do not have caveolae, making Cav-1 or -3 a requirement for both the formation and the maintenance of caveolae[11].

In addition to the caveolins, cavins are also a class of caveolae specific proteins. Cavins are adaptor proteins that regulate the curvature of caveolae membrane by anchoring Cav-1 to the cytoskeleton via its C-terminal region. The cavin protein family consists of 4 proteins, cavin 1, 2, 3 and 4 with cavin-1 being the most abundantly expressed and studied[12; 13]. However, before identifying cavin-1 as an adaptor protein for the caveolae structure, it was mainly known as Polymerase Transcript Release Factor 1 (PTRF-1) or cav-p60 due to it important role in ribosomal transcription termination by RNA Polymerase I (Pol I) since it binds to 3' end of the pre-mRNA allowing the allowing the release of pre-RNA and Pol I from the stalled transcription complex[14].

Previous work in smooth muscle rat aortic cells (A10) has shown that Gαq binds to the scaffold domain of Cav1 or Cav3 which enhances its activation[15]. Considering that Gαq continues to activate PLCβ when bound to caveolae (they do not share the same association site), the localization of Gαq to caveolae greatly enhances calcium signals. Hypo-osmotic conditions reduces Ca^{2+} signals by disrupting the Gαq/Cav1 interactions[16; 17]. It was also found that when cells are subjected to either bi-directional static or oscillating mechanical stretch, calcium release through activation of Gαq/PLCβ is intact, but contacts with caveolae are disrupted[18].
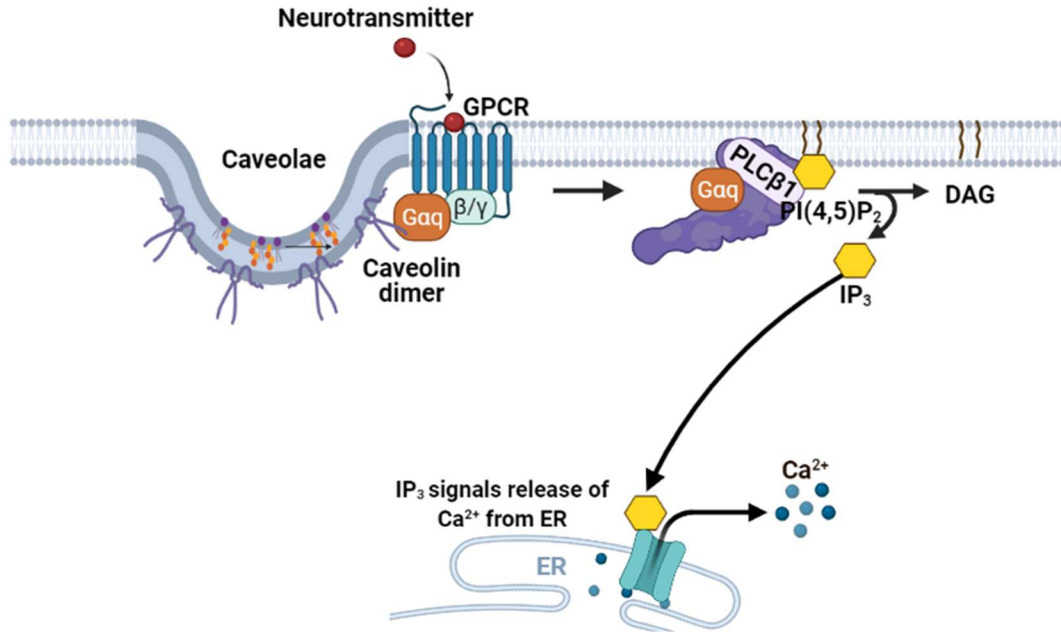
Figure 1. 2: Model representing PLCβ1's role on the plasma membrane. The hydrolysis of PI (4,5) P_2 is shown along with the Gαq binding to the Cav-1 dimer.

1.3 STRESS GRANULE FORMATION

While PLCβ1 is traditionally found on the plasma membrane catalyzing the hydrolysis of PIP_2, we found that a population of PLCβ also resides in the cytosol. When we isolated the cytosolic fractions of both undifferentiated PC12 (pheochromocytoma of the rat adrenal medulla) cells and A10 cells to identify potential binding partners for our protein of interest by mass spectrometry, we found that approximately one third of the bound proteins are classified as stress granule proteins.[19; 20]

Stress granules are membraneless cytoplasmic organelles that consist of non-translating mRNAs, translation initiation complexes (eIF5A), poly (A)-binding protein (PABPC1), RasGAP SH3 domain binding protein1 (G3BP1) and other RNA-related proteins including Argonaute 2 (Ago2) which is also part of the RNA induced silencing complex (RISC)[21; 22]. While the regulation of stress granule assembly and disassembly is not well understood, high resolution microscopy has shown that these aggregates lack a membrane envelope and therefore they partition themselves from the cytosol through liquid-liquid phase separation (LLPS)[23; 24]. The structure of stress granules contains two components: a concentrated core and a dynamic less-concentrated shell.

This entire structure, especially the shell, contains intrinsically disordered proteins (IDPs) that contribute to the stress granules liquid-like behavior. Therefore, the mixture of components that make up these aggregates have higher affinity of attraction to each other over the surrounding environment that makes up the cytosol, allowing these separate structures to coexist.

While the proper assembly and disassembly of the granules is fundamental for healthy cell function, it is important to understand this defense mechanism in more detail. When cells are exposed to environmental stress conditions such as mechanical stress, heat/cold shock, osmotic stress, oxidative stress, or nutrient deprivation, Gαq activation of PLCβ1 is greatly impeded [19]. In these cases, cells activate this defensive mode during which they halt production of several types of proteins and form stress granules in the cytoplasm, where they store mRNAs and associated translation proteins[25]. Stress granules act as waiting stations that allow the cells to decide the fate of the mRNAs after the stress is removed. Some mRNAs will follow degradation pathways; others will get stored, and some will enter the translational machinery[26; 27].

1.4 BIOLOGICAL SIGNIFICANCE

Studies focusing on all the FDA approved drugs from 1942 to 2016 interestingly show that approximately 40% of the total drugs available in the market per year of interest, are GPCR related drugs. When looking at the success rates of these drugs for each phase of their clinical trial, GPCR targets had success rates of 78%, 39% and 29% for phases I, II and III respectively which are significantly higher that the success rates of all the other drugs[28]. Some of the most important areas that GPCR targets impact are genetic disorder, neoplasm, cardiovascular diseases and respiratory system. When looking at the highest number of GPCR targets in trial the majority of them target diabetes and neoplasms while the highest ration of GPCR targets versus approved targets belongs to Alzheimer disease, obesity and Parkinson disease [29].

Other studies focusing on caveolae show that Cav3 knock out mice display cardiomyopathy characterized by hypertrophy, dilation and reduced contractility while Cav-1 null mice are prominent to develop cardiac hypertrophy[30; 31]. Additionally, Gαq plays a key role in hypertension, vascular remodeling and hypertrophy of vascular smooth muscle cells[32]. It is known that Gαq/PLCβ1 is a key mediator of scarring after heart infractions[33]. In other words,

changes in Gαq activation may influence the normal disassembly of stress granules causing atrophy, heart attack or heart failure[34]. Understanding the link between caveolae, Gαq activation and stress granules may increase the overall understanding of cardiac disease cause and progression on the cellular level.

High blood pressure or hypertension is a common condition in which the pressure of the blood within the blood vessels is higher than 130 over 80 mmHg. Blood pressure is determined both by the amount of blood your heart pumps and the amount of resistance to blood flow in your arteries. The long-term high force of the blood against the arteries can eventually cause serious health problems such as heart disease and stroke. This condition along with hypertrophy are the most common conditions studied in cardiovascular investigations. The leading cause of death in the United States as of 2020 is heart disease with stroke being second. Generally, one out of three US adults suffer from hypertension, which corresponds to approximately 75 million people worldwide, usually affecting individuals over 55 years old[35; 36].

1.5 INNOVATION

This study seeks to tie together Cav1/Gαq signaling with Gαq/PLCβ1 stress granule regulation and translation. The novelty of this proposal is the correlation between caveolae and stretch-induced stress granule formation through the Gαq/PLCβ1/GPCR signaling pathway. PLCβ1 has the ability to bind to many partners to prevent the premature formation of stress granules. In addition, caveolae act as stress sensors and mediators in smooth muscle cells, through both the Gαq/calcium signaling pathway and the mechanical function. Thus, Cav/Gαq/PLCβ1 may be regulating the coordinated assembly and disassembly of intracellular aggregates, impacting transcription and translation and affecting genes related to heart disease that may pave the development of new drug technologies.

1.6 REFERENCES

[1] A.G. Gilman, G proteins: transducers of receptor-generated signals. Annu Rev Biochem 56 (1987) 615-49.
[2] P. Oh, and J.E. Schnitzer, Segregation of heterotrimeric G proteins in cell surface microdomains. G(q) binds caveolin to concentrate in caveolae, whereas G(i) and G(s) target lipid rafts by default. Mol Biol Cell 12 (2001) 685-98.

[3] H.W. Choe, J.H. Park, Y.J. Kim, and O.P. Ernst, Transmembrane signaling by GPCRs: insight from rhodopsin and opsin structures. Neuropharmacology 60 (2011) 52-7.

[4] L.M. Luttrell, Reviews in molecular biology and biotechnology: transmembrane signaling by G protein-coupled receptors. Mol Biotechnol 39 (2008) 239-64.

[5] L.W. Runnels, and S.F. Scarlata, Determination of the affinities between heterotrimeric G protein subunits and their phospholipase C-beta effectors. Biochemistry 38 (1999) 1488-96.

[6] D.V. Predescu, S.M. Cretoiu, D. Cretoiu, L.A. Pavelescu, N. Suciu, B.M. Radu, and S.C. Voinea, G Protein-Coupled Receptors (GPCRs)-Mediated Calcium Signaling in Ovarian Cancer: Focus on GPCRs activated by Neurotransmitters and Inflammation-Associated Molecules. Int J Mol Sci 20 (2019).

[7] J.W. Putney, and T. Tomita, Phospholipase C signaling and calcium influx. Adv Biol Regul 52 (2012) 152-64.

[8] A. Echarri, and M.A. Del Pozo, Caveolae - mechanosensitive membrane invaginations linked to actin filaments. J Cell Sci 128 (2015) 2747-58.

[9] R.G. Parton, V.A. Tillu, and B.M. Collins, Caveolae. Curr Biol 28 (2018) R402-R405.

[10] B. Razani, S.E. Woodman, and M.P. Lisanti, Caveolae: from cell biology to animal physiology. Pharmacol Rev 54 (2002) 431-67.

[11] J.P. Gratton, P. Bernatchez, and W.C. Sessa, Caveolae and caveolins in the cardiovascular system. Circ Res 94 (2004) 1408-17.

[12] J.J. Williams, and T.M. Palmer, Cavin-1: caveolae-dependent signalling and cardiovascular disease. Biochem Soc Trans 42 (2014) 284-8.

[13] J. Mohan, B. Moren, E. Larsson, M.R. Holst, and R. Lundmark, Cavin3 interacts with cavin1 and caveolin1 to increase surface dynamics of caveolae. J Cell Sci 128 (2015) 979-91.

[14] L. Liu, and P.F. Pilch, A critical role of cavin (polymerase I and transcript release factor) in caveolae formation and organization. J Biol Chem 283 (2008) 4314-22.

[15] K.S. Murthy, and G.M. Makhlouf, Heterologous desensitization mediated by G protein-specific binding to caveolin. J Biol Chem 275 (2000) 30211-9.

[16] L. Yang, and S. Scarlata, Super-resolution Visualization of Caveola Deformation in Response to Osmotic Stress. J Biol Chem 292 (2017) 3779-3788.

[17] Y. Guo, L. Yang, K. Haught, and S. Scarlata, Osmotic Stress Reduces Ca2+ Signals through Deformation of Caveolae. J Biol Chem 290 (2015) 16698-707.

[18] A. Qifti, O. Garwain, and S. Scarlata, Mechanical Stretch Redefines Membrane Galphaq-Calcium Signaling Complexes. J Membr Biol 252 (2019) 307-315.

[19] A. Qifti, L. Jackson, A. Singla, O. Garwain, and S. Scarlata, Stimulation of phospholipase Cbeta1 by Galphaq promotes the assembly of stress granule proteins. Sci Signal 14 (2021) eaav1012.

[20] S. Scarlata, A. Singla, and O. Garwain, Phospholipase Cbeta interacts with cytosolic partners to regulate cell proliferation. Adv Biol Regul 67 (2018) 7-12.

[21] P. Anderson, and N. Kedersha, RNA granules. J Cell Biol 172 (2006) 803-8.

[22] F.E. Paulin, L.E. Campbell, K. O'Brien, J. Loughlin, and C.G. Proud, Eukaryotic translation initiation factor 5 (eIF5) acts as a classical GTPase-activator protein. Curr Biol 11 (2001) 55-9.

[23] J.R. Wheeler, T. Matheny, S. Jain, R. Abrisch, and R. Parker, Distinct stages in stress granule assembly and disassembly. Elife 5 (2016).

[24] D.S.W. Protter, and R. Parker, Principles and Properties of Stress Granules. Trends Cell Biol 26 (2016) 668-679.

[25] A. Khong, T. Matheny, S. Jain, S.F. Mitchell, J.R. Wheeler, and R. Parker, The Stress Granule Transcriptome Reveals Principles of mRNA Accumulation in Stress Granules. Mol Cell 68 (2017) 808-820 e5.

[26] C.J. Decker, and R. Parker, P-bodies and stress granules: possible roles in the control of translation and mRNA degradation. Cold Spring Harb Perspect Biol 4 (2012) a012286.

[27] K.H. Shah, S.N. Varia, L.A. Cook, and P.K. Herman, A Hybrid-Body Containing Constituents of Both P-Bodies and Stress Granules Forms in Response to Hypoosmotic Stress in Saccharomyces cerevisiae. PLoS One 11 (2016) e0158776.

[28] H.C.S. Chan, Y. Li, T. Dahoun, H. Vogel, and S. Yuan, New Binding Sites, New Opportunities for GPCR Drug Discovery. Trends Biochem Sci 44 (2019) 312-330.

[29] A.S. Hauser, M.M. Attwood, M. Rask-Andersen, H.B. Schioth, and D.E. Gloriam, Trends in GPCR drug discovery: new agents, targets and indications. Nat Rev Drug Discov 16 (2017) 829-842.

[30] S.E. Woodman, D.S. Park, A.W. Cohen, M.W. Cheung, M. Chandra, J. Shirani, B. Tang, L.A. Jelicks, R.N. Kitsis, G.J. Christ, S.M. Factor, H.B. Tanowitz, and M.P. Lisanti, Caveolin-3 knock-out mice develop a progressive cardiomyopathy and show hyperactivation of the p42/44 MAPK cascade. J Biol Chem 277 (2002) 38988-97.

[31] A.W. Cohen, D.S. Park, S.E. Woodman, T.M. Williams, M. Chandra, J. Shirani, A. Pereira de Souza, R.N. Kitsis, R.G. Russell, L.M. Weiss, B. Tang, L.A. Jelicks, S.M. Factor, V. Shtutin, H.B. Tanowitz, and M.P. Lisanti, Caveolin-1 null mice develop cardiac hypertrophy with hyperactivation of p42/44 MAP kinase in cardiac fibroblasts. Am J Physiol Cell Physiol 284 (2003) C457-74.

[32] D.M. Harris, H.I. Cohn, S. Pesant, R.H. Zhou, and A.D. Eckhart, Vascular smooth muscle G(q) signaling is involved in high blood pressure in both induced renal and genetic vascular smooth muscle-derived models of hypertension. Am J Physiol Heart Circ Physiol 293 (2007) H3072-9.

[33] J. Hao, H. Ju, S. Zhao, A. Junaid, T. Scammell-La Fleur, and I.M. Dixon, Elevation of expression of Smads 2, 3, and 4, decorin and TGF-beta in the chronic phase of myocardial infarct scar healing. J Mol Cell Cardiol 31 (1999) 667-78.

[34] H.N. Fridolfsson, and H.H. Patel, Caveolin and caveolae in age associated cardiovascular disease. J Geriatr Cardiol 10 (2013) 66-74.

[35] R. Kones, Primary prevention of coronary heart disease: integration of new data, evolving views, revised goals, and role of rosuvastatin in management. A comprehensive survey. Drug Des Devel Ther 5 (2011) 325-80.

[36] H. Cramer, H. Hall, M. Leach, J. Frawley, Y. Zhang, B. Leung, J. Adams, and R. Lauche, Prevalence, patterns, and predictors of meditation use among US adults: A nationally representative survey. Sci Rep 6 (2016) 36760.

CHAPTER 2 – BACKGROUND

REGULATION OF BIFUNCTIONAL PROTEINS IN CELLS: LESSONS FROM THE PHOSPHOLIPASE CB/G PROTEIN PATHWAY

Lela Jackson, Androniqi Qifti, Katherine M. Pearce, Suzanne Scarlata

Department of Chemistry & Biochemistry, Worcester Polytechnic Institute, Worcester, MA

The following subsections appear in the Review Article Jackson et al. "Regulation of bifunctional proteins in cells: Lessons from the phospholipase Cβ/G protein pathway" Protein Science. (2019) and are reproduced here with permission. Addition information on the authors' contributions can be found in section 2.15.

2.1 ABSTRACT

Some proteins can serve multiple functions depending on different cellular conditions. An example of a bifunctional protein is inositide-specific mammalian phospholipase Cβ (PLCβ). PLCβ is activated by G proteins in response to hormones and neurotransmitters to increase intracellular calcium. Recently, alternate cellular function(s) of PLCβ have become uncovered. However, the conditions that allow these different functions to be operative are unclear. Like many mammalian proteins, PLCβ has a conserved catalytic core along with several regulatory domains. These domains modulate the intensity and duration of calcium signals in response to external sensory information and allow this enzyme to inhibit protein translation in a noncatalytic manner. In this review, we first describe PLCβ's cellular functions and regulation of the switching between these functions, and then discuss the thermodynamic considerations that offer insight into how cells manage multiple and competitive associations allowing them to rapidly shift between functional states.

2.2 PLCβ GENERATES Ca^{2+} SIGNALS IN RESPONSE TO EXTRACELLULAR SIGNALS

Most sensory information is received and processed by the G protein signaling system.[1] This pathway allows external hormones and neurotransmitters to elicit different cell responses, such as movement or morphology changes. G protein pathways are initiated when an extracellular agent binds to its specific G protein coupled receptor (GPCR). GPCRs are a large family of seven transmembrane proteins that interact and respond to a diverse array of ligands that include hormones, neurotransmitters, vasodilators, many pharmaceutical agents, and light. Ligand binding allows GPCRs to activate their associated G proteins by catalyzing the exchange of GDP for GTP on the Gα subunits peripherally bound to the plasma membrane.[2, 3] Heterotrimeric G proteins are composed of three subunits (α, β, and γ). In the GTP-bound state, Gα has a ~50-fold weaker affinity to Gβγ subunits,[4] which destabilizes the heterotrimer leaving the Gα and Gβγ to separately bind to

and activate specific proteins. Once the complex is destabilized, the Gα and the Gβγ subunits each act as effectors on specific targets. Depending on the Gα subunit family, Gα will act to stimulate or inhibit adenylyl cyclase (AC), activate phosphoinositide-specific phospholipase C (PI-PLC), or regulate RhoA proteins. Alternatively, Gβγ subunits are thought to play a role in calcium channel activity, and regulate protein kinases and small G-proteins, such as ERK1/2, JNK, phosphoinositide-3 kinase (PI3K), and mitogen-activated protein kinases (MAPKs).[5]

In contrast to the ~800 different GPCRs, there are only four families of heterotrimeric G proteins that are classified by their Gα subunits.[6] PLCβ is the main effector of Gαq [7], and activation of Gαq increases the binding affinity of PLCβ ~20–40-fold (Figure 2.1, 2.8). Gαq is coupled to receptors for neurotransmitters such as dopamine and acetylcholine, as well as hormones that mediate vasoconstriction and inflammation, such as bradykinin and angiotensin II. PLCβ is soluble but binds to membranes, where it catalyzes the hydrolysis of phosphatidylinositol 4,5 bisphosphate (PIP$_2$), which is found at low levels in the plasma membrane.[9] PIP$_2$ hydrolysis catalyzed by PLCβ leads to two products: the lipid portion, diacylglycerol, which activates protein kinase C, and the soluble head group, 1,4,5 inositol trisphosphate (IP$_3$). IP$_3$ diffuses to the endoplasmic reticulum (ER) where it binds to IP$_3$ receptors. These receptors are Ca^{2+} channels and when IP$_3$ binds, they open, releasing Ca^{2+} from intracellular stores into the cytoplasm. This increased level of calcium changes the activity of a wide range of enzymes that carry out key cellular events such as generating action potentials and neurotransmission in neurons, or initiating muscle contraction.[10-12] Besides being activated by Gαq, two of the four known isoforms of PLCβ can be activated by Gβγ subunits.[13] Although Gβγ subunits have the potential to be released by any G protein family, release is generally associated with Gαi subunits thus connecting PLCβ and calcium signals to large and diverse array of GPCRs.
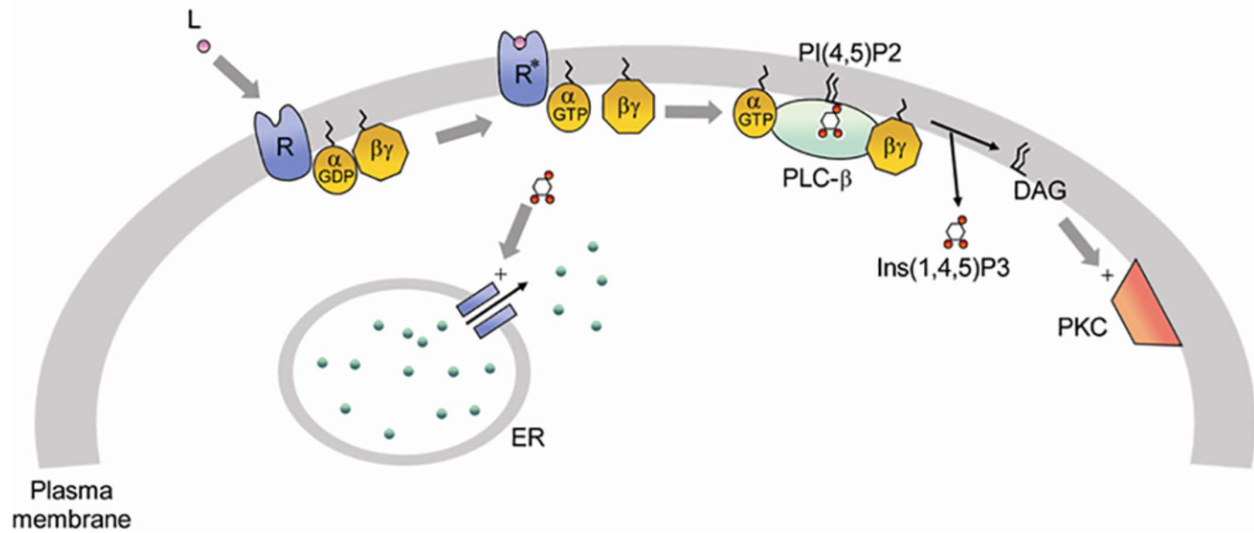
Figure 2.1: Cartoon of the Gαq/PLCβ signaling system showing simultaneous activation of PLCβ by both Gβγ and Gα subunits (see References 67, 68)

In order to access its substrate, PLCβ must bind to the plasma membrane. Binding of PLCβ to model membranes is strong and fairly nonspecific with partition coefficients ranging from 10 to 100 μM.[14] This range of affinities suggests a transient membrane association in the range of 0.1 to 1 s (see References [15, 16]). Studies using purified proteins and model membranes suggest that PLCβ initially binds to membranes where it diffuses and hops along the membrane until it encounters Gαq.[14] It is unclear whether a similar scenario occurs in cells since the amount of membrane available for binding may be lower, and if this is the case, PLCβ will bind directly to Gαq. Once activated, the affinity between Gαq and PLCβ1 increases 20-fold.[4] The high affinity between Gαq and PLCβ (K_d ~1 nM) is attributed to the tucking of Gαq into a nook between the C2 domain and C-terminal tail (Figure 2.2) of PLCβ1.[17]

Structure of the PLCβ3- Gαq Complex
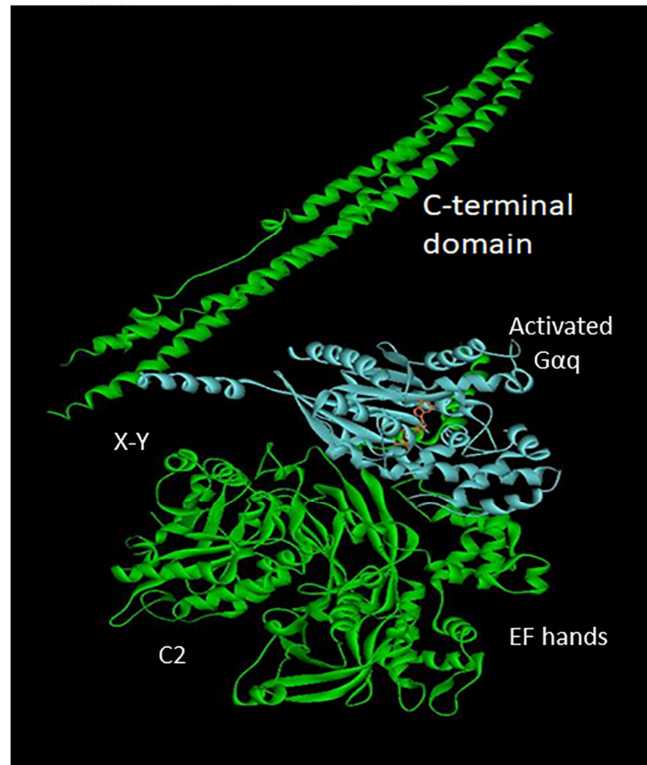
Figure 2.2: Crystal structure (PDB Id: 4GNK) of the PLCβ2 (green) -Gαq (blue) complex showing the extended C-terminal domain and where the various domains are indicated. Missing is an unstructured 52aa connector between the C2 and C-terminal domains

The initial activation of PLCβ and subsequent calcium release results in a series of coordinated events involving changes in protein associations, modifications, and localization.[18] Calcium release is enhanced by two major effects.[11] One is the activation of PLCδ. PLCδ has a similar structure as PLCβ but is not activated by G proteins. Instead, PLCδ becomes highly active when calcium levels in the cell rise, synergizing PLCβ activity (see Reference [19]). Additionally, increased calcium opens calcium-activated calcium channels on the plasma membrane, allowing external calcium to enter the cell.[20]

2.3 THE DOMAIN STRUCTURE OF PLCβ ALLOWS MULTI-FUNCTIONALITY

Like most mammalian signaling proteins, PLCβ is composed of several conserved domains (Figure 2.3). At the N-terminus is the pleckstrin homology (PH) which mediates activation by Gβγ. This domain is followed by two EF hands and the catalytic domain. Immediately following the

catalytic domain is the C2 domain and a long 400 amino acid coiled-coil domain that comprises the C-terminal domain. This region is distinctive of PLCβ enzymes and confers Gαq activation to the catalytic core. Gαq binds to the C-terminal domain close to the C2 domain (Figure 2.2), leaving the long-coiled coil extension to potentially interact with other species. As described below, it is this noncatalytic C-terminal region that allows PLCβ to impact protein translation.[21, 22]

Domain structure PLCβ Enzymes

PLCβ	PH Domain	EF hands	X – Y Catalytic Domain	C2 Domain	C-terminal Domain
	~ 1-120	~140-290	~320-650	~600-810	~800-1200
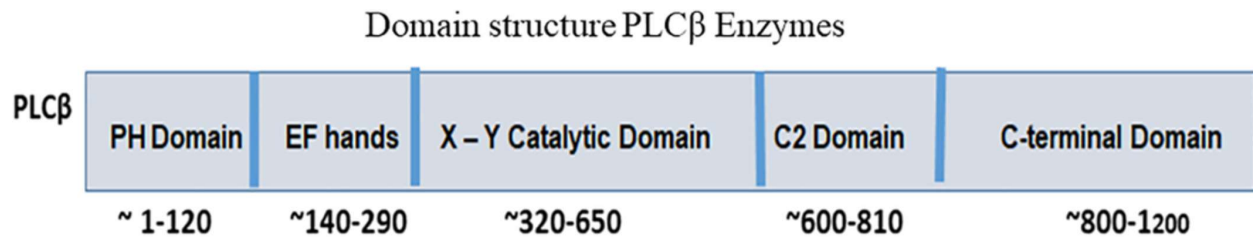
Figure 2.3: Schematic of the domain structure of PLCβ along with the amino acid number

2.4 PLCβ HAS AN ATYPICAL CYTOSOLIC POPULATION THAT IMPACT PROTEIN TRANSLATION

Even though PLCβ1 binds strongly to model membranes, cultured cells have a significant level of PLCβ in the cytosol (Figure 2.4). In previous years, the function of this cytosolic population was unclear because the activity of PLCβ in the absence of activated Gαq is very low, especially compared to PLCδ. To understand the role, if any, of this cytosolic population, our lab set out to identify novel binding partners of cytosolic PLCβ using two unbiased approaches: a yeast two hybrid study and identification of proteins associated with cytosolic PLCβ in an antibody pull-down.

EGFP-PLCβ1 expressed in a HEK293 cell
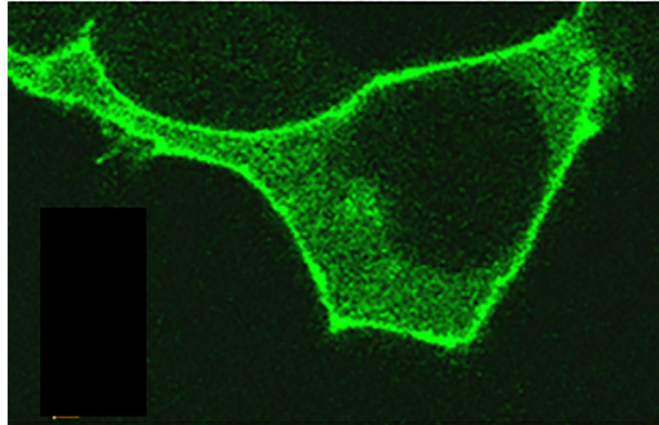
Figure 2.4: eYFP-PLCβ1 expressed in a HEK293 cells showing the prominent plasma membrane and cytosolic populations

2.5 PLCβ INHIBITS THE PROMOTER OF RNA-INDUCED SILENCING, C3PO, TO IMPACT POSTTRANSLATIONAL GENE REGULATION

A search for cytosolic PLCβ1 binding partners was first carried out by a yeast two-hybrid study using the C-terminal region as bait with the idea that an unknown cytosolic partner might activate PLCβ in a similar manner as Gαq, and allow the enzyme to modify the PIP_2 levels in internal membranes. These studies identified the nuclease TRAX (translin-associated factor X).[23] TRAX is a small helical protein that shuttles between the cytoplasm and nucleus.[24] TRAX is always found complexed with the oligonucleotide binding protein translin in a 6:2 (translin:TRAX) octamer called C3PO (Component 3 Promoter of the RNA Induced Silencing Complex), and expression of the two proteins is linked.[25] C3PO is found in all cells with similar structure from sponges to humans (Figure 2.5). The C3PO octamer is a dimer of tetramers with the oligonucleotide binding site located in a channel between the two hemispheres.[26] Single or double stranded oligonucleotides bind nonspecifically to the translin subunits where they are subsequently hydrolyzed by the TRAX subunits. PLCβ was found to bind primarily to the TRAX subunits at a 1:1 (C3PO:PLCβ) stoichiometry and a K_d ~8 nM.[23, 27] PLCβ1 binding blocks the release of product, inhibiting release and C3PO activity.

Structure of C3PO
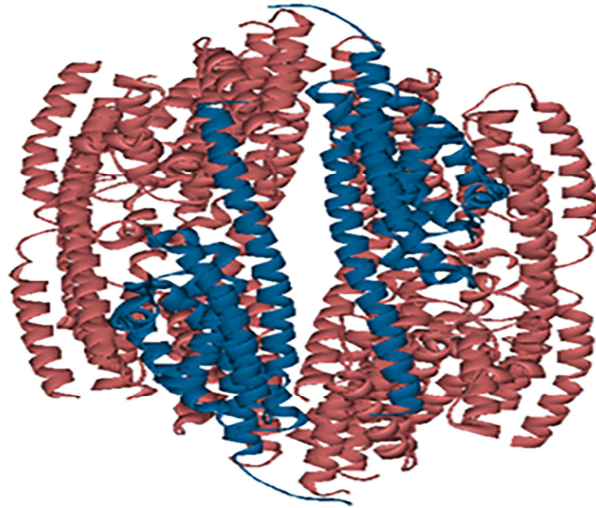
Figure 2.5: Structure of human C3PO where translin subunits are in red and TRAX are in blue PDB Id: 3PJA

While the exact cellular role of C3PO is under debate, there is evidence that C3PO promotes the activity of the RNA-induced silencing complex, RISC.[28] RISC is a ribonucleoprotein complex that silences gene expression by cleaving and degrading mRNA. Its activity is initiated by the RNase III enzyme Dicer to process dsRNA into ~22 nucleotide microRNA's (miRNA or miR).[29, 30] For degradation to happen, a guide strand of miRNA acts as a template for a complementary mRNA passenger strand to bind. With perfect pairing, Argonaute 2 (Ago2) will nick the miRNA passenger strand and C3PO will help further degrade it, allowing the complementary mRNA to hybridize to the guide strand. Once this happens, Ago2 will nick the mRNA between the 10th and 11th nucleotide, causing it to be degraded.[31, 32] If the guide strand does not match the mRNA perfectly, the Ago2-mRNA complex will stall and form aggregates, such as stress granules (Figure 2.6).

Diagram of Ago2 and C3PO's role in RNA-induced silencing
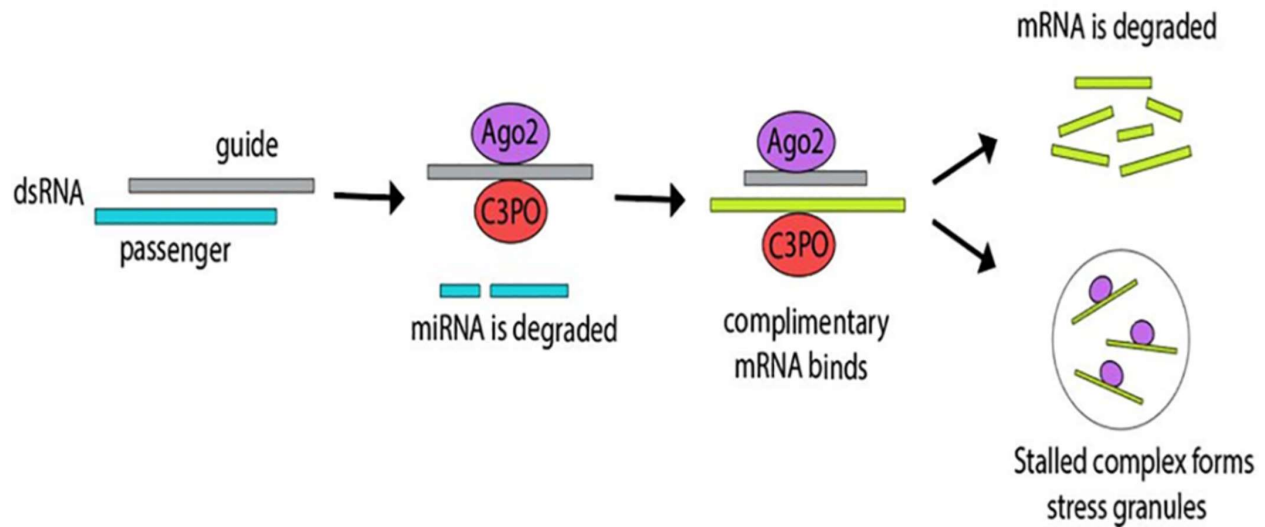
Figure 2.6: RNA silencing as a result of cleavage of miRNA by Ago2 and degradation by C3PO

In general, inhibition of C3PO by PLCβ can reverse silencing by exogenously added siRNAs, although this is not always the case. Part of the selectivity of the oligonucleotides that are silenced by PLCβ is dictated by the relative concentration of the specific miR, the presence of any competing miRs, and the stability of the miRs. Insight into the conditions that allow PLCβ to impact hydrolysis of specific oligonucleotides can be found in the thermodynamic cycle:[33]
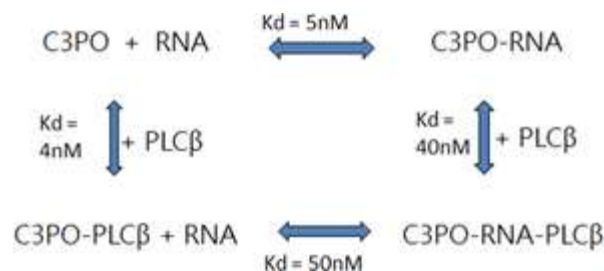
This schematic lists the association of RNA to C3PO, of PLCβ to C3PO and formation of ternary complexes where the Kd values are taken from model oligonucleotides.[33] The studies show that miRs that are slowly hydrolyzed (i.e., high melting T, high GC content) and are held in the active site of C3PO for relatively long times, are subject to inhibition by PLCβ. Alternately, less stable

RNAs whose hydrolysis and product release occur during the off-rate of PLCβ, are unaffected by PLCβ binding.

In cultured neuronal cells under basal conditions, only a minor population of PLCβ binds C3PO. However, when sympathetic neurons from pheochromocytoma of rat adrenal medulla (PC12) cells, a common model for neuronal cell development ([34]), are induced to differentiate, PLCβ increases its association to C3PO, and these complexes diminish as differentiation ends.[35] Surprisingly, loss of either PLCβ or C3PO reverses differentiation causing stem cell markers to be expressed and shifting miR populations to those associated with the differentiated state (Garwain et al., submitted). These results suggest that small amounts of PLCβ-C3PO complexes are required to maintain the differentiated state.

It is important to stress the dynamics of PLCβ in inhibiting RNA-induced silencing. Activation of Gαq shifts PLCβ away from C3PO allowing silencing to continue, whereas transfection of siRNAs, promotes cytosolic localization and reduces calcium signals (Figure 2.7 [36]). Thus, PLCβ is in dynamic equilibrium between these two partners.
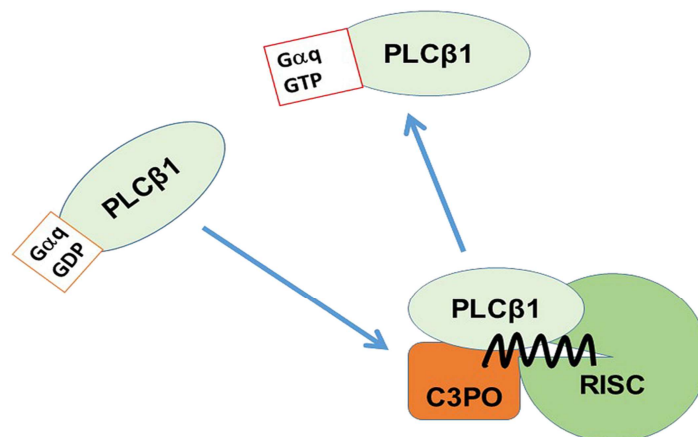
Figure 2.7: Cartoon showing the exchange of the PM and cytosolic populations of PLCβ

2.6 PLCβ IMPACTS STRESS GRANULE ASSEMBLY

While the functional significance of PLCβ-C3PO association is traced to shifting miR populations to establish and maintain neuronal differentiation, under basal conditions, only a minor population of PLCβ associates with C3PO suggesting that PLCβ may have additional roles. To identify

additional functions, we set out to identify additional binding partners. To this end, we isolated the cytosolic fractions of both undifferentiated PC12 cells and A10 cells (smooth muscle cell line derived from thoracic aorta of rats) and pulled-down PLCβ with a monoclonal antibody to identify the bound proteins by mass spectrometry. Surprisingly, we find that approximately one third of the bound proteins are classified as stress granule proteins.[37]

Stress granules are membraneless aggregates of stalled mRNA that prioritize protein synthesis until the stress is relieved.[38] Cells try to alleviate environmental stressors such as a change in osmotic pressure, heat, or oxidative stress by localizing untranscribed miRs into compact granules.[38, 39] These granules do not have an encapsulating membrane or envelope, and are effective in partitioning themselves from the cytosol and other organelles in a liquid-like state. Stress granules give the cell an opportunity to sort mRNAs and decide whether they should be degraded, stored, or translated.[28, 40] It is important to note that assembly and disassembly of stress granules are vital to healthy neuronal function and plasticity, and the inability to disassemble has been associated with some types of neurological diseases.[41]

Stress granules are mainly composed of untranslated mRNA, but also include proteins such as Argonaute 2 (Ago2), polyadenylate binding protein 1 (PABPC1), fragile X mental retardation proteins 1 and 2 (FXR1/2), Ras, GTPase activating protein-binding Protein 1 (G3BP1), and multiple eukaryotic translation initiation factors.[41-43] We find that all of these proteins are bound to cytosolic PLCβ1.[37] Furthermore, stress granules are independent of P bodies (processing bodies), which are similar membraneless aggregates that traditionally do not contain translation initiation factors and only store degraded mRNA.[44]

Our studies show that reducing cytosolic levels of PLCβ1 by downregulation or by activating Gαq to drive PLCβ to the membrane, increases the formation of stress granules containing Ago2, PABPC1 and G3BP1 in several types of cultured cells (Figure 2.8[37]). These observations suggest that the binding of PLCβ to stress granule proteins helps to prevent their aggregation.[45] The composition of the stress granules formed by the loss of cytosolic PLCβ and the identities of the transcripts contained are under investigation.
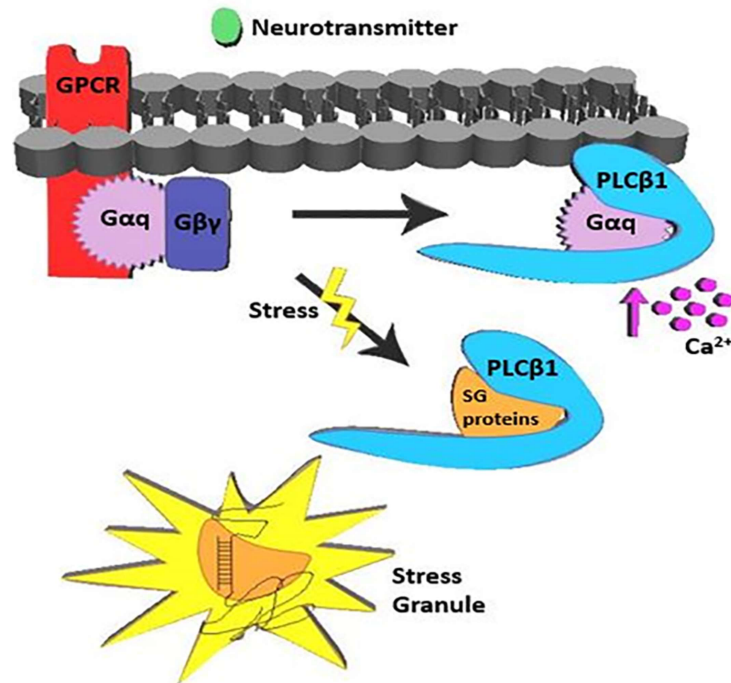
Figure 2.8: **Model of PLCβ1's dynamic exchange between G proteins on the plasma membrane and stress granules**

2.7 MODEL FOR THE ROLE OF CYTOSOLIC PLCβ

When PLCβ1 is bound to C3PO, many small, interfering RNAs (siRNAs) fail to downregulate protein expression. C3PO competes with Gαq for the same binding site on PLCβ1,[45] so it is believed that the role of PLCβ1 is split between the plasma membrane, when binding with Gαq, or the cytosol when interacting with C3PO or stress granule proteins. Thus, PLCβ1 binding to Gαq reverses its inhibition of C3PO while binding to C3PO inhibits calcium signaling through Gαq activation.[45] The need to shuttle PLCβ1 between the cytosol and plasma membrane depends on the concentration of these proteins within the cell and these processes are especially important to understand since they may impact key events, such as PC12 cell differentiation.

Another surprising, but more limited function of PLCβ is to inhibit CDK16, which is a neuronal and testis-specific cyclin-dependent kinase that inhibits an inhibitor of proliferation, p27kip.[46, 47] At the onset of PC12 cell differentiation, expression of PLCβ1 increases several-fold.[35] Besides binding to C3PO to promote differentiation, this bolus of PLCβ also binds to

CDK16 to inhibit proliferation.[48] The mechanism of inhibition is not clear. Based on testing of several cell lines, it appears that the ability of PLCβ1 to impact proliferation is limited to neuronal cells where CDK16 is expressed.

2.8 CONTROLLING THE TRANSITION OF PLCβ'S PLASMA MEMBRANE VERSUS CYTOSOLIC FUNCTION

Transition between PLCβ's two functions, that is, G protein/Ca^{2+} signaling on the plasma membrane versus inhibition of RNA-induced silencing in the cytosol, is primarily controlled by the activation of Gαq, which may override all of PLCβ's cytosolic functions. However, switching between these functions is subject to other cellular factors.

2.8.1 Control Gαq/GPCR localization

The localization of Gαq/GPCR will affect the localization of the plasma membrane population of PLCβ that exchanges with the cytosolic population. Several studies have shown that GPCRs are not homogeneous on the plasma membrane but can sequester in distinct areas, and the factors that control localization are numerous. First, it has been found that the shape of the cell regulates GPCR/Gαq localization affecting both signal transduction processes within the cell and second messenger dynamics between the plasma membrane (PM) and the endoplasmic reticulum.[49] An example of differences in calcium release in the body and neurons of PC12 cells is shown in Figure [9]. Localization patterns may play important roles in cells with varied morphologies such as neurons and podocytes. It is notable that in neurons GPCRs play an important role in presynaptic and postsynaptic signaling leading to their necessity to be localized all along the cell not just located within the synaptic cleft.[18] These findings lead to the interesting idea that localization of the receptors and their attached G proteins on tips and protrusions of cells may help sequester PLCβ from C3PO and stress granule proteins eliminating PLCβ's cytosolic function.
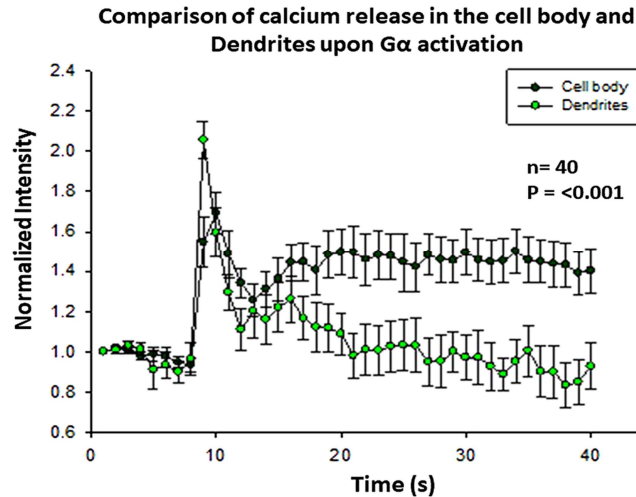
Figure 2.9: Differences in calcium signals in the dendrites versus the cell body of PC12 cells upon acetylcholine stimulation, from Garwain and Scarlata, unpublished

2.8.2 Stabilization of Gαq

The most stable and well-characterized microdomains on the plasma membrane are caveolae, and it has been shown that the presence of caveolae has profound effects on Gαq/PLCβ signaling.[50] Caveolae are protein dense invaginations on the plasma membrane. Structurally, caveolae are composed of caveolin-1 (Cav1) and/or caveolin-3 (Cav-3) where Cav-3 is muscle specific along with other proteins.[51, 52] Caveolin molecules only penetrate the inner leaflet in a "U" shape, and aggregation of ~140 of these proteins results in the invaginations that are a hallmark of these domains.[53, 54]

Several signaling complexes localize to caveolae leading to the idea that caveolae helps sequester and organize functionally related proteins.[52, 55-57] Our lab has found that Cav-1 or -3 specifically binds Gαq and their affinity increases when Gαq is activated.[58] The stabilization of activated Gαq by Cav1/3, coupled with release of Gβγ from caveolae domains during the activation cycle, has the net effect of prolonging PLCβ activation and increasing the extent and duration of Ca^{2+} responses.[59] The interaction between Cav1/3 not only localizes Gαq to caveolae domains, but also in turn allows Gαq to scaffold its associated GPCRs leading to a localized and potentially synergistic response.[60]

Caveolae are prominent in smooth muscle cells and provide mechanical strength by flattening during stretch to provide more membrane area.[61, 62] We have found that the flattening of these domains by mechanical stretch or hypo-osmotic conditions eliminates stabilization of activated Gαq by caveolin molecules reducing Ca^{2+} signals.[63, 64] Additionally, osmotic stress reduces the cytosolic level of PLCβ eliminating its cytosolic function.[37] Thus, caveolae have the potential to regulate the cytosolic versus plasma membrane functions of PLCβ by modulating the localization of Gαq and the duration of its activated state (Figure 2.10).

Cartoon showing localization of Gαq in a caveola
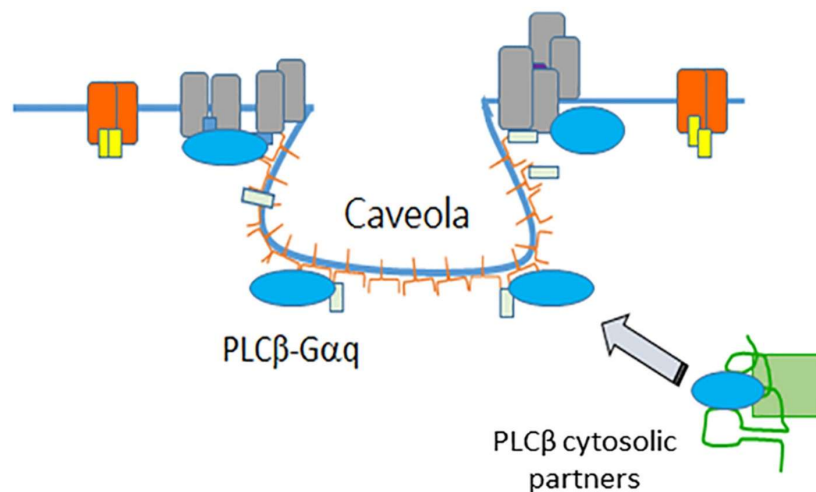
Figure 2. 10: Model depicting localization of PLCβ (blue), **and Gαq** (light gray) **and their corresponding GPCRs** (dark gray) **in caveolae where caveolin molecules are in red.** GPCRs coupled to other G proteins are in red and yellow

2.9 PREDICTING THE IMPACT OF Gαq/PLCβ ACTIVATION ON CALCIUM SIGNALS VERSUS PROTEIN TRANSLATION

Being able to delineate the factors that regulate the localization and activation of Gαq is a first step in predicting the ability of PLCβ to generate calcium responses or modulating protein translation. While present day methods are moving toward accurate quantification of the molecular identities, quantities and localization of proteins in cells, these values can only be estimated. Nevertheless, we can formulate a thermodynamic analysis that should be applicable in predicting the regulation of multifunctional proteins.

2.10 FUNCTIONAL SWITCHING OF PROTEINS

PLCβ is an example of a protein that has multiple cellular functions that switch upon activation, growth, differentiation, or other cellular events. Functional switching involves three key factors: (a) *Changes in the local concentration of protein and its relative partners*; (b) *Changes in relative affinities*; *and* (c) *Changes in the concentration and relative affinities of extraneous but competing proteins*.

The most simple analysis assumes that the observed PLCβ function stems from the relative plasma membrane versus cytosolic concentrations resulting from two competing bimolecular associations; one that impacts Ca^{2+} signals and one that impacts protein translation (PT). The key feature for PLCβ, and possibly other systems, is that simultaneous binding of Gαq and C3PO does not occur (PLCβ's interaction region with other cytosolic partners has not yet been determined).

The equilibria of PLCβ's function (K_f), can be considered as the ratio of the concentration of PLCβ bound to Gαq (PLCβ-Gαq) versus C3PO and other cytosolic partners (PLCβ-CP).

$$Kf=[PLC\beta\cdot G\alpha q]/[PLC\beta\cdot CP]$$

Where these complexes are described by the dissociation constants associated with PLCβ's calcium function (Kd[f-Ca2+]) or PLCβ's cytosolic function (Kd[f-CP]):

$$PLC\beta+G\alpha q=PLC\beta\cdot G\alpha q; Kd(f\cdot Ca2+)=([PLC\beta]*[G\alpha q])/[PLC\beta\cdot G\alpha q]$$

$$PLC\beta+CP=PLC\beta\cdot CP Kd(f\cdot CP)=([PLC\beta]*[CP])/[PLC\beta\cdot CP]$$

Substituting and rearranging gives:

$$Kf=[G\alpha q]*Kd(f\cdot Ca2+)/[CP]*Kd(f\cdot CP)$$

The above expression shows that the observed function of PLCβ is surprisingly independent of concentration and only dependent of the relative cellular concentration of the competing partners. The dissociation constants for the PLCβ-Gαq (both in its inactivated and activated states) complexes and the complexes formed between PLCβ and C3PO and/or the putative stress granule binding partner eukaryotic initiation factor 5A, have been measured using purified proteins.[4, 23, 37] More relevant dissociation constants can be obtained using cell extracts that will allow for quantification of the dissociated species and their complexes. We know that the binding of C3PO to PLCβ1 is stronger than Gαq(GDP) but weaker than Gαq(GTP), and these differences are within a 10-fold range allowing cells to switch PLCβ functions as needed depending on cellular circumstances. These expressions are regulated by three major factors.

2.11 THE LOCAL CONCENTRATION OF PROTEIN AND ITS RELATIVE PARTNERS; EFFECTS OF COMPARTMENTALIZATION

Cell compartmentalization allows cells to sequester components to promote some interactions while preventing others. For the case of PLCβ, compartmentalization takes the form of concentrating PLCβ's main partner, Gαq on the PM surface. PLCβ association with Gαq in this compartment is regulated by its intrinsic membrane binding, which enhances its association with Gαq by a reduction of dimensionality.

$$PLC\beta(cytosol)=PLC\beta(PM) \quad PLC\beta cytosol=PLC\beta PM$$

$$PLC\beta(PM)+G\alpha q=PLC\beta \cdot G\alpha q(PM) \quad PLC\beta PM+G\alpha q=PLC\beta \cdot G\alpha q PM$$

The concentrating effect of the plasma membrane has been previously treated[4] by considering that membrane-bound proteins are confined in a reduced volume (v) in relation to the bulk volume (V_b). The relationship between the amount of protein bound to a membrane, $[P]_{(membrane)}$ to its unbound concentration in the bulk $[P]_{(bulk)}$ effect can be expressed

$$[P](membrane)=[P](bulk)*(V_b/v) \quad Pmembrane=Pbulk*V_b/v$$

$$v=4\pi r2d \quad v=4\pi r2d$$

where v is the reduced volume of a spherical membrane with a known radius (r) and diameter (d). The apparent dissociation constant will be reduced by:

$$Kd=(Vb/v)KappKd=Vb/vKapp$$

This equation quantifies the increased affinity of two membrane-bound proteins versus their association in bulk solution and can be readily modified to a single membrane-bound species or multiple membrane associations. Analysis for proteins reconstituted on lipid vesicles is straightforward but more challenging for cellular systems because of uncertainty in the membrane surface area that the protein is confined; that is, proteins might diffuse in a limited surface area due to protein barriers, be confined to a domain such as caveolae, and/or a combination of the two. While these parameters are important for integral membrane proteins such as GPCRs, peripheral membrane proteins such as PLCβ undergo dissociation and reassociation events as dictated by their partition coefficients. Gαq, which is stably bound to the membrane by two palmitoyl groups[65] and bound to GPCR, has much more stable binding. Despite these complications, single molecule measurements may be used to estimate the amount of protein per surface area and the impact of plasma membrane partitioning on protein affinities.

In the case of Gαq/PLCβ association in cells, it is not clear whether the observed plasma membrane population is bound to membrane or Gαq. While PLCβ partitions to model bilayers with the partition coefficient, Kp ~1–10 μM[14] the amount of lipid available for binding is unclear. Thus, it is likely that the plasma membrane population PLCβ is complexed to Gαq in both its deactivated and activated, and this is supported by FRET studies.[66]

2.12 CHANGES IN RELATIVE AFFINITIES

All cellular events can be traced to changes in protein association due to changes in affinity. These changes in affinity can be brought about by the binding of ligands to extracellular or intracellular targets, phosphorylation/dephosphorylation, ATP hydrolysis, and so forth. For the Gαq/PLCβ pathway, activation of Gαq increases its affinity for PLCβ 20-fold,[4] which is stronger than the affinity measured for PLCβ /C3PO,[23] and possibly the affinities with other cytosolic proteins.

Notably, the cumulative affinities of these cytosolic proteins may not completely compete with activated Gαq. Thus, the net effect of Gαq activation is to shift cytosolic populations of PLCβ to the membrane surface and away from cytosolic partners. Additionally, because Gαq resides on the quasi two-dimensional surface of a membrane, increase in affinity is enhanced.

Measuring affinities of proteins is difficult in intact cells and changes in affinities are taken from data using purified proteins, but it is assumed that the magnitude of the changes in affinity seen in solution occur in cells. Besides affinities, it is important to estimate the local concentrations of the associating proteins, which depend on the number of molecules, the compartmentalization and competing proteins (*see below*). One method to estimate relative affinities is by measuring the loss in FRET between two labeled proteins as known amounts of competitors using fluorescent-tagged proteins. These estimates are certain to become more quantitative as more sophisticated methods are available.

2.13 CONCENTRATION AND RELATIVE AFFINITIES OF EXTRANEOUS, COMPETING PROTEINS

The least known variable in predicting exchange of protein partners in the complex milieu of the cell is the presence of competing proteins. Some of these interactions may have unclear functional relevance. It is likely that many of these interactions Here, we discuss several types of competing associations that might simplify analysis when predicting the switching of bifunctional proteins.

2.13.1 The presence of multiple isoforms of a given enzyme localized in the same compartment

Some cells express multiple isoforms of a protein that localize in similar compartments which, because of slightly varying affinities and activation profiles, allow cells to fine-tune responses. This is certainly the case for PLCβ where many cells express several isoforms at varying levels. Solution studies show that PLCβ1-3 bind to Gαq within an order of magnitude.[4] Additionally, all bind to Gβγ subunits but their activation profiles are very different; PLCβ1 is not activated by Gβγ while PLCβ2-3 are activated 2–10-fold.

When considering multiple isoforms of a protein and the affinities between the partners involved in the switching are not large, it is easiest to consider the isoforms as a single species that has a range of dissociation constants.

2.13.2 Competitors whose binding overlaps a primary binding site

If a competitive protein binds to a partner, there would be less of the partner available for binding and functional switching. The impact will depend on its affinity and local concentration.

We can estimate these effects:

For the association of A and B: $A + B = AB$

$$K(AB) = [AB]/([A] * [B])$$

If competitor C binds to B: $C + B = CB$

$$K(CB) = [BC]/([C] * [B])$$

Substituting and rearranging gives:

$$K(AB)/K(CB) = ([AB]/[A]) * ([BC]/[C])$$

Thus, in order for a reaction of weaker affinity to affect the primary reaction, the local concentration must compensate for the lower affinity.

2.13.3 Competitors whose binding only partially overlap the binding site

Many proteins have multiple binding sites that include the binding of other proteins, such as those discussed above, or allow partial exposure of the binding site. The degree of exposure will shift the impact from negligible for a small degree of occlusion to the equations above for complete exclusion.

2.14 CONCLUSIONS AND TAKE-HOME LESSONS

PLCβ is an example of a protein that has evolved to perform multiple functions in cells. These interdependent functions allow cells to respond in multiple and complementary ways to extracellular sensory information, that is, through pathways that involve calcium fluxes and through changes in the translation of different proteins. While the primary calcium function has been well characterized, PLCβ's secondary functions are just beginning to be uncovered.

Multifunctional proteins switch between various cellular roles through changes in protein associations. These changes may be brought about by chemical modifications, such as phosphorylation, or local changes in concentration of a protein partner through the appearance of an activated cofactor or changes in compartmentalization. Although we are still far from accurate quantitation of the factors that allow functional switching in living cells and tissue, we have begun to formulate analysis from when they become available.

2.15 AUTHOR CONTRIBUTIONS

L.J., A.Q., K.P. and S.S. designed experiments. L.J. developed the CEPO/RISK subsections. L.J & A.Q developed the stress granule formation related sections including the model. A.Q. developed the Gαq stabilization section through caveolae. K.P. developed the calcium signaling related section. L.J., A.Q., K.P., and S.S. interpreted the data. L.J, A.Q., K.P. and S.S. wrote the manuscript.

2.16 ACKNOWLEDGMENTS

2.17 REFERENCES

1. Hepler JR, Gilman AG. G-proteins. *Trends Biochem Sci*. 1992; **17**: 383– 387.
2. Jong YI, Harmon SK, O'Malley KL. Intracellular GPCRs play key roles in synaptic plasticity. *ACS Chem Neurosci*. 2018; **9**: 2162– 2172.
3. Devi LA. Heterodimerization of G-protein-coupled receptors: Pharmacology, signaling and trafficking. *Trends Pharmacol Sci*. 2001; **22**: 532– 537.

4. Runnels LW, Scarlata S. Determination of the affinities between heterotrimeric G protein subunits and their phospholipase C- b effectors. *Biochemistry*. 1999; **38**: 1488– 1496.

5. Penela P, Ribas C, Sánchez-Madrid F, Mayor F. G protein-coupled receptor kinase 2 (GRK2) as a multifunctional signaling hub. *Cell Mol Life Sci*. 2019; **76**: 4423– 4446.

6. Neves SR, Ram PT, Iyengar R. G protein pathways. *Science*. 2002; **296**: 1636– 1639.

7. Lee CH, Park D, Wu D, Rhee SG, Simon MI. Members of the Gq alpha subunit gene family activate phospholipase C beta isozymes. *J Biol Chem*. 1992; **267**: 16044– 16047

8. Drin G, Scarlata S. Stimulation of phospholipase C[beta] by membrane interactions, interdomain movement, and G protein binding – how many ways can you activate an enzyme? *Cell Signal*. 2007; **19**: 1383– 1392.

9. Bittner MA, Holz RW. Phosphatidylinositol-4,5-bisphosphate: Actin dynamics and the regulation of ATP-dependent and -independent secretion. *Mol Pharmacol*. 2005; **67**: 1089– 1098.

10. Dickinson GD, Ellefsen KL, Dawson SP, Pearson JE, Parker I. Hindered cytoplasmic diffusion of inositol trisphosphate restricts its cellular range of action. *Sci Signal*. 2016; **9**:ra108.

11. Rosenberg SS, Spitzer NC. Calcium signaling in neuronal development. *Cold Spring Harb Perspect Biol*. 2011; **3**:a004259.

12. Stiber JA, Rosenberg PB. The role of store-operated calcium influx in skeletal muscle signaling. *Cell Calcium*. 2011; **49**: 341– 349.

13. Park D, Jhon D, Lee CW, Lee KH, Rhee SG. Activation of phospholipase C isozymes by G protein βγ subunits. *J Biol Chem*. 1993; **268**: 4573– 4576.

14. Runnels LW, Jenco J, Morris A, Scarlata S. Membrane binding of phospholipases C-b$_1$ and C-b$_2$ is independent of phosphatidylinositol 4,5-bisphosphate and the a and bg subunits of G proteins. *Biochemistry*. 1996; **35**: 16824– 16832.

15. Yang B, Pu M, Khan HM, et al. Quantifying transient interactions between bacillus phosphatidylinositol-specific phospholipase-C and phosphatidylcholine-rich vesicles. *J Am Chem Soc*. 2015; **137**: 14– 17.

16. Suzuki KGN, Fujiwara TK, Edidin M, Kusumi A. Dynamic recruitment of phospholipase C gamma at transiently immobilized GPI-anchored receptor clusters induces IP3-Ca2+ signaling: Single-molecule tracking study 2. *J Cell Biol*. 2007; **177**: 731– 742.

17. Lyon AM, Dutta S, Boguth CA, Skiniotis G, Tesmer JJ. Full-length Galpha(q)-phospholipase C-beta3 structure reveals interfaces of the C-terminal coiled-coil domain. *Nat Struct Mol Biol*. 2013; **20**: 355– 362.

18. Huang Y, Thathiah A. Regulation of neuronal communication by G protein-coupled receptors. *FEBS Lett*. 2015; **589**: 1607– 1619.

19. Rebecchi M, Pentylana S. Structure, function and control of phosphoinositide-specific phospholipase C. *Physiol Rev*. 2000; **80**: 1291– 1335.

20. Hill-Eubanks DC, Werner ME, Heppner TJ, Nelson MT. Calcium signaling in smooth muscle. *Cold Spring Harb Perspect Biol*. 2011; **3**:a004549.

21. Lyon AM, Tesmer JJ. Structural insights into phospholipase C-beta function. *Mol Pharmacol*. 2013; **84**: 488– 500.

22. Wu D, Jiang H, Katz A, Simon MI. Identification of critical regions on phospholipase C-beta 1 required for activation by G-proteins. *J Biol Chem*. 1993; **268**: 3704– 3709.

23. Aisiku OR, Runnels LW, Scarlata S. Identification of a novel binding partner of phospholipase Cβ1: Translin-associated factor X. *PLoS ONE*. 2010; **5**:e15001.

24. Cho YS, Chennathukuzhi VM, Handel MA, Eppig J, Hecht NB. The relative levels of translin-associated factor X (TRAX) and testis brain RNA-binding protein determine their nucleocytoplasmic distribution in male germ cells. *J Biol Chem*. 2004; **279**: 31514– 31523.

25. Yang S, Cho YS, Chennathukuzhi VM, Underkoffler LA, Loomes K, Hecht NB. Translin-associated factor X is post-transcriptionally regulated by its partner protein TB-RBP, and both are essential for normal cell proliferation. *J Biol Chem*. 2004; **279**: 12605– 12614.

26. Tian Y, Simanshu DK, Ascano M, et al. Multimeric assembly and biochemical characterization of the Trax–translin endonuclease complex. *Nat Struct Mol Biol*. 2011; **18**: 658– 664.

27. Sahu S, Philip F, Scarlata S. Hydrolysis rates of different small interfering RNAs (siRNAs) by the RNA silencing promoter complex, C3PO, determines their regulation by phospholipase Cβ. *J Biol Chem*. 2014; **289**: 5134– 5144.

28. Liu Y, Ye X, Jiang F, et al. C3PO, an endoribonuclease that promotes RNAi by facilitating RISC activation. *Science*. 2009; **325**: 750– 753.

29. Lo Vasco VR, Longo L, Polonia P. Phosphoinositide-specific phospholipase C β1 gene deletion in bipolar disorder affected patient. *J Cell Commun Signal*. 2013; **7**: 25– 29.

30. Kurian MA, Meyer E, Vassallo G, et al. Phospholipase C beta 1 deficiency is associated with early-onset epileptic encephalopathy. *Brain*. 2010; **133**: 2964– 2970

31. Golebiewska U, Scarlata S. High pressure promotes alpha-synuclein aggregation in cultured neuronal cells. *FEBS Lett*. 2015; **589**: 3309– 3312.

32. Narayanan V, Scarlata S. Membrane binding and self-association of α-synucleins. *Biochemistry*. 2001; **40**: 9927– 9934.

33. Sahu S, Williams L, Perez A, et al. Regulation of the activity of the promoter of RNA-induced silencing, C3PO. *Protein Sci*. 2017; **26**: 1807– 1818.

34. Greene LA, Tischler AS. Establishment of a noradrenergic clonal line of rat adrenal pheochromocytoma cells which respond to nerve growth factor. *Proc Natl Acad Sci U S A*. 1976; **73**: 2424– 2428.

35. Garwain O, Scarlata S. Phospholipase Cβ-TRAX association is required for PC12 cell differentiation. *J Biol Chem*. 2016; **291**: 22970– 22976

36. Philip F, Sahu S, Golebiewska U, Scarlata S. RNA-induced silencing attenuates G protein-mediated calcium signals. *FASEB J*. 2016; **30**: 1958– 1967.

37. Qifti A, Jackson L, Singla A, Garwain O, Scarlata S (2019) Stimulation of Gαq promotes stress granule formation. bioRxiv:521369

38. Philip F, Sahu S, Caso G, Scarlata S. Role of phospholipase C-β in RNA interference. *Adv Biol Regul*. 2013; **53**: 319– 330.

39. Li L, Gu W, Liang C, Liu Q, Mello CC, Liu Y. The Translin-TRAX complex/C3PO is a ribonuclease in tRNA processing. *Nat Struct Mol Biol*. 2012; **19**: 824– 830.

40. Park AJ, Havekes R, Fu X, et al. Learning induces the translin/trax RNase complex to express activin receptors for persistent memory. *elife*. 2017; **6**:e27872.

41. Pratt AJ, MacRae IJ. The RNA-induced silencing complex: A versatile gene-silencing machine. *J Biol Chem*. 2009; **284**: 17897– 17901.

42. Babar IA, Slack FJ, Weidhaas JB. miRNA modulation of the cellular stress response. *Future Oncol*. 2008; **4**: 289– 298.

43. Buchan JR, Parker R. Eukaryotic stress granules: The ins and out of translation. *Mol Cell*. 2009; **36**: 932– 941.

44. Hyman AA, Weber CA, Jülicher F. Liquid-liquid phase separation in biology. *Ann Rev Cell Devel Biol*. 2014; **30**: 39– 58.

45. Decker CJ, Parker R. P-bodies and stress granules: Possible roles in the control of translation and mRNA degradation. *Cold Spring Harb Perspect Biol*. 2012; **4**:a012286

46. Mikolcevic P, Sigl R, Rauch V, et al. Cyclin-dependent kinase 16/PCTAIRE kinase 1 is activated by cyclin Y and is essential for spermatogenesis. *Mol Cell Biol*. 2012; **32**: 868– 879.

47. Yanagi T, Matsuzawa S-i. PCTAIRE1/PCTK1/CDK16: A new oncotarget? *Cell Cycle*. 2015; **14**: 463– 464.

48. Garwain O, Valla K, Scarlata S. Phospholipase Cβ1 regulates proliferation of neuronal cells. *FASEB J*. 2018; **32**: 2891– 2898.

49. Rangamani P, Lipshtat A, Azeloglu Evren U, et al. Decoding information in cell shape. *Cell*. 2013; **154**: 1356– 1369.

50. Weinstein H, Scarlata S. The correlation between multidomain enzymes and multiple activation mechanisms–the case of phospholipase Cbeta and its membrane interactions. *Biochim Biophys Acta*. 2011; **1808**: 2940– 2947.

51. Gratton JP, Bernatchez P, Sessa WC. Caveolae and caveolins in the cardiovascular system. *Circ Res*. 2004; **94**: 1408– 1417.

52. Bastiani M, Parton RG. Caveolae at a glance. *J Cell Sci*. 2010; **123**: 3831– 3836.

53. Murthy KS, Makhlouf GM. Heterologous desensitization mediated by G protein-specific binding to caveolin. *J Biol Chem*. 2000; **275**: 30211– 30219.

54. Echarri A, Del Pozo MA. Caveolae - mechanosensitive membrane invaginations linked to Actin filaments. *J Cell Sci*. 2015; **128**: 2747– 2758.

55. Anderson RG. The caveolae membrane system. *Annu Rev Biochem*. 1998; **67**: 199– 225.

56. Kovtun O, Tillu VA, Ariotti N, Parton RG, Collins BM. Cavin family proteins and the assembly of caveolae. *J Cell Sci*. 2015; **128**: 1269– 1278.

57. Schlegel A, Volonte D, Engelman JA, et al. Crowded little caves: Structure and function of caveolae. *Cell Signal*. 1998; **10**: 457– 463.

58. Sengupta P, Philip F, Scarlata S. Caveolin-1 alters Ca2+ signal duration through specific interaction with the G{alpha}q family of G proteins. *J Cell Sci*. 2008; **121**: 1363– 1372.

59. Guo Y, Golebiewska U, Scarlata S. Modulation of Ca2+ activity in cardiomyocytes through caveolae-G[alpha]q interactions. *Biophys J*. 2011; **100**: 1599– 1607.

60. Calizo RC, Scarlata S. A role for G-proteins in directing G-protein-coupled receptor– caveolae localization. *Biochemistry*. 2012; **51**: 9513– 9523.

61. Sinha B, Köster D, Ruez R, et al. Cells respond to mechanical stress by rapid disassembly of caveolae. *Cell*. 2011; **144**: 402– 413.

62. Yang L, Scarlata S. Super-resolution visualization of caveola deformation in response to osmotic stress. *J Biol Chem*. 2017; **292**: 3779– 3788.

63. Guo Y, Yang L, Haught K, Scarlata S. Osmotic stress reduces Ca2+ signals through deformation of caveolae. *J Biol Chem*. 2015; **290**: 16698– 16707.

64. Qifti A, Garwain O, Scarlata S. Mechanical stretch redefines membrane Galphaq-calcium signaling complexes. *J Membr Biol*. 2019; **252**: 307– 315.

65. Wedegaertner P, Wilson P, Bourne H. Lipid modifications of trimeric G proteins. *J Biol Chem*. 1995; **270**: 503– 506.

66. Dowal L, Provitera P, Scarlata S. Stable association between G alpha(q) and phospholipase C beta 1 in living cells. *J Biol Chem*. 2006; **281**: 23999– 24014.

67. Philip F, Kadamur G, Silos RG, Woodson J, Ross EM. Synergistic activation of phospholipase C-^{2}3 by G±q and G^{23} describes a simple two-state coincidence detector. *Curr Biol*. 2010; **20**: 1327– 1335.

68. Cabrera-Vera TM, Vanhauwe J, Thomas TO, et al. Insights into G protein structure, function, and regulation. *Endocr Rev*. 2003; **24**: 765– 781.

CHAPTER 3 - STIMULATION OF PHOSPHOLIPASE CB1 BY GAQ PROMOTES THE ASSEMBLY OF STRESS GRANULE PROTEINS

Androniqi Qifti[1*], Lela Jackson[1*], Ashima Singla[1‡], Osama Garwain[1§], Suzanne Scarlata[1†]

1Department of Chemistry and Biochemistry, Worcester Polytechnic Institute, Worcester, MA 01609, USA.

*These authors contributed equally to this study.

‡Current address: SCO 2A Madhya Marg, Sector 7-C, Chandigarh, 160007 India.

§Current address: Agilent Technologies, Santa Clara, CA 95051

†Corresponding author. Email: sfscarlata@wpi.edu

The following chapter appears in Qifti et al. "Stimulation of phospholipase Cβ1 by Gαq promotes the assembly of stress granule proteins." Science Signaling. (2021) and is reproduced here with permission from Biophysical Science Signaling. Supporting information from the manuscript was brought into the body of the chapter. Addition information on the authors' contributions can be found in section 3.6.

3.0 ABSTRACT

During adverse conditions, mammalian cells regulate protein production by sequestering the translational machinery in membrane-less organelles known as stress granules. Here, we found that activation of the G protein subunit $G\alpha_q$ promoted the formation of particles that contained stress granule proteins through a mechanism linked to the presence of phospholipase Cβ1 (PLCβ1) in the cytosol. In experiments with PC12 and A10 cells, we showed that under basal conditions, cytosolic PLCβ1 bound to stress granule-associated proteins, including PABPC1, eIF5A, and Ago2. Knockdown of cytosolic PLCβ1 with siRNA or promoting its relocalization to the plasma membrane by activating $G\alpha_q$ resulted in the formation of particles containing the stress granule markers, PABPC1, G3BP1, and Ago2. Our studies showed that the composition of these particles resemble those formed under osmotic stress and are distinct from those formed by other stresses. Our results fit a simple thermodynamic model in which cytosolic PLCβ1 solubilizes stress granule proteins such that its movement to activated $G\alpha_q$ releases these particles to enable the formation of stress granules. Together, our data are suggestive of a link between $G\alpha_q$-coupled signals and protein translation through stress granule formation.

3.1 INTRODUCTION

When cells are subjected to environmental stresses, they halt the production of many housekeeping proteins to preserve resources for the synthesis of proteins that will help the cell alleviate the particular stress. These stalled translation complexes, called stress granules, are thought to act as triage sites that protect non translated mRNAs from degradation until the stress is removed, while enabling the synthesis of other proteins (*1, 2*). Stress granules are distinct from processing bodies (P-bodies) that store and process mRNA, although these have also been observed under nonstress conditions. Depending on the cellular conditions, the mRNA held in these stalled complexes may be degraded, translated, or stored until needed. Additionally, studies in yeast subjected to hypo-osmotic stress found that P-bodies and stress granules may form hybrid structures (*3*), although this behavior has not yet been observed in higher eukaryotes. Physically, stress granules are phase-separated domains composed of nontranslating mRNAs, translation initiation complexes, poly (A)–binding protein, and many additional mRNA-related proteins (*4*). They consist of a packed core with loosely associated peripheral proteins (*5*). Stress granules appear when cells are subjected to environmental conditions such as cold- or heat-shock, exposure to toxic molecules, oxidative stress, hypo- or hyper-osmolarity, UV irradiation, or nutrient deprivation. The molecular mechanisms that transduce these different stresses into the cellular interior remain largely unresolved. Although stress granules appear in many types of cells, we focused here on those that form in mammalian cells. Stress granules have been implicated in the pathogenesis of various diseases, such as cancer, neurodegeneration, and viral infections (*1, 6*). Many stress granule proteins contain disordered regions, which play important roles in the liquid-like nature of stress granules. Neuronal cells, in particular, contain many proteins with disordered regions, and so it is not surprising that some neurological diseases (for example, amyotrophic lateral sclerosis) have been attributed to the abnormal stability of stress granules (*7*). Thus, it is important that cells have mechanisms to prevent the premature formation of stress granules, as well as to ensure their reversible assembly and disassembly.

Whereas stress granules primarily contain proteins associated with translation, note that argonaute 2 (Ago2) can be found in these regions (*8*). Ago2 is the main nuclease component of the RNA-induced silencing complex (RISC) (*9*). Ago2 binds to small interfering RNAs (siRNAs) in their double-stranded form and holds the guide strand after the passenger strand is degraded to enable

hybridization with a target mRNA. If pairing between the passenger strand and the mRNA is perfect, as is the case with exogenous siRNAs, then Ago2 will undergo conformational changes that result in mRNA degradation. Alternatively, if pairing is imperfect, as is frequently the case for endogenous microRNAs (miRNAs), the conformational changes that enable Ago2 nuclease activity do not occur, which results in the formation of a stalled complex (*10*). Thus, the formation and stability of these stalled complexes and their incorporation into stress granules alter protein populations, which may modify downstream protein-protein interactions that may ultimately change the properties of the cell.

The mechanisms through which environmental changes are transduced into the cell to promote stress granule formation are unclear and are likely to differ with different types of stress. Here, we showed that extracellular signals can affect stress granule formation through heterotrimeric guanine nucleotide–binding proteins (G proteins) to stall protein translation. Signaling through G proteins is initiated when external ligands bind to their target G protein–coupled receptors (GPCRs), which activates intracellular Gα subunits. The Gα$_q$ family of G proteins is activated by GPCRs for agents such as acetylcholine, dopamine, bradykinin, serotonin, and histamine (*11, 12*). Activated Gα$_q$ in turn activates phospholipase Cβ (PLCβ), which catalyzes the hydrolysis of the signaling lipid phosphatidylinositol-4, 5-bisphosphate, which eventually results in an increase in intracellular calcium (Ca^{2+}) signaling. There are four known members of the PLCβ family differ in their tissue distribution and their ability to be activated by G proteins (*12*). Here, we focused on PLCβ1, which is the isoform most highly activated by Gα$_q$ and is prominent in neuronal tissue. Whereas the major population of PLCβ1 lies at the plasma membrane, where it binds to Gα$_q$ and accesses its substrate, PLCβ1 is also found in the cytosol in every cell type examined and under different conditions (*13, 14*).

We previously found that cytosolic PLCβ1 binds to C3PO, the promoter of RNA-induced silencing, and showed that this binding can reverse the RNA-induced silencing of specific genes (*14, 15*). The association between these two proteins occurs in the same region through which Gα$_q$ binds to PLCβ1 and is upstream of the active site. Thus, although the catalytic activity of PLCβ1 is not affected by the binding of C3PO, its ability to be activated by Gα$_q$ is eliminated. Subsequent studies showed that the association between PLCβ1 and C3PO is critical for PC12 cell

differentiation (*16, 17*); however, little or no association is seen in nondifferentiating cells, leading to the question of whether cytosolic PLCβ1 has other binding partners. We also found that PLCβ1 binds to and inhibits a neuronal-specific enzyme required for cellular proliferation, CDK16 (*18, 19*), and that this association enables cells to cease proliferation and transition into a differentiated state (*17*). Again, this association is confined to a specific event that drives neuronal cells out of stemness, and suggests that under nonproliferating, nondifferentiating conditions, cytosolic PLCβ1 serves some other function. Here, we showed that a major population of cytosolic PLCβ1 was bound to stress granule–associated proteins and that this binding prevented premature stress granule formation. Removal of PLCβ1 from the cytoplasm in response to stress or by $G\alpha_q$-mediated stimulation promoted stress particle assembly. The interaction between PLCβ1 and stress granule proteins suggests a previously uncharacterized feedback mechanism between the external environment and the protein translation machinery.

3.2 MATERIALS AND METHODS

3.2.1 Cell Culture

Rat phenochromocytoma (PC12) and rat aortic smooth muscle (A10) cells were obtained from ATCC. Wistar-Kyoto rat 3M22 (WKO-3M22) cells, originally obtained from ATCC, were a generous gift from M. Rolle (Department. of Biomedical Engineering, Worcester Polytechnic Institute). PC12 cells were cultured in high-glucose DMEM (GIBCO) with 10% heat-inactivated horse serum (GIBCO) and 5% fetal bovine serum (FBS, Atlanta Biologicals). A10 cell lines were cultured in high-glucose DMEM with 10% FBS and 1% sodium pyruvate. WKY-3M22 cell lines were cultured in high-glucose DMEM (Corning) without L-glutamine with 10% FBS, 1% sodium pyruvate, 1% non-essential amino acids (VWR), and 1% L-glutamine (VWR). All cells were incubated at 37°C in 5% CO_2. Cells were synchronized in the G2/M phase as described previously (*17*). Briefly, 2 mM thymidine was added to the cells for 24 hours, after which the medium was removed and replaced by fresh complete culture medium for 8 hours, which was followed by the addition of nocodazole (40 ng/ml).

3.2.2 Plasmids

The EGFP-hArgonaute-2 (eGFP-Ago2) plasmid was purchased from (Addgene plasmid # 21981) and was prepared in the laboratory of Philip Sharp (MIT). The mCherry-Ago2 plasmid was a gift

from Alissa Weaver (Vanderbilt University). EGFP-G3BP1 was purchased from Addgene (plasmid # 119950) and was prepared in the laboratory of Jeffrey Chao (Friedrich Miescher Institute). The mCherry-TRAX-C1 plasmid was constructed by inserting the cDNA encoding *TRAX* between the Bam HI and Eco RI restriction sites in the mCherry-C1 backbone with T4 DNA ligase (NEB). Cell transfections with plasmids and siRNAs were performed with Lipofectamine 3000 (Invitrogen) in antibiotic-free medium. The culture medium was changed to one containing antibiotic (1% Penicillin/Streptomycin) 12 to 18 hours after transfection. For every FLIM experiment, two separate samples were prepared: donor alone and donor in the presence of acceptor.

3.2.3 Co-immunoprecipitations

PC12 cells were lysed in buffer containing 1% Triton X-100, 0.1% SDS, 1x protease inhibitor cocktail, and 10 mM Tris (pH 7.4), after which 200 μg of soluble protein was incubated with 2 μl of anti-PLCβ1 or anti-Ago2 antibody overnight at 4°C. After the addition of 20 mg of protein A-Sepharose 4B beads (Invitrogen), the mixture was gently rotated for 4 hours at 4°C. Beads were washed three times with lysis buffer, and bound proteins were eluted with sample buffer for 5 min at 95°C. Precipitated proteins were loaded onto two 10% polyacrylamide gels. After SDS-PAGE, one gel was transferred to nitrocellulose membranes and proteins were detected by Western blotting analysis with anti-PLCβ1 (D-8, Santa Cruz) and anti-Ago2 (Abcam ab32381 Lot# GR3195666-1) antibodies.

3.2.4 Application of stress conditions

For hypo-osmotic stress conditions, the culture medium was diluted with 50% water for 5 min before it was removed and replaced with Hanks' Balanced Salt Solution (HBSS) for imaging. For the arsenite treatment, a stock solution of 100 mM arsenite in water was prepared. Cells were exposed to a final concentration of 0.5 mM arsenite for 10 min before the medium was removed and replaced by HBSS for imaging. For heat shock conditions, cells were incubated at 40°C for 1 hour, whereas for cold-shock, cells were incubated at 12°C for 1 hour. For the oxidative stress treatment, a stock solution of 1 M $CoCl_2$ was prepared, and the cells were exposed to a final concentration of 1 mM $CoCl_2$ for 12 to 16 hours (overnight) at 37°C before the medium was

removed. Treatment of both PC12 cells and WKO-3M22 cells with puromycin (20 µg/l) was performed for 30 min at 37ºC.

3.2.5 FRET studies between purified PLCβ1 and eIF5A

PLCβ1 was purified by over-expression in HEK293 cells as previously described (*29*). Purification of eIF5A was performed as described previously (*27*). Purified eIF5A in a pET28-mhl vector was expressed in bacteria (Rosetta 2 DE3 plysS) by inoculating 100 ml of an overnight culture grown in Luria-Bertani medium into 2 L of Terrific Broth medium in the presence of kanamycin (50 µg/ml) and chloramphenicol (25 µg/ml) at 37°C. When the culture reached an optical density at 600 nm (OD 600) of ~3.0, the temperature of the medium was reduced to 15°C and the culture was treated with 0.5 mM IPTG to induce protein production. The cells were allowed to grow overnight before they were harvested and stored at -80°C. Frozen cells from 1.8 L of TB culture were thawed, resuspended in 150 ml of lysis buffer [20 mM HEPES (pH 7.5), 300 mM NaCl, 5% glycerol, 2 mM β-mercaptoethanol (BME), 5 mM imidazole, 0.5% CHAPS, protease inhibitor cocktail, and 5 µl of DNAase), and lysed with a panda homogenizer. The lysate was centrifuged at 30,000*g* for 45 min, added to a cobalt column in binding buffer [20 mM HEPES (pH 7.5), 300 mM NaCl, 5% glycerol, 2 mM BME, 5 mM imidazole], and equilibrated in 4 x 1 mL of a 50% slurry of cobalt resin. We passed 150 ml of supernatant through each cobalt column at approximately 0.5 ml/min, washed first with 20 mM HEPES (pH 7.5), 300 mM NaCl, 5% glycerol, 2 mM BME, 30 mM imidazole, and second with 20 mM HEPES (pH 7.5), 300 mM NaCl, 5% glycerol, 2 mM BME, 75 mM imidazole, and eluted with 20 mM HEPES (pH 7.5), 300 mM NaCl, 5% glycerol, 2 mM BME, 300 mM imidazole. Protein-protein associations were assessed by FRET using sensitized emission. Briefly, PLCβ1a and eIF5A were covalently labeled on their N-termini with Alexa Fluor 488 and Alexa Fluor 594 (Invitrogen), respectively, and the increase in acceptor emission when the samples were excited at the donor wavelength in the presence of Alexa Fluor 488–PLCβ1 was measured. Studies were repeated by pre-binding catalytically inactive C3PO with Alexa Fluor 488–PLCβ1.

3.2.6 MS analysis

MS measurements were performed at the University of Massachusetts Medical School as previously described (*66*). Cytosolic fractions were isolated from cells, and proteins that bound to

monoclonal anti-PLCβ1a antibody (Santa Cruz, D-8) were separated by electrophoresis. Protein bands were isolated by cutting the gels into 1x1-mm pieces, which were placed in 1.5-ml eppendorf tubes with 1 ml of water for 30 min. The water was removed, and 200 µl of 250 mM ammonium bicarbonate were added. Disulfide bonds were reduced by incubation with DTT at 50°C for 30 min, which was followed by the addition of 20 µl of 100 mM iodoacetamide for 30 min at room temperature. The gel slices were washed twice with 1-ml water aliquots. The water was then removed, 1 ml of 50:50 50 mM ammonium bicarbonate:acetonitrile was placed in each tube, and the samples were incubated at room temperature for 1 hour. The solution was then removed and 200 µl of acetonitrile was added to each tube, at which point the gel slices turned white and became opaque. The acetonitrile was removed, and the gel slices were further dried in a Speed Vac (Savant Instruments, Inc.). Gel slices were rehydrated in 100 µl of sequencing-grade trypsin (4 ng/µl, Sigma) in 0.01% ProteaseMAX Surfactant (Promega): 50 mM ammonium bicarbonate. Additional bicarbonate buffer was added to ensure complete submersion of the gel slices. Samples were incubated at 37°C for 18 hours. The supernatant of each sample was then removed and placed into a separate 1.5-ml eppendorf tube. Gel slices were further extracted with 200 µl of 80:20 acetonitrile:1% formic acid. The extracts were combined with the supernatants of each sample. The samples were then completely dried down in a Speed Vac. Tryptic peptide digests were reconstituted in 25 µl of 5% acetonitrile containing 0.1% (v/v) trifluoroacetic acid and separated on a NanoAcquity (Waters) UPLC. Briefly, a 2.5-µl injection was loaded in 5% acetonitrile containing 0.1% formic acid at 4.0 µl/min for 4.0 min onto a 100-µm inner diameter (I.D.) fused-silica pre-column packed with 2 cm of 5-µm (200 Å) Magic C18AQ (Bruker-Michrom) and eluted with a gradient at 300 nl/min onto a 75-µm I.D. analytical column packed with 25 cm^3 of 3-µm (100 Å) Magic C18AQ particles to a gravity-pulled tip. The solvents used were solvent A [water (0.1% formic acid)] and solvent B [acetonitrile (0.1% formic acid)]. A linear gradient was developed from 5% solvent A to 35% solvent B in 90 min. Ions were introduced by positive electrospray ionization through a liquid junction into a Q Exactive hybrid mass spectrometer (Thermo). Mass spectra were acquired over m/z 300 to 1750 at 70,000 resolution (m/z 200) and data-dependent acquisition selected the top 10 most abundant precursor ions for tandem mass spectrometry by HCD fragmentation using an isolation width of 1.6 Da, a collision energy of 27, and a resolution of 17,500. Raw data files were peak-processed with Proteome Discoverer software (version 2.1, Thermo) before undergoing database searching with Mascot Server (version 2.5)

against the Uniprot_Rat database. Search parameters included trypsin specificity with two missed cleavages or no enzymatic specificity. The variable modifications of oxidized methionine, pyroglutamic acid for N-terminal glutamine, phosphorylation of serine and threonine, N-terminal acetylation of the protein, and a fixed modification for carbamidomethyl cysteine were considered. The mass tolerances were 10 ppm for the precursor and 0.05 Da for the fragments. Search results were then loaded into the Scaffold Viewer (Proteome Software, Inc.) for peptide/protein validation and label-free quantitation. These data were analyzed using percentage of total spectra in Scaffold4 software before plotting with Sigma Plot 14.

3.2.7 N&B measurements

N&B theory and measurement were fully described previously (*36*). Experimentally, we collected ~100 cell images in which we viewed either free eGFP (control) or eGFP-Ago2 at a 66 nm/pixel resolution and at a rate of 4 µs/pixel. Regions of interest (256x256 box) were analyzed from a 320x320 pixel image. Offset and noise were determined from the histograms of the dark counts performed every two measurements. N&B data were analyzed with SimFC software (www.lfd.uci.edu).

3.2.8 N&B analysis

N&B defines the number of photons associated with a diffusing species by analyzing the variation of the fluorescence intensity in each pixel in the cell image. In this analysis, the apparent brightness, B, in each pixel is defined as the ratio of the variance, σ, over the average fluorescence intensity <k>:

$$B = \sigma2/< k >.$$

and

$$< k > = \epsilon n$$

where n is the number of fluorophores. The determination of the variance in each pixel is obtained by rescanning the cell image ~100 times as described earlier. The average fluorescence intensity, <k>, is directly related to the molecular brightness, ε, in units of photons per second per molecule, and n. B can also be expressed as:

$$B = \epsilon + 1$$

The apparent number of molecules, N, is defined as:

$$N = \epsilon n / (\epsilon + 1)$$

3.2.9 Fluorescence lifetime imaging measurements (FLIM)

FLIM measurements were performed on the dual-channel confocal fast FLIM (Alba version 5, ISS Inc.) equipped with photomultipliers and a Nikon Eclipse Ti-U inverted microscope. A 60× Plan Apo (1.2 NA, water immersion) objective and a mode-locked, two-photon titanium-sapphire laser (Tsunami; Spectra-Physics) were used in this study. The lifetime of the laser was calibrated each time before experiments by measuring the lifetime of Atto 435 in water with a lifetime of 3.61 ns (Ref) at 80, 160, and 240 MHz. The samples were excited at 800/850 nm, and emission spectra were collected through a 525/50 bandpass filter. For each measurement, the data were acquired until the photon count was >300. Fluorescence lifetimes were calculated by allowing $\omega = 80$ MHz:

$$\tau = \frac{S}{G * 2\pi * \omega}$$

3.2.10 Statistical analysis

Data were analyzed with the Sigma Plot 13 statistical packages, which included the student's *t* test and one-way analysis of variance (ANOVA).

3.2.11 Dynamic light scattering (DLS)

DLS measurements were performed on a Malvern Panalytical Zetasizer Nano ZS instrument. For these experiments, mRNA from PC12 cells was extracted with the Qiagen Mini Kit (Cat #: 74104) according to the manufacturer's instructions. Before the mRNA was extracted, the cells were exposed to stress, treated with siRNA(PLCβ1a), or transfected with plasmid expressing constitutively active $G\alpha_q$RC (*67*). For these measurements, approximately 50 μl of extracted mRNA in RNase-free water was added in a Hellma Fluorescence Quartz Cuvette (QS-3.00mm).

Each sample was run three times for 10 min per run. Control samples were repeated six times, the PLCβ knockdown sample twice, and the $G\alpha_q$ over-expression sample once.

3.2.12 Particle analysis

Samples were imaged with a 100X/1.49 oil TIRF objective to microscopically count the number of particles per μm^2 formed under different conditions. For each condition, 10 to 20 cells were randomly selected, and z-stack measurements were taken (1.0 µm/frame). Analysis was performed with ImageJ and Fiji ImageJ software in two ways. First, each measurement was thresholded before analyzing, and the number of particles per frame per measurement was averaged. Second, all z-stack measurements were combined to generate a 3D image for each sample before analyzing the number of particles per sample and averaging the results. Both methods produced identical results.

3.2.13 Microinjection studies

Microinjection of a solution of 100 nM eIF5A into PC12 cells was performed with an Eppendorf Femtojet Microinjector mounted on Nikon Eclipse Ti-U inverted confocal microscope under 0.35 PSI pressure and 0.5 s per injection.

3.2.14 Immunofluorescence

Cells were fixed with 3.7% formaldehyde, permeabilized with 0.1% triton X-100 in PBS, and then blocked with 10% goat serum, 5% BSA, 50 mM glycine in PBS. Cells were then stained with the appropriate primary antibodies (Abcam), incubated for 1 hour, washed, and treated with a secondary antibody for 1 hour. After another wash, the cells were viewed on a Zeiss Meta 510 laser confocal microscope. Data were analyzed with Zeiss LSM software and Image J. The secondary antibodies used were Alexa Fluor 488–conjugated anti-rabbit antibody for Ago-2 and Alexa Fluor 647–conjugated anti-mouse antibody for PABPC1.

3.2.15 Ca^{2+} signal imaging

Single-cell Ca^{2+} measurements were performed by labeling the cells with Calcium Green (Thermofisher), incubating the cells in HBSS for 45 min, and then washing the cells twice with HBSS. The release of intracellular Ca^{2+} in live PC12 cells was initiated by the addition of 2 µM

carbachol before imaging the time series on a Zeiss LSM 510 confocal microscope with excitation at 488 nm using the time series mode as previously described (*68*).

3.2.16 Western blotting analysis

Samples were placed in 6-well plates and collected in 250 μl of lysis buffer, which included NP-40 and protease inhibitors as mentioned earlier. Sample buffer was added at 20% of the total volume. After SDS-PAGE electrophoresis, proteins were transferred to nitrocellulose membranes (Bio-Rad). The primary antibodies used included: anti-PLCβ1 (Santa Cruz sc-5291), anti-Ago2 (abcam ab32381), anti-PABPC1 (Santa Cruz sc-32318), anti-G3BP1 (Santa Cruz sc-81940), anti-actin (abcam ab8226), anti-HSP90 (Santa Cruz sc-69703), anti-eGFP (Santa Cruz sc-8334) and siRNA PLCβ1 (Ambion 4390771). Membranes were treated with antibodies diluted 1:1000 in 0.5% milk and washed three times for 5 min each before applying the appropriate secondary antibody (anti-mouse or anti-rabbit, Santa Cruz) at a 1:2000 dilution. Membranes were washed three times for 10 min each before being imaged on a BioRad chemi-doc imager to determine the relative band intensities. Band intensities were measured at several sensitivities and exposure times to ensure that the intensities were in a linear range. Data were analyzed with ImageJ software.

3.3 RESULTS

3.3.1 PLCβ1 binds to stress granule–associated proteins

We began this work by performing experiments to determine previously uncharacterized binding partners of cytosolic PLCβ1 in PC12 cells under nondifferentiating conditions. Our approach was to isolate the cytosolic fractions of unsynchronized, undifferentiated PC12 cells and use a monoclonal antibody to pull down proteins bound to PLCβ1. We collected the PLCβ1-bound proteins and identified them by mass spectrometry (MS) analysis. Unexpectedly, we found that ~30% of the total proteins associated with cytosolic PLCβ1 were markers for stress granules (table S3.1) (*1, 20*), and we determined the percentage of their contribution to the total intensity (Fig. 3.3.1 A). In contrast, control studies with cytosolic fractions of cells with reduced amounts of PLCβ1 identified nonspecific proteins, such as tubulin, actin, and mitochondrial proteins (table S3.2).
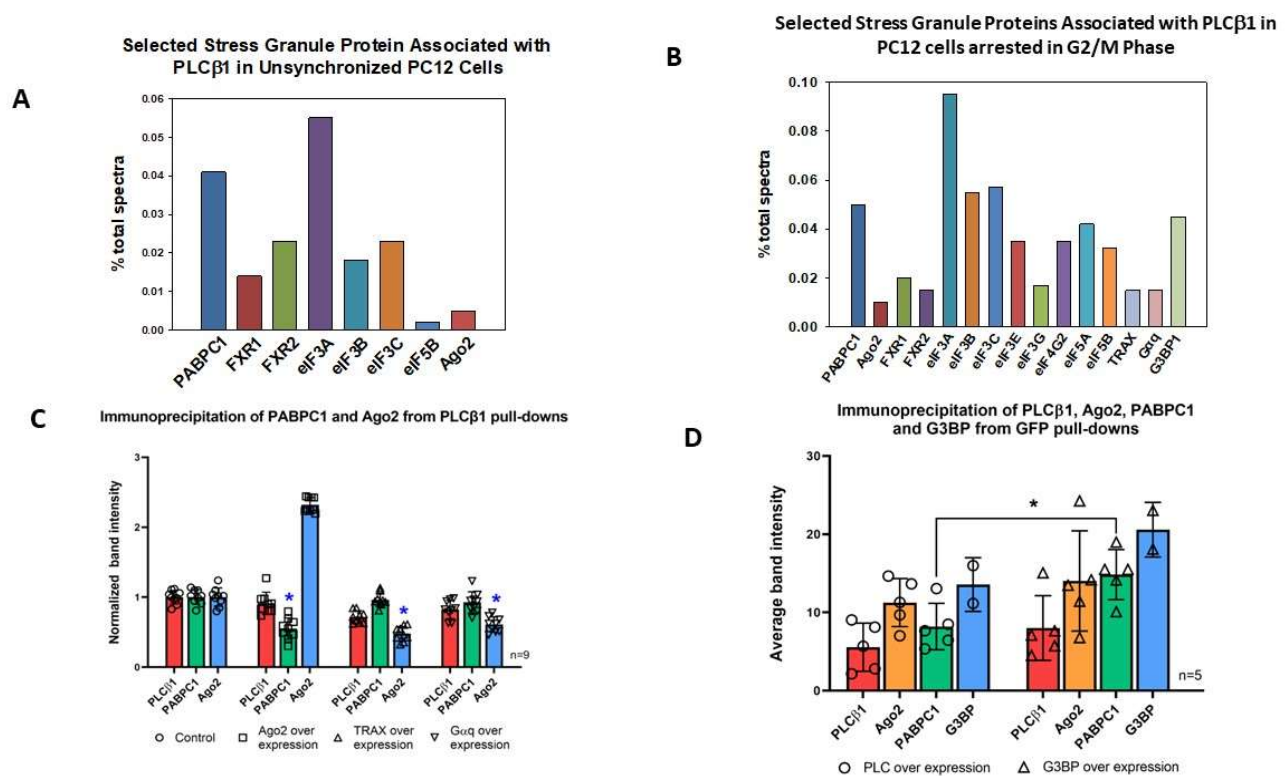
Figure 3.1: Major binding partners of PLCβ1 in PC12 cells. (A and B) Proteins associated with PLCβ1 were pulled down with a monoclonal antibody from the cytosolic fractions of unsynchronized PC12 cells primarily in the G1 phase (A) or PC12 cells arrested in the G2/M phase (B) and then subjected to MS analysis. The relative amounts of the indicated proteins were calcuated as described in Materials and Methods. All of the proteins identified in (A), except for eIF5B, were also found in an identical experiment in which proteins associated with Ago2 were pulled down (table S4). Proteins that were found to be phosphorylated included (A) FXR2 and (B) eIF3A, eIF3B, and eIF3C. Data were gathered from a single set of MS measurements and key features were validated biochemically as described in the text. (C and D) The cytsolic fractions of undifferentiated PC12 cells that were untransfected (control) or were transfected to overexpress Ago2, TRAX, or constitutively active Gαq were incubated with a monoclonal anti-PLCβ1 antibody to pull down PLCβ1-associated proteins. The pull-down samples (10 □g) were then analzyed by Western blotting with antibodies against PLC□1, PABC1, and Ago2, as indicated in the representative blots (fig.S1), and a compilation of the relative intensties of the bands of interest was determined by densitometry (see Materials and Methods). Data are means ± SD of eight

experiments. *P < 0.001. The relative amounts of C3PO and Gαq that were pulled down with PLCβ1 were not significantly different from that of PABPC1: P = 0.81 and P = 0.54, respectively. (D) A similar study to that described in (C) was performed with a monoclonal anti-GFP antibody to isolate either eGFP-PLCβ1 or eGFP-G3BP1 and their associated proteins from whole transfected PC12 cells. The relative amounts of the indicated proteins that were pulled down were determined by densitometry. Data are means ± SD of five experiments for PLCβ1, PABPC1, and Ago2 and of two experiments for G3BP1. Full-sized Western blots for representative samples can be see in fig. S3.1.

These studies (Fig. 3.1 A) were performed with unsynchronized cells where ~90% were in the G1 phase (17). However, our previous studies suggested that PLCβ1 may change binding partners as cells move through the cell cycle (21). Additionally, PLCβ1 has a nuclear population that may exchange with the cytosolic one (22). Therefore, we repeated the studies in cells in which the nuclear population of PLCβ1 was also available for binding by arresting cells in the G2/M phase, during which the nuclear matrix has broken down (Fig. 3.1B and table S3.3). Again, we found that 32% of the proteins bound to PLCβ1 were markers for stress granules, with the most prominent being eukaryotic initiation factor 5A (eIF5A) and polyadenylate binding protein C1 (PABPC1) (Fig. 3.1B). Additionally, other stress granule and translation proteins appeared in both groups, including FXR1/2, G3BP1, and other eIF proteins. Note that Ago2, which is associated with both RISCs and stress granules (8), appeared in these cells.

The proteomics studies described earlier are only indicative of potential protein partners of PLCβ1, because the candidates were identified under nonphysiological conditions. Therefore, we verified the binding of PLCβ1 to stress granule proteins through several other methods. First, we again performed pull-down experiments with the same monoclonal antibody that we used earlier, and we detected the association of two stress granule proteins by Western blotting analysis. The first, PABPC1, is an established marker for stress granules (20). The second, Ago2, moves into granules under stress conditions (8). Using unsynchronized, undifferentiated PC12 cells, we verified that PABPC1 and Ago2 bound to PLCβ1 (Fig. 3.1, C and D). We then determined whether the amounts of these proteins changed when two of the established binding partners of PLCβ1, Gα$_q$ and C3PO, were over-expressed (Fig. 3.1 C, fig. S3.1, A and B, and fig. S3.2 A and B). We found that the

amount of Ago2 that bound to PLCβ1 was reduced when that of either of the binding partners was increased, suggesting that Ago2 bound to similar regions of PLCβ1. However, the amount of PABPC1 that was pulled down with PLCβ1 did not significantly change with over-expression of either Gα$_q$ or C3PO ($P = 0.81$ and $P = 0.54$, respectively) and was reduced when Ago2 was over-expressed. The simplest interpretation of these data is that the interaction between PLCβ1 and PABPC1 differs from that between PLCβ1 and Ago2, and that the reduction in PABPC1 abundance in cells overexpressing Ago2 may be due to a redistribution of the PLCβ1 pool.

We wanted to verify that similar results could be obtained from experiments in which a different PLCβ1 antibody was used. Noting that PLCβ1 differs from other PLCβ family members mainly in the long 400 amino acid C-terminal domain to which Gα$_q$ and C3PO bind, and where some stress granule proteins may bind, we repeated the pull-down experiments under conditions in which antibody binding to its epitope in PLCβ1 would not occlude any potential binding partners. Specifically, we transfected undifferentiated, unsynchronized PC12 cells with a plasmid expressing eGFP-PLCβ1 where the eGFP tag is tethered to the N terminus of PLCβ1 and performed the pull-down experiments with anti-eGFP antibody. The results (Fig. 3.1C and D and fig. S3.3) showed associations between PLCβ1 and PABPC1, Ago2, and G3BP1. Together, these data support the idea that cytosolic PLCβ1 interacts with stress granule-associated proteins.

3.3.2 PLCβ1 associates with Ago2 but not G3BP1 in live cells

Our earlier studies suggested that the interaction between PLCβ1 and Ago2 might be modulated by G protein stimulation and cellular events associated with C3PO. Keeping in mind that C3PO promotes RNA-induced silencing, we set out to characterize the factors that regulated the PLCβ1-Ago2 association. We first isolated the cytosolic fractions of unsynchronized, undifferentiated PC12 cells, pulled down proteins associated with Ago2, and identified them by MS. We found that PLCβ1 was included in the data set (table S3.4). Note that all of the proteins that were associated with PLCβ1 (Fig. 3.1 A) were also pulled down with Ago2 (table S3.4).

We measured the extent of the association between PLCβ1 and Ago2 in live PC12 cells by Förster resonance energy transfer (FRET) as monitored by fluorescence lifetime imaging microscopy (FLIM). In this method, FRET efficiency is determined by the reduction in the time that the donor

spends in the excited state, or the fluorescence lifetime, before transferring energy to an acceptor fluorophore (*23*). If the donor molecule is excited with light that has a modulated intensity, the lifetime can be determined by the reduction in modulated intensity (M) as well as the shift in phase (φ) of the emitted light. If FRET occurs when the donor is in the excited state, the fluorescence lifetime will be reduced as indicated by a reduced change in modulation and phase shift. The amount of FRET can then be directly determined from the raw data by plotting the lifetimes in each pixel in the image on a phasor plot [S versus G, where S = M*sin (φ) and G = M*cos (φ)] (*24*). In these plots, the lifetimes in each pixel in a FLIM image will fall on the phasor arc for a single population. However, when two or more lifetimes are present, the points will be a linear combination of the fractions, with the points inside the phase arc that move towards the right due to shortened lifetimes such as when FRET occurs. Note that phasor representation is simply the Fourier transform of the lifetime decay curves but readily displays lifetimes directly from raw data without the need for model-dependent fitting of the lifetimes or other corrections.
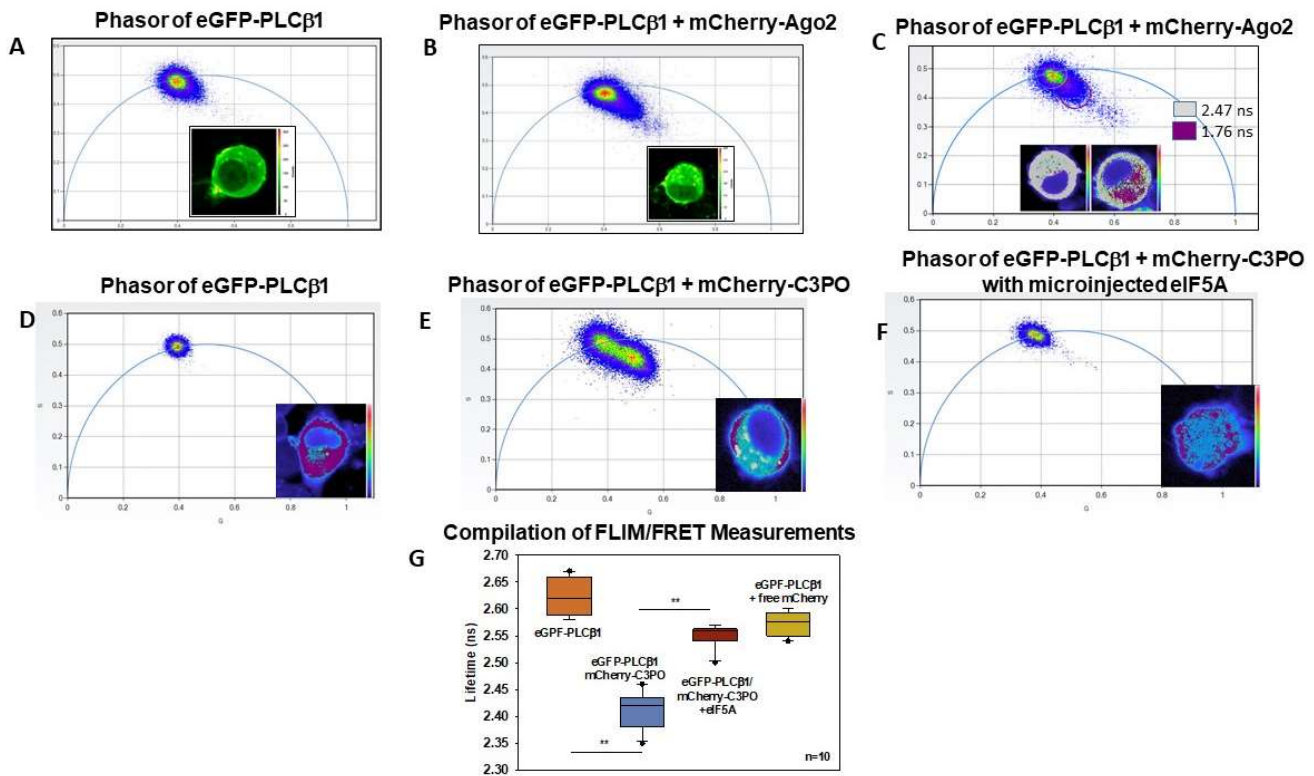
Figure 3.2: Binding of PLCβ1 to Ago2 and eIF5A in PC12 cells. (A to C) Representative phasor plots from transfected PC12 cells expressing (A) eGFP-PLCβ1 alone or (B) eGFP-PLCβ1 and

mCherry-Ago2. The raw lifetimes are plotted in polar coordinates, as indicated from the phase and modulated fluorescence lifetimes (see Results). Each point in the phasor plots corresponds to the lifetime of the eGFP-PLCβ1 emission measured in each pixel from the corresponding cell image shown in the graph. Images are representative of five to eight cells from three independent experiments. (C) A phasor diagram in which the non-FRET and FRET points are selected and the pixels are shown in the cell images. Note that no significant FRET was detected in control studies of eGFP-C3PO and mCherry-Ago2 (fig. S3.2). (D) Example of a phasor plot and the corresponding image from a FLIM measurement of eGFP-PLCβ1 expressed in a PC12 cell. The heat map indicates eGFP signal intensity. (E) A similar study to that described in (B) except that PC12 cells were cotransfected with plasmids expressing eGFP-PLCβ1 and mCherry-C3PO (TRAX). Purple dots indicate pixels represented in the phasor plot. (F) A similar study to that described in (E) except that this cell was microinjected with purifed, unlabeled eIF5A. (G) Compilation of eGFP-PLCβ1 lifetime results from two independent studies with n = 10 cells for each study and in which free mCherry was used as a negative control. Comparison of data before and after eIF5A microinjection was statistically significant: **P < 0.001.

Thus, we generated the phasor plot and the corresponding image of a PC12 cell expressing eGFP-PLCβ1 presenting the phase and modulation lifetime of each pixel in the image (Fig. 3.2, A to C). As expected for a single lifetime species, all points fell on the phasor arc (Fig. 3.2 A). When we repeated this experiment with cells expressing both eGFP-PLCβ1 and mCherry-Ago2, where mCherry is a FRET acceptor, the average donor lifetime was reduced from 2.5 to 1.7 ns and the points moved inside the phasor (Fig. 3.2 B). This reduction in lifetime and movement of the points into the phasor showed the occurrence of FRET between the probes. Because the amount of FRET depends on the distance between the fluorophores to the sixth power and given that the distance at which 50% transfers for the eGFP-mCherry pair is ~30 Å (25), our results suggest a direct interaction between PLCβ1 and Ago2 in the cytosol. We could select points in the phasor plots and visualize their localization in the cell image. We found that the points corresponding to FRET, and thus eGFP-PLCβ1:mCherry-Ago2 complexes, were localized in the cytoplasm (Fig. 3.2C). In contrast, points corresponding to eGFP-PLCβ1 alone were found both on the plasma membrane and in the cytoplasm. Additionally, we tested the extent of the association between eGFP-PLCβ1 and eGFP-G3BP1 using homo-FRET or FRET between identical species. No changes in lifetime,

and thus no FRET, were detected (fig. S3.2). This absence of FRET indicates that the two fluorophores were separated by more than ~45 Å, which suggests that any association between the two proteins is indirect.

3.3.3 eIF5A binds to PLCβ1 competitively with C3PO and Gαq

To remain cytosolic, stress granule proteins would need to bind to PLCβ1 in a manner competitive with $G\alpha_q$ or it would localize to the plasma membrane. We previously showed that PLCβ1 binds to C3PO through the same C-terminal region with which it binds to $G\alpha_q$ (15), and that competition between C3PO and $G\alpha_q$ regulates the ability of PLCβ1 to generate Ca^{2+} signals through $G\alpha_q$ activation or the ability of siRNAs to promote silencing, respectively (26). With this in mind, we searched the proteins identified in our MS analysis for stress granule proteins that could sequester PLCβ1 from $G\alpha_q$. We noted that eIF5A, which is a GTP-activating protein (27), has homologous regions to the GTPase region of $G\alpha_q$ and appeared in our MS screen as a PLCβ1-binding protein, so we chose it for further testing.

In an initial study, we purified PLCβ1 and covalently labeled it with a FRET donor, Alexa Fluor 488. We then purified eIF5A, labeled it with the FRET acceptor Alexa Fluor 594, and measured the association between the two proteins in solution by fluorescence titrations similarly to previous studies (28). We found that the two proteins bound to each other with strong affinity ($K_d = 27 \pm 5$ nM). However, when we formed the Alexa488-PLCβ1-C3PO complex and titrated Alexa594-eIF5A into the solution, we could not detect FRET (fig. S3.4). This result suggests that eIF5A binds to the same region of PLCβ1 as does C3PO, and similarly, to $G\alpha_q$ (15). To determine whether eIF5A competed with C3PO for binding to PLCβ1 in cells, we transfected PC12 cells with plasmids expressing eGFP-PLCβ1 and mCherry-TRAX to produce fluorescent C3PO (29). We detected an association between the two proteins by FLIM/FRET measurements (Fig. 3.2, D and E). We then microinjected purified eIF5A into the cells to increase its intracellular concentration by ~10 nM and found that FRET was eliminated (Fig. 2F). This result suggests that eIF5A displaces C3PO from PLCβ1 and that both proteins bind to a similar region of PLCβ1 (Fig. 2G).

We confirmed our hypothesis that eIF5A binds to the C-terminal region of PLCβ1 in experiments with purified proteins in solution. In these studies, we formed the eIF5A-PLCβ1 complex,

chemically cross-linked the proteins, digested the samples, separated the fragments by electrophoresis, and sequenced the peptides by MS (fig. S3.5, table S3.5). We found several interaction sites between the two proteins, but one of the most prominent was between residues 1085 to 1095 of PLCβ1and residues 97 to 103 of eIF5A (table S3.5), which are expected to be close to the Gα$_q$ activation region. Together, these studies suggest that eIF5A competes with both Gα$_q$ and C3PO for binding to PLCβ1 and thus could direct PLCβ1 to complexes containing stress granule proteins.

3.3.4 Osmotic stress has different effects on PLCβ1 isoforms

To determine whether PLCβ1 could affect stress granule formation, we subjected cells to mild, hypo-osmotic stress (300 to 150 mOsm), which we previously showed has reversible effects on the Gα$_q$-PLCβ signaling pathway in muscle cells as seen in figure 3.3 (A-E) (*30, 31*). We first determined whether hypo-osmotic stress affected the association between PLCβ1 and stress granule proteins within 5 min before adaptive changes in the cell occurred.
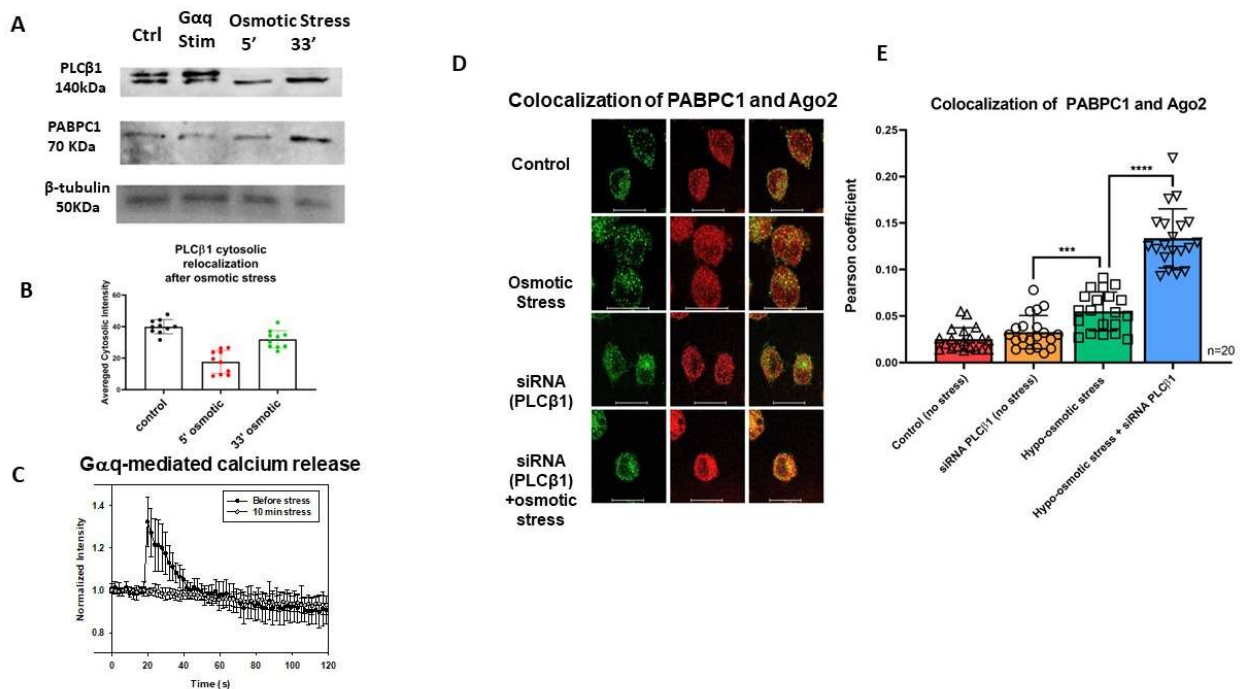
Figure 3.3: The effect of osmotic stress on cytosolic PLCβ1 in PC12 cells. (A) Representative Western blotting analysis of the cytosolic fractions of PC12 cells for PLCβ1 where PLCβ1a is the upper band of the doublet and PLCβ1b is the lower band. Cells were subjected to 10 min of

incubation with 5 µM carbachol to stimulate Gαq activity or were subjected to osmotic stress (150 mOsm) for 5 and 30 min. PABPC1 and β-tubulin bands are shown for comparison. (B) Results of a study in which undifferentiated PC12 cells transfeccted to express eGFP-PLCβ1 were subjected to osmotic stress as indicated, and changes in cytosolic fluorescence intensity in a slice in middle of the cell were quantified. Data are from nine independent experiments. Compared to control cells, those subjected to osmotic stress for 5 min had significantly different fluorescence intensity ($P < 0.001$). (C) Analysis of the change in Ca2+ release when PC12 cells labeled with Calcium Green were stimulated with 5 µM carbachol under basal conditions (300 mOsm) and hypo-osmotic stress (150 mOsm) for 10 min. Data are from n = 12 cells from three experiments and bars indicate SD. (D) Images of PC12 cells immunstained for Ago2 (green) and PABPC1 (red) under basal conditions (control), when the osmolarity was lowered from 300 to 150 mOsm (osmotic stress), and when cells that had been treated with siRNA(PLCβ1) were subjected to normal conditions or osmotic stress. Scale bars, 20 µm. (E) Compiled colocalization data showing the extent of colocalization of PABPC1 and Ago2 in cells from the experiments shown in (D). Data are from three experiments with 20 cells per experiment. ***$P = 0.002$ and **** $P < 0.001$.

Of the two major subtypes of PLCβ1 (1a and 1b), the 1a form is the best characterized and most prevalent subtype, having additional residues in its C terminus (residues 1142 to 1216) compared to the 1b isoform (32). Although both isoforms are similarly activated by Gα$_q$, some studies showed differences in their localization, although these differences appear to be cell type–specific (33-35). We found that 5 min of exposure of PC12 cells to osmotic stress caused a marked reduction in PLCβ1a abundance, whereas the amount of PLCβ1b was relatively unchanged (Fig. 3.3A). Gα$_q$ stimulation by the addition of carbachol did not affect the abundance of either isoform. Tracking the total amount of PLCβ1 with an antibody that recognizes both isoforms, we found that the cytosolic fraction of PLCβ1 was preferentially reduced by osmotic stress (Fig. 3.3B). Considering that the half-life of total PLCβ1 in PC12 cells is 20 min (17), our findings (Fig. 3, A and B) suggest that osmotic stress enhances PLCβ1a degradation. After 30 min of stress, the abundance of PLCβ1b increased compared to that in control cells, as did the amount of PABPC1, but PLCβ1a abundance remained low as the cells adapted (Fig. 3.3B). Because we could not distinguish between the 1a and 1b isoforms of PLCβ1 in most of our experiments, we will refer only to PLCβ1.

We determined the ability of hypo-osmotic stress to affect Ca^{2+} signals generated by $G\alpha_q$ in response to 1 μM carbachol. Using the fluorescent calcium indicator, Calcium Green (see Materials and Methods), we first verified that reducing the osmolarity from 300 to 150 mOsm did not affect the intracellular Ca^{2+} concentration. However, osmotic stress quenched the increase in Ca^{2+} signaling in response to activation of the $G\alpha_q$-PLCβ1 pathway (Fig. 3.3C). This loss was consistent with the reduced PLCβ1 abundance in cells under hypo-osmotic stress.

3.3.5 The abundance of cytosolic PLCβ1 affects stress granule assembly

It is possible that PLCβ1 binds to stress granule–associated proteins to prevent the premature assembly of stress particles. To test this idea, we followed stress granule formation in PC12 cells under hypo-osmotic stress by counting the number of particles that formed in undifferentiated, unsynchronized PC12 cells using a 100x objective lens under normal (300 mOsm) and hypo-osmotic (150 mOsm) conditions. Note that at this resolution, we may not have captured the formation of small particles (5), and we might have observed the assembly of primary particles, as well as the fusion of small pre-formed ones. In our experiments, we analyzed particle numbers and sizes in 1.0-μm slices though several cells and reported particle sizes in area as seen for each slice. Note also that converting the particles into three dimensions and analyzing the particles gave identical results but with reduced resolution.

We fixed PC12 cells under normal and hypo-osmotic conditions and stained them with monoclonal antibodies against the stress granule marker, PABPC1. In this analysis, we measured the size and number of particles in each slice of a confocal volume (see Materials and Methods) and plotted the additive values of these data. Thus, the highest value plotted (Fig. 3.4) corresponds to the total area of the cell occupied by stress granule particles. In control cells, PABPC1 antibody staining showed ~750 particles that were less than 25 μm^2 in area (Fig. 3.4A). When PLCβ1 abundance was reduced by siRNA, we observed an increase in PABPC1 particle size from 25 to 100 μm^2, suggesting that the loss of PLCβ1 promoted the formation of larger particles. When we applied osmotic stress to the cells, we observed an increase in the number of PABC1-containing particles between 25 and 50 μm^2 in area (Fig. 3.4B) However, osmotic stress did not change the size or number of PABC1-containing particles in cells in which PLCβ1a had been reduced, suggesting

that osmotic stress and the loss of PLCβ1 were not additive effects. In another series of experiments, we stimulated cells with carbachol to activate $G\alpha_q$ (Fig. 3.4C). We found that such stimulation induced the formation of a high number of particles of up to ~150 μm^2 in area and that reducing PLCβ1 abundance did not substantially affect either the size or number of PABPC1-containing particles. Together, these findings suggest that depletion of cytosolic PLCβ1, through siRNA treatment, osmotic stress, or recruitment to activated $G\alpha_q$, promoted the incorporation of PABPC1 into larger aggregates. We then used immunofluorescence analysis to test the effect of PLCβ1 on the size and number of particles associated with Ago2. For Ago2, the number of smaller particles substantially increased when PLCβ1 abundance was reduced (Fig. 3.4D). Unlike PABPC1-associated particles, the size and number of Ago2-associated particles were not affected by osmotic stress, although an increase in the number of small particles was still seen when PLCβ1 abundance was reduced (Fig. 3.4E). Additionally, carbachol-dependent stimulation of $G\alpha_q$ resulted in an increase in the number of Ago2-containing small particles (Fig. 3.4F).
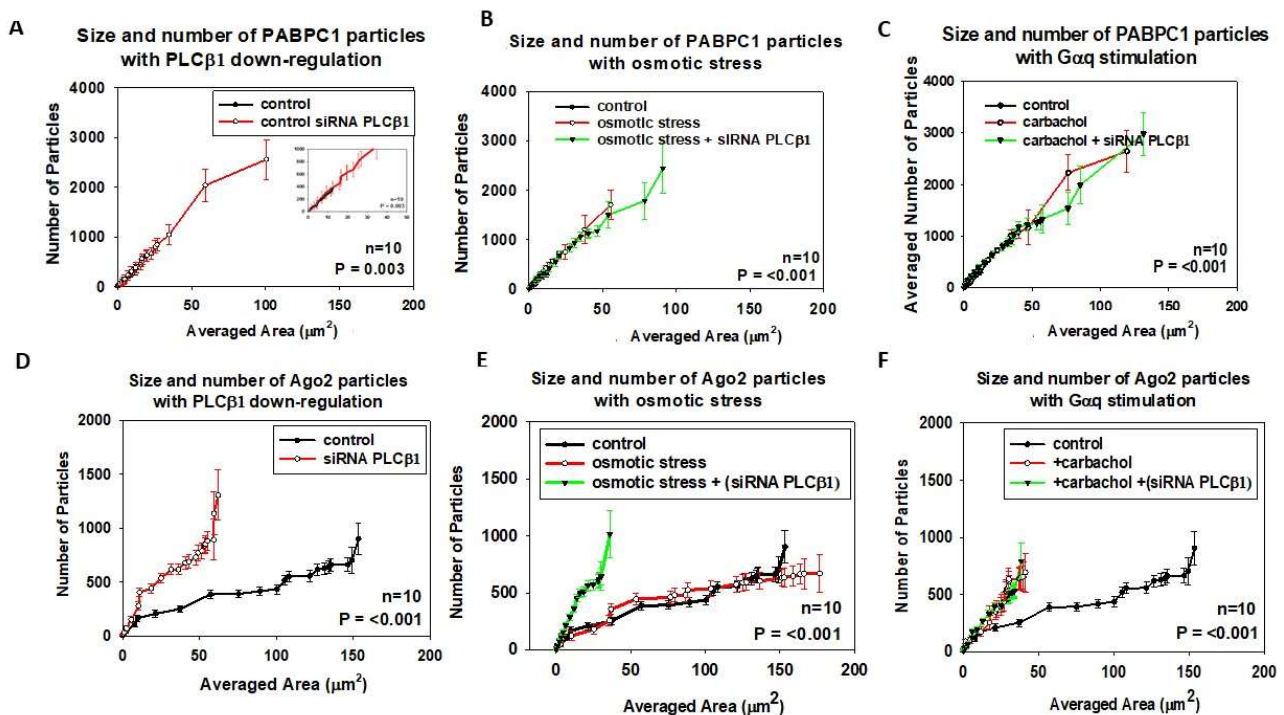
Figure 3.4: The effect of PLCβ1 on the formation of PABPC1- and Ago2-associated particles in PC12 cells. (A to C) The sizes and numbers of particles associated with monoclonal anti-PABPC1 in the cytosol of fixed and immunostained PC12 cells were measured with a 100x

objective and analyzed by Image J software (see Materials and Methods). (A) Treatment of cells with siRNA(PLCβ1) relative to mock-transfected controls. Inset: An enlarged version of the plot is shown to enable better comparison. (B) Analysis of the effect of osmotic stress (150 mOsm, 5 min) on the size and number of PABPC1-associated particles in control PC12 cells and in PC12 cells treated with siRNA(PLCβ1). (C) Analysis of the effect of Gαq stimulation by treatment with 5 µM carbachol on the size and number of PABPC1-associated particles in control PC12 cells and in PC12 cells treated with siRNA(PLCβ1). (D to F) Size and number of Ago2-associated particles as determined by immunofluorescence analysis with a monoclonal antibody of for cells that were treated with siRNA(PLCβ1) and compared to control cells (D). Control cells subjected to 5 min of osmotic stress (150 mOsm) were compared to cells treated with siRNA(PLCβ1) under osmotic stress (E). Control cells treated with 5 µM carbachol to stimulate Gαq were compared to cells treated siRNA(PLCβ1) and stimulated with 5 µM carbachol (F). Data are an average of three independent experiments that each sampled 10 cells. Error bars represent SD. The P values compare control conditions to the specific condition and were determined by ANOVA.

The experiments described earlier were performed with fixed, stained cells. We also followed particle formation in live PC12 cells transfected with plasmids expressing mCherry-Ago2 or eGFP-G3BP1. Although the number and areas of the particles varied somewhat with the extent of transfection, the results showed the same trend as those from the immunostained samples (fig. S3.6, A and B), that $G\alpha_q$ stimulation or osmotic stress increased the number of Ago2-associated smaller particles. These studies suggest that reduction of cellular PLCβ1 abundance increases the number of particles of proteins associated with stress granules. Whereas the increase in particle assemblies could be due to the loss of cellular PLCβ1, it may also be due to the removal of PLCβ1 from pre-formed particles. To address this question, we transfected PC12 cells with plasmid expressing eGFP-PLCβ1 and analyzed their particles (fig. S3.6C). We could not detect many particles less than 400 $µm^2$ in area, beyond which, the number the number of particles increased to ~1000. No substantial differences were found in cells subjected to osmotic stress. These data suggest that PLCβ1 does not associate with large particles in the cell.

The differences in the size and number of PABPC1- versus Ago2- or G3BP1-containing particles suggest that they might partition into different types of granules. We tested this idea by monitoring

the effect of both PLCβ1 and osmotic stress on the colocalization between Ago2 and PABPC1 (Fig. 3.3, D and E). Under normal osmolarity, we found little colocalization between the proteins in cells either with endogenous amounts of PLCβ1 or in cells in which PLCβ1 was knocked down. However, when the cells were subjected to osmotic stress, colocalization between Ago2 and PABPC1 increased, and this increase was greater in cells in which PLCβ1 was knocked down. These results suggest that PABPC1 and Ago2 form distinct particles that may begin to fuse or associate under high stress conditions, such as loss of cytosolic PLCβ1 or osmotic stress.

3.3.6 Assembly of Ago2- and G3BP1-containing aggregates depends on the type of environmental stress

It is probable that osmotic stress produces granules that are different in size, number, and composition than those produced by other stresses. We compared the formation of Ago2- and G3BP1-containing particles under different types of stress by Number & Brightness (N&B) analysis (see Materials and Methods). This method measures the number of fluorescent molecules associated with a diffusing particle in live cells (*36*). Thus, N&B measurements of cells expressing eGFP-Ago2 would indicate the conditions that promote the formation of aggregates.

We followed Ago2 aggregation in PC12 cells subjected to various stress conditions (Fig. 3.5 A to C). Subjecting cells to osmotic stress shifted the distribution of eGFP-Ago2 particles to the point where ~60% of the eGFP-Ago2 were significantly larger than monomers (Fig. 3.5B). Note that these Ago2-containing particles formed throughout the cytoplasm, and that only 75 to 80% of the cells showed aggregation. We compared the aggregation of eGFP-Ago2 in cells subjected to other stresses: cold shock (12°C for 1 hour), heat shock (40°C for 1 hour), treatment with 0.5 mM arsenite for 10 min (fig. S3.8 A to C), and oxidative stress (1 mM $CoCl_2$ for 8 hours; fig. S3.8D). Unlike osmotic stress, these other stresses produced changes in all of the cells observed; however, eGFP-Ago2 aggregates were seen as a few large particles rather than being evenly distributed through the cell. In a final series of experiments, we stimulated cells under normal conditions with carbachol to activate $G\alpha_q$ and promote the relocalization of cytosolic PLCβ1 to the plasma membrane (Fig. 3.5C). Unlike for the other stresses, we observed the formation of small eGFP-Ago2 aggregates distributed throughout the cytosol. This behavior was seen in every cell tested. These data suggest that different stresses, including $G\alpha_q$ activation, result in patterns of formation

of particles containing multiple Ago2 molecules. We also viewed the aggregation of eGFP-G3BP1 expressed in undifferentiated, unsynchronized PC12 cells (Fig. 3.5D to G). Unlike cells expressing eGFP-Ago2, PC12 cells expressing eGFP-G3BP1 showed aggregation under untreated conditions, (Fig. 3.5D), and the extent of this aggregation increased with hypo-osmotic stress (Fig. 3.5E), treatment with PLCβ1-specific siRNA, (3.5F), and carbachol treatment (Fig. 3.5G). Unlike the punctate pattern seen for eGFP-Ago2, eGFP-G3BP1 aggregates were more diffuse and occurred close to the plasma membrane, suggesting that eGFP-G3BP1 was present in a range of different stress granules.
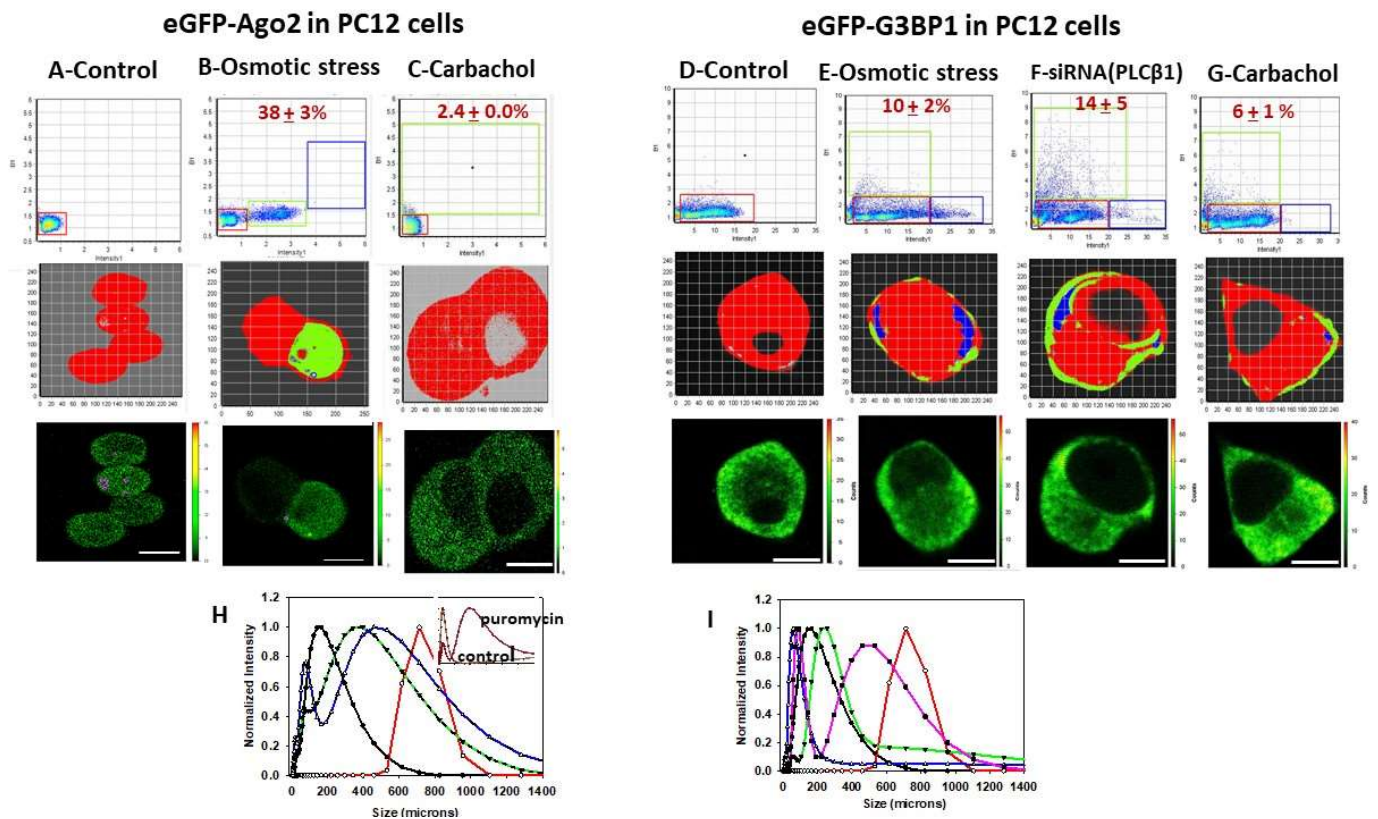
Figure 3.5: Aggregation of Ago2 and G3BP1 in PC12 cells as monitored by N&B analysis. (A to G) N&B studies of PC12 cells expressing eGFP-Ago2 (A to C) and eGFP-G3BP1 (D to G) and subjected to the indicated conditions. Top: The graphs display N&B values for each pixel where the y-axis corresponds to the brightness of the particle and the x-axis shows particle intensity. The pixels contained in the red boxes are the values found for free eGFP and correspond to monomeric eGFP-Ago2 (A to C) or eGFP-G3BP1 (D to G). Points outside the red boxes, shown in green and blue, correspond to higher-order species of Ago2 or G3BP1. Middle: Images show

the pixels corresponding to monomeic (red) and higher-order eGFP-Ago2 or eGFP-G3BP1 aggregates (green and blue) from the data shown in the graphs directly above. Bottom: Images are from fluorescence microscopy analysis with ISS software. The purple pixels denote Ago2 or G3BP1 aggregates. Data in (A) and (D) show control cells (n = 8 experiments); data in (B) and (E) show cells subjected to hypo-osmotic stress (150 mOsm, 5 min) (n = 8 experiments); and data in (C) and (G) show cells subjected to carbachol stimulation (5 µM, 10 min) (n = 5 experiments). data in (F) show cells treated with siRNA(PLCβ1) (n = 4 Scale bars, 10 µm. (H) The size distribution of cytosolic RNAs isolated from the indicated PC12 cells was measured by dynamic light scattering for control conditions (black), hypo-osmotic stress (150 mOsm, 5 min, green), over-expression of constiutively active Gαq (blue), and treatment with siRNA(PLCβ1) (pink). Inset: DLS spectra of cytosolic RNAs extracted from control cells and from cells treated with puromyocin; the x-axis range is from 0 to 3000 nm. (I) The size distribution of cytosolic RNAs where data for control cells (black) is included for easier comparison to cells subjected to hypo-osmotic stress (150 mOsm 5min, red), heat shock at 40°C for 1 hour (green), cold shock at 12oC for 1 hour (blue), and treatment with 0.5 mM arsenite for 10 min (pink). Inset: A comparison of control and puromysin-treated cells. Note that no changes were observed in cells subjected to oxidative stress (treatment with 12 mM $CoCl_2$ for 8 hours; fig. S7). Normalized data are shown. Each sample was scanned three times with 10 minutes per run. The numbers of independent samples were six (control) and two (PLCβ1 knockdown, Gαq over-expression, heat shock, cold shock, arsenite) and four (hypo-osmotic stress).

3.3.7 Cytosolic PLCβ1 abundance affects the size of cytosolic RNAs

The formation of stress granules is expected to be accompanied by an increase in the size distribution of cytosolic RNA as mRNA accumulates due to the arrest of translation. We measured the sizes of cytosolic RNA by dynamic light scattering (DLS) (Fig. 3.5, H and I). Subjecting cells to osmotic stress caused a significant shift to larger sizes. Reducing PLCβ1 abundance resulted in a small peak at low molecular weights and a broad peak at larger sizes that was shifted to the right when compared to that for the control cells. This small peak was consistent with enhanced C3PO activity due to the relief of inhibition by PLCβ1 (28). Over-expressing Gα$_q$ resulted in a similar behavior as did treatment with siRNA (PLCβ1). As a control, we measured the DLS spectra of cytosolic RNA from untreated cells and in cells treated with the antibiotic puromycin, which halts

mRNA translation, rendering mRNA in stress granules (*37*). The RNAs from puromycin-treated cells were almost two-fold greater in molecular weight compared to those in control cells and showed a small peak that corresponded to the sizes seen in control cells. These data (Fig. 3.5, H and I) are consistent with the translational arrest and the accumulation of higher molecular weight RNAs that occurred when PLCβ1 abundance was reduced.

3.3.8 Cytosolic PLCβ1 abundance affects stress granules in smooth muscle cells

Myocytes and other cell types may experience changes in osmotic conditions during their lifetime. With this in mind, we extended our studies to two different smooth muscle cell types: rat aortic smooth muscle (A10) cells and Wistar-Kyoto rat 3M22 (WKO-3M22) cells. We identified PLCβ1-associated proteins in A10 cells under control conditions and after 5 min of osmotic stress by pulling down PLCβ1 complexes with a monoclonal antibody and identifying the proteins by MS analysis (table. S3.6). A large fraction of the proteins pulled down with PLCβ1 are associated with transcription, which is most likely due to the nuclear population of PLCβ (*38*). The stress granule–associated proteins were less abundant than the transcription-associated proteins. Many of the stress granule–associated proteins were also found in PC12 cells, for example, PABPC1 and eIF5A (Fig. 3.6A), whereas others, such as Ago2 and FXR, were not detected. We repeated these experiments with A10 cells that had been subjected to hypo-osmotic stress for 5 min before undergoing lysis. We detected a loss of almost all of the transcription-associated proteins and most of the stress granule–associated proteins (Fig. 3.6B). These results suggest that PLCβ1 binds to stress granule–associated proteins in A10 cells, as well as in PC12 cells, and that osmotic stress results in their release from PLCβ1. Whereas the cellular amount of PLCβ1 in A10 cells was reduced by osmotic stress, this effect was much lower than that in PC12 cells (fig. S3.7).
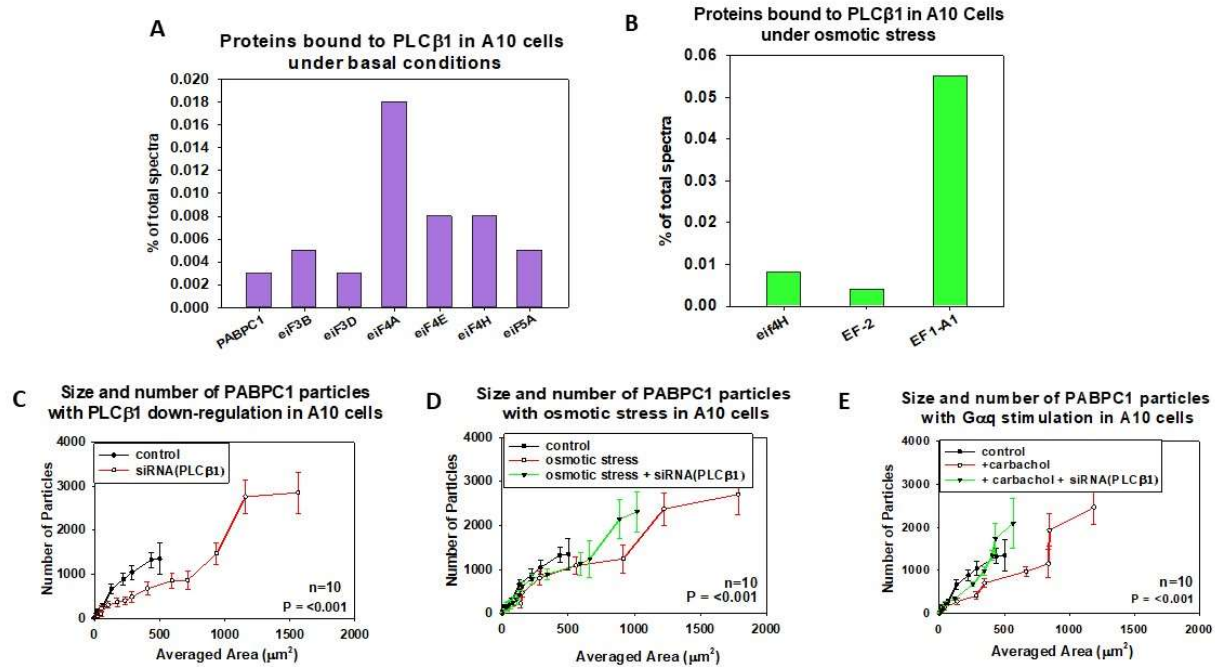
Figure 3.6: The effect of PLCβ1 on stress granule formation in A10 cells. (A and B) MS analysis of the proteins associated with PLCβ1 in A10 cells under normal osmotic conditions (A) and after being subjected to hypo-osmotic stress (150 mOsm) for 5 min (B). The full data set is shown in table S6. (C to E) Analysis of the sizes and numbers of particles associated with anti-PABPC1 in the cytosol of control A10 cells and A10 cells treated with siRNA(PLCβ1) as measured with a 100x objective and analyzed with Image J software (see Materials and Methods). The indicated cells were analyzed under basal conditions (C), after being subjected to osmotic stress (150 mOsm) (D), and after treatment with 5 μM carbachol to stimulate Gαq (E). All measurements are an average of three independent experiments with 10 cells sampled per experiment. Error bars indicate SD. P values were determined by ANOVA.

We then measured the formation of PABPC1 particles in A10 cells in which the cytosolic abundance of PLCβ1 was perturbed, such as by osmotic stress, siRNA(PLCβ1) treatment, and Gα$_q$ stimulation (Fig. 3.6, C to E). These cells exhibited particles that were ~10-fold larger than those in PC12 cells. Similar to PC12 cells, reducing PLCβ1 abundance in the A10 cells resulted in the formation of larger particles, which also occurred because of osmotic stress. In addition,

stimulation with carbachol (to activate $G\alpha_q$) also resulted in a significant increase in the number of larger particles. Together, these data indicate that the size and number of PABPC1-containing particles depend on the abundance of PLCβ1 in the cytosol.

Both osmotic stress and carbachol also promoted the formation of Ago2-containing particles in WKO-3M22 cells. We analyzed the N&B results of these cells subjected to osmotic stress, carbachol stimulation (Fig. 3.7 A to C), and arsenite (fig. S3.10). As occurred with PC12 cells, both osmotic stress and carbachol stimulation promoted Ago2 aggregation in the WKO-3M22 cells, whereas arsenite stress had only a minor effect (fig. S3.10). Reducing the abundance of PLCβ1 promoted Ago2 aggregation in both control (Fig. 3.7, D and E) and arsenite-stressed cells (fig. S10). In a final series of experiments, we monitored shifts in the sizes of cytosolic RNA in WKO-3M22 cells subjected to osmotic stress or carbachol stimulation and found statistically significant increases in the RNA sizes under both conditions (Fig. 3.7F). Note that the particles and cytosolic RNAs in WKO-3M22 cells appeared to be larger than those found in PC12 cells (Fig. 3.5 versus Fig. 3.7).
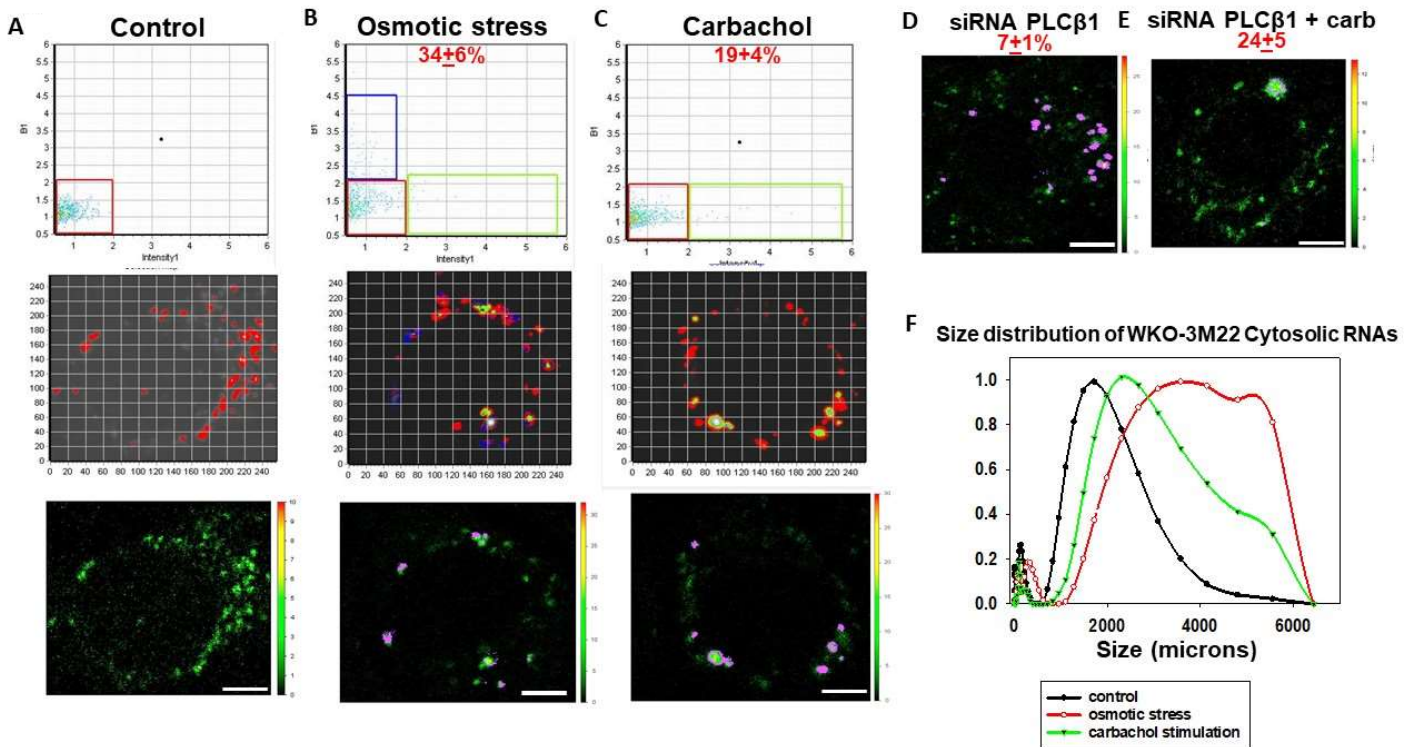
Figure 3.7: N&B analysis of eGFP-Ago2 aggregation in WKO-3M22 cells. (A to C) N&B analysis of brightness versus intensity for PC12 cells under the indicated conditions with the pixels of the colored boxes corresponding to specific regions in the cells (middle). Bottom: corresponding fluorescence microscopy images. Red boxes correspond to monomeric eGFP-Ago2 as determined by free eGFP. Points outside this box and in the green and blue boxes correspond to higher-order species and where the percentage of aggregation is given in red. Data in (A) show control cells, data in (B) show cells subjected to hypo-osmotic stress (150 mOsm, 5 min), and data in (C) show cells subjected to carbachol stimulation (5 μM, 10 min). (D and E) Data in (D) show cells treated with siRNA(PLCβ1), whereas data in (D) and (E) show cells treated with siRNA(PLCβ1) and stimulated with osmotic stress (150 mOsm). Data are from three experiments with nine cells analyzed per experiment. (F) Plot of the size distribution of cytosolic RNAs of WKO-3M22 cells as measured by dynamic light-scattering for control conditions (black), osmotic conditions (150 mOsm 5 min, red), and stimulation of Gαq with carbachol (5 μM, 10 min, green).

3.3.9 Stress granule formation depends on the abundance of PLCβ1

To understand the dependence of stress granule formation on the abundance of PLCβ1, we assumed that eIF5A was the primary contact between PLCβ1 and stress granule–associated proteins; however, eIF5B or another factor might be involved. We can then express the partitioning of eIF5A from the cytosol (c) to the particulate phase (p) as:

$$Kp = \frac{eIF5A^p}{eIF5A^c}$$

where eIF5A^p is the stress granule phase, also termed G. The total amount of eIF5A is given by:

$$E_T = eIF5A^p + eIF5A^c,$$

$$\text{where } eIF5A^c = eIF5^{free} + eIF5A\text{-}PLC\beta.$$

We can then express the association between PLCβ and eIF5A in terms of a bimolecular dissociation constant:

$$K_d = \frac{[PLC\beta][eIF5A]}{[PLC\beta - eIF5A]}$$

In this equation, PLCβ refers to cytosolic PLCβ. We only considered the cytosolic population and not the membrane-bound population in accordance with our results showing that the loss of cytosolic PLCβ appeared to promote stress granule formation. Thus, the total cytosolic amount of PLCβ is given by:

$$P_T = PLC\beta^{free} + PLC\beta\text{-}eIF5A$$

If we combine these equations to determine the relationship between the number of particles and the concentration of PLCβ, we obtain an equation that is quadratic in G (eIF5A).

$$G^2\left(1+\frac{1}{K_p}\right) + G\left(P_T - E_T + K_pK_d + K_d\right) - K_pK_dE_T = 0$$

To give:

$$G = \frac{-\left(P_T - E_T + K_d\left(1 + K_p\right)\right) \pm \sqrt{P_T^2 + E_T^2 + K_d^2\left(1 + K_p\right)^2 + 2K_d\left(1 + K_p(P_T + E_T)\right) - 2P_TE_T}}{\left(\dfrac{2\left(1 + K_p\right)}{K_p}\right)}$$

To determine the applicability of this model, we first needed to estimate values for G. We found a linear dependence between the number of particles and the average area of the particles for PABPC1 in PC12 and in A10 cells (Fig. 3.8, A and B). This linearity enabled us to estimate G using either of these measurements. Note that this linearity did not occur for Ago2-containing particles for which stress primarily increased the number of particles rather than their size (Fig. 3.4).
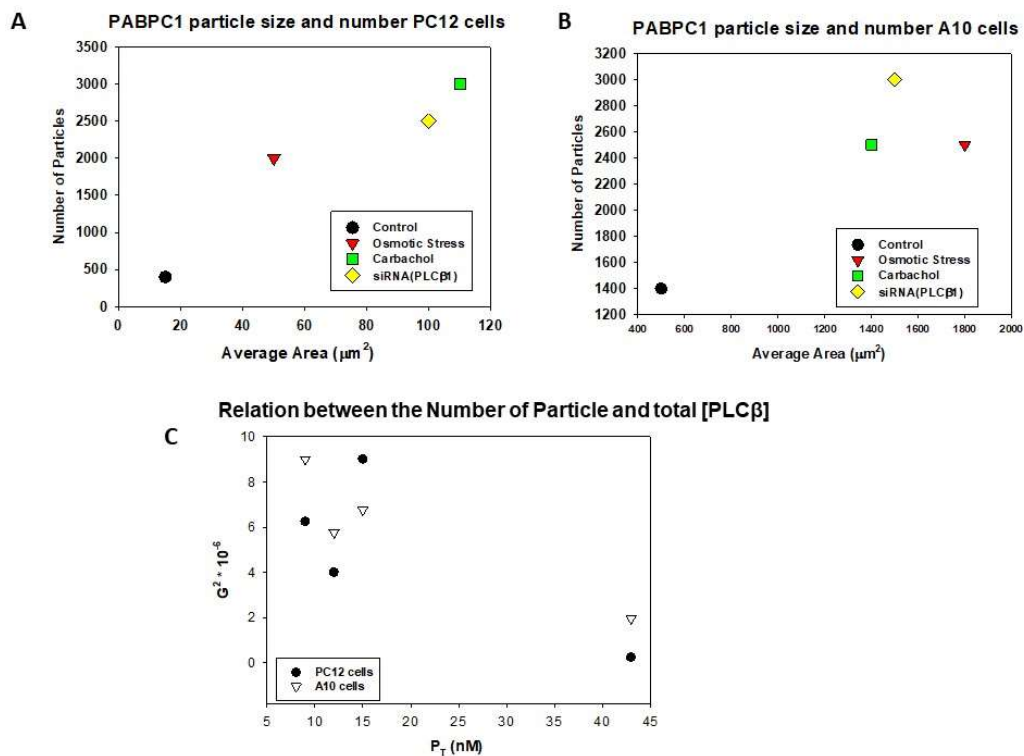
Figure 3. 8: Relationship between particle formation and PLCβ1 abundance. (A and B) Analysis of the relationship between the number of PABPC1 particles and their average area in (A) PC12 cells and (B) A10 cells that were treated as indicated. (C) Analysis of the relationship between the number of PABPC1 particles determined in Fig. 4, A to C, and Fig. 6, C to E and the estimated concentration of total cytosolic PLCβ1 in PC12 and A10 cells where the intensity is compared to a calibration scale using Alexa488 and measuring in confocal volume in an FCS instrument (26, 69).

We could estimate the total amount of cytosolic PLCβ by single molecule fluorescence measurements comparing the intensity of eYFP-PLCβ1 to an intensity scale constructed with Alexa488 as measured with a multiphoton laser in an fluorescence correlation instrument (see Materials and Methods). Briefly, we measured the number of eYFP-PLCβ1 molecules diffusing in a specific confocal volume after calibration with Alexa488. Note that we typically over-express ~two-fold more protein as indicated by Western blotting analysis. Our measurements enabled us to estimate a cytosolic eYFP-PLCβ1 concentration of ~43 nM in PC12 cells and ~49 nM in A10 cells, which was reduced to 10 to 15 nM under hypo-osmotic conditions. This decline can be

compared with the ~2.5-fold reduction in cytosolic PLCβ1 abundance that occurred in response to carbachol stimulation (Fig. 3.8B) and the 80 to 90% reduction in PLCβ1 abundance caused by siRNA treatment as seen in S9. Although these values for PLCβ1 are approximate, we used them to determine its dependence on stress granules as expressed as G^2. These data (Fig. 3.8C) showed the dependence of the size and number of stress granules when cyotsolic changes of PLCβ1 abundance occur.

3.4 DISCUSSION

The experiments presented here support the idea that cells direct signals through the reversible sequestration of proteins in membrane-less organelles. In some cases, these structures promote protein-protein interactions by reducing the local concentration and mobility of the proteins, whereas in other cases they effectively halt a functional pathway (*39, 40*). In this work, we showed that the atypical cytosolic population of PLCβ1 organized particles containing stress granule proteins in response Gα$_q$ signals. The specific types of stress granules that resulted from Gα$_q$-PLCβ1 signals appeared to be similar to those that occurred under osmotic stress but were distinct from those resulting from cold or heat shock, oxidative stress, or arsenite treatment. Our findings suggest that PLCβ1 regulates the entry of Ago2 and other stress granule proteins into particulates through a simple thermodynamic binding mechanism that is competitive with Gα$_q$ and that is dependent on the cytosolic concentration of PLCβ.

The traditional function of PLCβ is to generate Ca^{2+} signals in response to signaling molecules that lead to the activation of Gα$_q$, such as acetylcholine, dopamine, serotonin, melatonin, histamine, and angiotensin II. Note that without Gα$_q$ stimulation, the enzymatic activity of PLCβ1 is very low, and because Gα$_q$ resides at the plasma membrane and is not found in the cytosol, cytosolic PLCβ1 is not expected to be a substantial modifier of inositol phospholipids in internal membranes. Thus, any effect of these cytosolic binding partners on the enzymatic function of PLCβ1 would be immaterial; however, their ability to regulate its access to Gα$_q$ may be important for Ca^{2+} generation.

PLCβ1 plays multiple roles in cellular functions that are usually attributed to its enzymatic function. Studies showed that PLCβ1 can localize to the nucleus to regulate cell growth and differentiation, possibly through modulation of PIP$_2$ abundance in the nuclear envelope (*41, 42*).

We previously found that a stable, cytosolic population of PLCβ1 affects various cell functions, such as RNA silencing and neuronal cell differentiation and proliferation independently of its catalytic activity (*43, 44*). These alternative cytosolic functions of PLCβ only occur at specific and limited times in the cell cycle. For this reason, we set out to determine whether cytosolic PLCβ1 binds to other proteins in nondifferentiating cells under nonstimulated conditions. With these parameters in mind, we used a proteomics approach to uncover potential interacting proteins and validated some of these interactions in live cells. Our experiments showed that under basal conditions, cytosolic PLCβ1 interacted with stress granule–associated proteins in intact cultured cells.

Stress granules are RNA-protein aggregates that enable cells to halt the translation of mRNAs encoding nonessential proteins when the cells are subjected to environmental stress. We found that many of the proteins that associated with PLCβ1 in complexes directly contribute to RNA-processing and ribosome assembly, and that these proteins were found in PLCβ1-containing complexes isolated from PC12 cells and A10 cells. During the initiation stage of mRNA translation, the polyadenylate binding protein PABP binds to the tail of the mRNA, which then associates with eIF4, enabling the mRNA-protein complex to bind to the 40S subunit (*45*). A cytosolic form of PABP, PABPC1, was found in our PLCβ1 pulldown assay together with eIF4 subtypes, which bind to PABPC1 (see https://www.uniprot.org/uniprot/P11940). Several other eIF proteins were also identified in our analysis.

An important step in the progression of translation is the hydrolysis of GTP on eIF2, which is catalyzed by the GTPase activity of eIF5. Our results suggest that eIF5A may be a primary binding partner to mediate the association of PLCβ1 with stress granule proteins. eIF5A is found at very high abundance in cells arrested at the G2/M checkpoint when protein translation is expected to be low. eIF5A has several regions in its sequence that are homologous to those of Gα$_q$, including a region through which Gα$_q$ directly binds to PLCβ (amino acid residues 147 to 162), as indicated by homologous sequence alignment and chemical cross-linking (*46*). We directly tested the association between PLCβ1 and eIF5A in experiments with purified proteins. Not only was the PLCβ1-eIF5A binding affinity in the same range as the affinity between PLCβ1 and C3PO (*15*), but the binding was competitive both in solution and in cells. Because the site in PLCβ1 through

which it binds to C3PO overlaps with its binding site for $G\alpha_q$, the association of PLCβ1 with eIF5A should depend on the extent of $G\alpha_q$ activation, and this behavior was observed in our experiments. Thus, in the absence of $G\alpha_q$ stimulation, a population of cytosolic PLCβ1 may associate with eIF5A until specific events, such as cellular differentiation, cause PLCβ1 binding to shift to C3PO and inhibit RNA-induced silencing.

We found that cytosolic PLCβ1 also bound to Ago2 as seen in our pull-down studies, co-immunoprecipitation experiments, and FRET/FLIM analysis. Our ability to disrupt the PLCβ1-Ago2 interaction by the addition of purified eIF5A is suggestive of a direct interaction. Ago2 is the key nuclease component of the RISC (*47*), and our previous work suggested an association between PLCβ1 and Ago2 (*14*). Sequence alignment of Ago2 and the TRAX subunits of C3PO shows four homologous regions ranging from ~20 to 40 amino acid residues in length and from 21 to 30% identity and 40 to 56% homology (residues 2 to 54, 87 to 119, 202 to 228, and 109 to 136 in C3PO and residues 788 to 826, 555 to 598, 188 to 202, and 831 to 858 in Ago2). Note that at least three of the C3PO regions are potential interaction sites for binding to PLCβ1, and at least one of these may be available for binding to PLCβ1-Ago2 (*28*). By this argument, it is possible that PLCβ1 directly binds to Ago2 through interactions similar to those through which it binds to C3PO.

We determined whether PLCβ1 affected stress granule formation by monitoring the behavior of two established stress granule markers, Ago2 and PABPC1. We initially used mild osmotic stress that may occur physiologically. Hypo-osmotic stress initiates a series of cellular events to reduce the number of osmolytes in the cell, such as the synthesis of glycogen from glucose, as well as ion flow (*48*). Whereas we expected osmotic strength to change the ability of PLCβ1 to interact with stress granule proteins by causing changes in tertiary or quaternary structure, we were surprised to find a large reduction in PLCβ1a abundance in PC12 cells when osmotic stress was initially applied, although this effect was far less pronounced in A10 cells. The PLCβ1a and PLCβ1b isoforms differ by ~20 amino acids in the C-terminal region, but they are similarly activated by $G\alpha_q$. Piazzi *et al*. found that PLCβ1b, but not PLCβ1a, prevents cell death under oxidative conditions by affecting the amounts of key signaling proteins (*49*). Additionally, these two PLCβ1 isoforms may localize differently depending on cell type (*32-35, 50, 51*). Whereas our experiments

could not adequately distinguish between these two isoforms, it would be interesting to investigate any separate roles they may play in stress granule formation. Note that in addition to the changes in PLCβ1 abundance or properties that occurred because of osmotic stress, we also varied cytosolic PLCβ1 abundance by stimulating $G\alpha_q$ to recruit PLCβ1 from the cytosol to the plasma membrane, and we also reduced total PLCβ1 abundance with siRNA(PLCβ1). All of these methods showed a connection between cytosolic PLCβ1 abundance and the formation of particles.

Our experiments showed that the stress granules formed by osmotic stress differed from those formed in response to other stresses. Whereas we observed a substantial assembly of Ago2 under osmotic stress, we found that arsenite, oxidative stress, and temperature shock produced particles that contained monomeric Ago2. In addition, osmotic stress resulted in a large increase in the size distribution of cytosolic RNAs, whereas arsenite, oxidative stress, and temperature shock did not. Studies in *S. cerevisiae* (*3*) indicate that hypo-osmotic stress promotes the formation of particles composed of markers of both P-bodies and stress granules, supporting our findings that subjecting mammalian cells to hypo-osmotic stress forms particles with compositions that differ from those formed in response to other types of stress. Our results also suggest that these latter granules, which have low Ago2 content and are rich in proteins associated with RNA-processing, such as G3BP, are poised to prevent the translation of mRNAs whose protein products would not survive arsenite stress or oxidation, such as those involved in phosphorylation (*52*). In contrast, Ago2-rich granules, whose formation is mediated by the $G\alpha_q$-PLCβ1 pathway, may shift translation to mRNAs whose protein products enable cells to better respond to external signals. Thus, unlike arsenite or other stresses, $G\alpha_q$ activation may give rise to more physiologically relevant particles.

We monitored the appearance of stress granules under hypo-osmotic conditions structurally by fluorescence imaging and functionally by the accumulation of large cytosolic RNAs. Wheeler *et al*. showed that initially, stress granules are small and grow in size in a time-dependent manner (*5*). Here, we resolved particles greater than 10 μm^2 in area that formed in the cytoplasm, and the size and number of these particles did not vary between 5 and 10 min after stress induction. Additionally, whereas a very small population of eGFP-PLCβ1 incorporated into particles of ~400 μm^2, these were unchanged under conditions of osmotic stress, suggesting that PLCβ1 might deliver proteins into particles without incorporating into them. PABPC1 was associated with a

high number of aggregates whose numbers were affected by the abundance of cytosolic PLCβ1 as determined by immunofluorescence analysis. Formation of Ago2-associated particles, as monitored by both immunofluorescence and live-cell imaging, was sensitive to $G\alpha_q$ stimulation but not to other stresses. Furthermore, the formation of stress granules associated with G3BP1, which did not appear to bind directly to PLCβ1, appeared to be sensitive to cytosolic PLCβ1 abundance and showed extensive and diffuse aggregation. These data suggest that cells respond to $G\alpha_q$ activation by sequestering Ago2, G3BP1, and other proteins into stress granules to halt the production of specific proteins.

Our results also suggest that the stress granules generated by $G\alpha_q$ activation are more similar to those formed by reducing PLCβ1 abundance or inducing osmotic stress in terms of Ago2 aggregates and are distinct from those produced by thermal or oxidative stress. Specifically, cold, heat, oxidative, or arsenite stress did not result in Ago2 aggregation and did not substantially affect the sizes of cytosolic RNAs, even though oxidative stress reduced the abundance of PLCβ1 together with that of many cellular proteins (*53*). Our results are consistent with the variability of stress granule composition formed in response to different types of stress (*37, 54, 55*). Our studies also suggest that a loss of cytosolic PLCβ1 may arrest the translation of mRNAs for specific proteins by promoting the formation of mRNA-Ago2–associated stress granules. The idea that sustained $G\alpha_q$ activation can regulate the production of specific proteins is intriguing and a comprehensive study of all of the transcripts affected by PLCβ1 is underway.

Neurons and cardiomyocytes are long-lived cells, and their viability depends on the reversible assembly of stress granules. We used PC12 cells as a model for the role of stress granules in neurological diseases and A10 cells as a model for muscle cells that regularly experience changes in osmolarity. We also used WYK-3M22 rat aortic smooth muscle cells as another model of muscle cells, which is used as the normotensive control for spontaneously hypertensive rats, which are a common model of hypertension (*56*). We found a similar set of stress-related proteins in PLCβ1-containing complexes in the two cell lines, with the exception of neural-specific proteins and RISC proteins, such as Ago2 and C3PO. Thus, PLCβ1 may serve a similar role in many cell types by mediating stress granule formation but not in regulating RNA processing.

We constructed a simple thermodynamic model in which the partitioning of eIF5A into particulates is regulated by its association with PLCβ1, but we note that eIF5A can easily be replaced with Ago2. The expression derived from this model shows the scope by which PLCβ1 could affect stress granule formation. Specifically, if the total amount of eIF5A is much greater than that of PLCβ1, then stress granule formation will be independent of PLCβ1. Considering the high concentration of ribosomes in cells, it is difficult to estimate the amount of eIF5A that would be available to bind to PLCβ1. We know that microinjection studies that delivered ~10 nM eIF5A into cells resulted in the displacement of C3PO from PLCβ1, which can give us a quantitative handle for future studies. Regardless of the specific nature of eIF5A and its associated proteins, our data suggest that there is a concentration range of PLCβ1 that sensitizes cells to stress granule formation and that this range is under the control of $G\alpha_q$ activation. Additionally, endogenous amounts of PLCβ1 may help to control premature stress responses.

In summary, our studies suggest a model in which cytosolic PLCβ1 binds to stress granule protein complexes to keep these proteins disperse under basal conditions. Activation of $G\alpha_q$ shifts the cytosolic population of PLCβ1 to the plasma membrane, displacing stress granule proteins and promoting the formation of particles. This dynamic nature of PLCβ1 is consistent with FCS studies showing the rapid movement of the enzyme between the cytosol and plasma membrane (*28*). We propose a model (Fig. 3.9) in which cells use cytosolic PLCβ1 abundance to regulate the formation and timing of protein synthesis and to prevent the formation of irreversible aggregates. Note that the quenching of $G\alpha_q$-PLCβ1–dependent Ca^{2+} signals in cells under osmotic stress suggests that the stress granules may effectively block this signaling pathway.

We previously found that PLCβ1 plays an important but uncharacterized role in neuronal cell development. Specifically, the expression of PLCβ1a increases substantially within the first 24 hours of PC12 cell differentiation and then slowly decreases (*16*), leading to the question of why its abundance is so variable. PLCβ1 is highly expressed in neuronal tissue in which dysfunction in stress granule assembly has been implicated in disease (*57, 58*). Our data suggest that PLCβ1 may act as a chaperone to keep stress granule proteins dispersed under basal conditions. Note that reductions in the amount PLCβ1 are associated with a host of neurological disorders that may result from disruptions in Ca^{2+} signaling and the proliferation and differentiation of neuronal cells

(*59-62*). Schizophrenia and suicide specifically involve varying amounts of PLCβ1a and PLCβ1b in the prefrontal cortex (*61*). Note also that the PLCβ1-associated proteins identified here play important roles in neuronal function. FXR proteins are associated with the most common form of hereditary mental retardation (*63, 64*), whereas eIF5A is associated with neuronal growth and brain development (*65*). It is interesting to speculate about connections between PLCβ1-associated neurological disorders and those associated with FXR and eIF5A, which may involve dysfunction in stress granule assembly and disassembly.
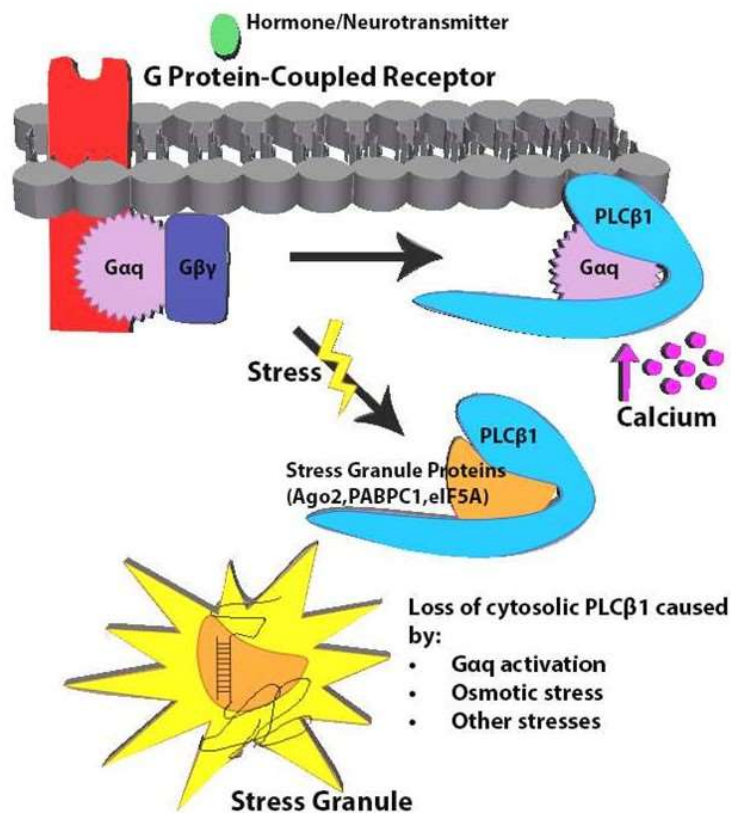
Figure 3.9: Model of the multiple interactions of PLCβ1 in cells. Under basal conditions, PLCβ1 is distibuted both at the plasma membrane and in the cytosol where it may interact with stress granule–associated proteins. The activation of Gαq (through the stimulation of a GPCR by its ligand) promotes the movement of PLCβ1 to the plasma membrane, thereby releasing the stress granule–associated proteins and promoting particle formation.

3.5 SUPPORTING INFORMATION
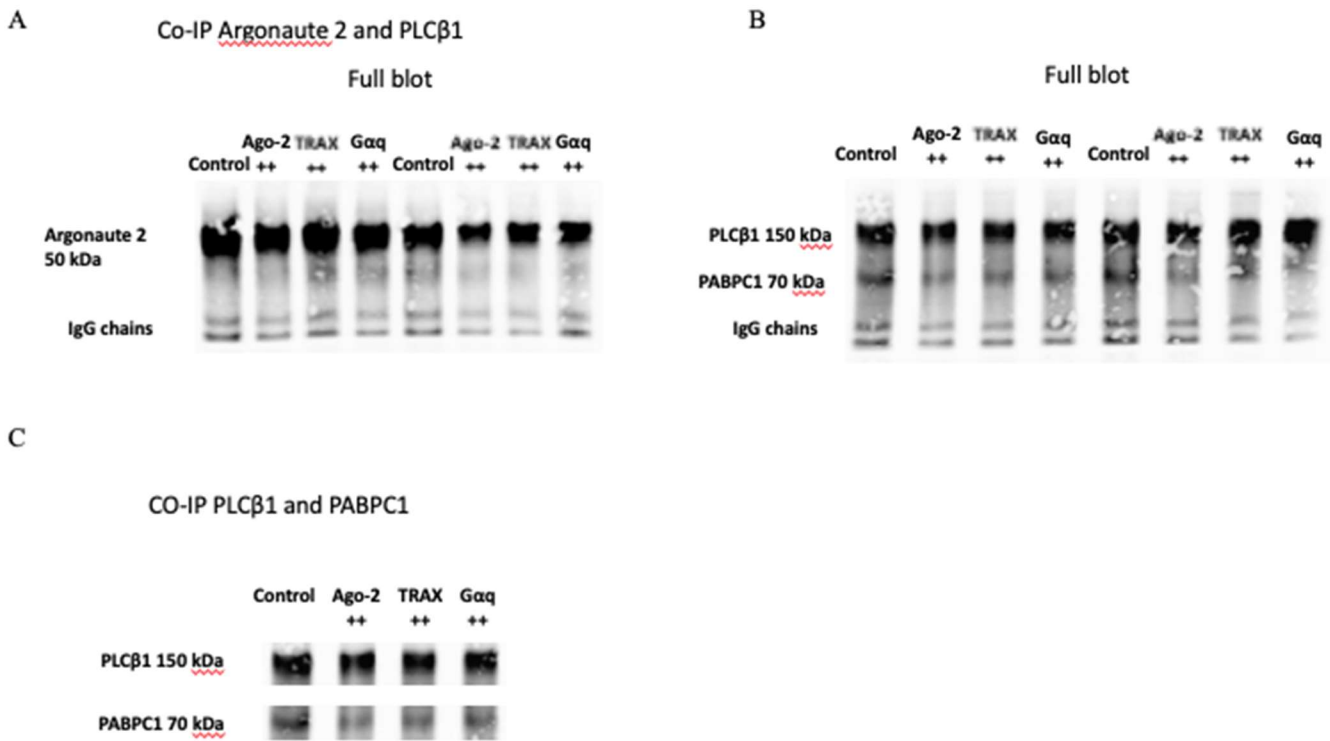
Figure S3.1: Western blotting analysis of proteins co-immunoprecipitated with Ago2 and PLCβ1. (A and B) Co-immunoprecipitation (CoIP) of PLCβ1 and Ago2 from the lysates of transfected PC12 cells expressing Ago2, TRAX, or Gαq as indicated. Antibodies used for CoIP and Western blotting are indicated. Blots are representative of two independent experiments. (C) CoIP of PLCβ1 and PABPC1 from the lysates of transfected PC12 cells expressing Ago2, TRAX, or Gαq as indicated. Antibodies used for CoIP and Western blotting are indicated. Blots are representative of two independent experiments.

FLIM/FRET studies of eGFP-Ago2 and mCherry-C3PO(TRAX)

Lifetime: 2.27 ns
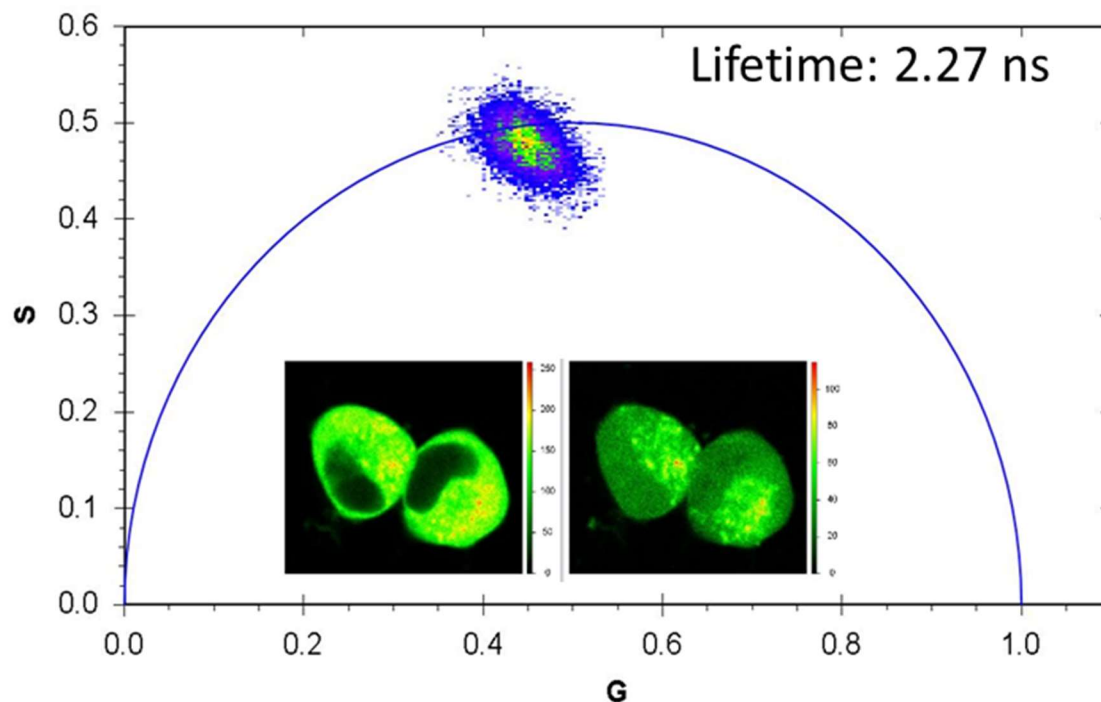
Figure S3.2: FLIM/FRET analysis showing the lack of association between mCherry-Ago2 and eGFP-C3PO. FLIM of eGFP-Ago2 and mCherry-C3PO(TRAX). Example of phasor plots in which PC12 cells were transfected with plasmids encoding eGFP-Ago2 and mCherry-TRAX and where the raw lifetimes are plotted as S versus G (see Results). Each point in the phasor plots corresponds to the lifetime from the eGFP-Ago2 emission seen in each pixel from the corresponding cell image shown in the graph. No FRET was detected. Data are representative of eight experiments.
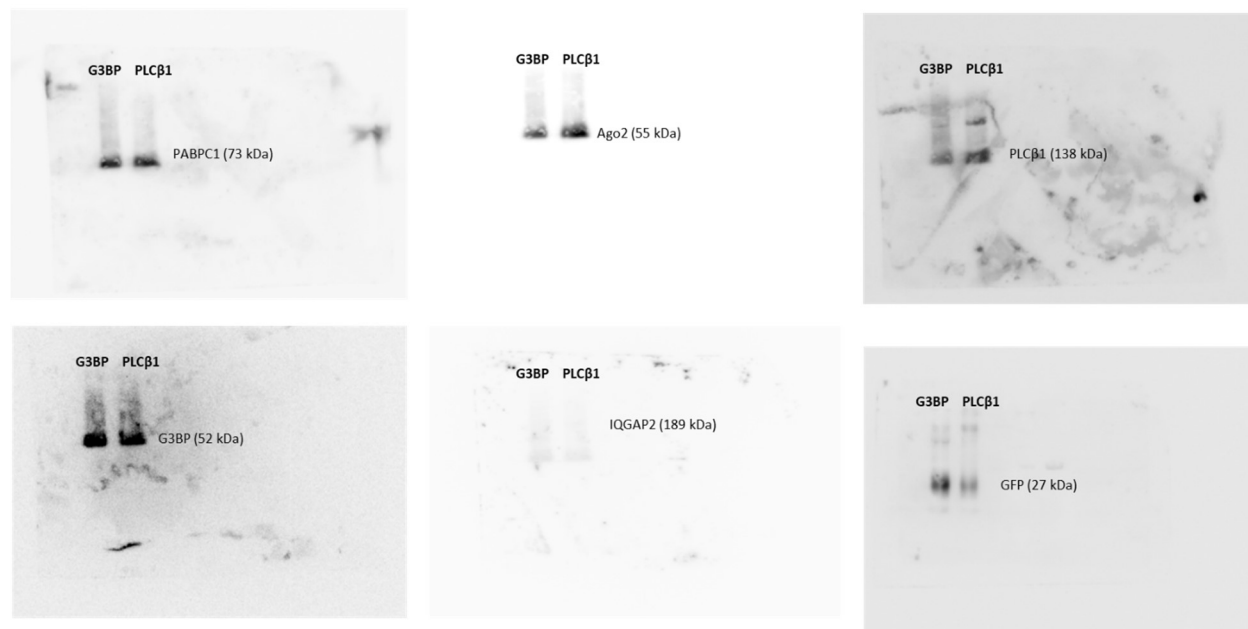
Figure S3.3: Pull-down of eGFP-PLCβ1 and eGFP-G3BP1 in PC12 cells. CoIP of GFP from the lysates of transfected PC12 cells expressing eGFP-PLC☐1 or eGFP-G3BP as indicated. Western blots are representative of five experiments for PLCβ1, PABPC1 and Ago2, and of two experiments for G3BP1. A nonbinding control, IQGAP2, was undetectable. Antibodies used for CoIP and Western blots are G3BP1, PABPC1, Ago2, PLCβ1, IQGAP2 and GFP.
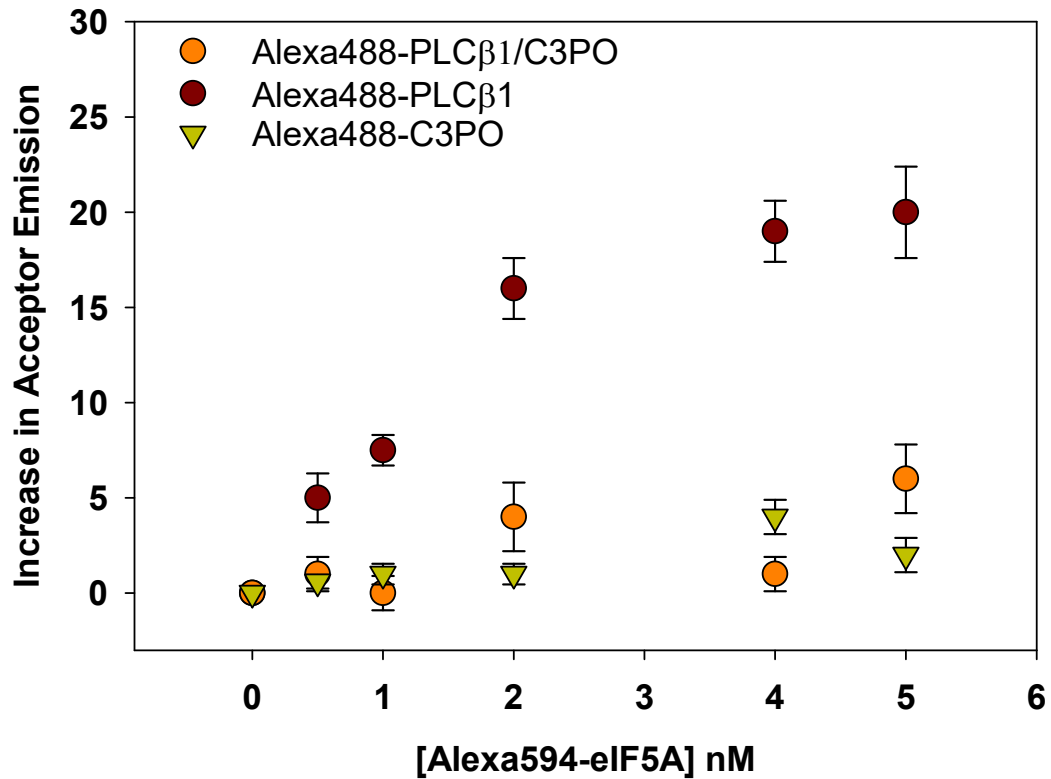
Figure S3.4: Competition between eIF5A and C3PO for binding to PLCβ1 in PC12 cells.
Fluorescence binding studies showing changes in FRET between purified Alexa594-eIF5A titrated into solutions of Alexa488-PLCβ1(brown circles), the Alexa488-PLCβ1:C3PO complex (orange circles), or Alexa488-C3PO (green triangles). FRET was determined by subtracting the fluorescence intensity of Alexa594-eIF5A alone from its intensity in the presence of the different labeled proteins (sensitized emission). Data were corrected for background and are from three experiments; bars represent SD.
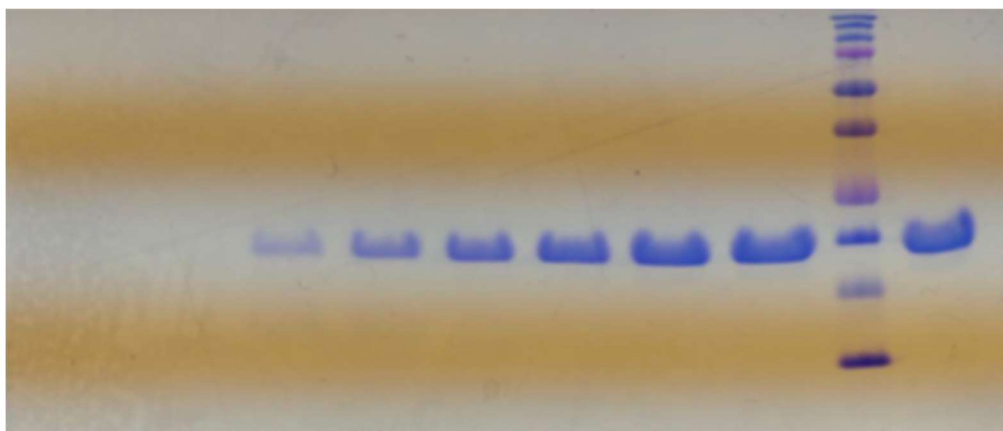
Figure S3.5: Analysis of eIF5A purity. Proteins were purified and labeled with fluorescent probes as described in the Materials and Methods. The Coomassie-stained SDS-PAGE gel shows the purity of eIF5A. Data are representative of 7 experiments.
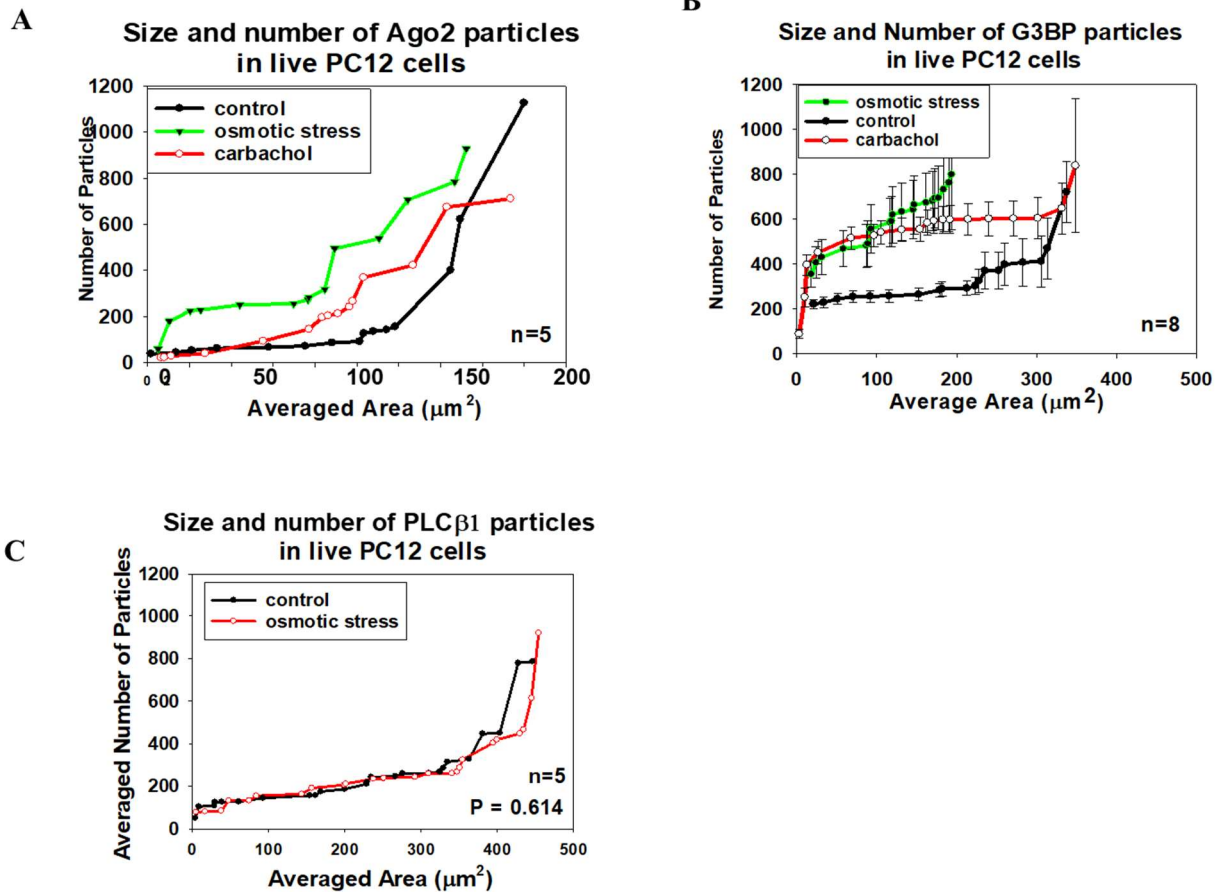
Figure S3.6: The effect of Gαq activation and hypoosmotic stress on the formation of Ago2, G3BP1-, and PLCβ1-associated particles in PC12 cells. (A) Analysis of particles associated with mCherry-Ago2 in live PC12 cells under control conditions, after exposure to 150 mOsm osmotic stress for 5 min, and after stimulation with 5 μM carbachol. (B) Analysis of particles associated with eGFP-G3BP1 in live PC12 cells under control conditions, after exposure to 150 mOsm osmotic stress for 5 min, and after stimulation with 5 μM carbachol. (C) Particles associated with eGFP-PLCβ1 in live cells under basal (300 mOsm) conditions and after osmotic stress (150 mOsm, 5 min). These data are an average of three independent experiments that each sampled five cells. For (B) and (C), bars indicate SD, whereas for (A), bars indicate SEM. The P values compare control versus osmotic stress conditions and were determined by ANOVA.
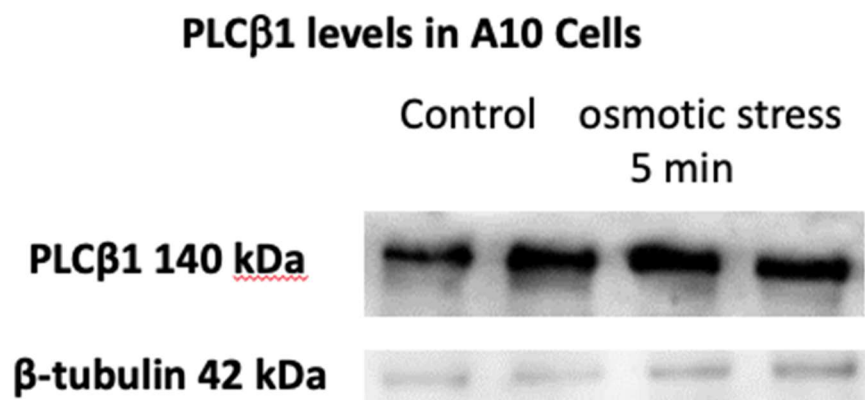
Figure S3.7: Western blot showing changes in the level of PLCβ1 in A10 cells under basal conditions and subjected to hypo-osmotic stress (150 mOsm for 5 min) (n=2). Densitometry comparing lanes 1 and 2 to 3 and 4, and accounting for differences in sample loading, show a 30-50% reduction in PLCβ1 levels.
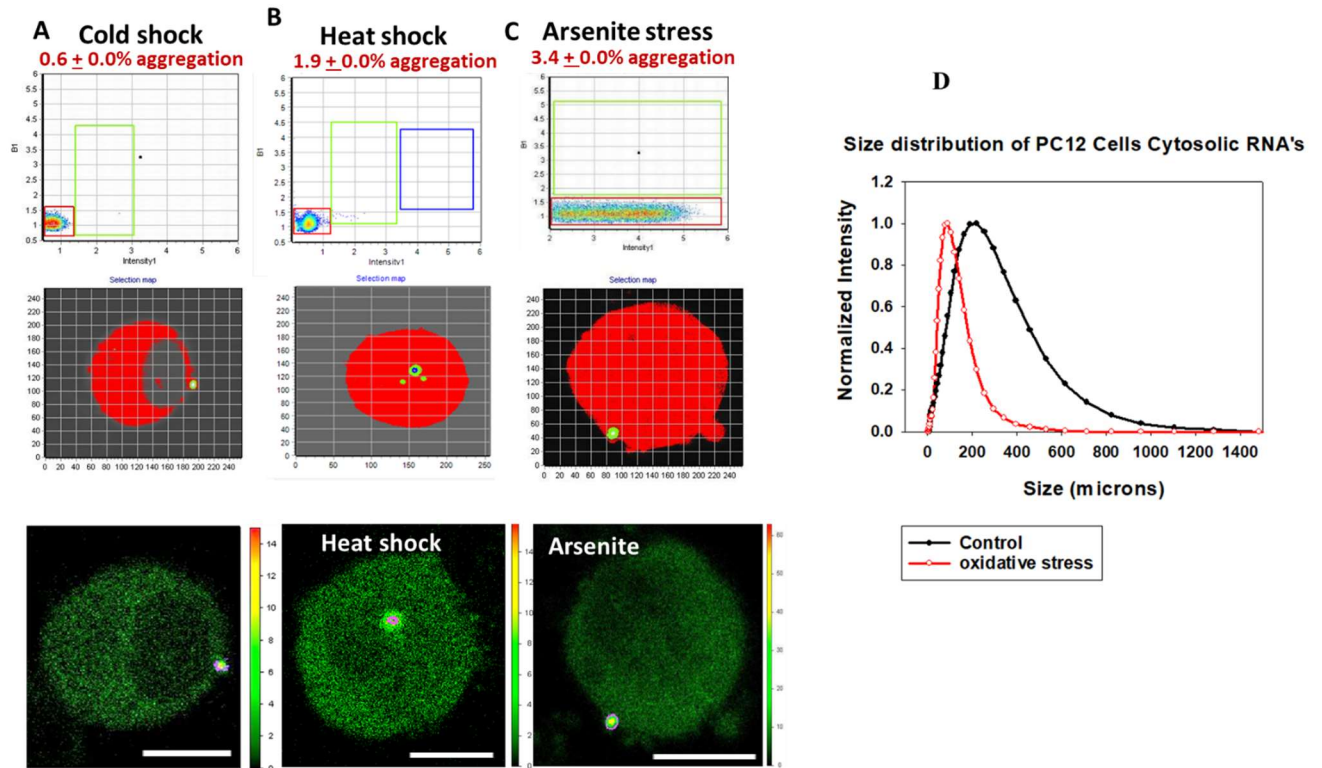
Figure S3.8: N&B analysis of eGFP-Ago2 aggregation in PC12 cells. (A to C) Data are from (A) cells subjected to cold shock at 12oC for 1 hour (n = six experiments), (B) cells subjected to heat shock at 40oC for 1 hour (n = six experiments); and (C) cells subjected to arsenite stress (0.5 mM, 10 min) (n = five experiments), Scale bars, 10 μm. (D) The size distribution of cytosolic RNA isolated from PC12 cells was measured by dynamic light scattering (n = three experiments) for control conditions (black) and oxidative stress (1 mM CoCl2 for 12 to 16 hours, red).
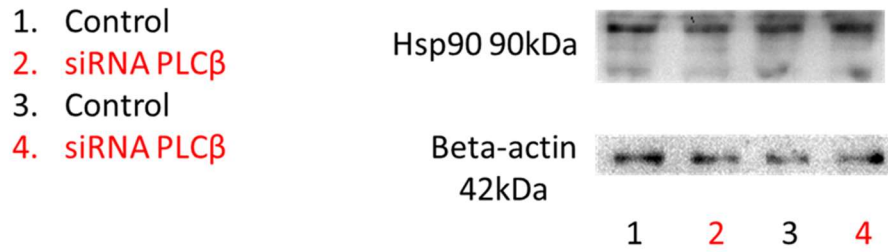
Figure S3.9: Effect of siRNA(PLCβ1) on Hsp90 abundance. Western blotting analysis of changes in Hsp90 abundance in undifferentiated PC12 cells that were treated with siRNA(PLCβ1). Cell treatments and Western blotting analysis were performed as described in the Results. Data are from two experiments.
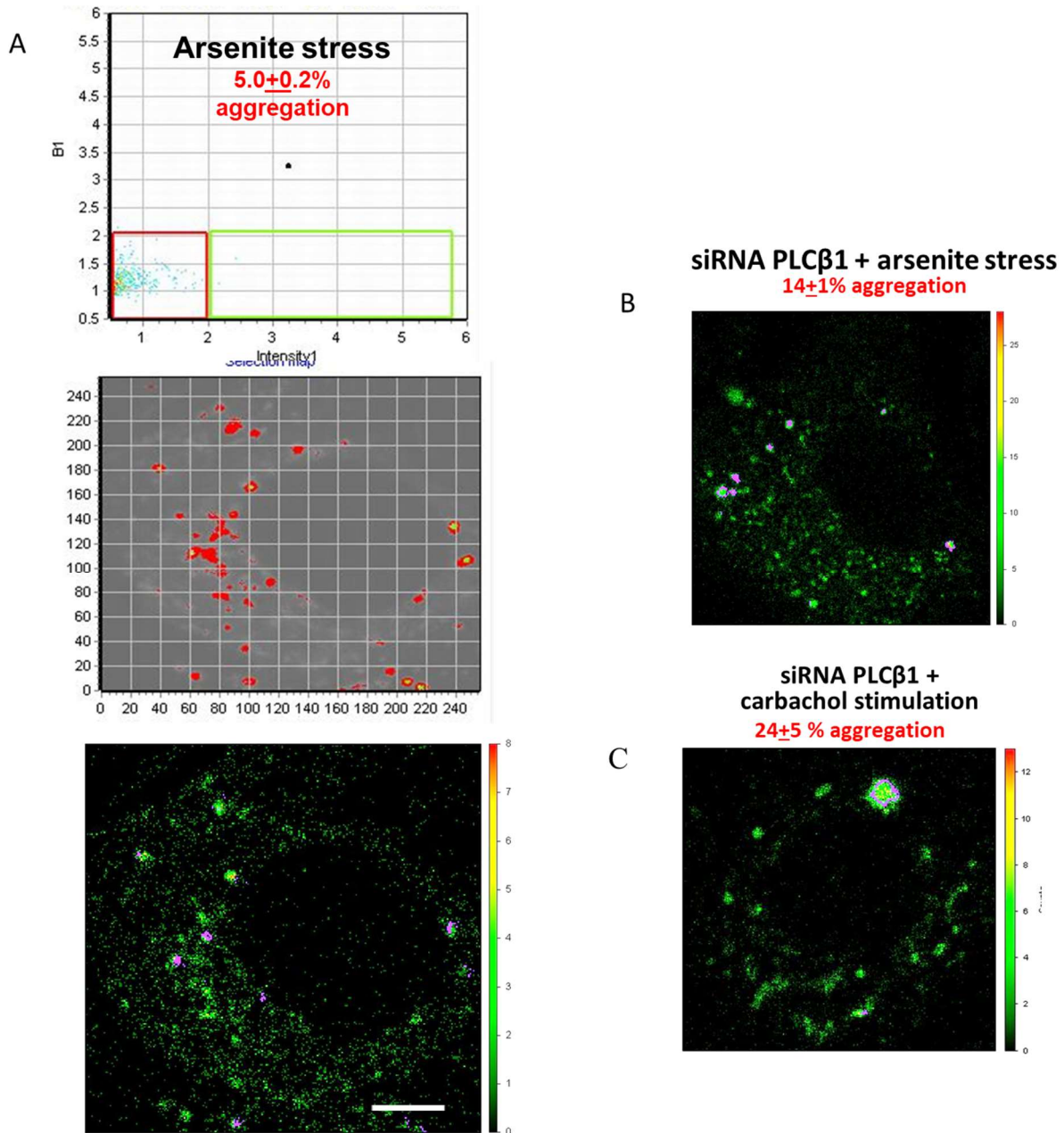
Figure S3.10: The effect of PLCβ1 on the formation of Ago2-associated particles in WKO-3M22 cells as monitored by N&B analysis. (A) N&B analysis of brightness versus intensity for PC12 cells under arsenite stress with the pixels of the colored boxes corresponding to specific regions in the cells with SIM-FCS 4. These cells were subjected to arsenite stress (0.5 mM for 10 min). Red boxes correspond to monomeric eGFP-Ago2 as determined by free eGFP. Points outside this box and in the green and blue boxes correspond to higher-order species. Scale bars are 10 μm. The corresponding fluorescence microscopy images in ISS are shown. (B and C) Data in (B) show cells treated with siRNA(PLCβ1) and arsenite (0.5 mM for 10 min) whereas data in (C) show cells

treated with siRNA(PLCβ1) and stimulated with carbachol (5 μM for 10 min). Data are from three experiments with nine cells analyzed per experiment.

3.6 AUTHOR CONTRIBUTIONS

A.Q., L.J., O.G., A.S. S.S. designed experiments.

A.Q. conducted and analyzed the following experiments: PLC cytosolic localization, all Western Blots for both PC12 and A10 cells, PABPC1 and Ago2 Particle Analysis in live and fixed PC12 cells, PABPC1 particle analysis in A10 cells, Number and Brightness of eGFP-Ago2 in PC12 and WKO-3M22 cells and Dynamic Light Scattering experiments.

L.J. conducted all FLIM/FRET experiments, Number and Brightness of eGFP-G3BP1in PC12 cells, GFP pulldown experiment and mass spectrometry analysis.

O.G. conducted the colocalization experiment between Ago2 and PABPC1, CoIP experiment and FLIM/FRET analysis.

A.S. conducted the mass spectrometry experiment and the calcium release experiment.

A.Q., L.J., and S.S developed signaling model. A.Q., L.J., O.S., A.S., and S.S. interpreted the data. A.Q., L.J., and S.S. wrote the manuscript.

3.7 ACKNOWLEDGEMENTS

interests: The authors declare that they have no competing interests. **Data and materials availability:** All data needed to evaluate the conclusions in the paper are present in the paper or the Supplementary Materials

3.8 REFERENCES

1.   P. Anderson, N. Kedersha, RNA granules. *J Cell Biol* **172**, 803-808 (2006); published online EpubMar 13 (10.1083/jcb.200512082).

2.   D. S. W. Protter, R. Parker, Principles and Properties of Stress Granules. *Trends Cell Biol* **26**, 668-679 10.1016/j.tcb.2016.05.004).

3.   K. H. Shah, S. N. Varia, L. A. Cook, P. K. Herman, A Hybrid-Body Containing Constituents of Both P-Bodies and Stress Granules Forms in Response to Hypoosmotic Stress in Saccharomyces cerevisiae. *PLoS One* **11**, e0158776 (2016)10.1371/journal.pone.0158776).

4.   A. Khong, T. Matheny, S. Jain, S. F. Mitchell, J. R. Wheeler, R. Parker, The Stress Granule Transcriptome Reveals Principles of mRNA Accumulation in Stress Granules. *Molecular Cell* **68**, 808-820.e805 10.1016/j.molcel.2017.10.015).

5.   J. R. Wheeler, T. Matheny, S. Jain, R. Abrisch, R. Parker, Distinct stages in stress granule assembly and disassembly. *eLife* **5**, e18413 (2016); published online Epub2016/09/07 (10.7554/eLife.18413).

6.   P. Anderson, N. Kedersha, Stress granules. *Current Biology* **19**, R397-R398 10.1016/j.cub.2009.03.013).

7.   M. Ramaswami, J. P. Taylor, R. Parker, Altered Ribostasis: RNA-Protein Granules in Degenerative Disorders. *Cell* **154**, 727-736 10.1016/j.cell.2013.07.038).

8.   A. Detzer, C. Engel, W. Wunsche, G. Sczakiel, Cell stress is related to re-localization of Argonaute 2 and to decreased RNA interference in human cells. *Nucleic Acids Res* **39**, 2727-2741 (2011); published online EpubApr (10.1093/nar/gkq1216).

9.   S. M. Hammond, A. A. Caudy, G. J. Hannon, Post-transcriptional gene silencing by double-stranded RNA. *Nat Rev Genet* **2**, 110-119 (2001); published online EpubFeb (

10.   J. Lopez-Orozco, J. M. Pare, A. L. Holme, S. G. Chaulk, R. P. Fahlman, T. C. Hobman, Functional analyses of phosphorylation events in human Argonaute 2. *RNA* **21**, 2030-2038 (2015)10.1261/rna.053207.115).

11.   P. Suh, J. Park, L. Manzoli, L. Cocco, J. Peak, M. Katan, K. Fukami, T. Kataoka, S. Yun, S. Ryu, Multiple roles of phosphoinositide-specific phospholipase C isozymes. *BMB reports* **41**, 415-434 (2008).

12.   M. Rebecchi, S. Pentylana, Structure, function and control of phosphoinositide-specific phospholipase C. *Physiological Reviews* **80**, 1291-1335 (2000).

13.   L. Dowal, P. Provitera, S. Scarlata, Stable association between G alpha(q) and phospholipase C beta 1 in living cells. *J Biol Chem* **281**, 23999-24014 (2006); published online EpubAug 18 (

14.   F. Philip, Y. Guo, O. Aisiku, S. Scarlata, Phospholipase Cβ1 is linked to RNA interference of specific genes through translin-associated factor X. *The FASEB Journal* **26**, 4903-4913 (2012); published online EpubDecember 1, 2012 (10.1096/fj.12-213934).

15.   O. R. Aisiku, L. W. Runnels, S. Scarlata, Identification of a Novel Binding Partner of Phospholipase Cβ1: Translin-Associated Factor X. *PLoS One* **5**, e15001 (2010).

16.   O. Garwain, S. Scarlata, Phospholipase Cβ-TRAX Association Is Required for PC12 Cell Differentiation. *Journal of Biological Chemistry* **291**, 22970-22976 (2016); published online EpubOctober 28, 2016 (10.1074/jbc.M116.744953).

17.   O. Garwain, K. Valla, S. Scarlata, Phospholipase Cβ1 regulates proliferation of neuronal cells. *The FASEB Journal* **In press**, fj.201701284R (2018)10.1096/fj.201701284R).

18.   T. Yanagi, M. Krajewska, S.-i. Matsuzawa, J. C. Reed, PCTAIRE1 Phosphorylates p27 and Regulates Mitosis in Cancer Cells. *Cancer Research* **74**, 5795-5807 (2014)10.1158/0008-5472.can-14-0872).

19.   T. Yanagi, S.-i. Matsuzawa, PCTAIRE1/PCTK1/CDK16: a new oncotarget? *Cell Cycle* **14**, 463-464 (2015); published online Epub2015/02/16 (10.1080/15384101.2015.1006539).

20.   H. Mahboubi, U. Stochaj, Cytoplasmic stress granules: Dynamic modulators of cell signaling and disease. *Biochim Biophys Acta* **1863**, 884-895 (2017); published online EpubApr (10.1016/j.bbadis.2016.12.022).

21.   O. Garwain, K. Valla, S. Scarlata, Phospholipase Cβ1 regulates proliferation of neuronal cells. *The FASEB Journal* **32**, 2891-2898 (2018)10.1096/fj.201701284R).

22.   L. Cocco, A. M. Martelli, R. S. Gilmour, S. G. Rhee, F. A. Manzoli, Nuclear phospholipase C and signaling. *Biochim Biophys Acta* **1530**, 1-14 (2001); published online EpubJan 15 (

23. J. Lakowicz, *Principles of Fluorescence Spectroscopy, Second Edition*. (Plenum, New York, 1999).

24. M. A. Digman, V. R. Caiolfa, M. Zamai, E. Gratton, The Phasor Approach to Fluorescence Lifetime Imaging Analysis. *Biophysical Journal* **94**, L14-L16 (2008); published online Epub11/02

25. G. H. Patterson, D. W. Piston, B. G. Barisas, Forster distances between green fluorescent protein pairs. *Anal Biochem* **284** 438-440 (2000).

26. F. Philip, S. Sahu, U. Golebiewska, S. Scarlata, RNA-induced silencing attenuates G protein-mediated calcium signals. *Faseb j* **30**, 1958-1967 (2016); published online EpubMay (10.1096/fj.201500140).

27. F. E. Paulin, L. E. Campbell, K. O'Brien, J. Loughlin, C. G. Proud, Eukaryotic translation initiation factor 5 (eIF5) acts as a classical GTPase-activator protein. *Curr Biol* **11**, 55-59 (2001); published online EpubJan 9 (

28. S. Sahu, L. Williams, A. Perez, F. Philip, G. Caso, W. Zurawsky, S. Scarlata, Regulation of the activity of the promoter of RNA-induced silencing, C3PO. *Protein Science* **26**, 1807-1818 (2017)10.1002/pro.3219).

29. S. Sahu, F. Philip, S. Scarlata, Hydrolysis Rates of Different Small Interfering RNAs (siRNAs) by the RNA Silencing Promoter Complex, C3PO, Determines Their Regulation by Phospholipase Cβ. *Journal of Biological Chemistry* **289**, 5134-5144 (2014); published online EpubFebruary 21, 2014 (10.1074/jbc.M113.531467).

30. Y. Guo, L. Yang, K. Haught, S. Scarlata, Osmotic Stress Reduces Ca2+ Signals through Deformation of Caveolae. *J Biol Chem* **290**, 16698-16707 (2015); published online EpubJul 3 (10.1074/jbc.M115.655126).

31. L. Yang, S. Scarlata, Super-resolution Visualization of Caveola Deformation in Response to Osmotic Stress. *J Biol Chem* **292**, 3779-3788 (2017); published online EpubMar 03 (10.1074/jbc.M116.768499).

32. Y. Y. Bahk, Y. H. Lee, T. G. Lee, J. Seo, S. H. Ryu, P. G. Suh, Two forms of phospholipase C-beta 1 generated by alternative splicing. *Journal of Biological Chemistry* **269**, 8240-8245 (1994); published online EpubMarch 18, 1994 (

33. Y. Bahk, H. Song, K. J. Baek, B. Y. Park, H. Kim, S. H. Ryu, P. G. Suh, Localization of two forms of phospholipase Cb1, a and b, in C6Bu-1 cells. *Biochem Biophys Acta* **1389**, 76-80 (1998).

34. C. G. Kim, D. Park, S. G. Rhee, The role of carboxyl-terminal basic amino acids in G_qa-dependent activation, particulate association, and nuclear localization of phospholipase C-b_1. *J Biol Chem* **271**, 21187-21192 (1996); published online EpubAug 30 (

35. D. R. Grubb, O. Vasilevski, H. Huynh, E. A. Woodcock, The extreme C-terminal region of phospholipase Cbeta1 determines subcellular localization and function; the "b" splice variant mediates alpha1-adrenergic receptor responses in cardiomyocytes. *Faseb j* **22**, 2768-2774 (2008); published online EpubAug (10.1096/fj.07-102558).

36. M. A. Digman, R. Dalal, A. F. Horwitz, E. Gratton, Mapping the Number of Molecules and Brightness in the Laser Scanning Microscope. *Biophys J* **97**, 2320-2332 (2008).

37. A. Aulas, M. M. Fay, S. M. Lyons, C. A. Achorn, N. Kedersha, P. Anderson, P. Ivanov, Stress-specific differences in assembly and composition of stress granules and related foci. *J Cell Sci* **130**, 927-937 (2017); published online EpubMar 1 (10.1242/jcs.199240).

38. L. Cocco, I. Faenza, R. M. Fiume, S. R. Gilmour, F. A. Manzoli, Phosphoinositide-specific phospholipase C (PI-PLC) [beta]1 and nuclear lipid-dependent signaling. *Biochem Biophys Acta* **1761**, 509-521 (2006).

39. L. B. Case, X. Zhang, J. A. Ditlev, M. K. Rosen, Stoichiometry controls activity of phase-separated clusters of actin signaling proteins. *Science* **363**, 1093-1097 (2019)10.1126/science.aau6313).

40. W. Y. C. Huang, S. Alvarez, Y. Kondo, Y. K. Lee, J. K. Chung, H. Y. M. Lam, K. H. Biswas, J. Kuriyan, J. T. Groves, A molecular assembly phase transition and kinetic proofreading modulate Ras activation by SOS. *Science* **363**, 1098-1103 (2019)10.1126/science.aau5721).

41. L. Cocco, L. Manzoli, I. Faenza, G. Ramazzotti, Y. R. Yang, J. A. McCubrey, P. G. Suh, M. Y. Follo, Modulation of nuclear PI-PLCbeta1 during cell differentiation. *Adv Biol Regul* **60**, 1-5 (2016); published online EpubJan (10.1016/j.jbior.2015.10.008).

42. G. Ramazzotti, I. Faenza, R. Fiume, A. M. Billi, L. Manzoli, S. Mongiorgi, S. Ratti, J. A. McCubrey, P. G. Suh, L. Cocco, M. Y. Follo, PLC-beta1 and cell differentiation: An

insight into myogenesis and osteogenesis. *Adv Biol Regul* **63**, 1-5 (2017); published online EpubJan (10.1016/j.jbior.2016.10.005).

43.   S. Scarlata, O. Garwain, L. Williams, I. G. Burguera, B. Rosati, S. Sahu, Y. Guo, F. Philip, U. Golebiewska, Phospholipase Cbeta connects G protein signaling with RNA interference. *Adv Biol Regul* **61**, 51-57 (2016); published online EpubMay (10.1016/j.jbior.2015.11.006).

44.   S. Scarlata, A. Singla, O. Garwain, Phospholipase Cβ interacts with cytosolic partners to regulate cell proliferation. *Advances in Biological Regulation*, (2017); published online Epub2017/09/09/ (https://doi.org/10.1016/j.jbior.2017.09.004).

45.   B. Alberts, D. Bray, J. Lewis, M. Raff, K. Roberts, J. Watson, *Molecular Biology of the Cell*. (Garland, New York, 1994).

46.   A. M. Lyon, V. M. Tesmer, V. D. Dhamsania, D. M. Thal, J. Gutierrez, S. Chowdhury, K. C. Suddala, J. K. Northup, J. J. G. Tesmer, An autoinhibitory helix in the C-terminal region of phospholipase C-β mediates Gαq activation. *Nat Struct Mol Biol* **18**, 999-1005 (2011)http://www.nature.com/nsmb/journal/vaop/ncurrent/abs/nsmb.2095.html#supplementary-information).

47.   G. Hutvagner, M. J. Simard, Argonaute proteins: key players in RNA silencing. *Nature Reviews Molecular Cell Biology* **9**, 22 (2008); published online Epub01/01/online (10.1038/nrm2321).

48.   K. Dietmar, Osmotic stress sensing and signaling in animals. *The FEBS Journal* **274**, 5781-5781 (2007)doi:10.1111/j.1742-4658.2007.06097.x).

49.   M. Piazzi, W. L. Blalock, A. Bavelloni, I. Faenza, M. Raffini, F. Tagliavini, L. Manzoli, L. Cocco, PI-PLCβ1b affects Akt activation, cyclin E expression, and caspase cleavage, promoting cell survival in pro-B-lymphoblastic cells exposed to oxidative stress. *The FASEB Journal* **29**, 1383-1394 (2015)10.1096/fj.14-259051).

50.   A. M. Martelli, R. S. Gilmour, V. Bertagnolo, L. M. Neri, L. Manzoli, L. Cocco, Nuclear localization and signalling activity of phosphoinositidase C beta in Swiss 3T3 cells. *Nature* **358**, 242-245 (1992); published online EpubJul 16 (

51.   T. M. Filtz, D. R. Grubb, T. J. McLeod-Dryden, J. Luo, E. A. Woodcock, Gq-initiated cardiomyocyte hypertrophy is mediated by phospholipase Cβ1b. *The FASEB Journal* **23**, 3564-3570 (2009); published online EpubOctober 1, 2009 (10.1096/fj.09-133983).

52. M. F. Hughes, Arsenic toxicity and potential mechanisms of action. *Toxicol Lett* **133**, 1-16 (2002); published online EpubJul 7 (

53. Y. Guo, S. Scarlata, A Loss in Cellular Protein Partners Promotes α-Synuclein Aggregation in Cells Resulting from Oxidative Stress. *Biochemistry* **52**, 3913-3920 (2013); published online Epub2013/06/04 (10.1021/bi4002425).

54. J. Y. Youn, W. H. Dunham, S. J. Hong, J. D. R. Knight, M. Bashkurov, G. I. Chen, H. Bagci, B. Rathod, G. MacLeod, S. W. M. Eng, S. Angers, Q. Morris, M. Fabian, J. F. Cote, A. C. Gingras, High-Density Proximity Mapping Reveals the Subcellular Organization of mRNA-Associated Granules and Bodies. *Mol Cell* **69**, 517-532.e511 (2018); published online EpubFeb 1 (10.1016/j.molcel.2017.12.020).

55. S. Jain, Joshua R. Wheeler, Robert W. Walters, A. Agrawal, A. Barsic, R. Parker, ATPase-Modulated Stress Granules Contain a Diverse Proteome and Substructure. *Cell* **164**, 487-498 10.1016/j.cell.2015.12.038).

56. J. M. Lemire, C. W. Covin, S. White, C. M. Giachelli, S. M. Schwartz, Characterization of cloned aortic smooth muscle cells from young rats. *The American journal of pathology* **144**, 1068-1081 (1994).

57. B. Wolozin, Physiological Protein Aggregation Run Amuck: Stress Granules and the Genesis of Neurodegenerative Disease. *Discovery medicine* **17**, 47-52 (2014).

58. L. Chen, B. Liu, Relationships between Stress Granules, Oxidative Stress, and Neurodegenerative Diseases. *Oxidative Medicine and Cellular Longevity* **2017**, 10 (2017)10.1155/2017/1809592).

59. A. J. Hannan, P. C. Kind, C. Blakemore, Phospholipase C-β1 expression correlates with neuronal differentiation and synaptic plasticity in rat somatosensory cortex. *Neuropharmacology* **37**, 593-605 (1998); published online Epub4/5/ (http://dx.doi.org/10.1016/S0028-3908(98)00056-2).

60. C. E. McOmish, E. L. Burrows, M. Howard, A. J. Hannan, PLC-β1 knockout mice as a model of disrupted cortical development and plasticity: Behavioral endophenotypes and dysregulation of RGS4 gene expression. *Hippocampus* **18**, 824-834 (2008)10.1002/hipo.20443).

61. M. Udawela, E. Scarr, S. Boer, J. Y. Um, A. J. Hannan, C. McOmish, C. C. Felder, E. A. Thomas, B. Dean, Isoform specific differences in phospholipase C beta 1 expression in the

prefrontal cortex in schizophrenia and suicide. *npj Schizophrenia* **3**, 19 (2017); published online Epub2017/04/19 (10.1038/s41537-017-0020-x).

62.   H.-j. Kim, H.-Y. Koh, Impaired Reality Testing in Mice Lacking Phospholipase Cβ1: Observed by Persistent Representation-Mediated Taste Aversion. *PLoS One* **11**, e0146376 (2016)10.1371/journal.pone.0146376).

63.   C. Agulhon, P. Blanchet, A. Kobetz, D. Marchant, N. Faucon, P. Sarda, C. Moraine, A. Sittler, V. Biancalana, A. Malafosse, M. Abitbol, Expression of FMR1, FXR1, and FXR2 genes in human prenatal tissues. *J Neuropathol Exp Neurol* **58**, 867-880 (1999); published online EpubAug (

64.   B. Bardoni, A. Schenck, J.-L. Mandel, The Fragile X mental retardation protein. *Brain Research Bulletin* **56**, 375-382 (2001); published online Epub2001/11/01/ (https://doi.org/10.1016/S0361-9230(01)00647-5).

65.   Y. Huang, D. S. Higginson, L. Hester, M. H. Park, S. H. Snyder, Neuronal growth and survival mediated by eIF5A, a polyamine-modified translation initiation factor. *Proceedings of the National Academy of Sciences of the United States of America* **104**, 4194-4199 (2007); published online Epub02/28

12/07/received (10.1073/pnas.0611609104).

66.   S. Iwata, Lee, J.W., Okada, K., Lee, J.K. Iwata, M., Rasmussen, B., Link T.A., Ramaswamy, S. and Jap, B.K., Complete at of the 11 subunit bovine mitochondrial cytochrome bc1 complex. *Science* **281**, 64-71 (1998).

67.   T. E. Hughes, H. Zhang, D. Logothetis, C. H. Berlot, Visualization of a functional Gaq-green fluorescent protein fusion in living cells. *J.Biol.Chem.* **276**, 4227-4235 (2001).

68.   R. C. Calizo, S. Scarlata, A Role for G-Proteins in Directing G-Protein-Coupled Receptor–Caveolae Localization. *Biochemistry* **51**, 9513-9523 (2012)10.1021/bi301107p).

69.   C. A. Royer, S. F. Scarlata, in *Methods in Enzymology*. (Academic Press, 2008), vol. 450, pp. 79-106.

CHAPTER 4 - DEFORMATION OF CAVEOLAE IMPACTS TRANSCRIPTION AND TRANSLATIONAL THROUGH CAVIN-1 RELOCALIZATION

Androniqi Qifti, Shravani Balaji, and Suzanne Scarlata*

Dept of Chemistry and Biochemistry, Worcester Polytechnic Institute Worcester, MA 01609

Corresponding author – S. Scarlata, 100 Institute Rd., Worcester, MA 01609, USA, sfscarlata@wpi.edu, 508-831-6803

Running title –Cavin-1 relocalizes with membrane stress

TOC – Mechanical stretch impacts translation and transcription through cavin-1 localization

The following subsections appear in Qifti et al. "DEFORMATION OF CAVEOLAE IMPACTS TRANSCRIPTION AND TRANSLATIONAL THROUGH CAVIN-1 RELOCALIZATION" *Accepted*, Journal of Biological Chemistry. (2022) and are reproduced here with permission. Sections with an asterisk (*) indicate additional sections not included in the original article. Addition information on the authors' contributions can be found in section 4.6.

4.0 ABSTRACT

Caveolae are membrane domains that provide mechanical strength to cells and localize signaling molecules. Caveolae are composed of caveolin-1 or -3 (Cav1/3) molecules that assemble into domains with the help of cavin-1. Besides organizing caveolae, cavin-1, also known as polymerase I and transcript release factor (PTRF), promotes ribosomal RNA transcription in the nucleus. Here, we find that deforming caveolae by subjecting cells to mild osmotic stress (300 to 150 mOsm), changes levels of GAPDH, Hsp90 and Ras only when Cav1/cavin-1 levels are reduced suggesting link between caveolae deformation and protein expression. We find that this link may be due to relocalization of cavin-1 to the nucleus upon caveolae deformation. Cavin-1 relocalization is also seen when Cav1-Gαq contacts change upon stimulation. Cav1 and cavin-1 levels have profound effects on cytosolic RNA levels that in turn impact the ability of cells to form stress granules and RNA-processing bodies (p-bodies) which protect mRNA when cells are subjected to environmental stress. Studies using a cavin-1 knock-out cell line show adaptive changes in cytosolic RNA levels but a reduced ability to form stress granules. Our studies show that caveolae, through release of cavin-1, communicates extracellular cues to the cell interior to impact transcriptional and translational processes.

4.1 INTRODUCTION

Caveolae are flask-shaped membrane invaginations that can flatten to provide more membrane area and are implicated in mechano- and electric sensation, endocytosis, and vasodilation through modulating the NO pathway (1-4). In previous studies, our lab found that populations of Gαq and their receptors reside in caveolae domains and this localization is assisted by interactions between Gαq and caveolin molecules (5,6). Activation of Gαq by hormones or neurotransmitters strengthens these interactions resulting in enhancement calcium signals. Deformation of caveolae by mild osmotic stress disrupts this stabilization and returns calcium signals to levels observed in

the absence of caveolae (7-9). Additionally, when cells are subjected to either bi-directional static or oscillating mechanical stretch, calcium release through activation of Gαq/PLCβ is intact, but contacts between Gαq and caveolin are disrupted (10,11). In separate series of studies, our lab found that activation of the Gαq/PLCβ triggers a novel calcium-independent pathway that is linked to regulation of GAPDH protein production but not Hsp90 (see (12)).

Cavins are a family of four proteins that regulate the curvature of the caveolae membrane by anchoring caveolins to the cytoskeleton (for reviews see (13-15)). The most abundantly expressed is cavin-1, also known as polymerase 1 and transcript release factor (PTRF) or cav-p60. Since its discovery in 1998, cavin-1 has been found to be a necessary component of caveolae formation, by mediating the sequestration of caveolin molecules into immobile caveolae domains (see (13)). Several studies, including those here, strongly suggest that expression of cavin-1 and caveolin are interdependent; Cav-1 knockout mice have nearly no cavin-1 expression, and cavin-1 knockout mice have diminished Cav-1 expression (15,16). When fibroblasts are swelled by a 10-fold decrease in osmotic strength, cavin-1 is released from the plasma membrane as caveolae disassemble to provide more membrane area (17).

Before cavin-1 was identified as a structural adaptor for caveolae, it was recognized for its role in modulating cellular transcriptional activity (18). Cavin-1/PTRF promotes ribosomal DNA transcription by binding to the 3' pre-RNA, allowing the release of pre-RNA and Polymerase I from the transcription complex (19). Cavin-1 not only plays a role in transcript release, but it increases the overall rate of transcription in a concentration-dependent manner. In adipocytes, insulin stimulation causes phosphorylation of cavin-1 promoting its translocation from caveolae to the nucleus (19) suggesting a role in signal transduction. The importance of cavin-1 expression is seen in knock-out mice that show diverse abnormalities consistent with impaired ribosome biogenesis including abnormal growth failure, loss in fat, resistance to obesity, impaired exercise ability, muscle hypertrophy, altered cardiac and lung function (see (20)). Pertinent for this study are reports suggesting that increased cavin-1 expression promotes cellular stress responses to toxic agents which many be traced to binding to p53 in the cytosol (21).

The connection between cavin-1's ability to regulate caveolae structure and promote ribosomal RNA suggests that any mechanism that destabilizes cavin-1's interactions with caveolin including caveolae deformation, would impact transcription and transitional processes through cavin-1. Here, we show that changes in environmental conditions, such as mild osmotic stress, addition of neurotransmitter, or exposure toxins drives cavin-1 from the plasma membrane to impact RNA transcription and two processes that regulate protein translation (i.e. stress granule and p-body formation). Our results suggest that cavin-1 molecules of caveolae acts as sensors to inform the cell interior of environmental stress.

4.2 MATERIALS AND METHODS

4.2.1 Cell Culture

Rat aortic smooth muscle (A10) cells were purchased from ATCC and used as described (8). Wystar Kyoto rat 3M22 (WKO-3M22) cells, originally obtained from ATCC, were a generous gift from Dr. Marsh Rolle. Mouse Embryonic Fibroplasts (MEFs) were a generous gift from Dr Liu Libin (Boston University School of Medicine). WKO-3M22 cell lines were cultured in high glucose DMEM (Corning) without L-glutamine with 10% fetal bovine serum, 1% sodium pyruvate, 1% non-essential amino acids (VWR) and 1% L-glutamine (VWR). MEFs were cultured in high glucose DMEM (Corning) without L-glutamine with 10% fetal bovine serum, 1% sodium pyruvate and 1% penicillin streptomycin. All cells were incubated at 37°C in 5% CO2.

4.2.2 Plasmids & Stains

EGFP-human-Argonaute-2 (eGFP-Ago2) was purchased from (Addgene plasmid # 21981) and was prepared in the laboratory of Philip Sharp (MIT). MCherry-Ago2 was a gift from Alissa Weaver (Vanderbilt University). EGFP-G3BP1 was purchased from Addgene (plasmid #119950) and was prepared in the laboratory of Jeffrey Chao (Friedrich Miescher Institute). EGFP- Cavin 1 was a generous gift of Dr Liu Libin (Boston University School of Medicine). CellMask Deep Red Plasma Membrane Stain was purchased by Thermofischer (cat# C10046) for the localization experiments. Plasmid transfections and siRNA knockdowns were done using Lipofectamine 3000 (Invitrogen) in antibiotic-free media. Medium was changed to one containing antibiotic (1% Penicillin/Streptomycin) 12-18 hours post transfection.

4.2.3 Applications of stress conditions

For the control measurements, the media was replaced with Hank's Balanced Salt Solution (HBSS) before imaging. For the hypo-osmotic stress conditions, the medium was diluted with 50% water for 5 minutes before it was removed and replaced with HBSS for imaging. For the arsenite treatment, a stock solution of 100mM arsenite in water was prepared and a total of 10 µL of stock solution was added to 2 mL of media. Cells were exposed to a final concentration of 0.5mM arsenite for 10 minutes before the medium was removed and replaced by HBSS for imaging. For Gαq stimulation, 10 µL of a stock solution of 1 mM carbachol was added to 2mL of media for a final concentration of 5µM. Bradykinin was also used to stimulate Gαq by adding 1 µL of a stock solution of 10 mM bradykinin was added to 2mL of media for a final concentration of 5µM. For the isoproterenol treatment 10 µL of a stock solution of 1 mM carbachol was added to 2mL of media for a final concentration of 5µM. For the heat shock, cells were incubated at 40°C for 1 hour.

4.2.4 RNA Extraction and Dynamic light scattering (DLS)

DLS measurements were carried out on a Malvern Panalytical Zetasizer Nano ZS instrument. For these experiments, total RNA from WKO-3M22 cells was extracted following the instructions from the Qiagen Mini Kit (Cat #: 74104). Prior to RNA extraction, cells were exposed to stress conditions. For these measurements, approximately 50µLof extracted RNA in RNase free water was added in a Hellma Fluorescence Quartz Cuvette (QS-3.00mm). Each sample was run 3 times, 10 minutes per run.

4.2.5 Quantification of cavin-1 cellular localization by fluorescence imaging

Cell localization of eGFP-cavin-1 was assessed by combining multiple images of cells whose compartments were identified with fluorescent markers to the nucleus (DAPI), and the plasma membrane (CellMask), and tracking the shifts in eGFP-cavin-1 fluorescence intensity distribution relative to these coordinates in real time when cells are subjected to various stress conditions. A Horizontal Line Profile (H-Line Profile) was generated with counts vs pixel X where each intensity pixel corresponded to a unique coordinate location in the cell. These unique coordinates were matched to the plasma membrane, cytosolic and nucleus compartments based on the location of

DAPI and the CellMask plasma membrane stain and the relative location of the eGFP-cavin1 to these compartments were calculated.

4.2.6 Immunostaining and Particle analysis

Cells were grown to ~75% confluency and exposed to stress conditions, then fixed with 3.7% formaldehyde, permeabilized using 0.2% Triton X-100 in PBS then blocked using 100% Fetal Bovine Serum (FBS). Cells were then stained with primary antibodies incubated for 2 hours at room temperature or overnight at 4°C, washed and treated with a fluorescent secondary antibody for 1 hour. Some of the primary antibodies that were used were anti-PABPC1 (Santa Cruz sc-32318), antiG3BP1 (Santa Cruz sc-81940) and anti-LSM14A ABclonal Cat NO: A16682). After another wash, the 35mm MatTek glass bottom culture dishes were then imaged on the ISS Alba FLIM 2-photon confocal microscope using a 100X/1.49 oil TIRF objective to microscopically count the number of particles formed under different conditions per µm2. For each condition, 10-12 cells were randomly selected, and z-stack measurements were taken (1.0 µ/frame). Analysis was performed using ImageJ where each measurement was thresholded before averaging the number of particles per frame per measurement. Statistical significance was calculated using SigmaPlot with either a Student's t-test, Tukey Test or Anova on Racks.

4.2.7 Number and Brightness (N&B) measurements

N&B theory and measurement has been fully described (see (30)). Experimentally, we collected ~100 cell images viewing either free eGFP (control) or eGFP-Ago2, at a 66nm/pixel resolution and at a rate of 4 µs/pixel. Regions of interest (256x256 box) were analyzed from a 320x320 pixel image. Offset and noise were determined from the histograms of the dark counts performed every two measurements. Number and Brightness (N&B) data was analyzed using SimFC (www.lfd.uci.edu).

4.2.8 N&B analysis

N&B defines the number of photons associated with a diffusing species by analyzing the variation of the fluorescence intensity in each pixel in the cell image. In this analysis, the apparent brightness, B, in each pixel is defined as the ratio of the variance, σ, over the average fluorescence intensity $<k>$:

$$BB = \sigma\sigma 2/< kk >. \text{ and } < kk > = \epsilon\epsilon\epsilon$$

where n is the number of fluorophores. The determination of the variance in each pixel is obtained by rescanning the cell image for ~100 times as described above. The average fluorescence intensity, <k> is directly related to the molecular brightness, €, in units of photons per second per molecule, and n. B can also be expressed as

$$BB = \epsilon\epsilon + 1$$

And the apparent number of molecules, N, as

$$NN = \epsilon\epsilon\epsilon\epsilon /(\epsilon\epsilon + 1)$$

4.2.9 Western blotting

Samples were placed in 6 well plates and collected in 250µL of lysis buffer that included NP-40 and protease inhibitors as mentioned before, sample buffer is added at 20% of the total volume. After SDS-PAGE electrophoresis, protein bands were transfer to nitrocellulose membrane (Bio-Rad, California USA). Primary antibodies include anti-PLCβ1 (Santa Cruz sc-5291), anti-Ago2 (abcam ab32381), anti-actin (abcam ab8226) and anti-eGFP (Santa Cruz sc-8334. Membranes were treated with antibodies diluted 1:1000 in 0.5% milk, washed 3 times for 5 minutes, before applying secondary antibiotic (anti-mouse or anti-rabbit from Santa Cruz) at a concentration of 1:2000. Membranes were washed 3 times for 10 minutes before imaging on a BioRad chemi-doc imager to determine the band intensities. Bands were measured at several sensitivities and exposure times to ensure the intensities were in a linear range. Data were analyzed using Image-J.

4.3 RESULTS

4.3.1 Expression of Cav1 alters protein expression in response to stress

We have previously found that the binding of cytosolic PLCβ to the promoter of RISC (C3PO) inhibits its activity to regulate the silencing of select genes, and that this effect is reversed upon Gαq activation (12,22-24). Specifically, we found that activation of Gαq drives cytosolic PLCβ to the plasma membrane releasing inhibition of the promoter of RISC and reversing silencing of

GAPDH by siRNA, but not Hsp90. We tested the idea that, because the caveolae enhances activation of Gαq (5), which shifts the cytosolic population of PLCβ to the plasma membrane, then caveolae expression could indirectly regulate of GAPDH.

Using rat aortic smooth muscle (A10) cells, we quantified the production of GAPDH, along with Hsp90 and Ras for comparison, when Cav1, Gαq and PLCβ were downregulated. We first found that reducing Cav1 changes the level of actin and reduces the level of other cellular proteins (see below) making direct impact of Cav1 levels difficult to assess. We therefore took a more indirect approach. Because caveolae provides mechanical strength to cells, we subjected cells to mild osmotic stress that will deform caveolae and eliminate its stabilization of the Gαq/PLCβ pathways (8). We reduced the osmolarity of the media from 300 to 150 mOsm in control cells and cells treated with siRNA(Cav1) and quantified changes in GAPDH, Hsp90 and Ras levels (**Fig. 4.1**, where samples blots are shown in *Supporting information 4.1*). Differences between the two cell groups were not immediate but appeared ~12 hours after continuous osmotic stress suggesting that Cav1 impacts slower transcription and/or translation processes rather than more rapid degradation or other down-regulation mechanisms. In contrast to Cav1, down-regulating Gαq had little or no effect, as did down-regulating PLCβ1 although these cells contain little PLCβ1 (25). These results argue that the Gαq/PLCβ pathway is not the primary factor underlying changes in protein production. These data suggest that Cav1 levels impact the ability of cells to produce proteins under hypo-osmotic stress conditions.
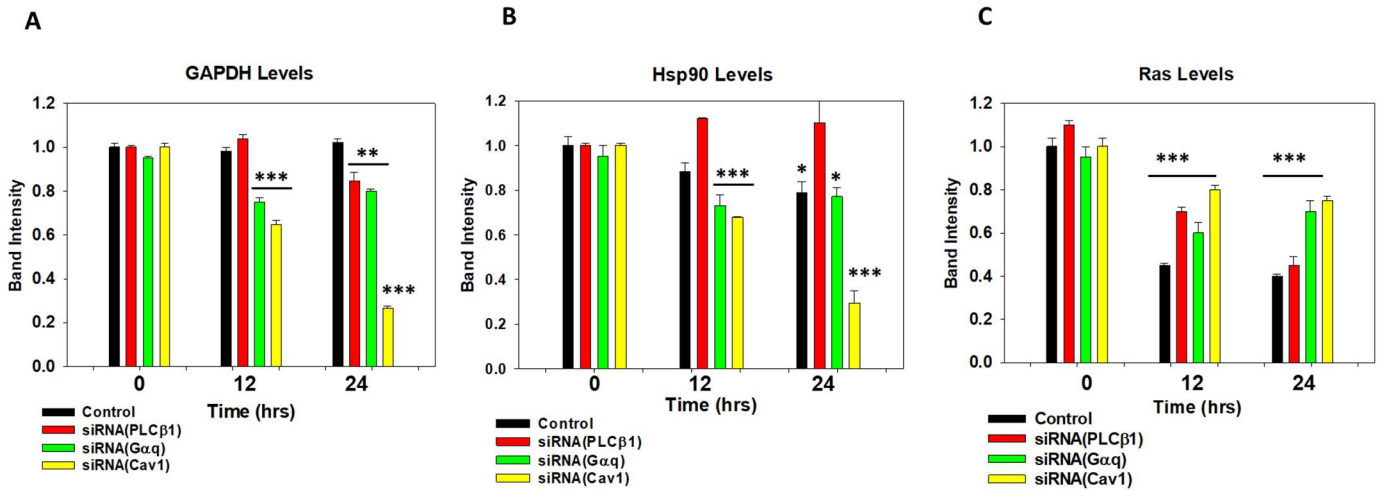
Figure 4.1: Down-regulation of Caveolin 1 impacts protein levels. Changes in proteins levels of A- GAPDH, B- Hsp90, C- Ras in rat aortic smooth muscle (A10) in control (black), siRNA PLC (red), siRNA Gαq (green) and siRNA Caveolin 1 (yellow) cells where n=3 and the asterisks correspond to p values with one asterisk being 0.1<p<0.5, two asterisks meaning p<0.05 and three asterisks indicating p<0.001. An example western blot is shown in Supporting information 1.

4.3.2 Cavin-1 shifts its cellular localization under osmotic stress

Expression of Cav1 and cavin-1 are interdependent ((16) and Supporting information 4.2A) and so we tested whether the protein changes observed in Fig.1 might be due to cavin-1 levels since cavin-1 promotes transcription of ribosomal RNA (18). While previous studies found that high osmotic stress disassembles caveolae releasing cavin-1 from the plasma membrane (17), it is unclear whether release will occur at the mild, physiological stress conditions used here which deforms but not disassembles caveolae (9).

Cavin-1 relocalization studies were carried out in intact Wistar Kyoto smooth muscle cells (WKO-3M22) which are flat and easily imaged. Cells were transfected with eGFP-cavin-1 and shifts in the cellular distribution of fluorescence intensity with hypo-osmotic stress by confocal were measured. Under basal conditions, we find that eGFP-cavin-1 localizes on the plasma membrane with small amounts in the cytoplasm and nucleus (**Fig. 4.2A**). Because the additional, transfected protein would increase total cellular cavin-1 and effect its localization, we repeated these studies

by first down-regulating cavin-1 by ~95% before transfecting with eGFP-cavin-1 (see *Supporting Information 4.2,4.3*). We than quantified the eGFP-cavin-1 fluorescence intensity on or close to the plasma membrane, the cytosol and the nucleus (see Methods). In this case, the observations were similar with the intensity being slightly lower on the plasma membrane as compared to the nucleus, and no intensity could be detected in the cytosol, suggesting that endogenous cavin-1 is mainly distributed between the plasma membrane and nuclear compartments (see *Supporting Information 4.3*).

When we subjected wild type eGFP-cavin-1 cells to mild hypo-osmotic stress, a large portion of the plasma membrane GFP-cavin-1 intensity shifts to the cytosol and the nucleus (**Fig. 4.2B-C**) again by tracking the fluorescence intensity relative to the plasma membrane, cytosol, and nucleus (see Methods). Interestingly, when cells are subjected to bradykinin stimulation, cavin-1 relocalizes to the nucleus. In contrast, when we subjected cells to isoproterenol which does not stimulate Gαq, eGFP-cavin-1 remains outside the nucleus (**Fig. 4.2C**). To test the idea that cavin-1 shifts to the nucleus when caveolae domains are disrupted, we down-regulated Cav-1 and found that little cavin-1 is associated with the plasma membrane under these conditions (**Fig. 4.2E-G**). Taken together, these data show that caveolae deformation, as well as disassembly, has the potential to promote nuclear localization of cavin-1 allowing it to function as a transcription activator.

We also tested whether other stress conditions impact cavin-1 localization. Because Cav1 / Gαq interactions strengthen when is activated, we determined whether Gαq stimulation would in turn change cavin-1/Cav1 interactions and cavin-1 localization. To this end, we find that addition of carbachol to activate Gαq promotes relocalization of GFP-cavin-1 to the nucleus (see Supporting Information). This relocalization is much more pronounced when Gαq is stimulated with bradykinin, since these cells are rich in bradykinin receptors (**Fig.4.2C-F**), and we note that siRNA(Cav1) slightly diminishes Gαq protein levels (*Supporting Information 4.2).* Additional cell images are displayed in *Supporting Information 4.4*). Because both carbachol and bradykinin can stimulate Gαi in addition to Gαq, we stimulated cells with isoproterenol, which does not activated Gαq. In this case, shifts in intensity to the nucleus are not observed (**Fig. 4.2C-D**). We also found that treating cells with arsenite, which promotes a p53 response and is correlated to

cavin-1 activity (26), also promotes cavin-1 nuclear localization, but to a lesser extent compared to Gαq activation. Interestingly, when caveolin-1 is down-regulated, cavin-1 nuclear relocalization is more pronounced in arsenite treated cells compared to carbachol stimulated ones (**Fig.4.2E-G**).

D

	Control	Osmotic Stress	Bradykinin	Isoproterenol
Merge				
eGFP-cavin-1				
DAPI				
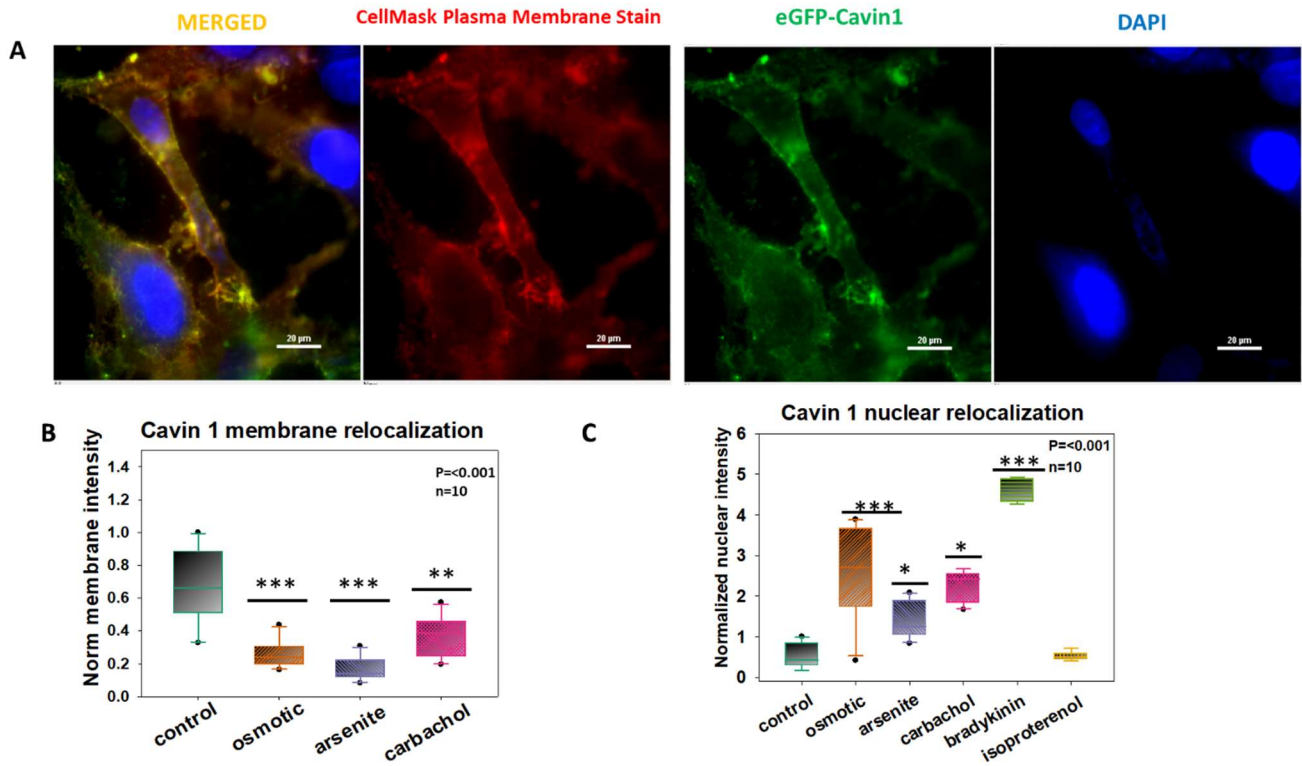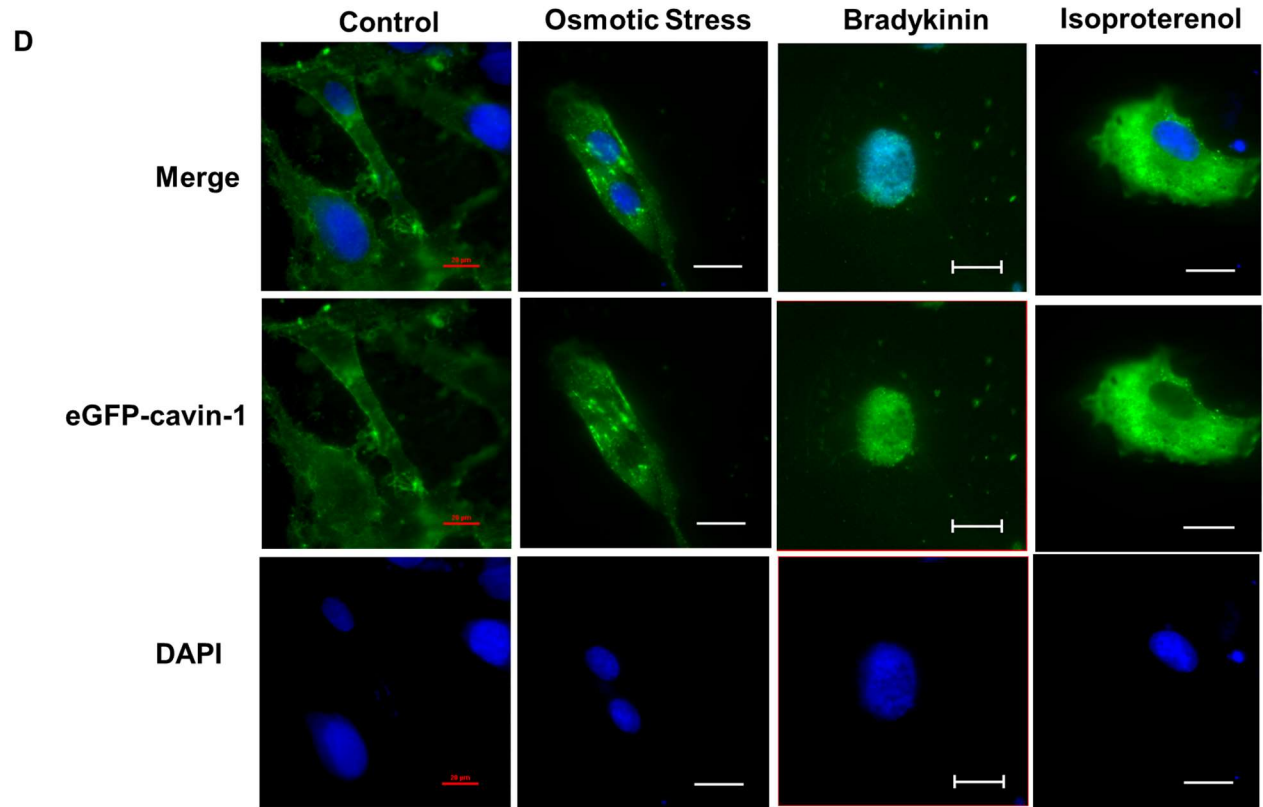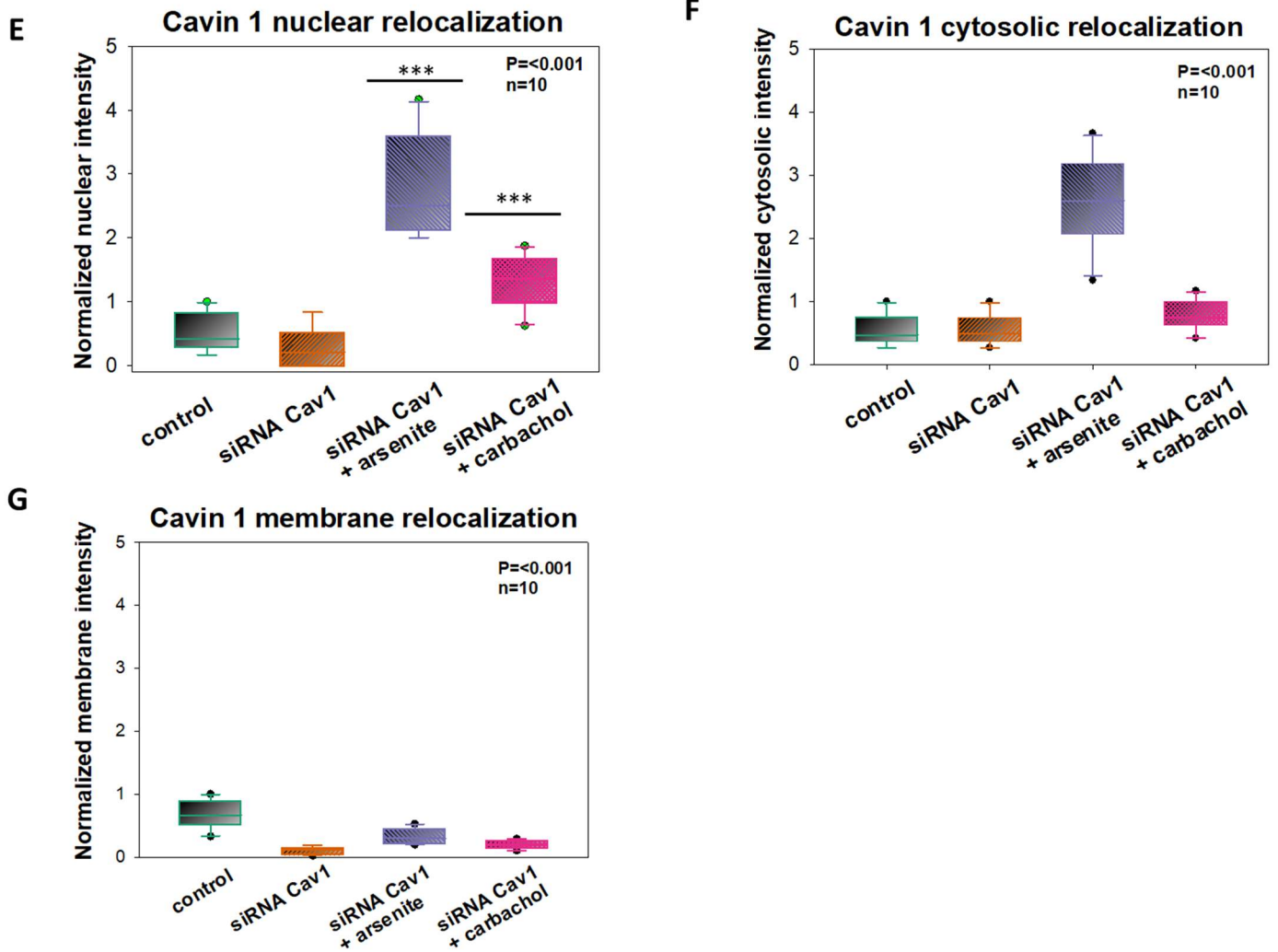
Figure 4. 2: Cavin-1 relocalization in WKO-3M22 cells. A- Sample fluorescence images of fixed WKO-3M22 cells transfected with eGFP-Cavin1 (green) and stained with CellMask Deep Red Plasma Membrane stain (red) and DAPI (blue) under control conditions as obtained at 60X magnification and focusing on the bottom of the cell. Scale bars are 20 μm long. B, C- Cell localization of eGFP-cavin-1 was assessed in subjected to hypo-osmotic (orange), arsenite (purple), Gαq stimulation with carbachol (pink), bradykinin stimulation (green) and isoproterenol treatment (yellow). eGFP-cavin-1 localization was determined by measuring the pixel intensities to coordinates to the plasma membrane, cytosolic and nucleus compartments based on the location of DAPI and the CellMask plasma membrane stain (see Methods). Changes in membrane (B) and nuclear localization (C) in wild type cells. Intensities were normalized to the plasma membrane control. The asterisks correspond to p values with one asterisk being $0.1 < p < 0.5$, two asterisks

meaning p<0.05 and three asterisks indicating p<0.001. D - Sample fluorescence images of fixed WKO-3M22 cells transfected with eGFP-Cavin1 (green) and stained DAPI (blue) under control, hypo-osmotic, bradykinin stimulation and isoproterenol treatment respectively as imaged by epifluorescence with 60X magnification. Scale bars are 20 μm long for the control samples and 10 μm long for the rest of the conditions. E-G- Cell localization of eGFP-cavin-1 in cells treated with siRNA(Cav1) in the nucleus (E), cytosol (F) and membrane compartments (G).. Intensities were normalized to the control of the nuclear population. All measurements are an average of 3 independent experiments that sampled 10 cells, where SD is shown and where the p values were determined using Student t-test where each data set was compared to control.

The data in **Fig.4.2** show that several stress conditions promote movement of cavin-1 from the plasma membrane to the nucleus, which would be expected to increase protein production based on cavin-1's nuclear function. However, this is not seen in **Fig.4.1** where similar or lower levels of proteins, normalized for actin and changes in total protein content, were observed. Therefore, we investigated other mechanisms through which Cav1 would influence protein levels.

4.3.3 Transient down-regulation of Cav1 or cavin-1 affects the amount of cytosolic RNAs and their size distribution

In the studies above, we observed that down-regulating Cav1 or cavin-1 results increases cell death by ~40% and ~52%, respectively, as estimated by comparing the number of transfected to control cells in 3-5 culture dishes. We postulated that this increase in mortality is due to decreased transcription and protein loss caused by reduced levels of cavin-1. To this end, we measured changes in the levels of cytosolic RNA (**Fig. 4.3A**). These studies were done by isolating the cytosolic fractions of WKO cells, removing the nuclear and lipid components, and isolating the RNA after protein digestion and lipid solubilization (see Experimental Procedures). We find that down-regulating Cav1 by 60% and cavin-1 by 38%, as estimated by western blotting in WKO-3M22 cells (*Supporting Information 4.2*), resulted in a 5-fold reduction of cytosolic RNA while down-regulating cavin-1 by 94% and Cav1 by 74% resulted in a ~13 fold reduction (**Fig. 4.3A**). Notably, subjecting cells to osmotic stress also reduced cytosolic RNA levels even though more cavin-1 was nuclear (**Fig. 4.2C**).

We characterized relative size distributions of the cytosolic RNA populations by dynamic light scattering (DLS). We find that the transcripts effected by Cav1 down-regulation are smaller in size suggesting a higher level of processing. The RNA seen when cavin-1 is down-regulated is very large suggesting reduced processing, and the relative amount of the larger sized population decreases with the application of stress (**Fig. 4.3B-E**). The loss in RNA with Cav1/cavin-1 is consistent with reduced proliferation due to reduced transcription, and the shifts in the sizes of cytosolic RNA suggests that Cav1/cavin-1 levels impact RNA processing. We interpret the changes in with carbachol as being due to the release of the nuclease C3PO under control conditions to process larger RNAs (12), and the loss of stabilization of activated Gαq when Cav1/cavin-1 are down-regulated (5).
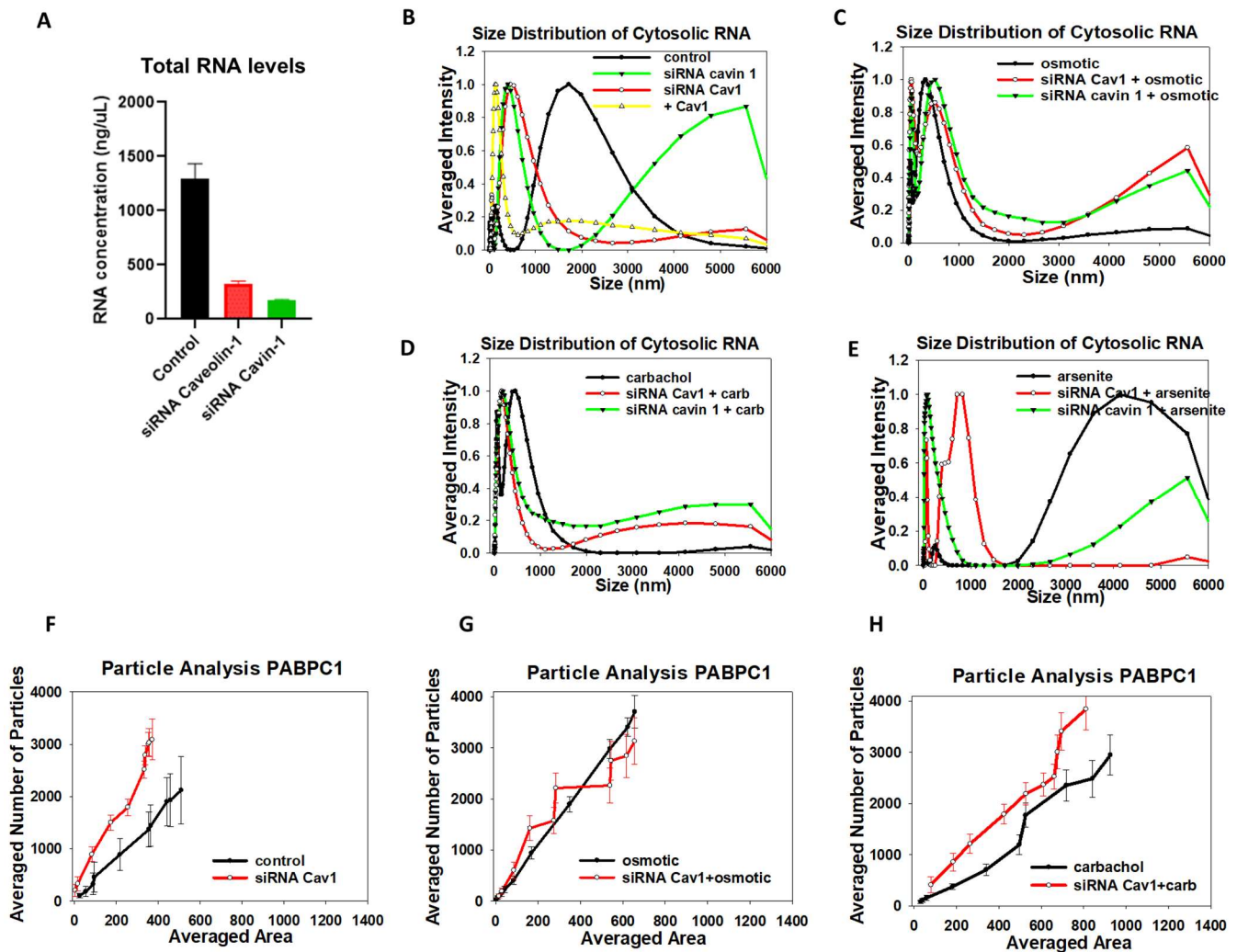
Figure 4. 3: Cav1 effects cytosolic RNA size distribution and stress granules in WKO-3M22 cells. A- RNA from WKO-3M22 cells treated with siRNA (Cav1) (red) and siRNA(cavin-1) (green) was extracted and quantified (see methods). B- Normalized DLS spectra showing the size distributions of cytosolic RNA isolated from WKO-3M22 cells under control conditions (black), siRNA(Cav1) treated cells (red), cavin-1 overexpression (yellow), and siRNA(cavin-1) (green) down-regulation. C- Similar study as in (B) for cells subjected to hypo-osmotic stress (150 mOsm 5min), and D- cells subjected to Gαq stimulation with carbachol treatment (5μM, 10min). Each sample was scanned 3 times with 10 minutes per run. The number of independent samples were 6 per condition. F-H - The size and number of particles associated with monoclonal anti-PABPC1 in the cytosol of fixed and immunostained WKO-3M22 cells was measured on a 100x objective and analyzed using Image J (see methods). Comparison of cells with siRNA (Cav1) to mock-transfected under basal conditions (F), hypo-osmotic stress (150 mOsm, 5 minutes) (G), Stimulation of Gαq by treatment with 5 μM carbachol (H). All measurements are an average of 3 independent experiments that sampled 10 cells, where SD shown and where the p values were determined using ANOVA.

Additionally, transfection of cavin-1 to WKO cells treated with siRNA(cavin-1) showed DLS spectra similar to control (*S4.7*). We note that the percentage of rRNA to cytosolic RNA levels is reduced when Cav1 or cavin-1 is down-regulated as indicated by weaker contribution of the 18S and 28S ribosomal RNA bands (*S4.4, S4.7*).

4.3.4 Transient loss of Cav1/cavin-1 impacts stress responses

The changes in size distributions in **Fig. 4.3** suggest that Cav1/cavin-1 levels or stress conditions impact cytosolic RNA processing. To better understand these changes, we looked at the two major mechanisms used by cells to handle cytosolic RNA: processing bodies (p-bodies) and stress granules. P-bodies are associated with RNA degradation as well as RNA storage (27), and stress granules are halted ribosomal RNA complex that protect mRNA during stress conditions, such as the hypo-osmotic conditions used here (28). Stress granules and p-bodies have an overlapping storage function and both contain Ago2 (29) which either stalls mRNA translation or degrades mRNA depending on the amount of base pairing between the Ago2-bound miR and the mRNA.

Since both stress granules and p-bodies require RNA, their assembly will be inhibited by the reduced RNA levels accompanying cavin-1 down-regulation.

We first tested whether Cav1/cavin-1 down-regulation changes the number and size of stress granules under basal conditions. These studies were carried out by immunostaining WKO-3M22 cells treated with either control or Cav-1 siRNA and immunostaining for the stress granule marker, polyadenylate binding protein (cytosolic) -1 (PABPC1). The size and area of PABPC1 particles were then quantified from high-resolution fluorescence confocal images (see Methods). In **Fig 4.3F,** we show a comparison of control and siRNA (Cav1) in cells under basal conditions. We find that loss of Cav1/cavin-1 results in more numerous but smaller particles consistent with smaller RNAs seen by DLS.

We then determined whether reducing Cav1/cavin-1 levels change the ability of cells to form PABPC1 particles (i.e. stress granules) under hypo-osmotic stress or carbachol stimulation (**Fig. 4.3G-H**). We find that reduced Cav1/cavin-1 levels did not affect particle formation in cells subjected to osmotic stress and produced a small increase in the number of fewer particles in cells stimulated with carbachol. These results suggest that the reduced levels of GAPDH and Hsp90 caused by Cav1 down-regulation (**Fig. 4.1)** are not due to confinement of their mRNAs into large stress granules.

The reduction in cytosolic RNA may result in smaller stress granules that might be missed in immunostaining studies. In a second series of studies, we monitored stress granule formation in live cells using the stress granule assembly protein G3BP1 tagged with eGFP. This construct allowed us to monitor small aggregates by a fluorescence correlation method (N&B) which senses small aggregates. N&B is a fluorescence method which follows the diffusion of a fluorophore in an image series, and compares the number of photons associated with this diffusion to a monomeric control, such as free eGFP (30). This method allows us to determine small particles that might be missed in confocal imaging.

In **Fig 4.4,** we show control cells transfected with eGFP-G3BP1 and subjected to various stress conditions. The amount of aggregation with each stress condition correlates to amount of cavin-1

relocalization seen in **Fig 4.2**; carbachol stimulation showed the highest amount of aggregation, followed by osmotic stress and then arsenite. When Cav1/cavin-1 was down-regulated, no changes in G3BP1 aggregation were observed except for osmotic stress which showed a small, residual change that might be due to residual Cav1. These results suggest that lowering Cav1/cavin-1 levels make cells less able to adopt mechanisms that protect them from environmental stress.
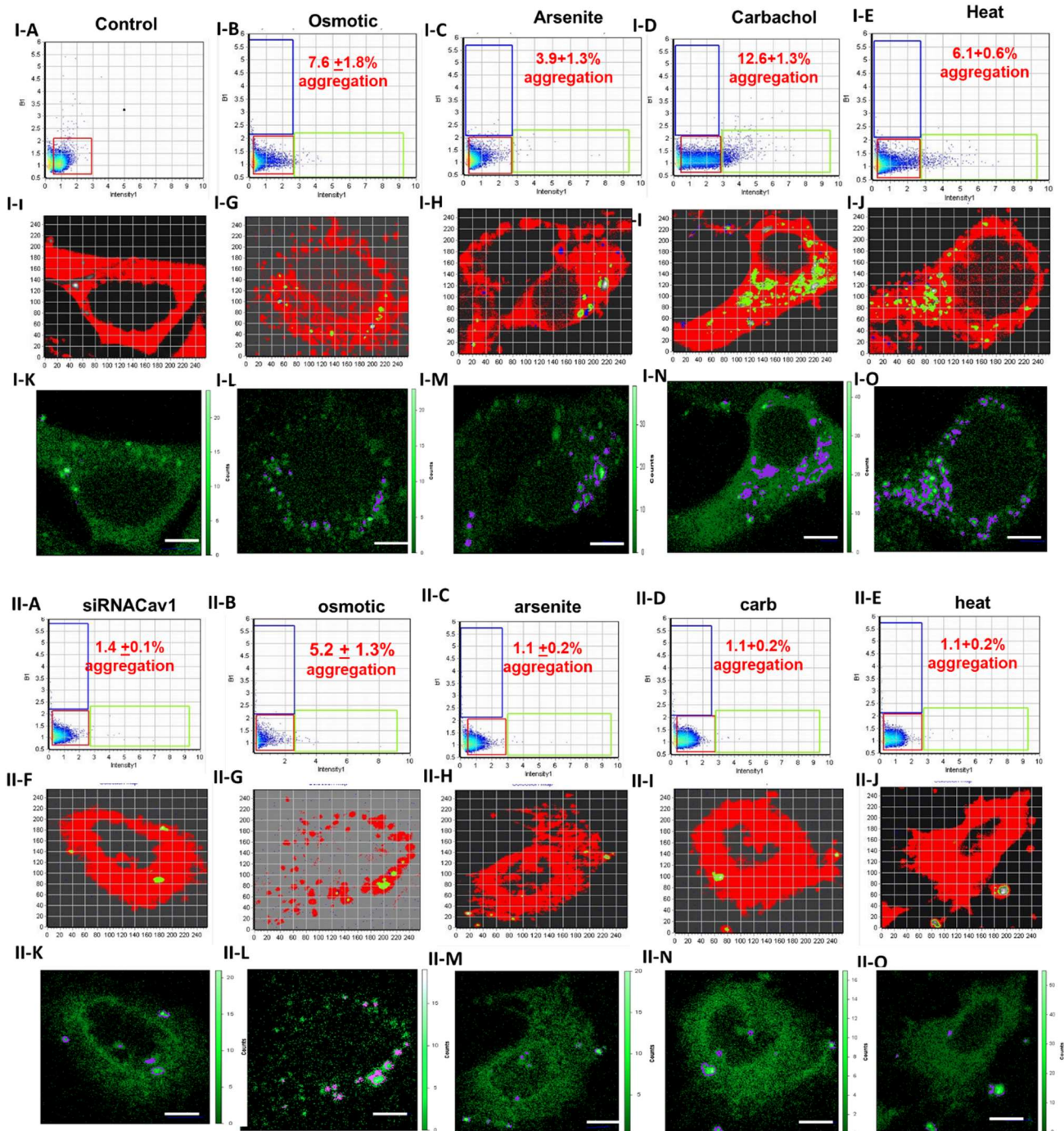
Figure 4.4: N&B analysis of eGFP-G3BP1 aggregation in WKO-3M22 cells. I- The top panels (I-A –I-E) show graphs of the brightness versus intensity with the pixels of the colored boxes corresponding to the specific regions in the cells (I-F – I-J) using SIM-FCS 4 software. The bottom panels show the corresponding fluorescence microscopy images in ISS (I-K –I-O). The red box corresponds to monomeric eGFP-G3BP1 while points outside this box and in the green and blue boxes correspond to higher order species. Panels I-A, I-F,I- K are control cells (n=8); Panels I-B, I-G, I-L are cells subjected to hypo-osmotic stress (150 mOsm, 5 min) (n=6); Panels I-C, I-H, I-M are cells subjected to arsenite stress (0.5mM, 10 min) (n=6); Panels I-D, I-I, I-N are cells subjected to carbachol stimulation (5µm, 10 min)(n=6); Panels I-E, I-J, I-O are cells subjected to heat shock (42°C, 60 min)(n=6); Scale bars are 10 µm long. Part II is similar to Part I for cells treated with siRNA(Cav1) (n=6). Scale bars are 10 µm long.

It is also possible that reduced cytosolic RNA with Cav1/cavin-1 knock-down will impact p-bodies. We used the p-body marker, LSM14A, which is associated with inactive mRNA storage, to monitor the formation of p-bodies on the micron scale (31,32). High-resolution confocal images were analyzed to determine the number and area of LSM14A particles. Compared to control cells, down-regulating Cav1 had little effect on p-bodies, but down-regulating cavin-1 results in a greater number of LSM14A particles (**Fig. 4.5**) showing that the available RNA available is not being processed, which is consistent with reduced ribosome activity (see *Discussion*). Additionally, we find that carbachol stimulation increases formation of LSM14A containing p-bodies while osmotic stress has no effect.
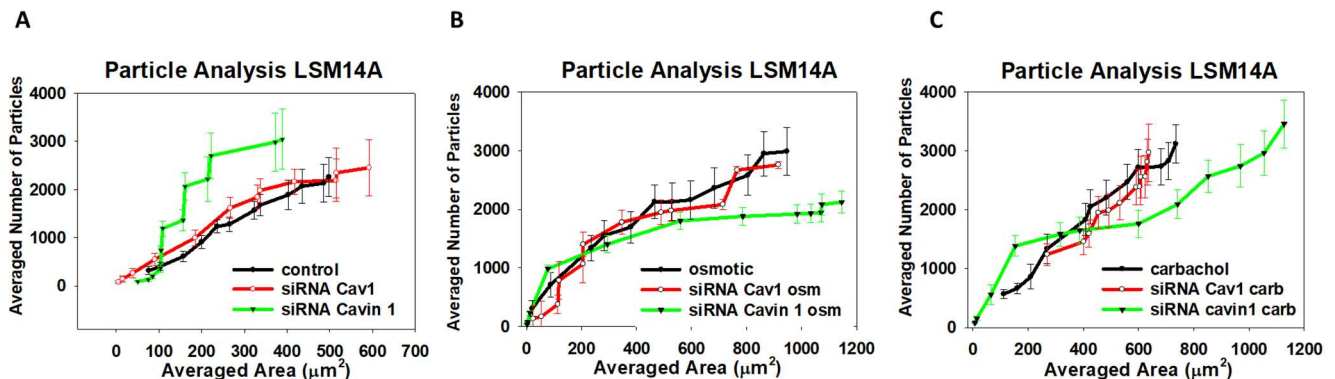
Figure 4.5: Cavin 1 impacts LSM14A containing P-body formation. The size and number of particles associated with monoclonal anti-LSM14A in the cytosol of fixed and immunostained WKO-3M22 cells was measured on a 100x objective and analyzed using Image J (see methods). Comparison of mock treated and cells treated with siRNA(cavin-1) or siRNA(Cav1) under basal conditions (A), hypo-osmotic stress (150 mOsm, 5 minutes) (B), and stimulation with 5 µM carbachol (C). All measurements are an average of 3 independent experiments that sampled 10 cells, where SD shown and where the p values were determined using ANOVA.

The studies above indicate that Cav1/cavin-1 levels primarily affect the formation of stress granules that form under various environmental conditions rather than p-bodies, which are associated with RNA storage and degradation under basal conditions. Therefore, we sought to investigate the effect of Cav1/cavin-1 on the formation of large and small aggregates containing Ago2, which aggregates in cells subjected to osmotic stress or Gαq activation (33). We monitored stress-induced aggregation of eGFP-Ago2 in live cells with Cav1/cavin-1 down-regulation. When viewing Ago2 aggregates in control cells by fluorescence microscopy, we find that environmental stress does not significantly impact the size and number of Ago2 particles (**Table 4.1** and *Supporting information 4.9*) and only minor changes, similar to PABPC1 particles, are seen for cells treated with siRNA (Cav1). When we view small Ago2 particles in control cells by N&B analysis, we find a large effect due to osmotic and carbachol stress but little change with heat and arsenite (**Table 4.1**). These results show that down-regulation of Cav1/cavin-1 reduces stress-induced aggregation, most likely due to reduced cytosolic RNA levels **(***Supporting information 4.10***).**

Table 4.1: Stress responses quantified by Particle Analysis and N&B. Shown are values for the slopes of the Particle Analysis curves (i.e. number versus area of particles), and the N&B values. Changes over four-fold are shown in red.

	Particle Analysis		N&B	
	Ago2	**PABPC1**	**Ago2**	**G3BP1**
Control	1.82	4.18	n/a	n/a
osmotic	1.63	**5.56**	**34**	**7.6**
carbachol	1.69	**3.21**	**19**	**12.6**
Arsenite	1.55	2.87	5	3.9
heat	1.46	3.07	3.9	**6.1**
siRNA Cav1	2.47	**7.62**	5.3	1.4
siRNA Cav1 + osmotic	1.69	4.27	2.3	**5.2**
siRNA Cav1 + carbachol	3.12	4.43	0.4	1.1
siRNA Cav1 + arsenite	1.74	**6.05**	1.3	1.1
SiRNA Cav1 + heat	**5.31**	4.46	**16.4**	1.1
siRNA cavin-1	2.27	3.45	**9.9**	1.3
siRNA cavin-1 + osmotic	1.39	2.89	3.6	1.6
siRNA cavin-1 + carbachol	**7.32**	**7.39**	4	1.2
siRNA cavin-1 + arsenite	1.76	**5.89**	2.9	1.2
siRNA cavin-1 + heat	3.01	2.97	2.6	1.2

.

4.3.5 Cavin-1 knock-out cells show widespread phenotypic changes as well as adaptive behavior

We obtained a strain of mouse embryonic fibroblasts (MEFs) where cavin-1 was knocked out using CRISPR/Cas9 genome editing technology (19). These knock-out cells have a threefold longer doubling time and a more trapezoid morphology as compared their wild type counterparts where the circularity dropped from 0.78+.2, n=16 to 0.55+.3, n=16. Additionally, we were unable to visualize caveolae by Cav1 immunostaining which is consistent with the absence of these caveolae, and these cells had a 55%-68% lower level of Cav-1 as quantified by western blot (Supporting information 2F). Surprisingly, we find that the cytosolic RNA levels of the knock-out cells were identical to the wild type in sharp contrast to transient down-regulation of Cav1/cavin-1.

4.3.6 Cavin-1 knock-out cells show different cytosolic RNA size distributions

The adaptive changes in cytosolic RNA in the KO cells gives us the opportunity to understand the effects of cavin-1 at constant levels of cytosolic RNA. We find that even though the cytosolic RNA levels in the cavin-1 KO are the same as wild type, their size distributions are very different (**Fig. 4.6A-C**). Cytosolic RNA of wild type cells has two populations: a major one at small RNA sizes and a minor one at larger sizes. These populations are reversed in the knock-out cells; the peak at small RNA sizes was only 1/3 as high as the one at larger sizes. When we increase the expression of cavin-1 by over-expressing Cav1 in the knock-out cells, we find a shift in RNA sizes towards wild type values.

The shift to larger cytosolic RNAs sizes in the knock-out cells could be due to reduced processing. To test this idea, we subjected wild type cells to carbachol or hypo-osmotic stress to halt mRNA processing. These stresses reduced the amount of small RNAs consistent with the halting of Ago2 activity due to stress granule formation. The loss of small cytosolic RNAs in the wild type cells results in a DLS spectrum similar to unstressed knock-out cells. In contrast, subjecting cavin-1 knock-out cells to stress did not significantly change the cytosolic RNA size distribution. Thus, we interpret the higher sizes in the knock-out cells as being caused by reduced RNA processing (**Fig. 4.6D-E).**
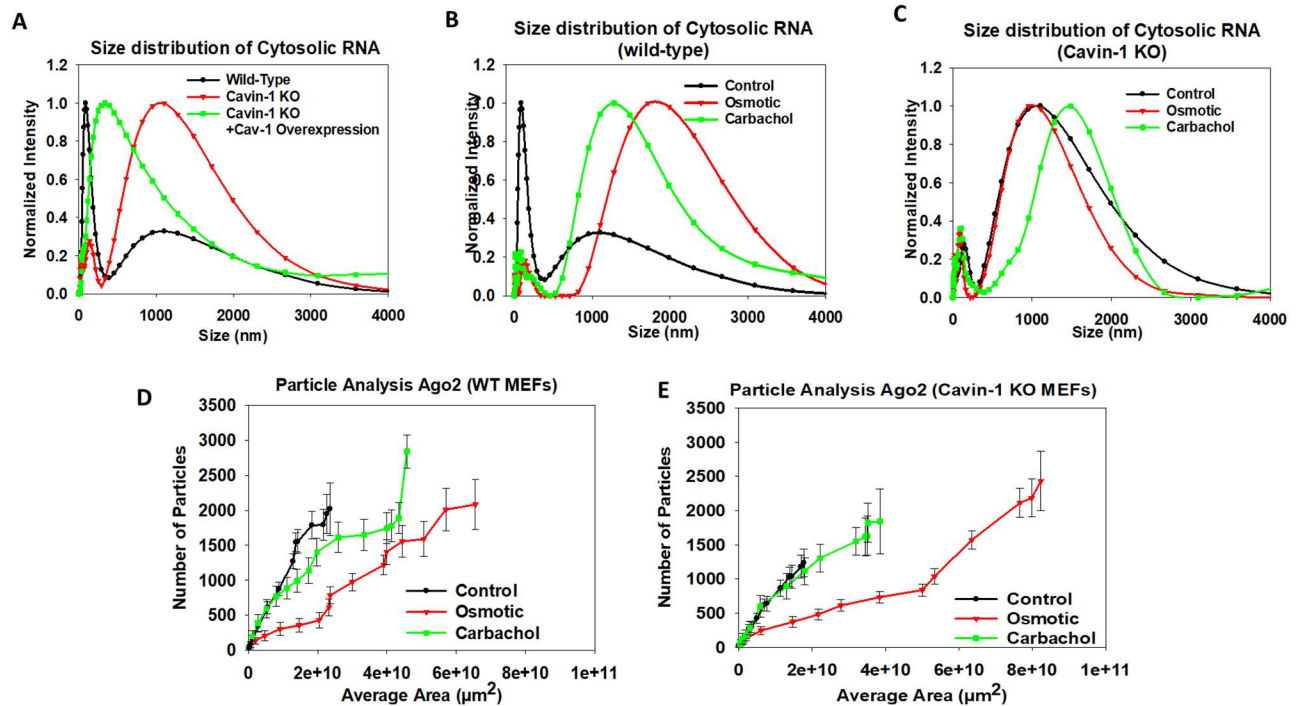
Figure 4.6: RNA size distribution and formation of eGFP-Ago2 particles in wild type and cavin-1 KO MEFs. A- Normalized DLS spectra showing changes in the size distribution of cytosolic RNA isolated from MEFs for mock treated control cells (black), cavin-1 knock-out cells (red) and cavin-1 KO cells over-expressing Cav1 (green). B- DLS spectra of cytosolic RNA from wild type MEFs under control conditions (black), hypo-osmotic stress (150 mOsm 5 min, red), cells over-expressing of constitutively active Gαq (green). C- An identical study showing the size distribution of cavin1 KO cells under control conditions (black), hypo-osmotic stress (150 mOsm 5min) (red) and carbachol stimulation (5 µM for 10 minutes, green). Each sample was scanned 3 times with 10 minutes per run. The number of independent samples were 6 per condition. D- Size and number of particles associated with anti-Ago2 in the cytosol of MEFs were measured on a 100x objective and analyzed using Image J (see methods) showing treatment of wild type cells with hypo-osmotic stress (150 mOsm, 5 minutes-red) and Gαq stimulation (5 µM carbachol, 10 minutes – green). E- Treatment of cavin-1 KO cells to 5 minutes of osmotic stress (150 mOsm) and carbachol stimulation (5 µM carbachol, 10 minutes – green). Measurements are an average of 3 independent experiments that sampled 10 cells. P values were determined using ANOVA.

The large sizes of cytosolic RNA may be consistent with stalled ribosomal complexes (i.e., stress granules), and we determined the ability of the cavin-1 knock out cells to form stress granules. Particle analysis of wild type and KO cells showed Ago2 particles have are similar in size and number in cells under basal conditions and cells subjected to hypo-osmotic while the knock-out cells produced fewer particles under carbachol stimulation as compared to wild type cells (**Table 4.1,** *Supporting information 4.11*). This reduction is consistent with the reduced levels of Gαq activation due to the loss of caveolae. The size of Ago2 particles formed were greatly enhanced upon Cav1/cavin-1 upregulation indicating some type of a compensatory mechanism (*Supporting Information Table 4.2, Fig. S4.11*). These cells were also highly sensitive to arsenite suggesting that one of the adaptive mechanisms used by these cells is energy dependent. We also viewed small eGFP-Ago2 particles in wild type and cavin-1 knock-out cells by number and brightness (N&B) (*Supporting Information Table 4.1*). As compared to control cells, we find that the cavin-1 knock-out cells have eGFP-Ago2 particles that contain more fluorophores and are more intense. When cells are subjected to hypo-osmotic stress, the knock-out cells show enhanced aggregation which was slightly reversed with Cav1 overexpression **(***Supporting Information 4.12***)**. Thus, even though cavin-1 depleted cells have less particles on the micron scale, they have a larger number of smaller particles, and environmental stress promotes the formation of small Ago2 particles.

4.3.7 Caveolin-1 KO primary smooth muscle cells unable to form stress granule formation *
The following studies were conducted at the Centro Nacional de Investigaciones Cardiovasculares (CNIC) in Madrid, Spain at the lab of Dr Miguel Angel Del Pozo and under the supervision of Dr Asier Echarri. These studies were part of an ongoing collaboration with main goal to understand the role of Cav-1 in stress granule accumulation through aging.

Various studies have been performed in Cav-1 null mice over the years correlating the role of this protein in cancel, diabetes, atherosclerosis, and cardiomyopathy[1]. However, there have been no previous studies examining the role of Cav-1 in defense mechanisms such as stress granule and p-body accumulation. When extracting primary smooth muscle cells from the aortas of different aged mice (4 weeks vs 19 weeks) we were able to examine the effects of aging in stress granule formation along with the role of Cav-1 in this process while using wild type and Cav-1 null mice. Older wild type mice showed more numerous and larger Ago2 stress granule compared to younger

mice. This phenomenon could be easily explained by aging and the fact that these wild type mice become more susceptible to changes the older they grow (**Fig 4.7B**). Previous studies have looked at stress granule formation, composition and dynamics due to aging[2]. Many of them have shown evidence of age-dependent decrease in expression of ATP-dependent chaperone machines along with proteosomes making cells, primarily neuronal, more susceptible. Other studies in skeletal muscle cells examined the role of oxidative stress in stress granule formation and found a delayed SG resolution due to aging[3].

While the role of caveolae and cav-1 in particular has not been properly examined in regards to the physiological stress granule assembly and disassembly, we were eager to understand the mechanisms initiated. When looking at the number and size of particles in cells extracted from 4-week-old wild type versus 4-week-old Cav-1 KO mice, we see that the absence of Caveolin-1 in these smooth muscle cells initiates defensive mechanisms normally due to adaptive mechanisms that have taken the place of cav-1 (**Fig. 4.7A,C,D**). In addition to the absence of Cav-1 when hypo-osmotic stress was applied to these cells for 5 minutes, there was a further increase in Ago2 related particles forming suggesting intact defense mechanisms being present in these cells (**Fig 4.7E**). However, the disassembly rate of these granules due to the exposure in hypo-osmotic stress remains unknown.

When we conducted the same experiment and analysis in older aged mice (19 weeks old) we did not observe similar results. Caveolin-1 KO cells were able to initiate the assembly and disassembly of stress granules as they age (**Fig 4.7G**). In addition, even though cells extracted from wild type 19-week-old mice showed a significant increase in the number and size of Ago2 associated particles, the same behavior was not observed in the Caveolin-1 KO cells suggesting changes in the cytosolic RNA levels and reduced RNA processing occurred (**Fig 4.7F, H,I**). In other words, the data obtained from primary cells support the findings that have been demonstrated throughout this chapter confirming that caveolae deformation affects RNA processing.
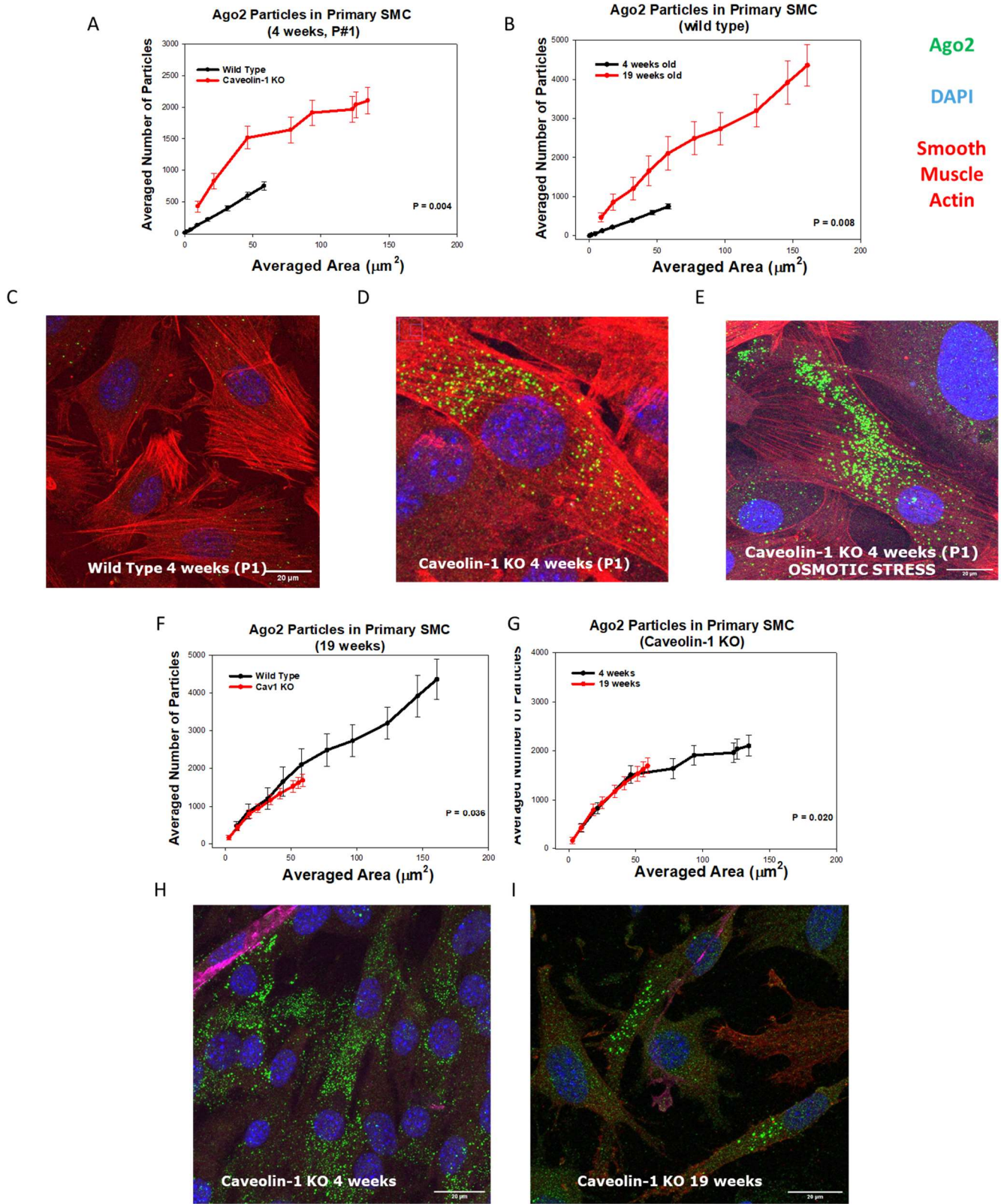
Figure 4.7: Formation of eGFP-Ago2 particles in primary smooth muscle cells. (A)Size and number of particles associated with anti-Ago2 in the cytosol of primary smooth muscle cells

extracted from 4-week-old wild type (black) and Caveolin-1 KO (red) mice. Particles were measured on a 100x objective and analyzed using Image J (see methods). (B) Size and number of particles associated with anti-Ago2 in the cytosol of primary smooth muscle cells extracted from 4-week-old wild type (black) and 19-week-old wild type (red) mice. Smooth muscle cells from wild type 4-week-old mice (C), Caveolin-1 KO 4-week-old mice (D) and Caveolin-1 KO 4-week-old mice exposed to 5 minutes hypo-osmotic stress (E) are shown with Ago2 stained in green, smooth muscle actin stained in red and DAPI stained in blue (see methods). (F) Size and number of particles associated with anti-Ago2 in the cytosol of primary smooth muscle cells extracted from 19-week-old wild type (black) and Caveolin-1 KO (red) mice. (G) Size and number of particles associated with anti-Ago2 in the cytosol of Caveolin-1 KO primary smooth muscle cells extracted from 4-week-old (black) and 19-week-old (red) mice. Smooth muscle cells from Caveolin-1 KO 4-week-old mice (H), Caveolin-1 KO 19-week-old mice (I) are shown with Ago2 stained in green, smooth muscle actin stained in red and DAPI stained in blue.

*4.3.7.1 References ***

[1] R. Hnasko, and M.P. Lisanti, The biology of caveolae: lessons from caveolin knockout mice and implications for human disease. Mol Interv 3 (2003) 445-64.
[2] X. Cao, X. Jin, and B. Liu, The involvement of stress granules in aging and aging-associated diseases. Aging Cell 19 (2020) e13136.
[3] C.J. Rodriguez-Ortiz, J.C. Flores, J.A. Valenzuela, G.J. Rodriguez, J. Zumkehr, D.N. Tran, V.E. Kimonis, and M. Kitazawa, The Myoblast C2C12 Transfected with Mutant Valosin-Containing Protein Exhibits Delayed Stress Granule Resolution on Oxidative Stress. Am J Pathol 186 (2016) 1623-34.

4.4 DISCUSSION

In this work, we have begun to delineate the complex connections between caveolae, mechanical stretch and cell physiology used hypo-osmotic stress to deform caveolae. Caveolae provide mechanical strength to cells and serve as platforms that localize signaling proteins (1). Several years ago, we found a connection between these two functions when we observed that Cav-1/-3 enhances Gαq / calcium signals, and that deformation of caveolae disrupts Cav/Gαq interactions (9). Here, we show that caveolae have an additional role by indirectly helping cells sense and respond to environmental stress conditions by modulating translational and transcriptional processes.

These studies were initiated by work showing that elevating cytosolic PLCβ reverses RNA-induced silencing of GAPDH but not Hsp90 through its inhibition of a promotor of RNA-silencing, C3PO (12). Activation of Gαq drives PLCβ to the plasma membrane promoting both RNA-induced silencing and stress granule formation (12,34). Because Cav-1/-3 stabilizes activated Gαq (5), we postulated that its presence might also affect protein production by modulating Gαq activity. Our initial studies measured the effect of reduced Cav1 on the expression of two housekeeping proteins GAPDH and Hsp90, and the growth-associated protein Ras. As detailed below, the impact of Cav-1 on the basal levels of these proteins was difficult to quantify because of its broad effect on cellular RNA, and so we focused on changes in the levels of these proteins when caveolae were deformed under mild osmotic stress. By comparing to control cells, we find that levels of all three proteins are influenced by Cav1 down-regulation. The impact of Cav1 on GAPDH and Hsp90 does not appear to primarily involve the Gαq/PLCβ signaling pathway since cells where either Gαq or PLCβ1 were downregulated showed either minor or no changes as compared to controls, although our studies suggest that Ras levels might be influenced by both Gαq and Cav1. Thus, these initial studies suggest that Cav1 may act through pathways distinct from Gαq/PLCβ to impact the levels of specific cellular proteins.

We searched for mechanisms that connect caveolae to protein levels in another cultured smooth muscle cell line that are easily imaged. We noted that cavin-1 plays a dual role in cells by stabilizing caveolae domains on the plasma membrane and by promoting the transcription of ribosomal RNA in the nucleus (3,35). Because expression of Cav1 and cavin-1 are linked, we were not surprised to find that down-regulating Cav1 results in a dramatic decrease in cytosolic RNA levels, which may influence cellular levels of proteins like GAPDH, while down-regulating cavin-1 causes a much larger reduction of RNA. The ability of cavin-1 to regulate transcription allowed us to use the level and properties of cytosolic RNA as a read-out for nuclear cavin-1 activity.

Cavin-1 has been found to be released from the plasma membrane when caveolae domains disassemble, or upon phosphorylation during insulin signaling (19). Here, we worked at osmotic conditions where caveolae deform enough to disrupt Cav-1/Gαq interactions and focused on cavin-1 relocalization in real time in intact cells (9). We find that even these milder conditions promoted

release of cavin-1 from the plasma membrane to the cytosol and nucleus. Not only did osmotic stress allow for cavin-1 relocalization, but carbachol stimulation did as well suggesting that strengthening Cav1-Gαq interactions weakened contacts with cavin-1. As expected, activation of Gαi did not promote nuclear localization of eGFP-cavin-1. We were surprised to find that arsenite treatment, which has pervasive effects in cells, also promotes cavin-1 relocalization to the nucleus. This relocalization may be due to initiation of cellular mechanisms to alleviate cell toxicity, or due to disintegration of caveolae-cytoskeletal contacts (36-38).

While cavin-1's functions on the plasma membrane and in the nucleus are known, and the large population of this protein localizes in these two compartments, its role in the cytosol has not yet been determined. It is possible that the cytosolic population acts as a reservoir for the other cellular compartments. It is notable that cavin-1 has been found to form complexes with cavin-2 in the cytosol (39). More recent work found that cavin-3, which interacts with both cavin-1 and caveolin-1 can also be released from the plasma membrane upon caveolae disassembly, interacts with a large number of cytosolic proteins and some of these interactions may overlap with cavin-1 (40,41). Pertinent for this study is the argument that cytosolic cavin-1 does not directly mediate stress granule formation since we have not detected cavin-1 in protein complexes associated with either PLCβ1 or Ago2 (33).

Our studies showed that reducing Cav1/cavin-1 levels and subjecting cells to osmotic stress reduced of GAPDH and Hsp90 levels relative to controls but increased Ras. We do not believe that these differential effects on these transcripts are specific to cavin-1 but instead are indirect through other pathways, or due to the rate of translation of transcript caused by reduction ribosomes levels. We explored this idea by assessing the relative size distribution of cytosolic RNAs. In WKO cells, lowering cavin-1 promotes the appearance of very large RNAs, while over-expressing cavin-1 increases small RNAs due to enhanced processing consistent with enhanced ribosomal activity. Reducing cytosolic PLCβ through stimulation of Gαq or application of osmotic stress shows the same shift towards smaller RNAs due to increased RISC activity while halting processing by arsenite causes a shift to very large sizes. These shifts are consistent with cavin-1's role in promoting cytosolic RNA processing by increasing ribosomal RNA levels (18).

Cavin-1 is highly expressed in proliferative tissues and ones rich in caveolae such as prostate cancer cells (PC-3), rhabdomyosarcoma (RMS), endothelial cells (ECs), etc. (42-45). Aside from making cells more susceptible to damage from mechanical stretch, down-regulating cavin-1 would be expected to slow cell growth due to reduced ribosomal RNA output, and these characteristics were observed in the MEF cavin-1 knock-out cells (19). Even though they grew much slower than wild type, the KO MEFs had similar levels of cytosolic RNA showing that these cells have adapted to reduced ribosomal RNA transcription. We noted that the sizes of the RNAs in the cavin-1 KO MEFs were much larger than control suggesting a reducing in processing. When we over-express Cav1 in the KO MEFs, we find a shift in RNA sizes towards control cells. This shift is not due to increased expression of cavin-1 by Cav1 over-expression because the cavin-1 gene has been eliminated from these cells. One possibility is that Cav1's stabilization of Gαq shifts the PLCβ population to the plasma membrane promoting RISC activity (12), and this idea is supported by previous FRET measurements (33).

Stress granule formation is initiated by cytosolic mRNA, and so it was not surprising that reducing Cav1/cavin1 results in cells that have impaired stress responses. We tested the importance of Cav1/cavin-1 on micron-sized particles by imaging marker proteins, and for MEFs, we were also able to image on smaller aggregates by N&B analysis of fluorescent-tagged markers. Under basal conditions, the cavin-1 KO MEFs showed a greater number of small aggregates of Ago2 but a lower number of larger aggregates as compared to wild type cells and transfecting with Cav1 did not affect the results since cavin-1 is required for caveolae.

The overall goal of this study was to understand how caveolae transmits mechanical stress into cells, and their ability to mediate Gαq signals. We used a mild osmotic stress where caveolae are deformed but not completely disassembled and one that emulate physiological conditions that can occur in the epithelial cells in the digestive tract and kidney and also in fish and invertebrate (9,46). While we knew that this stress would reduce Gαq/calcium signals, we were surprised to find that caveolae changed the ability of cells to handle stress as seen by changes in protein content, and changes in cytosolic RNA, and changes in stress granule number and area. Our data indicate that these changes are mediated by two factors: relocalization of cavin-1 from the plasma membrane to the nucleus to allow increased rRNA production and increased translation, and increased RNA

levels in the cytosol as described in the model shown in **Fig. 4.8**. The nature of the specific proteins translated are unclear and may depend on competing transcripts, miRs and the rate of translation. Low levels of rRNA reduces the formation of ribosomes allowing cytosolic mRNA to be susceptible to inclusion in p-bodies or degradation by RISC (47). The rRNA resulting from nuclear cavin-1 provides a protective effect for cells by increasing cytosolic RNA levels allow for stress granule formation, although reduction in ribosomes may shift more mRNA into p-bodies as our studies indicate. It is notable that caveolae are prevalent in cells where expression of Gαq is high. Thus, normal Gαq activation by agents such as bradykinin, angiotensin II, histamine, etc. (48), and the studies here suggest that normal, Gαq activation helps cycle cavin-1 to the nucleus in response to these signals. Taken together, these studies show that cavin-1 can act as a sensor that communicates environmental stress to the nucleus that allow cells to better initiate stress responses.
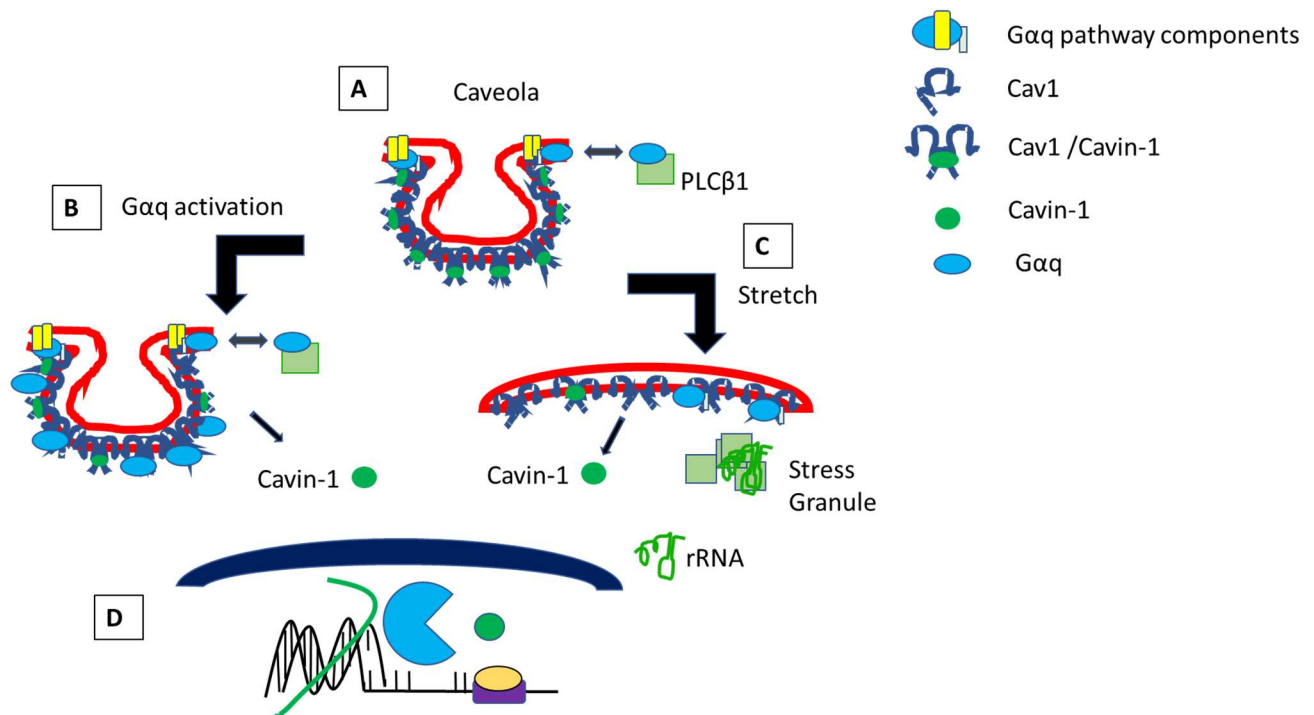
Figure 4.8: Model of cavin relocalization with stretch and Gaq activation. A- Gαq and PLCβ localize in caveolae; B- Enhancement of Gαq /Cav1 during activation releases a population of cavin-1 from the plasma membrane; C- mechanical stretch flattens the domains releasing cavin-1 from the plasma membrane and shifting PLCβ to the cytosol which leads to a reduced number of

stress granules; D –cavin-1 relocalizes to the nucleus to influence transcription of specific genes that lead to changes in cell structure.

4.5 SUPPORTING INFORMATION
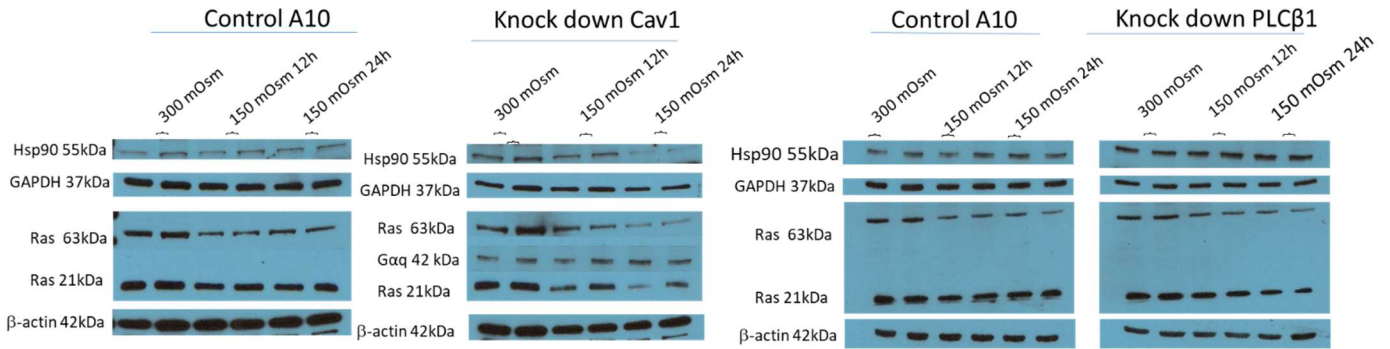
Figure S4.1 Down-regulation of Caveolin 1 impacts protein levels. Changes in proteins levels of GAPDH, Hsp90 and Ras in rat aortic smooth muscle (A10) were verified with western blot where n=3.
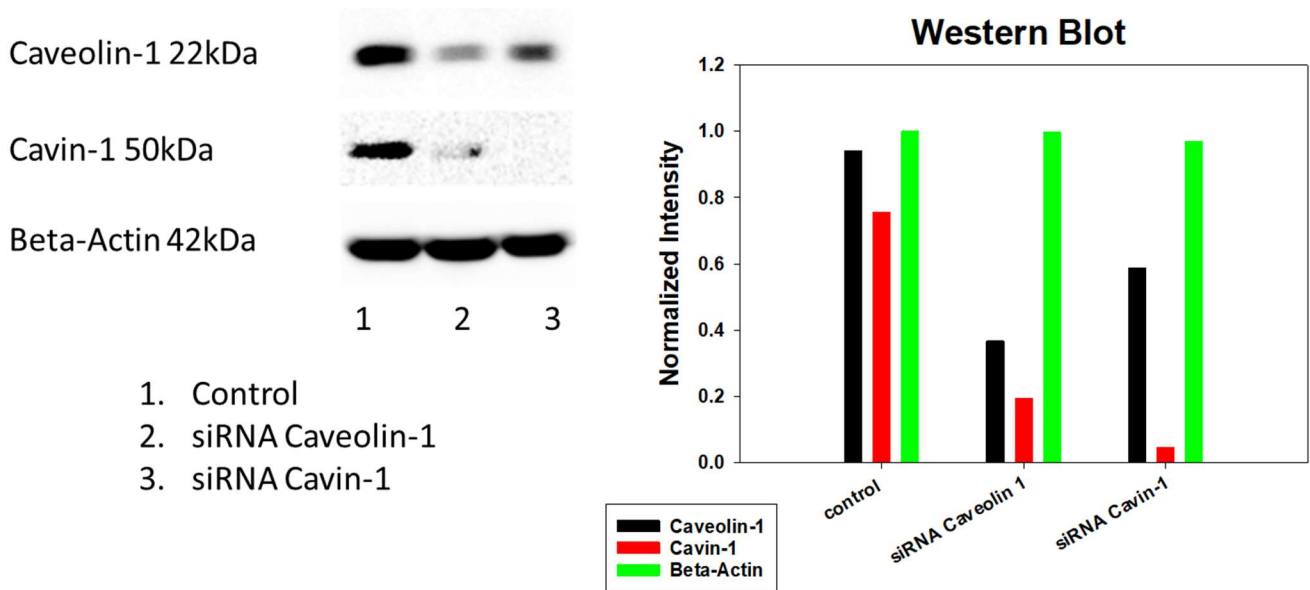
Figure S4.2: Quantification of protein levels in WKO-3M22 Cells. Downregulating caveolin 1 reduced the levels of the protein by 60% and the levels of cavin-1 by 38% while downregulating

cavin-1 reduced the levels of caveolin-1 by 74% and the levels of cavin-1 by 94% as seen by Western Blot since these proteins are interdependent (n=3).
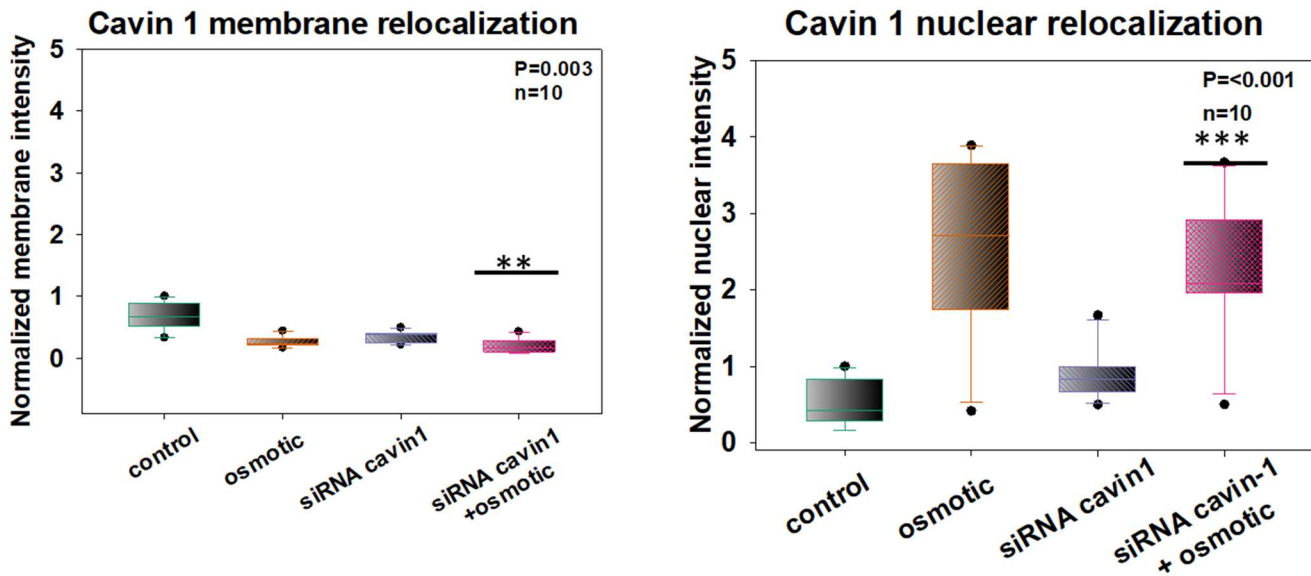
Figure S4.3: eGFP-Cavin-1 localization in cavin-1 downregulated WKO-3M22 cells. Downregulating cavin 1 before transfecting cells with cavin-1-GFP showed the same localization with cavin-1 levels slightly reduced in the plasma membrane compared to the nucleus and no cavin-1 present in the cytoplasm.
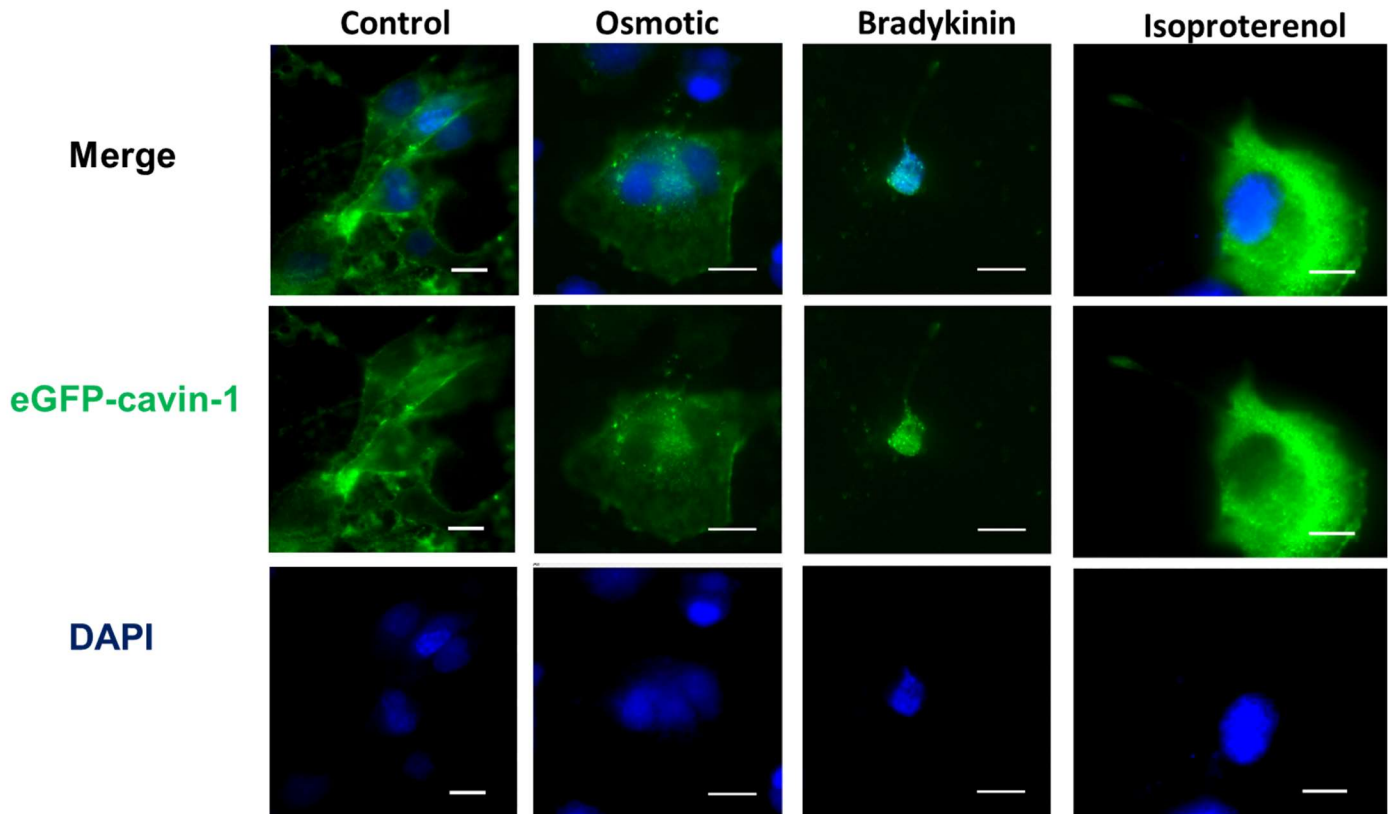
Figure S4.4: Additional cells showing Cavin-1 relocalization in WKO-3M22 cells. Sample fluorescence images of fixed WKO-3M22 cells transfected with eGFP-Cavin1 (green) and DAPI (blue) under control, osmotic, bradykinin and isoproterenol (see text) as obtained at 60X magnification. Scale bars are 20 μm long for the control and 10 μm for the rest of the conditions.

Gαq 42kDa

Beta-Actin 42kDa

1   2   3

1. Control
2. siRNA Caveolin-1
3. siRNA Cavin-1
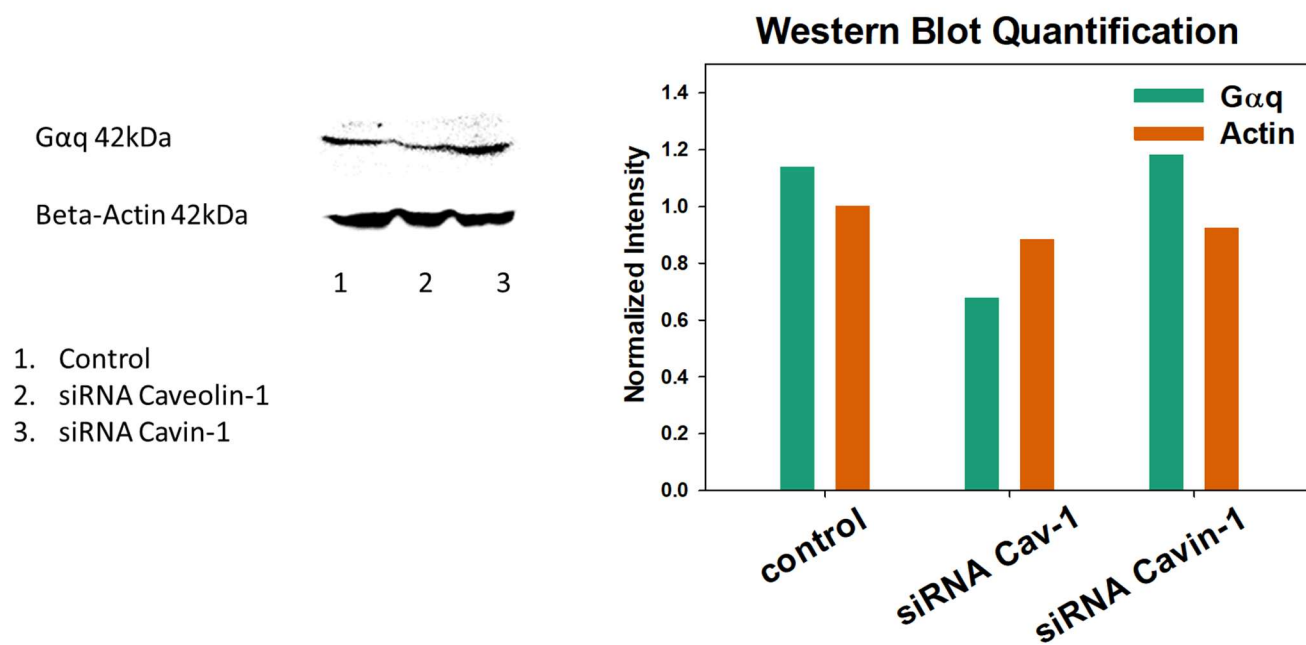
Figure S4.5: Quantification of protein levels in WKO-3M22 Cells. Downregulating caveolin 1 reduced the levels of the protein by 46% while downregulation of cavin-1 did not show the same affect as seen by Western Blot since these proteins are interdependent (n=3).
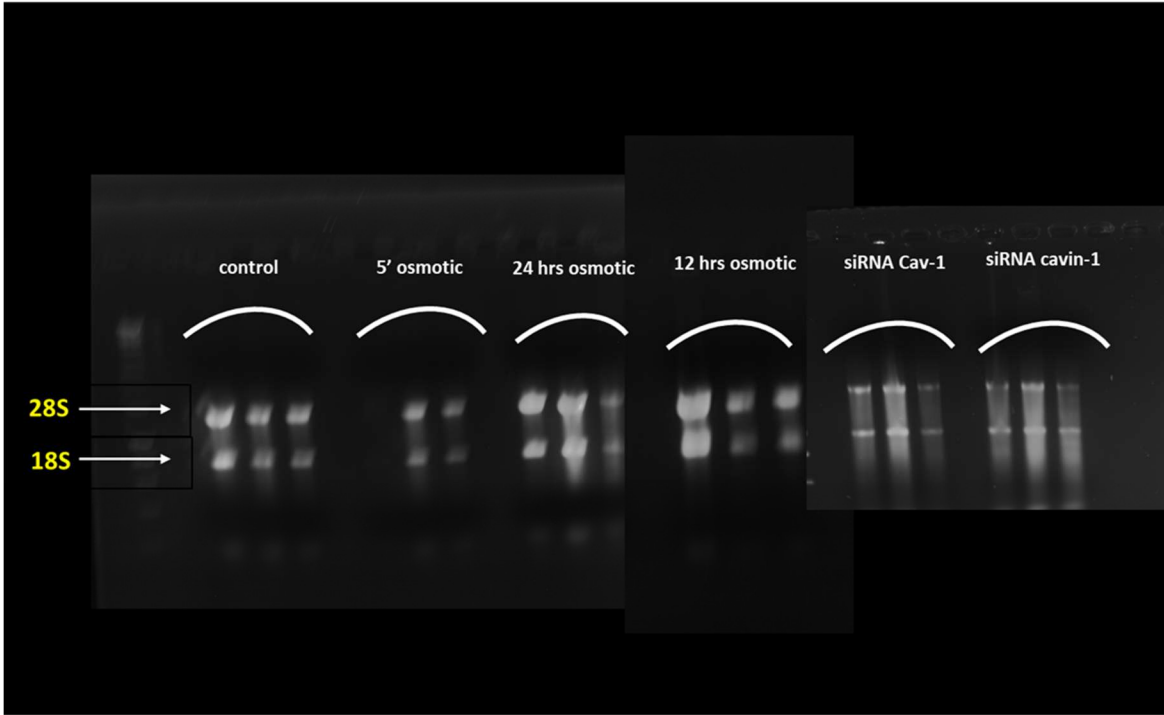
Figure S4.6: Bleach Agarose gels showing ribosomal RNA integrity. One to two µg of total RNA per band run on a 1% denaturing bleach-agarose gel where bands are independent samples. Agarose gels were prepared with 1X TBE buffer, bleach and ethidium bromide and run for 75 minutes at 100V.
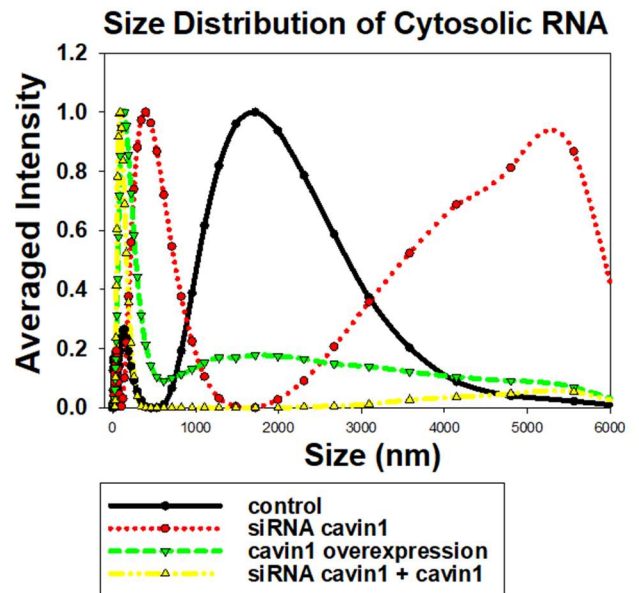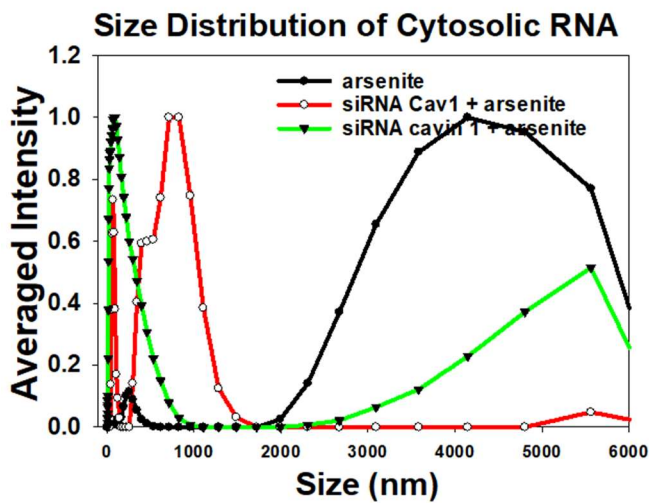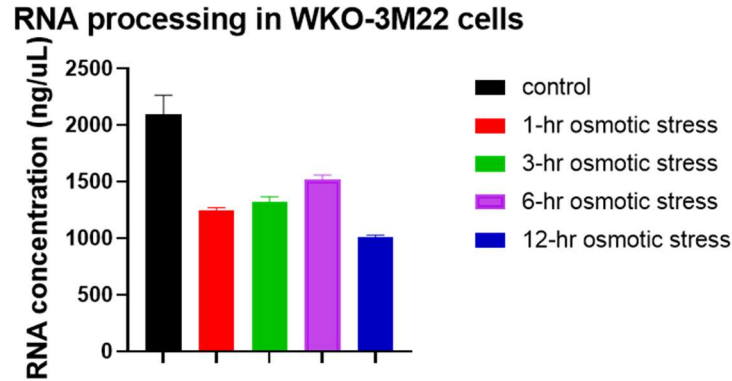
Figure S4. 7: The effect of arsenite on the size distribution of cytosolic RNAs (top-left), the rescue effect of Cavin-1 in cavin-1 depleted WKO-3M22 cells (top-right) along with the effects of osmotic stress in RNA processing (bottom). (Top-Left panel) Control cells (black) and Cav1 (red) and cavin-1 (green) down-regulated cells were treated with 0.5mM arsenite for 10 min. (Top-Right panel) Control cells (black), cavin-1 downregulated cells (red), cavin-1 overexpressed cells (green) and cavin-1 downregulated cells with cavin-1 overexpressed after the downregulation occurred. Samples were prepared as described in the Methods section and DLS spectra were taken according to the legend in Fig. 4.3 B-E in the text. (bottom panel) The RNA levels under control (black), 1 hour hypo-osmotic (red), 3 hours hypo-osmotic (green), 6 hours hypo-osmotic stress (purple) and 12 hours hypo-osmotic stress (blue) was extracted and analyzed.
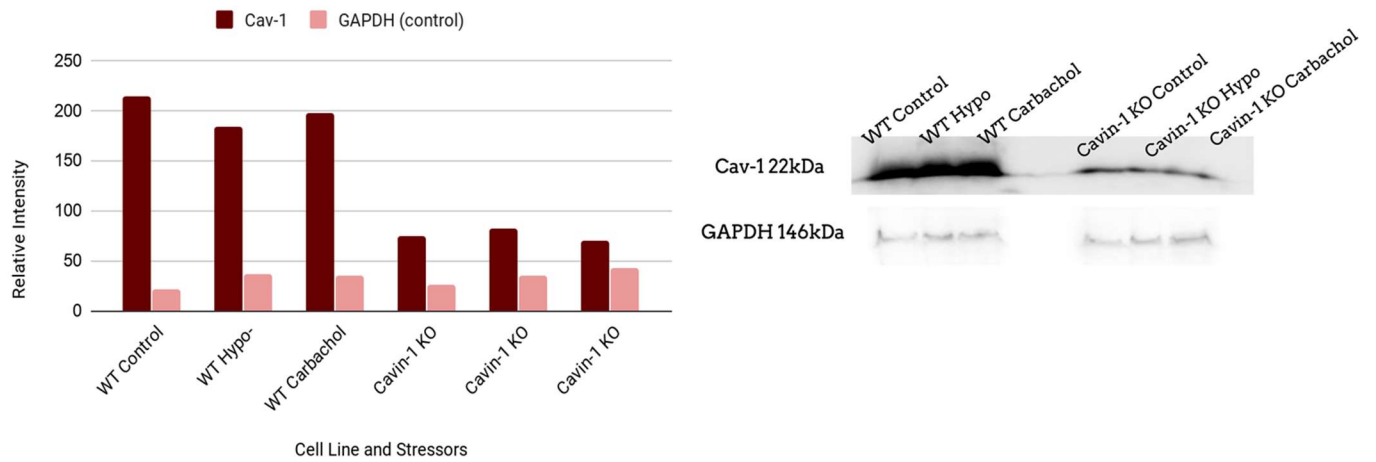
Figure S4. 8: Absence of Cavin 1 reduces the levels of Caveolin 1 in MEFs. The lack of cavin-1 in the cavin KO mouse embryonic fibroblasts reduced the levels of caveolin-1 by ~55-68% depending on the environmental stress applied as seen by Western Blot (n=3).
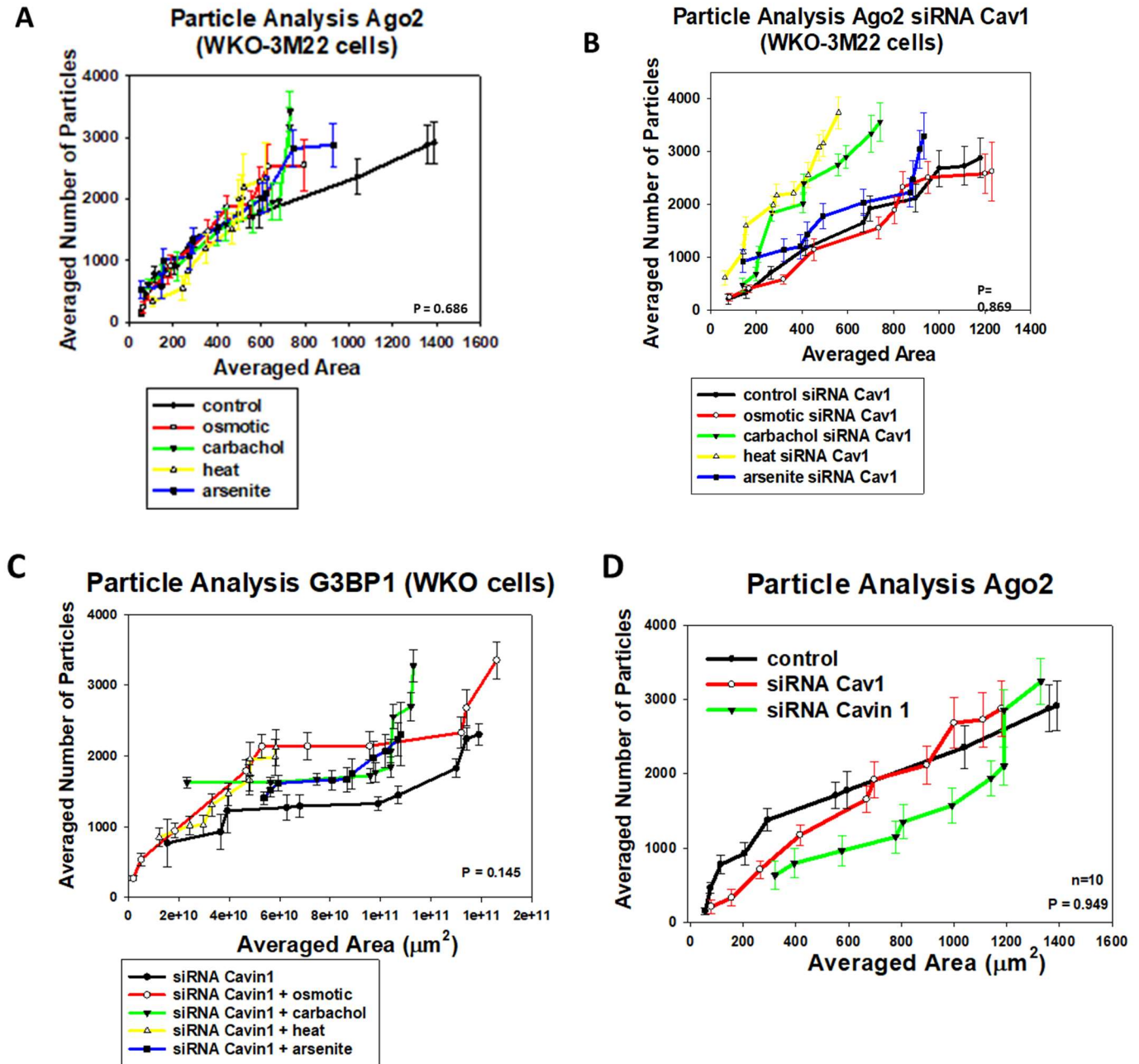
Figure S4. 9: Caveolin 1 and Cavin-1 do not affect Ago-2 related particles In WKO-3M22 Cells. The size and number of particles associated with monoclonal anti-Ago2 in the cytosol of fixed and immunostained WKO-3M22 cells was measured on a 100x objective and analyzed using Image J (see methods). Comparison of all environmental conditions in control cells (A) caveolin-1 down-regulated cells (B) and cavin-1 downregulated cells (C). A comparison between the control (black) caveolin-1 downregulation (red) and cavin-1 downregulation (green) can be seen in (D).

All measurements are an average of 3 independent experiments that sampled 10 cells, where SD shown and where the p values was determined using ANOVA.
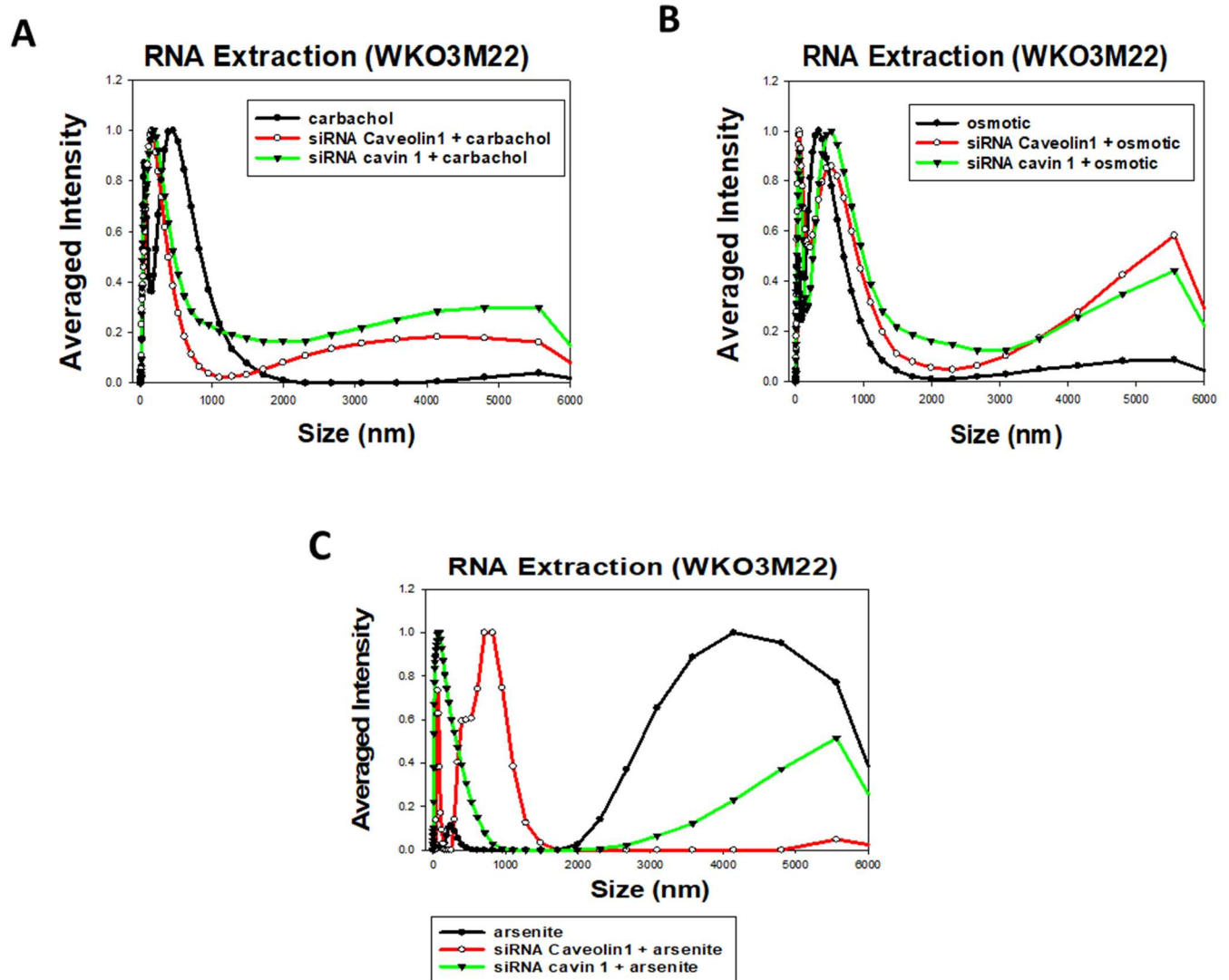
Figure S4. 10: Characterization of RNA in WKO-3M22 cells. A- RNA from WKO-3M22 cells treated with siRNA(Cav1) (red) and siRNA(cavin-1) (green) was extracted and quantified (see methods). Normalized DLS spectra showing the size distributions of cytosolic RNA isolated from WKO-3M22 cells under carbachol conditions (5µM, 10min) (black), siRNA(Cav1) and carbachol treated cells (red), and siRNA(cavin-1) and carbachol treated cells (green). B- Similar study as in (A) for cells subjected to hypo-osmotic stress (150 mOsm 5min), and C- arsenite treatment (0.5mM, 10 min). Each sample was scanned 3 times with 10 minutes per run. The number of independent samples were 6 per condition.
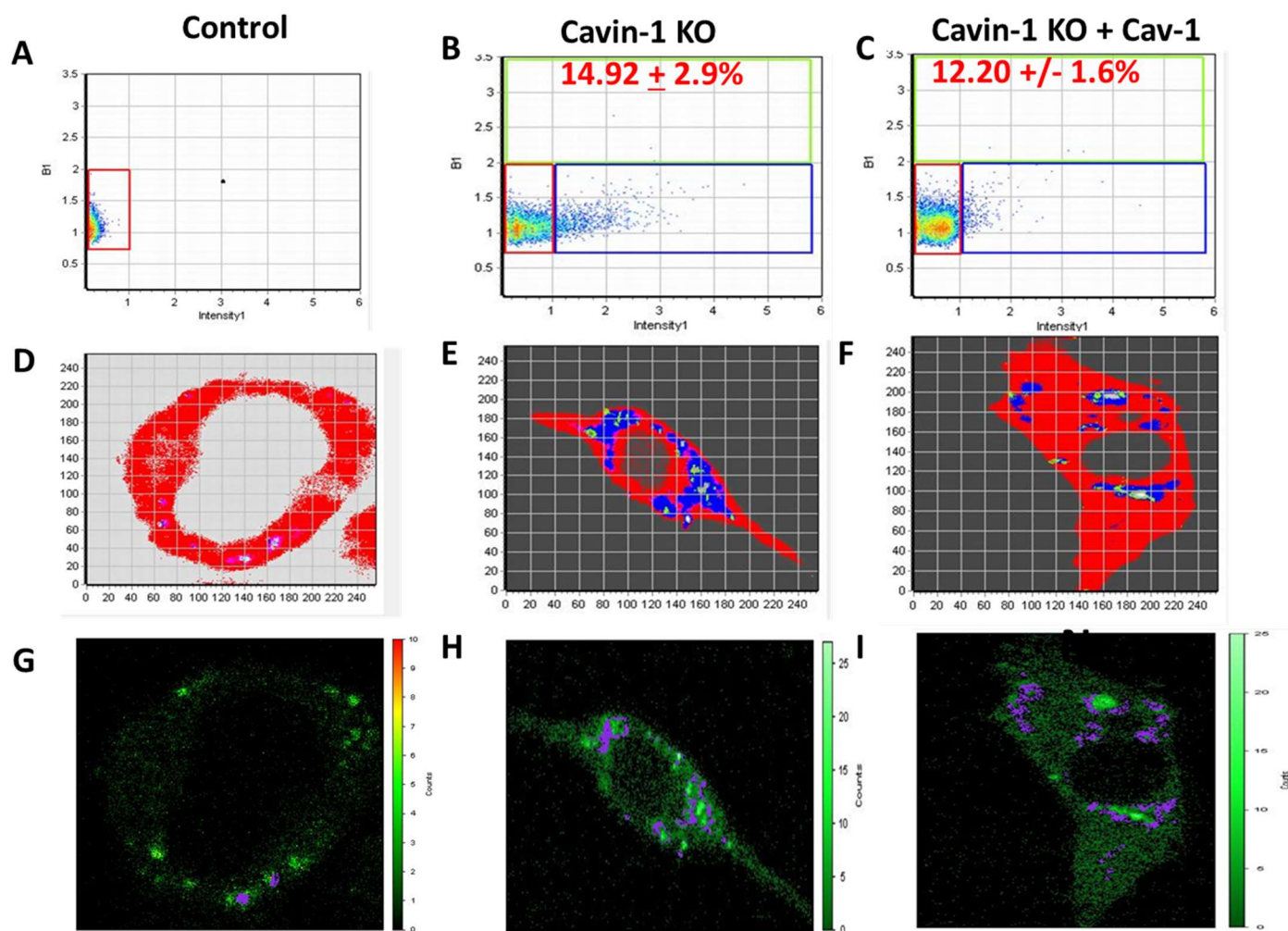
Figure S4. 11: N&B analysis of eGFP-Ago2 aggregation in MEF cells. I- The top panels (A – C) show graphs of the brightness versus intensity with the pixels of the colored boxes corresponding to the specific regions in the cells (D – F) using SIM-FCS 4 software. The bottom panels show the corresponding fluorescence microscopy images in ISS (G-I). The red box corresponds to monomeric eGFP-Ago-2 while points outside this box and in the green and blue boxes correspond to higher order species. Panels A, D,G are control cells (n=6); Panels B, E,H are cavin-1 knock-out cells, and Panels C, F, I are cavin-1 knock-out cells with caveolin-1 overexpression. Scale bars are 10 μm long.
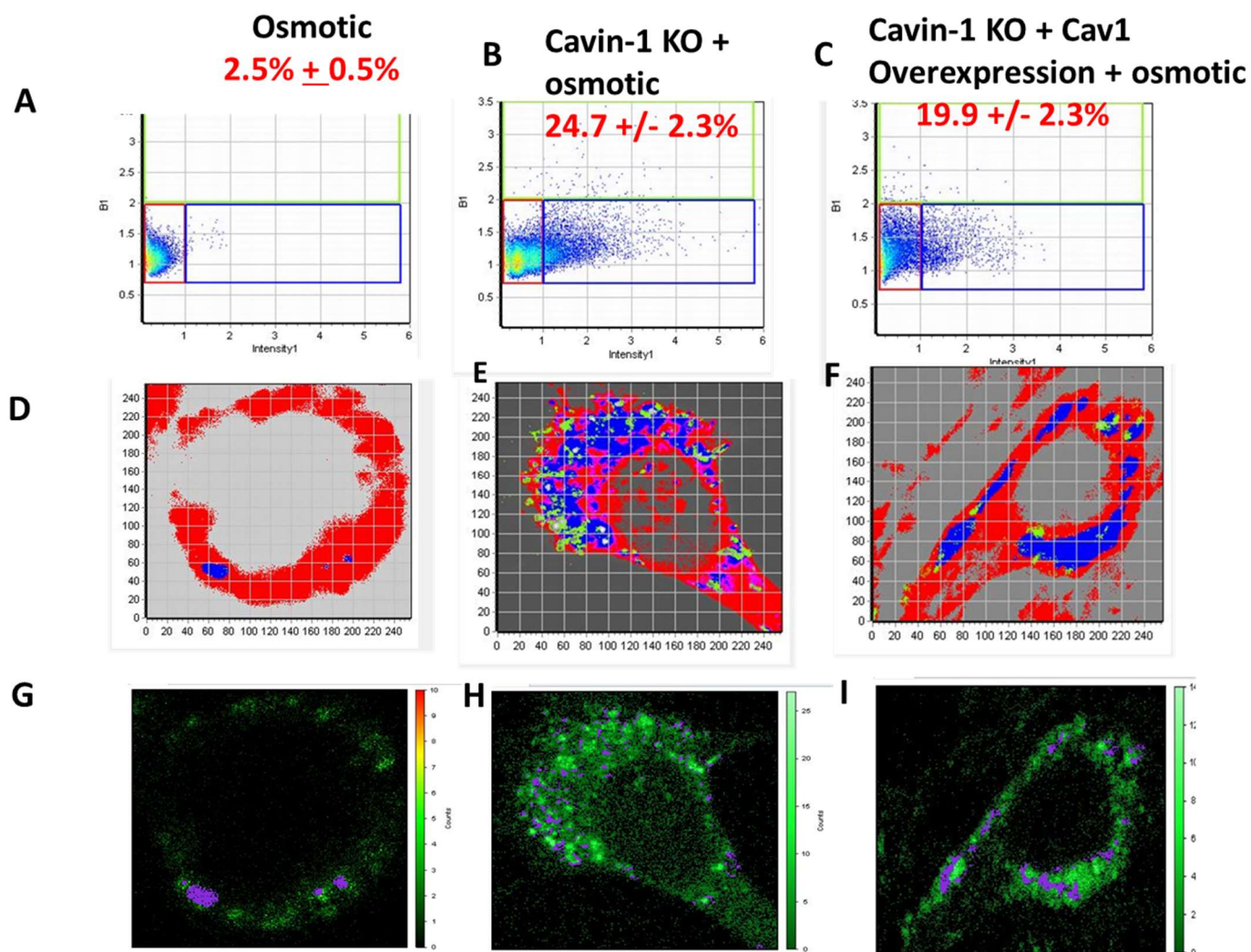
Figure S4. 12: N&B analysis of eGFP-Ago2 aggregation in osmotically stressed MEF cells. I-The top panels (A –C) show graphs of the brightness versus intensity with the pixels of the colored boxes corresponding to the specific regions in the cells (D – F) using SIM-FCS 4 software. The bottom panels show the corresponding fluorescence microscopy images in ISS (G-I). The red box corresponds to monomeric eGFP-Ago-2 while points outside this box and in the green and blue boxes correspond to higher order species. Panels A, D,G are control cells (n=6); Panels B, E,H are cavin-1 knock-out cells, and Panels C, F, I are cavin-1 knock-out cells with caveolin-1 overexpression. Scale bars are 10 μm long.

	Particle Analysis		N&B	
Wild type	Ago2		Ago2	
Control	-			
osmotic	++		-	
carbachol	+		+	
arsenite	++		+	
heat	+++		+	
cavin-1 KO				
control	-		++	
osmotic	++		+++	
carbachol	+		+	
arsenite	+++		++	
heat	+++		+	
Cavin-1 KO + Cav1 overexpression				
control	++		++	
osmotic	++		++	
carbachol	++		+	
arsenite	++		+	
heat	+		+	

For N&B:
+++ : > 20% aggregation
++: >10% and < 20%
+: >3% and < 10%
-   : >0 and < 3%

For Particle Analysis (where y=ax+b)

Ago2:
+++: a=0-2
++: a= 2-4
+: a= 4-6
-: a= 6-8

Table S4.1: Stress responses quantified by Particle analysis and N&B in MEFs.

4.6 AUTHOR CONTRIBUTIONS

A.Q., S.S. designed experiments. A.Q. conducted and analyzed all experiments conducted in WKO-3M22 cells along with the N&B analysis in mouse embryonic fibroblasts. S.B. conducted and analyzed experiments conducted in mouse embryonic fibroblasts. A.Q. and S.S developed signaling model. A.Q., S.B., and S.S. interpreted the data. A.Q. and S.S. wrote the manuscript.

4.7 ACKNOWLEDGEMENTS

4.8 REFERENCES

1.   Parton, R. G. (2018) Caveolae: Structure, Function, and Relationship to Disease. *Annual Review of Cell and Developmental Biology* **34**, 111-136

2.   Bernatchez, P., Sharma, A., Bauer, P. M., Marin, E., and Sessa, W. C. (2011) A noninhibitory mutant of the caveolin-1 scaffolding domain enhances eNOS-derived NO synthesis and vasodilation in mice. *J Clin Invest* **121**, 3747-3755

3.   Parton, R. G., Tillu, V. A., and Collins, B. M. (2018) Caveolae. *Curr Biol* **28**, R402-R405

4.   Buwa, N., Mazumdar, D., and Balasubramanian, N. (2020) Caveolin1 Tyrosine-14 Phosphorylation: Role in Cellular Responsiveness to Mechanical Cues. *The Journal of Membrane Biology* **253**, 509-534

5.   Sengupta, P., Philip, F., and Scarlata, S. (2008) Caveolin-1 alters Ca2+ signal duration through specific interaction with the G{alpha}q family of G proteins. *J Cell Sci* **121**, 1363-1372

6.   Calizo, R. C., and Scarlata, S. (2012) A Role for G-Proteins in Directing G-Protein-Coupled Receptor–Caveolae Localization. *Biochemistry* **51**, 9513-9523

7.   Guo, Y., Golebiewska, U., and Scarlata, S. (2011) Modulation of Ca2+ Activity in Cardiomyocytes through Caveolae-G[alpha]q Interactions. *Biophysical Journal* **100**, 1599-1607

8.   Guo, Y., Yang, L., Haught, K., and Scarlata, S. (2015) Osmotic Stress Reduces Ca2+ Signals through Deformation of Caveolae. *J Biol Chem* **290**, 16698-16707

9. Yang, L., and Scarlata, S. (2017) Super-resolution Visualization of Caveola Deformation in Response to Osmotic Stress. *J Biol Chem* **292**, 3779-3788

10. Aisiku, O., Dowal, L., and Scarlata, S. (2011) Protein kinase C phosphorylation of PLC[beta]1 regulates its cellular localization. *Archives of Biochemistry and Biophysics* **509**, 186-190

11. Qifti, A., Garwain, O., and Scarlata, S. (2019) Mechanical Stretch Redefines Membrane Galphaq-Calcium Signaling Complexes. *J Membr Biol* **252**, 307-315

12. Philip, F., Guo, Y., Aisiku, O., and Scarlata, S. (2012) Phospholipase Cβ1 is linked to RNA interference of specific genes through translin-associated factor X. *The FASEB Journal* **26**, 4903-4913

13. Briand, N., Dugail, I., and Le Lay, S. (2011) Cavin proteins: New players in the caveolae field. *Biochimie* **93**, 71-77

14. Kovtun, O., Tillu, V. A., Ariotti, N., Parton, R. G., and Collins, B. M. (2015) Cavin family proteins and the assembly of caveolae. *Journal of Cell Science* **128**, 1269-1278

15. Williams, J. J., and Palmer, T. M. (2014) Cavin-1: caveolae-dependent signalling and cardiovascular disease. *Biochem Soc Trans* **42**, 284-288

16. Liu, L., and Pilch, P. F. (2008) A critical role of cavin (polymerase I and transcript release factor) in caveolae formation and organization. *J Biol Chem* **283**, 4314-4322

17. Sinha, B., Köster, D., Ruez, R., Gonnord, P., Bastiani, M., Abankwa, D., Stan, R. V., Butler-Browne, G., Vedie, B., Johannes, L., Morone, N., Parton, R. G., Raposo, G., Sens, P., Lamaze, C., and Nassoy, P. (2011) Cells Respond to Mechanical Stress by Rapid Disassembly of Caveolae. *Cell* **144**, 402-413

18. Jansa, P., Mason, S. W., Hoffmann-Rohrer, U., and Grummt, I. (1998) Cloning and functional characterization of PTRF, a novel protein which induces dissociation of paused ternary transcription complexes. *EMBO J* **17**, 2855-2864

19. Liu, L., and Pilch, P. F. (2016) PTRF/Cavin-1 promotes efficient ribosomal RNA transcription in response to metabolic challenges. *eLife* **5**, e17508

20. Liu, L. (2020) Lessons from cavin-1 deficiency. *Biochemical Society Transactions* **48**, 147-154

21. Bai, L., Deng, X., Li, J., Wang, M., Li, Q., An, W., A, D., and Cong, Y.-S. (2011) Regulation of cellular senescence by the essential caveolar component PTRF/Cavin-1. *Cell Res* **21**, 1088-1101

22. Philip, F., Sahu, S., Golebiewska, U., and Scarlata, S. (2016) RNA-induced silencing attenuates G protein-mediated calcium signals. *Faseb j* **30**, 1958-1967

23. Sahu, S., Philip, F., and Scarlata, S. (2014) Hydrolysis Rates of Different Small Interfering RNAs (siRNAs) by the RNA Silencing Promoter Complex, C3PO, Determines Their Regulation by Phospholipase Cβ. *Journal of Biological Chemistry* **289**, 5134-5144

24. Sahu, S., Williams, L., Perez, A., Philip, F., Caso, G., Zurawsky, W., and Scarlata, S. (2017) Regulation of the activity of the promoter of RNA-induced silencing, C3PO. *Protein Science* **26**, 1807-1818

25. Disalvo, J., and Nelson, S. R. (1998) Stimulation of G-Protein Coupled Receptors in Vascular Smooth Muscle Cells Induces Tyrosine Kinase Dependent Increases in Calcium Without Tyrosine Phosphorylation of Phospholipase C Gamma-1. *FEBS Letters* **422**, 85-88

26. Kurki, S., Latonen, L., and Laiho, M. (2003) Cellular stress and DNA damage invoke temporally distinct Mdm2, p53 and PML complexes and damage-specific nuclear relocalization. *J Cell Sci* **116**, 3917-3925

27. Luo, Y., Na, Z., and Slavoff, S. A. (2018) P-Bodies: Composition, Properties, and Functions. *Biochemistry* **57**, 2424-2431

28. Anderson, P., and Kedersha, N. (2006) RNA granules. *J Cell Biol* **172**, 803-808

29. Sen, G. L., and Blau, H. M. (2005) Argonaute 2/RISC resides in sites of mammalian mRNA decay known as cytoplasmic bodies. *Nat Cell Biol* **7**, 633-636

30. Digman, M. A., Dalal, R., Horwitz, A. F., and Gratton, E. (2008) Mapping the Number of Molecules and Brightness in the Laser Scanning Microscope. *Biophys J* **97**, 2320-2332

31. Li, Y., Chen, R., Zhou, Q., Xu, Z., Li, C., Wang, S., Mao, A., Zhang, X., He, W., and Shu, H. B. (2012) LSm14A is a processing body-associated sensor of viral nucleic acids that initiates cellular antiviral response in the early phase of viral infection. *Proc Natl Acad Sci U S A* **109**, 11770-11775

32. Parker, R., and Sheth, U. (2007) P bodies and the control of mRNA translation and degradation. *Mol Cell* **25**, 635-646

33. Qifti, A., Jackson, L., Singla, A., Garwain, O., and Scarlata, S. (2019) Stimulation of Gαq Promotes Stress Granule Formation. *Science Signaling, Preprint - (https://www.biorxiv.org/content/10.1101/521369v1)* **in press**

34. Qifti, A., Jackson, L., Singla, A., Garwain, O., and Scarlata, S. (2021) Stimulation of phospholipase Cβ1 by Gα(q) promotes the assembly of stress granule proteins. *Sci Signal* **14**, eaav1012

35. Liu, L., and Pilch, P. F. (2016) PTRF/Cavin-1 promotes efficient ribosomal RNA transcription in response to metabolic challenges. *Elife* **5**

36. Parton, R. G., Joggerst, B., and Simons, K. (1994) Regulated internalization of caveolae. *J Cell Biol* **127**, 1199-1215

37. Head, B. P., Patel, H. H., Roth, D. M., Murray, F., Swaney, J. S., Niesman, I. R., Farquhar, M. G., and Insel, P. A. (2006) Microtubules and actin microfilaments regulate lipid raft/caveolae localization of adenylyl cyclase signaling components. *J Biol Chem* **281**, 26391-26399

38. Echarri, A., and Del Pozo, M. A. (2015) Caveolae - mechanosensitive membrane invaginations linked to actin filaments. *J Cell Sci* **128**, 2747-2758

39. Breen, M. R., Camps, M., Carvalho-Simoes, F., Zorzano, A., and Pilch, P. F. (2012) Cholesterol depletion in adipocytes causes caveolae collapse concomitant with proteosomal degradation of cavin-2 in a switch-like fashion. *PLoS One* **7**, e34516

40. Mohan, J., Moren, B., Larsson, E., Holst, M. R., and Lundmark, R. (2015) Cavin3 interacts with cavin1 and caveolin1 to increase surface dynamics of caveolae. *J Cell Sci* **128**, 979-991

41. McMahon, K. A., Wu, Y., Gambin, Y., Sierecki, E., Tillu, V. A., Hall, T., Martel, N., Okano, S., Moradi, S. V., Ruelcke, J. E., Ferguson, C., Yap, A. S., Alexandrov, K., Hill, M. M., and Parton, R. G. (2019) Identification of intracellular cavin target proteins reveals cavin-PP1alpha interactions regulate apoptosis. *Nat Commun* **10**, 3279

42. Moon, H., Lee, C. S., Inder, K. L., Sharma, S., Choi, E., Black, D. M., Le Cao, K. A., Winterford, C., Coward, J. I., Ling, M. T., Australian Prostate Cancer, B., Craik, D. J., Parton, R. G., Russell, P. J., and Hill, M. M. (2014) PTRF/cavin-1 neutralizes non-caveolar caveolin-1 microdomains in prostate cancer. *Oncogene* **33**, 3561-3570

43. Faggi, F., Chiarelli, N., Colombi, M., Mitola, S., Ronca, R., Madaro, L., Bouche, M., Poliani, P. L., Vezzoli, M., Longhena, F., Monti, E., Salani, B., Maggi, D., Keller, C., and Fanzani, A. (2015) Cavin-1 and Caveolin-1 are both required to support cell proliferation, migration and anchorage-independent cell growth in rhabdomyosarcoma. *Lab Invest* **95**, 585-602

44. Hill, M. M., Bastiani, M., Luetterforst, R., Kirkham, M., Kirkham, A., Nixon, S. J., Walser, P., Abankwa, D., Oorschot, V. M., Martin, S., Hancock, J. F., and Parton, R. G. (2008) PTRF-Cavin, a conserved cytoplasmic protein required for caveola formation and function. *Cell* **132**, 113-124

45. Davalos, A., Fernandez-Hernando, C., Sowa, G., Derakhshan, B., Lin, M. I., Lee, J. Y., Zhao, H., Luo, R., Colangelo, C., and Sessa, W. C. (2010) Quantitative proteomics of caveolin-1-regulated proteins: characterization of polymerase i and transcript release factor/CAVIN-1 IN endothelial cells. *Mol Cell Proteomics* **9**, 2109-2124

46. Dietmar, K. (2007) Osmotic stress sensing and signaling in animals. *The FEBS Journal* **274**, 5781-5781

47. Eulalio, A., Behm-Ansmant, I., and Izaurralde, E. (2007) P bodies: at the crossroads of post-transcriptional pathways. *Nat Rev Mol Cell Biol* **8**, 9-22

48. Hepler, J. R., and Gilman, A. G. (1992) G-proteins. *Trends Biochem. Sciences* **17**, 383-387

CHAPTER 5- IDENTIFYING THE GENES ASSOCIATED WITH THE CAVIN-1 RELOCALIZATION THAT OCCURS WITH OSMOTIC AND MECHNICAL STRESS

5.1 ABSTRACT

In the previous chapter, we showed that osmotic stress promotes caveolae deformation that causes cavin-1 to relocalize to the nucleus. Earlier in this thesis, we showed that osmotic stress induces the formation of stress granules in the cytoplasm of neuronal and smooth muscle cells. In this chapter, we will describe the use of smooth muscle cells (WKO-3M22) to identify the genes whose expression was changed during caveolae deformation. We used two different methods to deform caveolae; prolonged osmotic stress and bi-directional mechanical stress. In addition, we analyzed the effect of downregulation of Cav-1 and cavin-1 to understand the impact of caveolae removal on the transcriptome. These experiments produced interesting and original results. In particular, we found that osmotic deformation of caveolae affects the cell circadian rhythm while complete loss of caveolae triggers anti-viral immune responses. The potential significance and application of these findings will be discussed. Further experiments are needed to confirm these hypotheses and to identify the signaling pathways underlying these effects.

5.2 INTRODUCTION

In the previous chapter, we showed that after mechanical stretch (such as osmotic stress), cavin-1 relocalizes from the plasma membrane to the nucleus to impact transcription. Here, we use RNA-sequencing to identify the genes whose expression is affected by the expression levels and localization of cavin-1. We identified hundreds of genes whose expression was upregulated and downregulated. Among these, a few categories of genes were prominently represented, namely genes involved in circadian rhythm regulation, anti-viral immune responses, cancer and apoptosis (see results).

While these results are nonetheless interesting, the expectations of this project were to identify genes that are fundamental in smooth muscle cell survival and function. There are several studies showing that actin, myosin, elastin and ubiquitin related genes are severely impacted in vascular smooth muscle cells resulting in changes in contractility[1; 2; 3]. In addition, the ability or inability of these cells to successfully differentiate due to stress-induced caveolae deformation was expected

to impact smooth muscle myosin heavy chain, α-smooth muscle actin, calponin, SM22, α- and ß-tropomyosins, and αl integrin genes since they are transcriptionally regulated meaning that transcription of these genes is upregulated in differentiated SMCs but is downregulated in dedifferentiated SMCs [4; 5]. While the expression of some of these expected genes was impacted, their effect was not as dramatic as the ones we will be focusing on in the Results section. However, further analysis and optimization of those results need to be done in a separate study. Here we will focus on the most prominent and dramatic effects induced by cavin-1 relocalization.

5.2.1 Circadian Rhythm in mammals and cells

Many living organisms display a 24-hour cycle of activity and rest called the circadian rhythm. In mammals, many physiological processes are subject to circadian regulation such as sleep-wake cycles, body temperature, heartbeat, blood pressure, endocrine secretion, renal activity, and liver metabolism. The circadian clock is a timing system that consists of an input pathway adjusting the time, a central oscillator generating the circadian signal, and an output pathway eliciting the circadian physiology and behavior[6]. While most organisms are believed to regulate their circadian clocks according to changes in the duration of light, interestingly, many of them will operate in complete darkness.

The core of the mammalian circadian clock is a feedback loop composed of transcription factors. In the mammalian circadian clock, the transcription factor Circadian Locomotor Output Cycles Kaput (CLOCK) dimerizes with the transcription factor Brain and Muscle Arnt1-like-1 (BMAL1). The CLOCK/BMAL1 dimer binds to a response elements of the Enhancer boxes (or E-boxes) family and promotes the transcription of the Cryptochrome 1 and 2 genes, (*Cry1, Cry 2*), and of the period 1, 2, 3 genes (Per1, Per2 and Per3).

After transcripts of Per and Cry are translated in the cytoplasm, they dimerize and return to the nucleus where they interact with the CLOCK/BMAL1 dimer. This interaction interferes with the ability of CLOCK and BMAL1 to stimulate further transcription of the *per* and *cry* genes and transcription is halted. As Per and Cry proteins degrade, CLOCK and BMAL1 are freed to promote Per and Cry transcription again. Therefore, the cycle starts again, forming a negative feedback loop that generates 24-hour cycles affecting behavior and physiology.

A few studies have documented the existence of circadian rhythms in cultured cells. Previous studies in cultured rat fibroblasts have shown that serum addition to the culture media inhibits leucine zipper transcription factor TEF mRNA expression, whose expression follows a robust circadian rhythm [7]. These circadian oscillations last approximately 8 to12 hours suggesting that serum inhibition may be specific for transcripts with circadian accumulation in vivo. Highly regular oscillations in the levels of dissolved oxygen can be observed conveniently in chemostats that have been glucose starved and re-fed[8]. Other studies conducted in mouse embryonic fibroblasts identify cytosolic BMAL1 binding partners as known stress granule related proteins (eiF5a, PABPC1, etc)[9]. Upon phosphorylation, BMAL1 regulates ribosomal translation in cells, independently of its transcriptional activity while associating with several translation initiation factors.

Earlier in Chapter 3, we found that hypo-osmotic stress stimulates stress granule accumulation through a reduction in the level of cytosolic PLCβ1. Additionally, we find that hypo-osmotic stress deforms caveolae to release cavin-1 from the membrane, from where it travels to the nucleus to impact transcription. Here, we identified genes involved with hypo-osmotic stress through the formation of stress granules and changes in transcription due to the relocalization of cavin-1.

5.2.2 Viral entry and immune response

Viruses needs to invade a living cell to replicate. The viral particle, called the virion, consists of an RNA or DNA viral genome enclosed in an outer protein shell called the capsid. Some viruses have an envelope around the capsid that contains lipids and proteins, including glycoproteins and viral receptor proteins known as spikes [10]. There are two mechanisms by which enveloped viruses enter their host cells. In the first, the virion attaches to host cell receptors using the spikes. The envelope of the virus fuses with the plasma membrane of the host and the nucleocapsid is released directly into the cytoplasm, and the nucleic acid then separates from the protein coat. In the second mechanism, the enveloped virus absorbs to the host cell by specific proteins on its surface, and the virion is taken in by endocytosis. In the latter process, the host cell plasma membrane surrounds the virion forming a vesicle, and the nucleocapsid with the viral nucleic acid

is released into the host cytoplasm. The capsid protein is then removed, releasing the nucleic acid of the virus.

The endocytic pathways exploited by viruses to enter host cells include macropinocytosis, clathrin-dependent endocytosis, and caveolae-dependent endocytosis, as well as poorly characterized routes such as clathrin- and caveolae-independent endocytosis. Although most viruses use only one of these pathways to enter cells, studies have shown that some viruses use multiple mechanisms to gain entry into host cells [11]. Caveolae have been implicated in mediating several different endocytic events including internalizing ligands such as cholesterol, which is translocated to the endoplasmic reticulum [12]. Due to its composition, caveolae can cluster receptors and signaling molecules and have been proposed as a site for vesicle budding, docking and fusion. Several viruses such as the Simian virus 40 (SV40), polyoma virus and echovirus 1 are endocytosed through flask-shaped caveolae mediated by caveolin-1 upon entry and transported to the ER by an organelle known as caveosome [13; 14].

The host cell initiates various defense mechanisms to prevent the spread of viral infections. The first response to a viral infection is the rapid-onset innate response. There are several known mechanisms involved in innate immunity including interferons, natural killer cells and antigen-presenting cells. When the virus infects a cell, the cell produces and releases signaling proteins called interferons, which are a type of cytokine. Interferons act as a warning signal to neighboring cells where they bind to interferon receptors on uninfected cells. The cells then start producing anti-viral proteins which prevent the virus from replicating. Interferons are also able to induce nearby cells to increase the expression of major histocompatibility class I molecules, or MHC class I, on their surface. These molecules have two major signaling functions; first they present antigens, which are endogenous viral fragments, to adaptive immune cells, and second to innate immune cells. As mentioned above, we found that changes in expression levels of cavin-1 and Cav-1 affect the transcript levels of genes that are linked to early stages of viral entry.

5.2.3 Mechanical stretch and apoptosis
Another way used to promote the flattening of caveolae and induce the relocalization of cavin-1 from the plasma membrane to the nucleus is the oscillating mechanical stretch. Oscillating

mechanical stretch has been thoroughly examined in various cell lines and tissues including skeletal and smooth muscle cells, epithelial cells and fibroblasts. While the results vary with cell types, in most of them include cyclic mechanical stretch include cell proliferation and migration, endoplasmic reticulum stress induction, cancer regulation and apoptosis[15; 16; 17]. Our lab has previously shown that different forms of mechanical stretch affect calcium signaling through the Gαq/PLCβ pathway in a unique manner [18]. After stretching cells for various time points, we found that no cells survived after being stretched for more than 12 consecutive hours. Here, we show that after 12-hours bi-directional mechanical stretch at 1 Hz frequency in a sterile environment, several genes regulating cell survival and death are upregulated.

Apoptosis is an important cellular process that allows cells to die in a controlled fashion. This process plays an important role in growth and development. In addition, this process regulates the elimination of faulty cells when the DNA has been damaged beyond repair. A series of events are needed to initiate apoptosis, where signals can be extrinsic or intrinsic. Regardless of their origin, proteases called caspases are activated, setting off a chain of intracellular events leading to the cell's death by apoptosis.

5.3 MATERIALS AND METHODS

5.3.1 Cell Culture

Wystar Kyoto rat 3M22 (WKO-3M22) cells, originally obtained from ATCC, were a generous gift from Dr. Marsha Rolle at Worcester Polytechnic Institute. WKO-3M22 cell lines were cultured in high glucose DMEM (Corning) without L-glutamine with 10% fetal bovine serum, 1% sodium pyruvate, 1% non-essential amino acids (VWR) and 1% L-glutamine (VWR). All cells were incubated at 37°C in 5% CO2. For these experiments, cells were cultured in triplicates per condition of interest in 100mm X 25mm sterile, polystyrene cell culture dishes.

5.3.2 siRNA knock-down

Down-regulation of the Cav-1 gene was accomplished using SmartPool rat siRNA(Cav1) from Dharmacon Cat# L-093600-02-0005 to give greater than 85% down-regulation as estimated by western blotting. Silencing the PTRF-1 gene was accomplished using Smartpool siRNA PTRF from Millipore Sigma Cat# SASI_Rn02_0021-3052/PTRF (10.0NMOL). siRNA negative control

Sigma cat# SIC001was used. Transfection of siRNAs was accomplished using Lipofectamine 3000 (Invitrogen, Inc) as recommended by the manufacturer.

5.3.3 Plasmids

Tomato- pZac2.1 gfaABC1D-td adenovirus was purchased from Addgene (cat# 44332) and was prepared by the Baljit Khakh Lab (David Geffen School of Medicine). EGFP- Cavin 1 was a generous gift of Dr Liu Libin (Boston University School of Medicine).

5.3.4 Applications of stress conditions

For the hypo-osmotic stress conditions, the medium was diluted with 50% water for 5 minutes, 12 hours and 24 hours before it was removed, and the cells were collected. For the mechanical bi-directional stretch, PDMS stretchable plates were made using the Sylgard® 184 Silicone Elastomer kit. They were first sterilized by soaking in 70% ethanol, then coated with fibronectin for 30 min, washed with HBSS (Hanks' balanced salt solution) and coated again with fibronectin for 30 min. This double coating was necessary for the cells to attach and grow. WKO-3M22 cells adhered on the PDMS plates described above [i]were inserted into the stretching device described by Dr. Kristen Billiar and colleagues[19]. The device was then inserted inside the cell incubator where the stretching took place at 37ºC and 5% CO_2. All stress conditions had their appropriate controls that were treated identically besides the stress application.

5.3.5 mRNA sequencing

For each experiment, three 100-mm cell culture dishes were set up for each experimental condition and processed at 90% confluency. WKO-3M22 cells were cultured and stressed as described above and transfection was performed with Lipofectamine. Total RNA was extracted using the Qiagen RNA Mini kit (Cat #: 74104) and run on a sodium hypochlorite agarose denaturing gel to initially check ribosomal RNA integrity. The RNA Integrity Number has been correlated to the golden standard RIN and provides quantitative information about the integrity of total RNA. Here the RIN was determined using an Agilent TapeStation 4200 with a High Sensitivity RNA assay, as recommended by the manufacturer. High-quality RNA is required (RIN score > 7.0) in order to produce good quality RNAseq libraries. All our samples had RIN score between 9.2 and 10 (**Fig. 5.1**). For library preparation, we used 500 ng of each RNA

sample with the NEBNext Ultra II Directional RNA Library Preparation kit (New England Biolabs, cat# E7765S) with the Poly(A) mRNA Magnetic Isolation Module (NEB cat# E7490). The NEB Next Multiplex Oligos for Illumina (Index Primer Set 1 & 2, NEB cat # E7335S, E7500S) were used to barcode each library. RNA sequencing was performed by Novogene, Inc. on a NovaSeq sequencer (Illumina), according to the manufacturer's instructions. For each library, ~10G of raw data were obtained with a paired end PE150 cycle. Data analysis was performed using Database for Annotation, Visualization and Integrated Discovery (DAVID).

	RIN (out of 10)		RIN (out of 10)
control (for everything)	9.2	Control siRNAs1	10.0
control (for everything)	9.6	Control siRNAs2	10.0
control (for everything)	9.9	Control siRNAs3	9.9
5 minutes osmotic	9.9	siRNA Caveolin1.1	9.8
5 minutes osmotic	9.9	siRNA Caveolin1.2	9.9
5 minutes osmotic	9.8	siRNA Caveolin1.3	9.7
12 hours osmotic	9.9	siRNA Cavin1.1	9.8
12 hours osmotic	9.7	siRNA Cavin1.2	9.7
12 hours osmotic	9.8	siRNA Cavin1.3	9.8
24 hours osmotic	9.7	Control PDMS 1	9.7
24 hours osmotic	9.7	Control PDMS2	9.9
24 hours osmotic	9.6	12-h Mech. Stretch1	9.6
		12-h Mech. Stretch2	9.7

Figure 5. 1: RNA Integrity Number (RIN) for library preparation. All samples ran through an Agilent Bioanalyzer DNA Chip per the instructions of the manufacturer.

5.4 RESULTS

5.4.1 Prolonged osmotic stress affects circadian clock related genes

When analyzing the RNA sequencing data obtained after 5 minutes, 12 hours and 24 hours of hypo-osmotic stress (Fig. 5.2), it was evident that the five-minute time point was too short to trigger significant differences in gene expression. However, as expected, the longer the exposure,

the larger the array of genes that were affected due to osmotic stress. This effect ca be visualized in **Fig. 5.2[20]** where we used an MA plot, (an application of Bland-Altman plot, for visual representation of genomic data). The MA plot visualizes the data by transforming it into M (log ratio) and A (mean average) scales for two sets of data. If the two sets of data are represented as R and G, then M= ($\log_2$R- $\log_2$G) showing the difference between the two sets of data and A= ($\log_2$R+ $\log_2$G)/2 representing the geometric mean of the two sample sets. Due to the dynamic range of the samples from a few hundred to approximately fifty thousand, the log numbers are taken in order to shrink that range and make the calculations manageable. Therefore, the y axis represents the difference between the two groups while the x axis shows the average read counts.

When analyzing the genes whose expression was altered due to osmotic stress, we first looked at overlapping genes between the 12-hour and the 24-hour osmotic stress (**Fig. 5.3**). For the overlapping genes that were upregulated more than 3-fold, we found that they were involved in different functional pathways, suggesting that osmotic stress is pervasive and affects several processes simultaneously. One of the identified upregulated genes was *Pld4* (phospholipase D family member 4), which has been shown to regulate phagocytosis and endosomal nucleic-acid sensing[21; 22; 23].

While there were hundreds of genes overlapping for the 12-hour osmotic stress and the 24- hour osmotic stress condition, when we looked at the genes that were downregulated more than 3-fold, no overlapping genes were identified. After 12 hours of osmotic stress, only 2 genes were downregulated more than 3-fold with the first one being synaptotagmin 13 (syt13, - 3.4fold), which is involved in vesicle release. The second one identified was fatty acid 2-hydroxylase (fa2h, - 4.1fold), which is mainly involved in lipid metabolism. In particular human syt13 gene had been characterized as a key mediator in liver tumor suppression [24] while other studies have shown that syt13 is a novel biomarker in lung adenocarcinoma [25]. In addition, 58% of the genes that were downregulated more than 3-fold after 24-hour osmotic stress, are associated with plasma membrane functions, indicating the expected finding that osmotically induced stretch impact expression and function of membrane proteins.
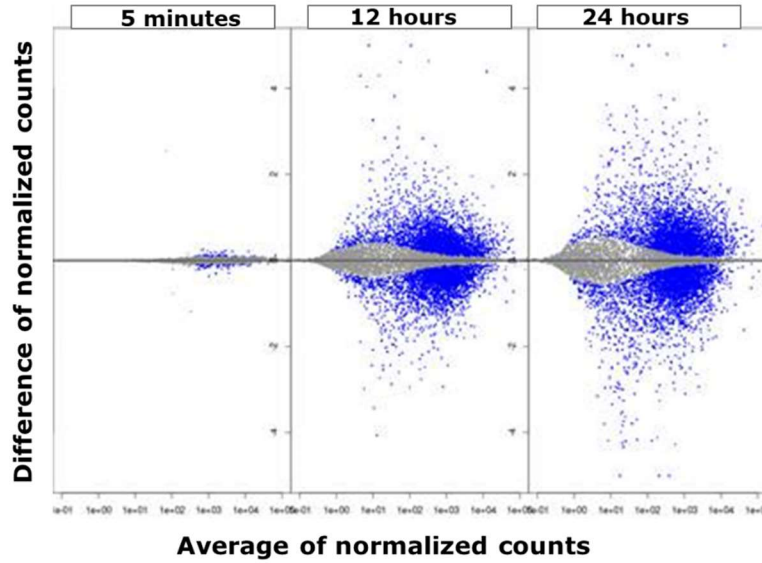
Figure 5. 2 MA plot visualizing the log ratio and mean average of the data. (left) After 5 minutes of osmotic stress there are almost no differentially expressed genes. After 12 hours osmotic stress (middle) and 24 hours of osmotic stress (right) a very large number of genes are changed. These lists of genes use a cutoff padj<0.1.
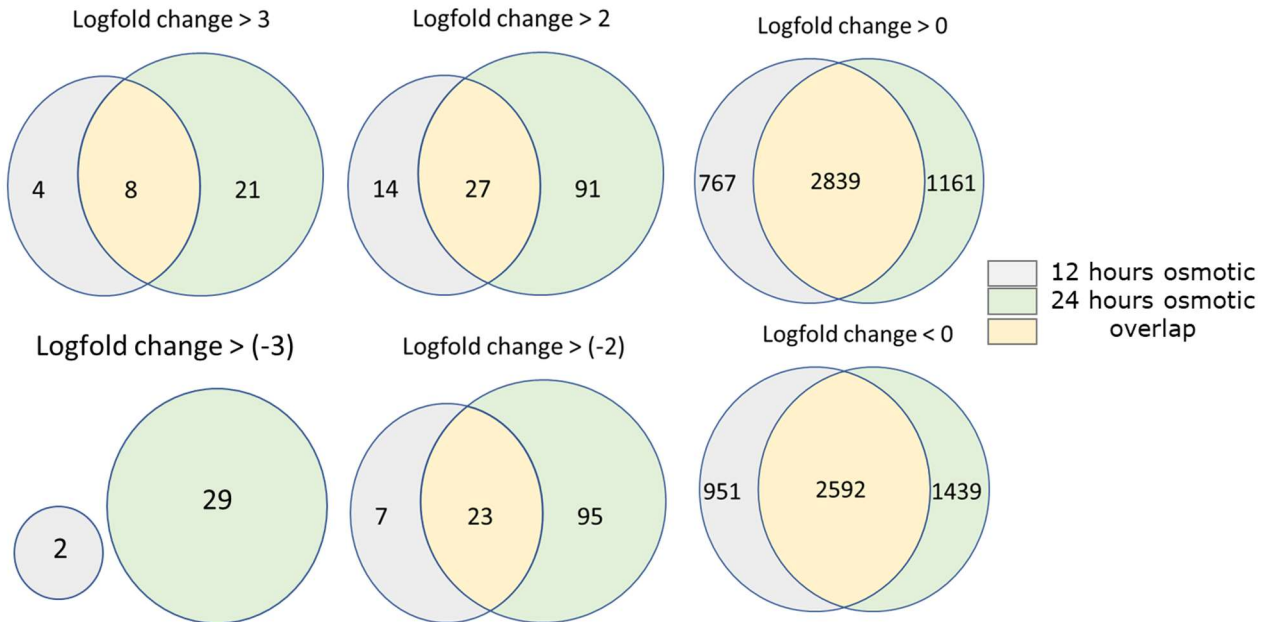
Figure 5. 3: Categorization of genes by fold change due to 12-hour/24-hour hypo-osmotic stress. Light gray corresponds to the number of genes whose production was altered after 12-hours

osmotic stress, light green indicated the genes for 24-hour osmotic stress and yellow represents the overlapping genes for the two conditions.

Our data analysis shows that more than 100 genes are differentially expressed between the 12 hours and 24 hours osmotic time points. Interestingly, we found that the most prominent ones are fundamental components of the circadian *CLOCK* genes. Examples of these genes can be found in **Table 5.1**. Specifically period 1, 2 and 3 (*per*1,2,3) are genes implicated in rhythm generation and entrainment[26]. While previous studies have shown that asynchronized cells become synchronized after oscillating serum starvation exposure, other studies relate osmotic stress with G1 cell cycle delay[27]. These data suggest that exposing cultured unsynchronized cells to prolonged osmotic stress may synchronize the cell cycle. In other words, BMAL1 not only has a vital role in the circadian clock but is also a translation factor involved in regulation of protein synthesis.

Our lab has previously shown the importance of osmotic stress in recruiting cytosolic PLCβ to the plasma membrane, leading to release of SG proteins and formation of stress granules[28]. However, there has been no direct correlation between PLCβ and BMAL1 transcription factor, or any of its effectors. Previous studies have correlated the activities of phospholipase C, adenylate cyclase (AC) and protein kinase A (PKA) with per2 rhythms in suprachiasmatic nucleus (SCN) neurons. Besides the transcriptional repression of Per genes, circadian rhythm oscillations are also dependent on vasoactive intestinal polypeptide (VIP) signaling between cells. Because VIP is released by SCN neurons in a circadian pattern, it was found that these synchronized oscillations occur due to parallel changes in PLCβ and adenylate cyclase. In addition, there are studies showing that angiotensin II induces circadian gene expression of CLOCK genes in cultured vascular smooth muscle cells suggesting a potential correlation between GPCR specific hormones, stress granule accumulation and cell cycle[29].

Differences in gene expression

Genes	12 hours osmotic stress	24 hours osmotic stress
ciart	-1.15	+2.76
dbp	-1.02	+1.90
nr1d1	-2.44	+1.64
per1	-1.60	+1.10
nr1d2	-1.31	+0.87
per3	-1.06	+0.54

Table 5. 1: Osmotic stress affects circadian gene expression. After 12 hours of osmotic stress the expression of the circadian clock genes decreased while it gets partially or fully restored after 24 hours of osmotic stress suggesting cell cycle synchronization.

5.4.2 Lowering Caveolin-1/Cavin-1 expression has similar impact on gene expression

Both Cav-1 and cavin-1 are needed to form stable caveolae domains. Cav-1 and cavin-1 expression is interdependent, and it was not surprising that we found several overlapping genes. (**Fig. 5.4**). When looking at the overlapping genes for the two conditions that were upregulated more than 4-fold, only one gene was identified as unique with caveolin-1 knock down while the remaining 48 genes were overlapping.
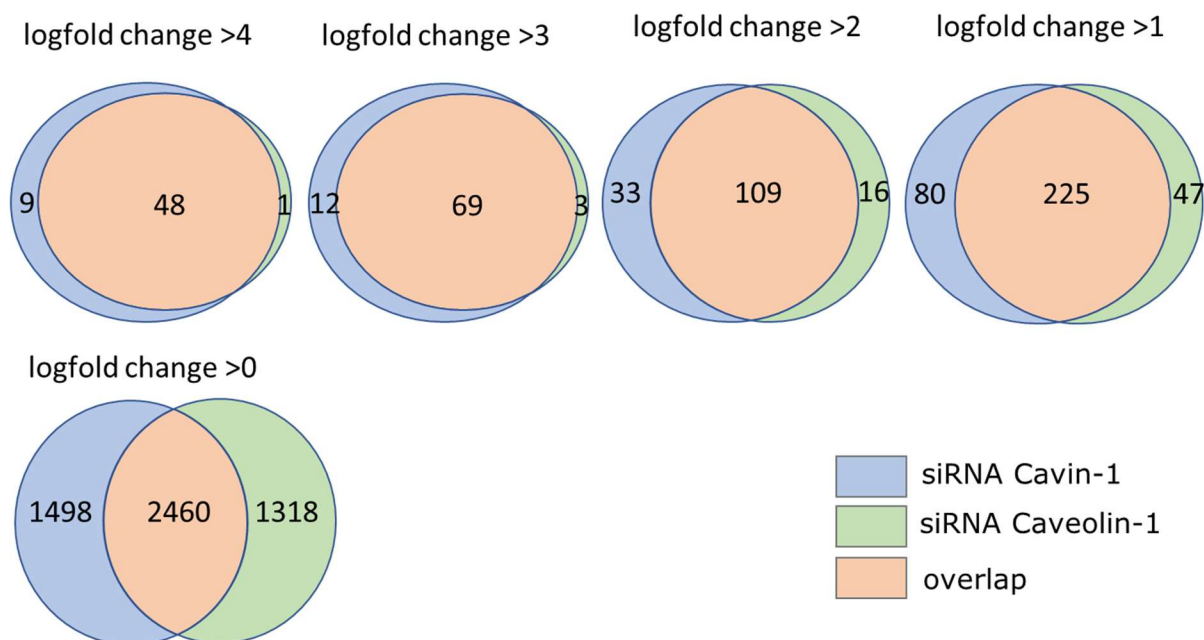
Figure 5. 4: Categorization of genes by fold change due to Caveolin-1/cavin-1 downregulation. Blue corresponds to the number of genes whose production was altered after cavin-1 was downregulated, green indicates the genes after caveolin-1 downregulation and orange represents the overlapping genes for the two conditions.

Interestingly, when looking at functional characteristics of the overlapping genes that were upregulated more than 3-fold, we found that 72% of them are involved in anti-viral responses with the remaining 28% being split almost equally between cancer biomarkers and cell apoptosis regulation. We have previously shown that when downregulating caveolin 1, there is an increase in cell death by ~40%, while downregulation of cavin-1 causes ~52% of cells to die. While the apoptotic genes were a somewhat expected result, the anti-viral immune response without the presence of viral RNA was a very interesting and intriguing finding that has been so far not documented in the literature to our knowledge.

The upregulated genes following Cav-1 and cavin-1 downregulation are shown in **Table 5.2**. As mentioned, some of the genes that were identified belong to the interferon and chemokine families, which are primary stimulators of anti-inflammatory signaling responses. A striking observation is their marked upregulation by up to 11-fold which suggests a quite robust and specific response. Most of the, 2460 upregulated and overlapping genes in total, were involved in cellular protein

modification, regulation of cell proliferation, regulation of apoptotic processes and neutrophil mediated immunity.

Genes	Gene Name	Viral Infection
mx1 (+11fold)	myxovirus (influenza virus) resistance 1	Influenza/Viral Encephalitis
zbp1 (+11fold)	serpin family A me Z-DNA binding protein 1	Herpes Simplex/Influenza
ifit3 (+10fold)	interferon-induced protein with tetratricopeptide repeats 3	Systematic Lupus Erythematosus
rsad2 (+10fold)	radical S-adenosyl methionine domain containing 2	Yellow Fever
ccl5 (+9fold)	C-C motif chemokine ligand 5	Human Immunodeficiency Virus Type 1
oasl (+8fold)	2'-5'-oligoadenylate synthetase-like	West Nile Virus Infection
ido1 (+7fold)	indoleamine 2,3-dioxygenase 1	Listeriosis/Chlamydia

Table 5. 2: Highest upregulated overlapping genes initiate anti-inflammatory responses.

To gain further insight into the activation of the cell immune response genes, we tested viral infectivity on the cells, using an adeno-associated virus. Adeno-associated viruses have been suggested to enter host cells through a caveolae-mediated mechanism, in addition to other mechanisms.[30]. We tested the ability of this virus to enter the cells and express a td tomato reporter gene under control conditions, or after caveolin-1/ cavin-1 downregulation (**Fig 5.5**). When caveolae are intact in control cells, approximately 21% of the cells are infected by the virus. Cavin-1 overexpression, decreases infectivity, indicating a protective effect of caveolae against viral infection. In support of this hypothesis, when caveolae are ablated, following caveolin-1 or cavin-1 downregulation, viral infectivity climbs to 71% and 82%, respectively. These down-regulated caveolin-1 or cavin-1 cells were then used for a rescue experiment where we transfected them with cavin-1-GFP to overexpress cavin-1 and allow the formation of caveolae. Indeed, with cavin-1 overexpression, there is a significant decrease in viral infectivity by more than 55 percent.
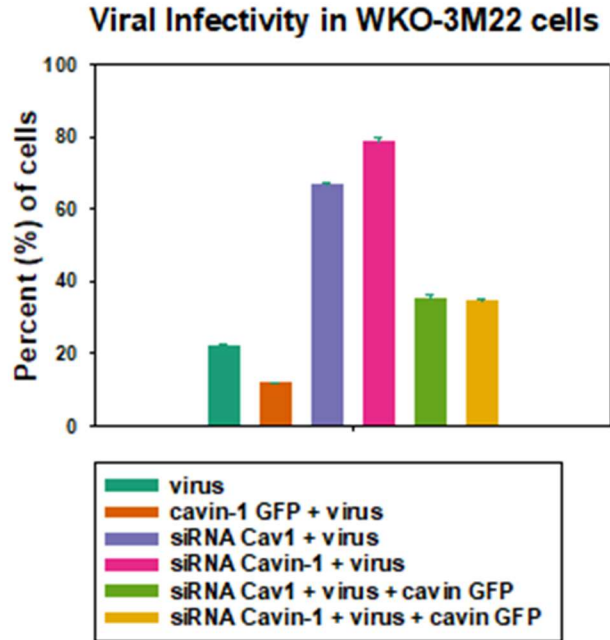
Figure 5. 5: Viral expression with caveolae deformation. Percent of control cells (green) transfected with the viral plasmid, co-transfected cells with viral plasmid and cavin-1 GFP (orange), caveolin-1 knock down cells expressing the virus (purple), cavin-1 knock down cells expressing the virus (pink). Rescue experiment with cavin-1 overexpression in Caveolin-1 knock down (green) and cavin-1 knock down (yellow) cells. Data shown from three independent experiment where n=120.

5.4.3 Caveolin-1 knock down decreases c-fos expression

While analyzing the genes whose expression decreased with the absence of Cav-1 or cavin-1, we did not find overlapping genes that were downregulated more than two-fold (**Fig. 5.5**). Specifically, no genes were downregulated more than 2-fold for the cavin-1 knock down. When downregulating caveolin-1, the production of two genes reduced more than 2-fold, *Actin Filament Associated Protein 1 Like 2* (*afap1l2,* -2.03 Fold) and *Fos Proto-Oncogene Ap-1 Transcription Factor Subunit* (*fos,* -3.0 Fold). Afap1l2 is a known adaptor protein involved in the PI3K-AKT pathway[31]. Loss has been implicated with changes in cell cycle, mainly proliferation rates and apoptosis. On the other hand, the *fos* gene family has been extensively investigated in a variety of different cell types and tissue. Along with FOSB, FOSL1, and FOSL2, FOS encodes leucine zipper proteins that can dimerize with proteins of the JUN family forming the transcription factor complex AP-1[32; 33]. Therefore, the FOS proteins have been implicated as regulators of cell

proliferation, differentiation, and transformation while in some cases they have also been implicated in cell apoptosis.
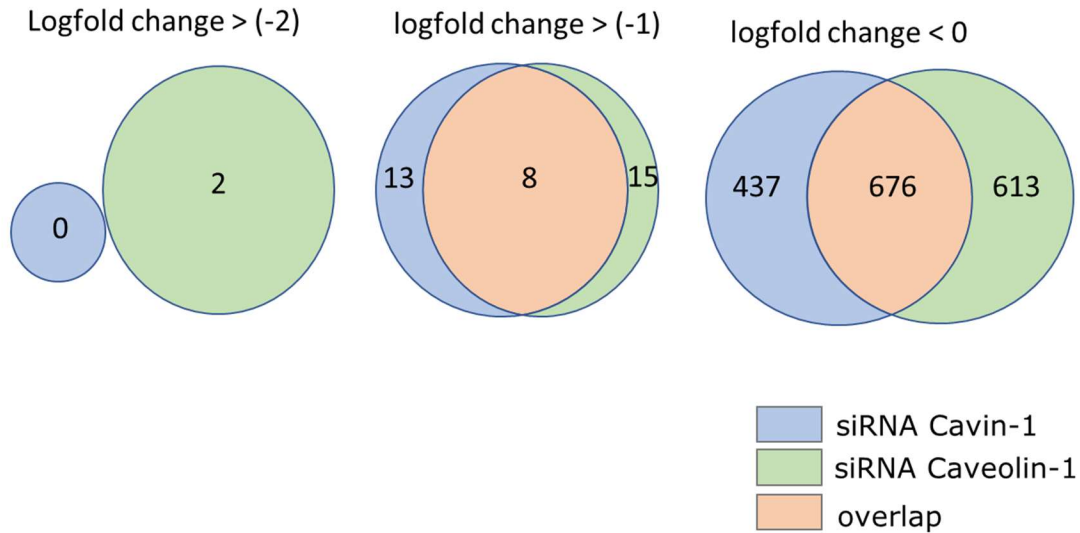
Figure 5.6: Categorization of genes by fold change due to Caveolin-1/cavin-1 downregulation. Blue corresponds to the number of genes whose production was altered after cavin-1 was downregulated, green indicates the genes after caveolin-1 downregulation and orange represents the overlapping genes for the two conditions.

5.4.4 Bi-directional cyclic mechanical stretch induces cell apoptosis in smooth muscle cells

When analyzing the genes whose production was altered following mechanical stretch, we found more upregulated genes than downregulated ones (**Fig 5.7**). When focusing on the downregulated genes, only two genes were identified with a profound change exceeding the 3-fold. These two genes were: *FAT Atypical Cadherin 3* (*fat3*, -3.2-fold) and *Gap Junction Protein Alpha 5* (*gja5*, -4.9-fold). FAT3 along with fat1, fat2 and fat4 are human homologs of Drosophila Fat involved in tumor suppression and planar cell polarity (PCP)[34]. Gap Junctions are functionally very important in smooth muscle cells since they mediate plasticity in arterial walls[35]. GJA5 specifically is known to modulate arterial identity and arteriogenesis. Different studies have also shown that mutations in GJA5 may predispose patients to idiopathic atrial fibrillation by impairing gap-junction assembly or electrical coupling[36; 37].
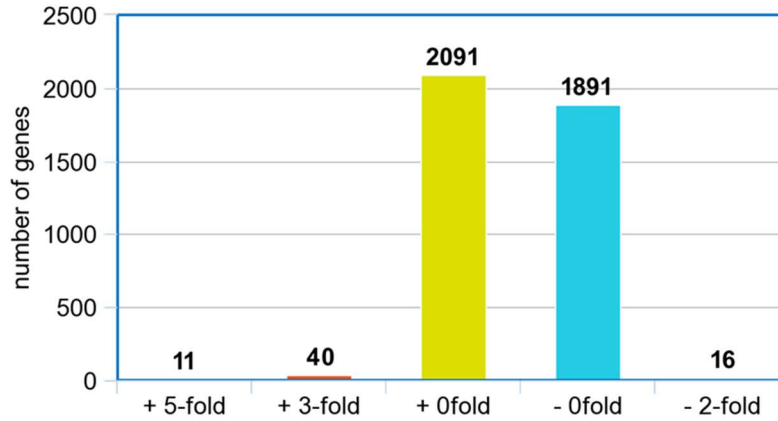
Figure 5. 7: Number of genes altered due to mechanical stretch organized by fold change. The total number of upregulated genes was 2091 (yellow) while the total number of downregulated ones was 1891 (cyan). Only 11 genes were upregulated more than 5-fold while 40 of them were upregulated more than 3-fold (red). Only 16 genes were downregulated more than 2-fold.

When looking at the biological processes that these genes were involved in, many of them were correlated with transcriptional misregulation and proteoglycans in cancer, while others affected processing in the endoplasmic reticulum, autophagy and apoptosis. The most upregulated genes for these conditions can be found in **Table 5.3**.

Genes	Gene Name
prss35 (+7fold)	protease, serine, 35
akr1c14 (+7fold)	aldo-keto reductase family 1, member C14
slc4a11 (+6.6fold)	solute carrier family 4 member 11
ptgs2 (+6.6fold)	prostaglandin-endoperoxide synthase 2
trem3 (+6.2fold)	triggering receptor expressed on myeloid cells 3
phex (+6fold)	phosphate regulating endopeptidase homolog, X-linked
lilrb4 (+6fold)	leukocyte immunoglobulin like receptor B4
slco4a1 (+6fold)	solute carrier organic anion transporter family, member 4a1

Table 5. 3 Highest upregulated genes due to mechanical stretch.

5.5 DISCUSSION

While we identified a plethora of genes related to the presence and expression level of cavin-1, it is difficult, in most cases, to infer their precise physiological roles. Nonetheless, a few findings were novel and paved the way for new hypotheses on the physiological roles of caveolae. Our results uncovered a previously undocumented link between hypo-osmotic stress and the expression of circadian rhythm genes. In Chapter 3, we reported that osmotic stress promotes the formation of stress granules in the cytosol of cells, where stress granule proteins and untranslated mRNA accumulate until the stress is released[28]. Other studies have shown that the circadian rhythm protein, BMAL1, dimerizes in the cytosol with the CLOCK transcription factor, and enters the nucleus where it binds to the enhancer box promoting the transcription of the *cry* and *per* family genes. Upon exposure to 12 hours of continuous hypo-osmotic stress, the dimerization of the two transcription factors in the cytoplasm of cells is not possible potentially because of dilution [9]. Therefore, there is no binding to the E-box leading to decreased transcription of *per* and *cry* genes (**Fig. 5.8**). The lack of dimer may lead to the phosphorylation of BMAL1, which binds to stress granule proteins and inhibits the formation of stress granules. However, the phosphorylated state of BMAL1 does not last indefinitely, and 12 hours later (total of 24 hours of hypo-osmotic stress) BMAL1 is free to dimerize with CLOCK and enter the nucleus, bind to the E-box and induce the transcription of *per* and *cry* genes. SG protein synthesis is still low explaining why there is no SG formation when caveolae is deformed. These precisely timed oscillations allow us to conclude that prolonged osmotic stress may lead to cell synchronization with BMAL1 phosphorylation playing a key role in this process. Even though preliminary data from our lab suggest that PLCβ1 is upregulated in the mitotic phase, the actual role of PLCβ in mediating stress granule formation through the circadian rhythm metabolism remains unclear.
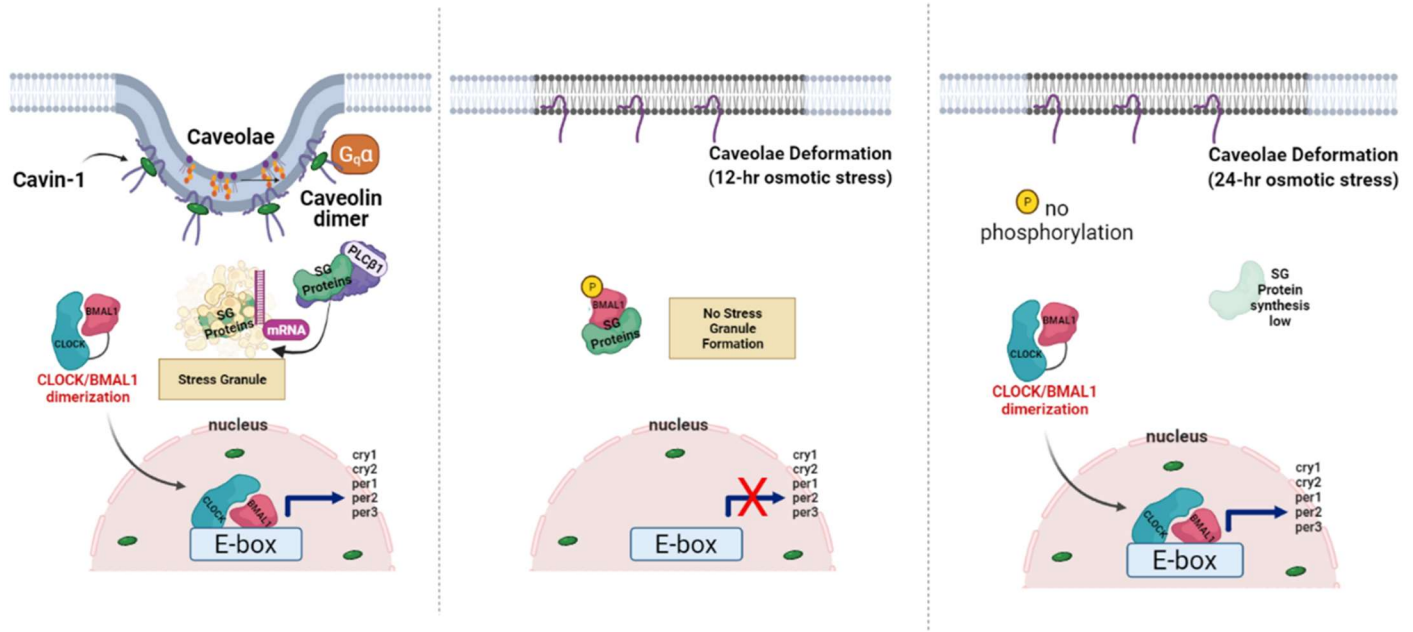
Figure 5. 8: Model for cell synchronization with prolonged osmotic stress exposure. (Left) control conditions showing CLOCK/BMAL1 dimerization in the cytoplasm, stress granule formation and caveolae structure intact, (middle) 12-hour osmotic stress causing BMAL1 phosphorylation, caveolae deformation and decreased transcription of *cry* and *per* family genes, (right) events unfolding after 24-hour osmotic stress with caveolae remaining deformed, SG protein synthesis low and no BMAL1 phosphorylation taking place.

Another major finding in our experiments is the stimulation of an anti-viral immune response with caveolae deformation. So far, we know that viral entry can occur through caveolae, where viral particles will cause their disruption, and that Cav-1 is required for caveolae dependent endocytosis[38]. It is also known that expression of Cav-1 and cavin-1 are interdependent, meaning that downregulating either of them will negatively affect the caveolae structures [39].

When either of these two proteins are downregulated, the cells initiate defense mechanisms triggering the activation and recruitment of the immune response cells. These, in turn produce inflammation that further enhance the immune response mediated by interferons and chemokines that send signals to initiate the production of anti-inflammatory genes. This anti-inflammatory response is needed to avoid tissue damage due to excessive immune cell activation and activity. The increased transcription of anti-viral genes without the presence of viral DNA or RNA

suggests that the disruption of caveolae and the absence of cavin-1 from the nucleus signals an alarm, ultimately activating expression and production of cytokines and hence triggering an immune response. It is possible, but unconfirmed, that the residual cavin-1 exit the nucleus in an attempt to assist Cav-1 in restoring caveolae structure. It is also possible that when cells are infected, they lack cavin-1 in the nucleus which may allow triggering of defense gene upregulation (**Fig. 5.9**). Additional experiments will need to be conducted in order to validate the precise signaling events.
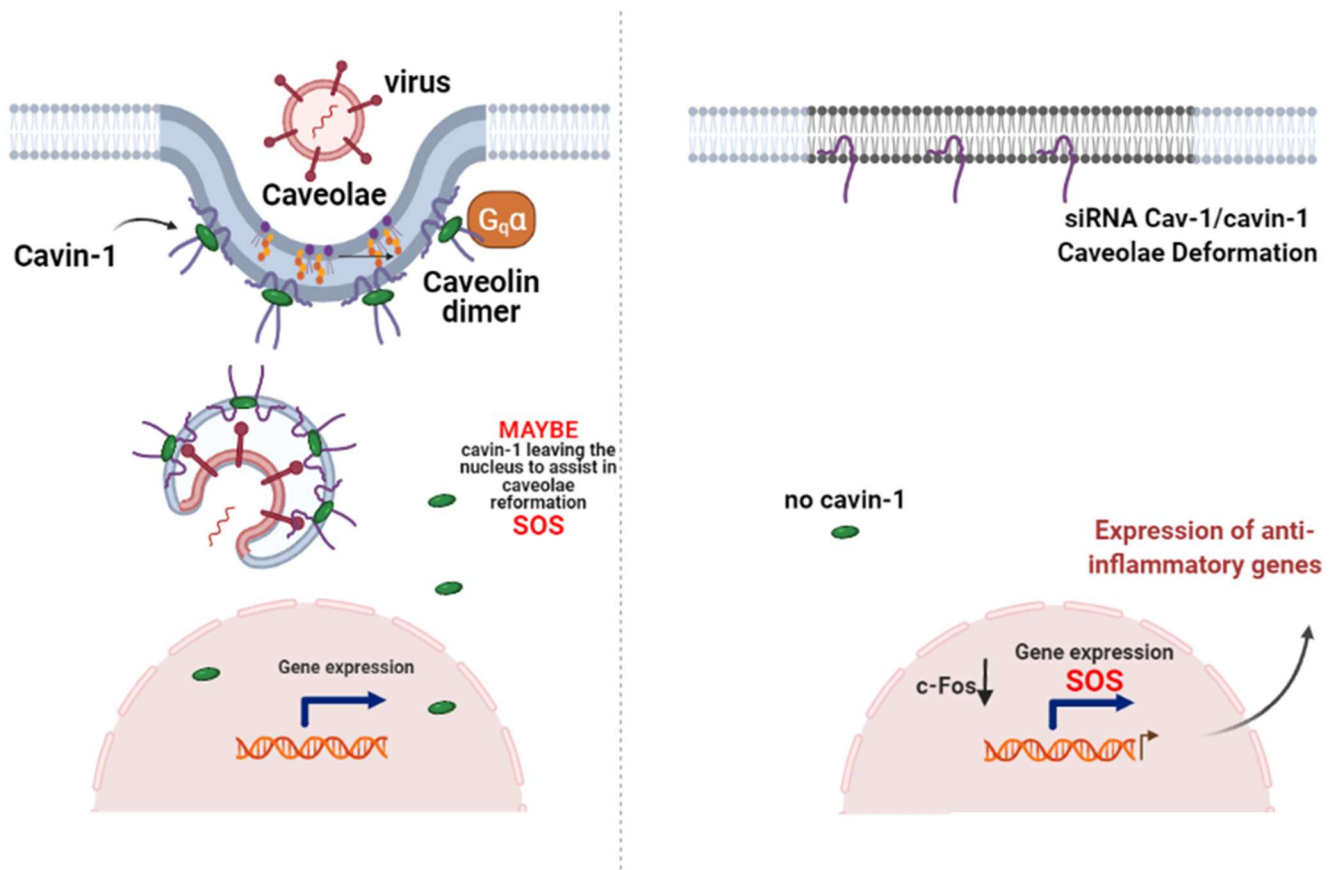
Figure 5. 9: Model for viral entry and caveolae deformation. (Left) caveolae disruption due to viral entry and cavin-1 exiting the nucleus assisting Cav-1 in caveolae reformation. (Right) Caveolae disruption due to knock down of Cav-1/cavin-1 and upregulation of anti-inflammatory gene expression.

While the effects of mechanical stretch in carcinogenesis and apoptotic behaviors have been studied extensively, the results obtained in this study raise new questions on the role of G-protein-

coupled receptor (GPCR) signaling in stem cell biology and cell survival. Even though the first candidate for a mechanosensitive GPCR has been the angiotensin-II type-1 (AT1) receptor[40], we identified other potential regulators of signaling transduction in the GPCR mediated signaling pathway. The effect extended to other GPCRs involved need to be further studied and analyzed.

5.6 ACKNOWLEDGEMENTS

5.7 REFERENCES

[1] H. Hao, G. Gabbiani, and M.L. Bochaton-Piallat, Arterial smooth muscle cell heterogeneity: implications for atherosclerosis and restenosis development. Arterioscler Thromb Vasc Biol 23 (2003) 1510-20.

[2] O. Espitia, M. Chatelais, M. Steenman, C. Charrier, B. Maurel, S. Georges, R. Houlgatte, F. Verrecchia, B. Ory, F. Lamoureux, D. Heymann, Y. Goueffic, and T. Quillard, Implication of molecular vascular smooth muscle cell heterogeneity among arterial beds in arterial calcification. PLoS One 13 (2018) e0191976.

[3] S.S. Rensen, P.A. Doevendans, and G.J. van Eys, Regulation and characteristics of vascular smooth muscle cell phenotypic diversity. Neth Heart J 15 (2007) 100-8.

[4] K. Sobue, K. Hayashi, and W. Nishida, Expressional regulation of smooth muscle cell-specific genes in association with phenotypic modulation. Mol Cell Biochem 190 (1999) 105-18.

[5] J. Solway, J. Seltzer, F.F. Samaha, S. Kim, L.E. Alger, Q. Niu, E.E. Morrisey, H.S. Ip, and M.S. Parmacek, Structure and expression of a smooth muscle cell-specific gene, SM22 alpha. J Biol Chem 270 (1995) 13460-9.

[6] T. Lange, S. Dimitrov, and J. Born, Effects of sleep and circadian rhythm on the human immune system. Ann N Y Acad Sci 1193 (2010) 48-59.

[7] A. Balsalobre, F. Damiola, and U. Schibler, A serum shock induces circadian gene expression in mammalian tissue culture cells. Cell 93 (1998) 929-37.

[8] S.J. Silverman, A.A. Petti, N. Slavov, L. Parsons, R. Briehof, S.Y. Thiberge, D. Zenklusen, S.J. Gandhi, D.R. Larson, R.H. Singer, and D. Botstein, Metabolic cycling in single yeast cells from unsynchronized steady-state populations limited on glucose or phosphate. Proc Natl Acad Sci U S A 107 (2010) 6946-51.

[9] J.O. Lipton, E.D. Yuan, L.M. Boyle, D. Ebrahimi-Fakhari, E. Kwiatkowski, A. Nathan, T. Guttler, F. Davis, J.M. Asara, and M. Sahin, The Circadian Protein BMAL1 Regulates Translation in Response to S6K1-Mediated Phosphorylation. Cell 161 (2015) 1138-1151.

[10] M.M. Poranen, R. Daugelavicius, and D.H. Bamford, Common principles in viral entry. Annu Rev Microbiol 56 (2002) 521-38.

[11] H. Wang, P. Yang, K. Liu, F. Guo, Y. Zhang, G. Zhang, and C. Jiang, SARS coronavirus entry into host cells through a novel clathrin- and caveolae-independent endocytic pathway. Cell Res 18 (2008) 290-301.

[12] M.J. Duncan, J.S. Shin, and S.N. Abraham, Microbial entry through caveolae: variations on a theme. Cell Microbiol 4 (2002) 783-91.

[13] A.L. Kiss, and E. Botos, Endocytosis via caveolae: alternative pathway with distinct cellular compartments to avoid lysosomal degradation? J Cell Mol Med 13 (2009) 1228-37.

[14] L. Pelkmans, and A. Helenius, Endocytosis via caveolae. Traffic 3 (2002) 311-20.

[15] F. Wernig, and Q. Xu, Mechanical stress-induced apoptosis in the cardiovascular system. Prog Biophys Mol Biol 78 (2002) 105-37.

[16] M. Sotoudeh, Y.S. Li, N. Yajima, C.C. Chang, T.C. Tsou, Y. Wang, S. Usami, A. Ratcliffe, S. Chien, and J.Y. Shyy, Induction of apoptosis in vascular smooth muscle cells by mechanical stretch. Am J Physiol Heart Circ Physiol 282 (2002) H1709-16.

[17] J. Sanchez-Esteban, Y. Wang, L.A. Cicchiello, and L.P. Rubin, Cyclic mechanical stretch inhibits cell proliferation and induces apoptosis in fetal rat lung fibroblasts. Am J Physiol Lung Cell Mol Physiol 282 (2002) L448-56.

[18] A. Qifti, O. Garwain, and S. Scarlata, Mechanical Stretch Redefines Membrane Galphaq-Calcium Signaling Complexes. J Membr Biol 252 (2019) 307-315.

[19] H. Cirka, M. Monterosso, N. Diamantides, J. Favreau, Q. Wen, and K. Billiar, Active Traction Force Response to Long-Term Cyclic Stretch Is Dependent on Cell Pre-stress. Biophys J 110 (2016) 1845-1857.

[20] D. Giavarina, Understanding Bland Altman analysis. Biochem Med (Zagreb) 25 (2015) 141-51.

[21] A.L. Gavin, D. Huang, C. Huber, A. Martensson, V. Tardif, P.D. Skog, T.R. Blane, T.C. Thinnes, K. Osborn, H.S. Chong, F. Kargaran, P. Kimm, A. Zeitjian, R.L. Sielski, M. Briggs, S.R. Schulz, A. Zarpellon, B. Cravatt, E.S. Pang, J. Teijaro, J.C. de la Torre, M. O'Keeffe, H. Hochrein, M. Damme, L. Teyton, B.R. Lawson, and D. Nemazee, PLD3 and PLD4 are single-stranded acid exonucleases that regulate endosomal nucleic-acid sensing. Nat Immunol 19 (2018) 942-953.

[22] A.C. Gonzalez, S. Stroobants, P. Reisdorf, A.L. Gavin, D. Nemazee, D. Schwudke, R. D'Hooge, P. Saftig, and M. Damme, PLD3 and spinocerebellar ataxia. Brain 141 (2018) e78.

[23] Y. Otani, Y. Yamaguchi, Y. Sato, T. Furuichi, K. Ikenaka, H. Kitani, and H. Baba, PLD$ is involved in phagocytosis of microglia: expression and localization changes of PLD4 are correlated with activation state of microglia. PLoS One 6 (2011) e27544.

[24] J.E. Jahn, and W.B. Coleman, Re-expression of tumorigenicity after attenuation of human synaptotagmin 13 in a suppressed microcell hybrid cell line. Int J Oncol 32 (2008) 441-9.

[25] L. Zhang, B. Fan, Y. Zheng, Y. Lou, Y. Cui, K. Wang, T. Zhang, and X. Tan, Identification SYT13 as a novel biomarker in lung adenocarcinoma. J Cell Biochem 121 (2020) 963-973.

[26] S. An, R.P. Irwin, C.N. Allen, C. Tsai, and E.D. Herzog, Vasoactive intestinal polypeptide requires parallel changes in adenylate cyclase and phospholipase C to entrain circadian rhythms to a predictable phase. J Neurophysiol 105 (2011) 2289-96.

[27] G. Belli, E. Gari, M. Aldea, and E. Herrero, Osmotic stress causes a G1 cell cycle delay and downregulation of Cln3/Cdc28 activity in Saccharomyces cerevisiae. Mol Microbiol 39 (2001) 1022-35.

[28] A. Qifti, L. Jackson, A. Singla, O. Garwain, and S. Scarlata, Stimulation of phospholipase Cbeta1 by Galphaq promotes the assembly of stress granule proteins. Sci Signal 14 (2021) eaav1012.

[29] H. Nonaka, N. Emoto, K. Ikeda, H. Fukuya, M.S. Rohman, S.B. Raharjo, K. Yagita, H. Okamura, and M. Yokoyama, Angiotensin II induces circadian gene expression of clock genes in cultured vascular smooth muscle cells. Circulation 104 (2001) 1746-8.

[30] H. Wang, Y. Li, F. Sun, Y. Feng, K. Jin, and X. Wang, 1,2,3,4-Tetrahydro-8-hydroxyquinoline-promoted copper-catalyzed coupling of nitrogen nucleophiles and aryl bromides. J Org Chem 73 (2008) 8639-42.

[31] N. Tanga, K. Kuboyama, A. Kishimoto, H. Kiyonari, A. Shiraishi, R. Suzuki, T. Watanabe, A. Fujikawa, and M. Noda, The PTN-PTPRZ signal activates the AFAP1L2-dependent PI3K-AKT pathway for oligodendrocyte differentiation: Targeted inactivation of PTPRZ activity in mice. Glia 67 (2019) 967-984.

[32] R. Chiu, W.J. Boyle, J. Meek, T. Smeal, T. Hunter, and M. Karin, The c-Fos protein interacts with c-Jun/AP-1 to stimulate transcription of AP-1 responsive genes. Cell 54 (1988) 541-52.

[33] P. Angel, and M. Karin, The role of Jun, Fos and the AP-1 complex in cell-proliferation and transformation. Biochim Biophys Acta 1072 (1991) 129-57.

[34] M. Katoh, Function and cancer genomics of FAT family genes (review). Int J Oncol 41 (2012) 1913-8.

[35] X.F. Figueroa, and B.R. Duling, Gap junctions in the control of vascular function. Antioxid Redox Signal 11 (2009) 251-66.

[36] I. Buschmann, A. Pries, B. Styp-Rekowska, P. Hillmeister, L. Loufrani, D. Henrion, Y. Shi, A. Duelsner, I. Hoefer, N. Gatzke, H. Wang, K. Lehmann, L. Ulm, Z. Ritter, P. Hauff, R. Hlushchuk, V. Djonov, T. van Veen, and F. le Noble, Pulsatile shear and Gja5 modulate arterial identity and remodeling events during flow-driven arteriogenesis. Development 137 (2010) 2187-96.

[37] M.H. Gollob, D.L. Jones, A.D. Krahn, L. Danis, X.Q. Gong, Q. Shao, X. Liu, J.P. Veinot, A.S. Tang, A.F. Stewart, F. Tesson, G.J. Klein, R. Yee, A.C. Skanes, G.M. Guiraudon, L. Ebihara, and D. Bai, Somatic mutations in the connexin 40 gene (GJA5) in atrial fibrillation. N Engl J Med 354 (2006) 2677-88.

[38] J.L. Smith, S.K. Campos, A. Wandinger-Ness, and M.A. Ozbun, Caveolin-1-dependent infectious entry of human papillomavirus type 31 in human keratinocytes proceeds to the endosomal pathway for pH-dependent uncoating. J Virol 82 (2008) 9505-12.

[39] Y. Zhou, N. Ariotti, J. Rae, H. Liang, V. Tillu, S. Tee, M. Bastiani, A.T. Bademosi, B.M. Collins, F.A. Meunier, J.F. Hancock, and R.G. Parton, Caveolin-1 and cavin1 act synergistically to generate a unique lipid environment in caveolae. J Cell Biol 220 (2021).

[40] U. Storch, M. Mederos y Schnitzler, and T. Gudermann, G protein-mediated stretch reception. Am J Physiol Heart Circ Physiol 302 (2012) H1241-9.

CHAPTER 6 - CONCLUSIONS, LIMITATIONS, AND FUTURE WORK

6.1 CONCLUSIONS

6.1.1 Conclusions Chapter 3 (Aim 1)

While the complexity and the multifunctionality of PLCβ is already known to be mainly taking part on the plasma membrane regulating calcium signaling, this dissertation contributed to the identification of cytosolic binding partners for the protein. Identifying these binding partners led to a series of novel findings including the accumulation of stress granule through the Gαq/PLCβ1 signaling pathway. In addition, so far stress granules were shown to form due to the application of oxidative stress through various concentrations of arsenite added to the media of cells and animal models. Here, we showed that different environmental stress showed a significant increase in stress granule formation **(Fig. 6.1).** It must be noted that differences depended on the type of stress that was applied. While promoting stress granule formation through external environmental conditions, we were able to not only quantify the differences between the various stressors but also visualize the formation of stress granules in real time. The methods used contributed to the better understanding of the composition of these granules and their triggers, providing fundamental insight for future experimental design and optimization.

However, the work conducted was mainly focused on the visualization of accumulated granules rather than their disassembly suggesting the need for future experiments focusing on that process and the signaling components that mainly regulate it. It is already known that delayed disassembly of these stress granules is implicated in several diseases and disorders including Amyotrophic Lateral Sclerosis and Autism Spectrum Disorder[1; 2; 3]. Therefore, identifying the components that assist or regulate this process would provide valuable insight for potential biomarkers in pharmaceutical discoveries and disease prevention.
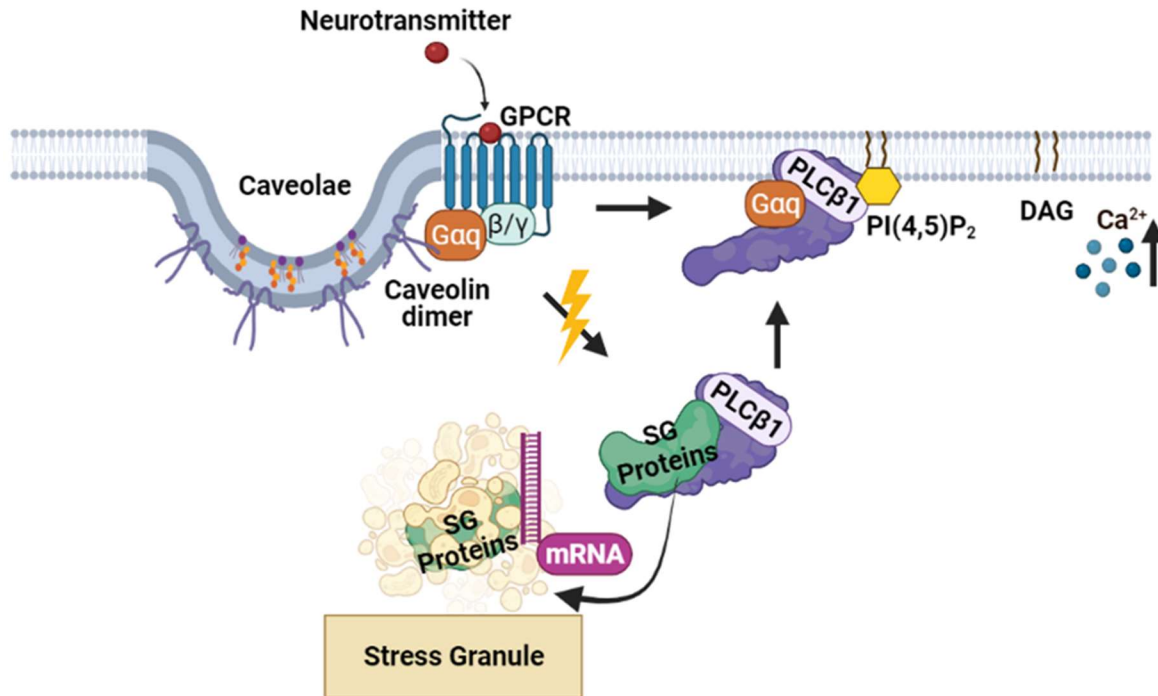
Figure 6.1: Model presenting stress granule formation through the Gαq/PLCβ1 signaling pathway.

6.1.2 Conclusions Chapter 4 (Aim 2)

Caveolae and its components, especially cav-1, have been identified as mediators in various processes including mechanosensation, endocytosis, cell mobility, and apoptosis[4; 5; 6; 7]. While the role of caveolae's components has been thoroughly examined over several decades, this dissertation provides valuable insight regarding the role of caveolae in stress adaptation and the signaling events that take place upon its deformation on the plasma membrane. With cav-1 not directly promoting the accumulation of stress granules and p-bodies, we found that cavin-1 mediates the signaling cascade initiated by caveolae deformation. While several studies have shown cavin-1 as an integral part of the plasma membrane ensuring the structure of caveolae[8; 9; 10] and other studies mention cavin-1 being present in the nucleus and assisting polymerase-1 in transcription termination, this dissertation provides evidence that cavin-1 relocalizes to the nucleus[11]. The relocalization occurs after applying hypo-osmotic stress or upon activation of the Gαq/ PLCβ1 by using carbachol or bradykinin. This property of cavin-1 must be further explored since this protein has the potential of being used as a pharmaceutical vehicle for delivering necessary drugs to the nucleus to halt or promote transcription and translation of genes of interest.

6.1.3 Conclusions Chapter 5 (Aim 3)

So far, this dissertation has presented evidence regarding the multifunctionality of both PLCβ1 and cavin-1 which are mediating fundamental processes in different compartments of the cell. Now, it is important for us to try and further understand and correlate the GPCR signaling pathway as we know it with the complexity of caveolae.

We focused on identifying changes occurring in the nucleus after caveolae deformation and through the PLCβ/Gαq signaling pathway. Some of the most striking findings that need to be further analyzed and understood involved changes in the expression of genes consisting of the circadian rhythm signaling regulation, the anti-inflammatory immune response, the apoptotic mechanism, as well as tumorigenesis and tumor suppression. Overall, these data suggest that the caveolae/Gαq/PLCβ1 pathway allow smooth muscle cells to adapt to changes and the summary of all signaling events described in this dissertation can be found in **Fig. 6.2**.
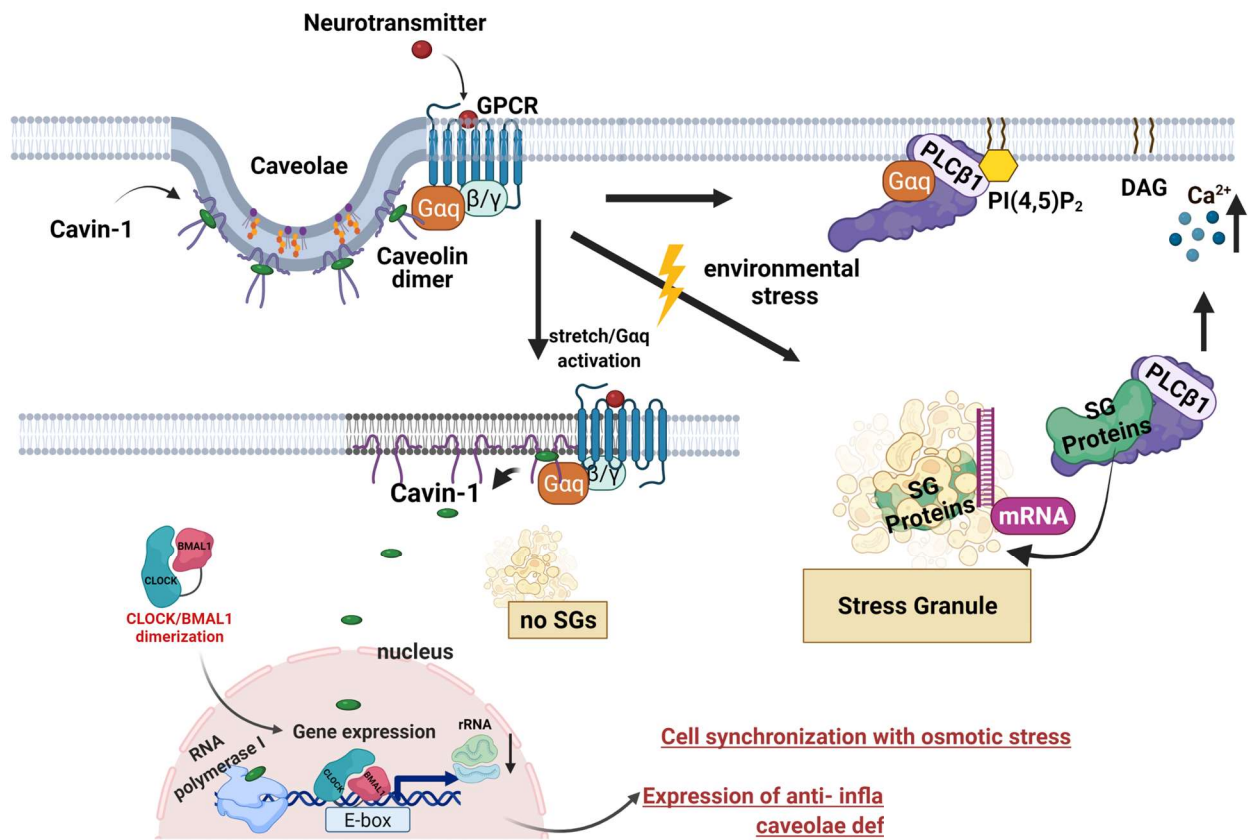
Figure 6. 2: Summary model of all chapters. This model presents the activation of PLCβ1 on the plasma membrane, the stress granule formation mediated by cytosolic PLCβ and the changes occurring in gene expression due to caveolae deformation and cavin-1 relocalization from the plasma membrane to the nucleus.

6.2 EXPERIMENTAL LIMITATIONS

There were several limitations that may contributed to our experiments (see below). These limitations did not take away from the overall findings that cavin-1 mediates information from the plasma membrane to the nucleus. However, next steps should address some of these limitations by improving experimental procedures.

6.2.1 Experimental Limitations Aim 1

6.2.1.1 Particle Analysis Data Presentation

In our first aim, we used Particle Analysis as a method to visualize the formation of stress granules in fixed cells upon immunostaining them with antibodies for specific stress granule marker

proteins such as PABPC1, Ago2 and G3BP1. We then used our 2-photon microscope to take optical slices along the z axis of each cell to generate a graph with the total number and size of the particles forming. When graphing the data, we arranged it as two independent sets of data with the number of particles represented on the y-axis and the size of particles represented on the x-axis. We chose this representation after trying several different ones including combining all optical slices into a 3-D figure before conducting the analysis as well as presenting the data in a histogram. From all our options, this was the easiest to visualize since we were mainly interested in looking at the cumulative total number of stress granules formed under each condition that the cells were exposed to, along with the cumulative total area that the stress granules were occupying in each cell. We understand that when the optical slices are taken on the z-axis some stress granule particles can occupy more than one optical slice and therefore may be double counted. However, this limitation was carried along all the conditions and for all the data analysis that took place, and we can confidently claim that even though it is a limitation it did not alter our findings or discoveries in this aim.

6.2.2 Experimental Limitations Aim 2

6.2.2.1 PDMS plates and transfection

One of the most important goals of this aim was to use bi-directional mechanical stretch to deform the caveolae structure and look at cavin-1 translocation. For us to track cavin-1 localization in the cell, we had to use a GFP tagged plasmid that allowed us to conduct this experiment microscopically and with great accuracy. In order for the cells to be mechanically stretched, we culture them in PDMS plates that can be attached into a stretch device. This available stretch device belongs to the Billiar lab in the Biomedical Engineering department of Worcester Polytechnic Institute. While the cells were able to properly adhere and grow on the PDMS plates, throughout this project we were unable to transfect them with any available plasmid.

We usually use lipofectamine 3000 as an advanced lipid nanoparticle technology for transfection. However, we were unable to transfect cells cultured on PDMS plates. We then tried different transfection methods including electroporation, which is a physical transfection method, FuGENE HD reagents, along with different types of viruses. While none of these methods were successful, we found that lentiviruses, which are considered a biological method of transduction, were able to

show a small transfection efficiency. However, the transfection efficiency was too low to draw accurate results.

6.2.3 Experimental Limitations Aim 3

6.2.3.1 PDMS plates and cell concentration

One of the conditions tested in this Aim was the 12-hours mechanical bi-directional stretch. We cultured cells in PDMS plates and placed the device inside the incubator for 12 hours before collecting the cells. This experiment had two major drawbacks with the first one being the low concentration of the cells and the second one being the device itself. While the other conditions used cells cultured 100mm dishes that fit 10mL of media each, each PDMS plate can only fit 2mL of media. Therefore, the number of cells collected after the stretch was significantly lower than other conditions. However, we made sure to have appropriate control dishes to overcome this issue. In addition, the PDMS dishes were uncovered inside the incubator raising concern regarding the sterility of the environment without however, any noticeable contamination present. Again, appropriate controls were included in this experiment, however optimizing this method and improving the stretch conditions would be highly recommended for future experimental designs.

6.3 FUTURE WORK

The data presented in this thesis have supported the connection between the Gαq/PLCβ pathway and stress granule formation along with the novel ability of cavin-1 to relocalize to the nucleus and affect the production of various genes due to caveolae deformation. This process is evident in various types of cells including different smooth muscle cells, mouse embryonic fibroblasts, and PC12 cells. In addition to the conditions that were presented in this thesis, there are additional properties, markers, and experiments that have yet to be tested. Future work will greatly strengthen our understanding of the relationship between caveolae deformation and stress-associated mechanoadaptation.

6.3.1 Chapter 4: Future Work

6.3.1.1 Caveolin-1, Gαq and PLCβ1 binding.

In the studies in Chapter 3 and 4, the binding of PLCβ to activated Gαq has been well discussed and served as an origin for the rest of the studies. The ability of Cav-1 to stabilize the activated

state of Gαq since it binds to a different binding site, has also been one of the key properties of this protein. What is interesting and worth investigating is whether these three components can interact at the same time. Future studies should focus on understanding to what extent these interactions occur simultaneously and whether that will affect downstream effectors such as the intensity of calcium efflux or the ability of PLC to move from the cytoplasm to the plasma membrane and vice versa. While these interactions are known, this model has never been quantified so far. An easy way of approaching this experiment is by doing a multicolor FLIM/FRET and looking at the changes in lifetime for three different fluorophores, each of which is targeting one of the three proteins of our interest.

6.3.1.2 Cavin-1 relocalization in different cell types and tissue

The most novel finding in Chapter 4, was the ability of cavin-1 to relocalize from the plasma membrane to the nucleus upon caveolae deformation through hypoosmotic stress or Gαq stimulation. While these results were striking in the cell line that was used (WKO-3M22), it is important to verify this finding in alternate cell lines. Future studies could potentially focus on mouse embryonic fibroblasts to repeat this experiment and track the localization of cavin-1. In addition, primary smooth muscle cells could also by utilized after they are extracted from different aged mice to understand whether aging plays an important role in cavin-1 localization and whether or not other signaling events are assisting or preventing this process from happening.

6.3.2 Chapter 5: Future Work

6.3.2.1 Circadian rhythm and cell synchronization

Our results in chapter 5 identified several genes that are downregulated after 12 hours and upregulated upon 24 hours of osmotic stress. This differential expression of certain genes for the two conditions was correlated with the circadian rhythm and cell cycle. While it is possible that prolonged osmotic stress is a way of synchronizing the cells, these results need to be verified. One way of approaching this challenge is by serum starving the cells and after collecting them run PCRs for the most prominent genes that were identified with our experiment.

In addition, it is important to understand whether these identified genes are cell-line specific or whether we are looking at a more universal phenomenon. If osmotic stress is indeed synchronizing

other cell lines, that is something to look at. Our lab has access to several different model cell lines such as Hela cell, HEK cells and PC12 cells which would be a good start for these experiments.

6.3.2.2 Cavin-1 and viral infectivity

The removal of caveolae through the absence of Cav-1 or cavin-1 initiated a dramatic immune response to the WKO-3M22 cells with some anti-inflammatory genes being upregulated up to 11-fold. While this is an interesting result with many possible interpretations (see Discussion section 5.5) it is crucial to understand what the role of cavin-1 during viral infection is and why is the presence of this protein do important for the survival of cells.

One way of approaching this would be to look at the nuclear envelop integrity with the presence and the absence of viral DNA and understand if cavin-1 is exiting the nucleus more easily due to the disruption of nuclear envelope. A great marker for this would be LEMD-2, a protein involved in nuclear structure organization. Absence of LEMD-2 can suggest nuclear disruption and irregular movement of cavin-1 to and from the nucleus which could lead to initiation of uncommon signaling events.

6.4 REFERENCES

[1] N. Fernandes, N. Eshleman, and J.R. Buchan, Stress Granules and ALS: A Case of Causation or Correlation? Adv Neurobiol 20 (2018) 173-212.

[2] Y. Gao, N. Goonawardane, J. Ward, A. Tuplin, and M. Harris, Multiple roles of the non-structural protein 3 (nsP3) alphavirus unique domain (AUD) during Chikungunya virus genome replication and transcription. PLoS Pathog 15 (2019) e1007239.

[3] Y.R. Li, O.D. King, J. Shorter, and A.D. Gitler, Stress granules as crucibles of ALS pathogenesis. J Cell Biol 201 (2013) 361-72.

[4] R.G. Parton, V.A. Tillu, and B.M. Collins, Caveolae. Curr Biol 28 (2018) R402-R405.

[5] A. Echarri, and M.A. Del Pozo, Caveolae - mechanosensitive membrane invaginations linked to actin filaments. J Cell Sci 128 (2015) 2747-58.

[6] B. Razani, S.E. Woodman, and M.P. Lisanti, Caveolae: from cell biology to animal physiology. Pharmacol Rev 54 (2002) 431-67.

[7] A.W. Cohen, D.S. Park, S.E. Woodman, T.M. Williams, M. Chandra, J. Shirani, A. Pereira de Souza, R.N. Kitsis, R.G. Russell, L.M. Weiss, B. Tang, L.A. Jelicks, S.M. Factor, V. Shtutin, H.B. Tanowitz, and M.P. Lisanti, Caveolin-1 null mice develop cardiac hypertrophy with hyperactivation of p42/44 MAP kinase in cardiac fibroblasts. Am J Physiol Cell Physiol 284 (2003) C457-74.

[8] F. Faggi, N. Chiarelli, M. Colombi, S. Mitola, R. Ronca, L. Madaro, M. Bouche, P.L. Poliani, M. Vezzoli, F. Longhena, E. Monti, B. Salani, D. Maggi, C. Keller, and A. Fanzani, Cavin-1 and Caveolin-1 are both required to support cell proliferation, migration and anchorage-independent cell growth in rhabdomyosarcoma. Lab Invest 95 (2015) 585-602.

[9] J.J. Williams, and T.M. Palmer, Cavin-1: caveolae-dependent signalling and cardiovascular disease. Biochem Soc Trans 42 (2014) 284-8.

[10] K.A. McMahon, Y. Wu, Y. Gambin, E. Sierecki, V.A. Tillu, T. Hall, N. Martel, S. Okano, S.V. Moradi, J.E. Ruelcke, C. Ferguson, A.S. Yap, K. Alexandrov, M.M. Hill, and R.G. Parton, Identification of intracellular cavin target proteins reveals cavin-PP1alpha interactions regulate apoptosis. Nat Commun 10 (2019) 3279.

[11] L. Liu, and P.F. Pilch, PTRF/Cavin-1 promotes efficient ribosomal RNA transcription in response to metabolic challenges. Elife 5 (2016).

Appendix: protocols

A1: Isolation and excision of murine aortas

Protocol modified and reproduced from Nathan Robbins, Allie Thompson (2014), *Isolation and Excision of Murine Aorta; A Versatile Technique in the Study of Cardiovascular Disease*, *https://www.jove.com/t/52172/isolation-excision-murine-aorta-versatile-technique-study?list=HVrjuD8u, doi: 10.3791/52172*

Preparation of mouse

1. Euthanize by exposing the animal to carbon dioxide inhaled to effect. This method cannot be used in mice that are less than 1-month old. Secondary method of euthanasia includes cervical dislocation which indicates breaking the neck/spine of the mice at the cervical area.

2. Sanitize the external surface of the mouse by spraying the fur along the abdominal region where the initial cuts will be made, with 70% ethanol so that the fur is wet with ethanol and no loose/dry hair enter the region.

3. Lay the mouse out on a surgical board in the spine position with upper and lower appendages extended outward.

4. Secure appendages to the board using push pins.

Isolation of the Heart and Aorta

1. Use forceps to locate and isolate abdominal skin just inferior of the sternum and use scissors to remove the superficial skin.

2. Dissect up into the thoracic cavity, going through the diaphragm, being sure not to lacerate the heart or any major blood vessels.

3. Extend the lateral incisions made in step 2.3 cranially to remove the anterior portion of the ribcage. If necessary, free the heart from the anterior chest wall using blunt dissection.

4. Clean the chest cavity of extraneous blood and fluid by using sterile gauze to absorb material. Once the area is more visible, remove the lungs to better expose the heart and aorta.

Perfusion of Heart and Aorta

1. Fill a 10-cc syringe with 10 ml of sterile ice cold 1x phosphate buffer solution (PBS), and attach a 25 gauge needle to the syringe.
2. Gently insert the needle into the left ventricle of the heart.
3. Cut the right atrium to alleviate pressure buildup from perfusion. Perfuse the contents of the syringe into the mouse over 2 - 3 min.
4. Use sterile gauze at the opening in the right atrium to absorb perfusion fluid.

Isolation and Excision of the aorta

1. Expose the gastrointestinal contents by cutting caudally through the abdominal wall, extending the incision to the suprapubic area. Extend the incision further towards the lower limbs bilaterally to create skin flaps which can be pinned down or excised.
2. Remove the lobes of the liver, pancreas, stomach, spleen, and intestines to better visualize the aorta. Take care when dissecting near the perirenal region, as the aorta is superficial at the branches of the renal arteries.
3. NOTE: Perform this step in a precise and matriculate manner as the gastrointestinal tract is rich with bacteria which increases the propensity for contamination.
4. Rinse the area with 1x PBS and remove all fluid by absorption with a sterile gauze.
5. Using sterile microscissors and microforceps, separate the aorta from the spine dorsally and the esophagus ventrally. It is best to use blunt dissection and utilizing a dissection microscope for this.
6. Remove the perivascular adipose tissue using fine microscissors being sure not to remove a portion of the aortic wall. This is essential to minimize the potential for fibroblast contamination when culturing aortic smooth muscle cells.

Notes:

- For one 35mm dish of primary smooth muscle cells, 3-4 aortas were used.
- The aorta is made up of three layers: the inner layer (tunica intima), the middle layer (tunica media), and the outer layer (tunica adventitia). The inner layer consists of endothelial cells, the middle layer has a large amount of elastin which can be visualized through microscopy

since it causes autofluorescence and the outer layer consists mainly of fibroblasts which need to be removed quickly since they proliferate rapidly and expand everywhere.

- To remove the outer layer, the aorta is digested in collagenase which allows the outer layer to loosen up and be removed with forceps like a sock.

A2: Preparation of Bleach Agarose Gels for RNA Visualization

Protocol provided from Dr McKinnon-Rosati's lab, Stony Brook University.

1. Add 1 g agarose to a 250 mL Erlenmeyer flask using the technical balance, making sure to clean up the balance with a brush after use.
1. In the gel room, add 99 mL 1X TBE buffer to flask and swirl.
2. Add 1 mL commercial bleach (e.g., Clorox; 6% sodium hypochlorite) to flask and incubate for 5 minutes at room temperature, swirling occasionally.
3. Melt agarose in microwave for 1 minute. In the meantime, prepare the casting tray in the
4. gel box, making sure the rubber gasket does not get twisted, and place combs in the tray So that spacers face top of gel.
5. Take flask out of the microwave with rubber pinch grip and swirl. Place flask back in
5. Microwave for another minute.
6. Make sure all the agarose has dissolved.
7. Add 5 µl of 10 mg/ml ethidium bromide to solution and swirl.
8. Pour solution into the casting tray and allow to solidify.
9. Add 1 µg RNA to 1.7 µl 6X DNA loading buffer and bring the final volume to 10 µl with water.
6. Load gel with RNA samples.
7. Run the gel for 75 min. at 100 V and visualize with UV light.

Solutions:

6X Loading Buffer (store at 4°C)
- M.W. for 10 mL Final Conc.
- Glycerol 92.09 3 mL 30%
- Bromophenol blue 0.025 g 1.5 mM
- Xylene cyanol 0.025 g 1.9 mM

A3: Immunofluorescence staining protocol for WKO-3M22 cells and mouse embryonic fibroblasts

1. Cells were fixed with 3.7% formaldehyde prepared in PBS for 30 minutes.
2. Cells were washed 3 times with PBS for 5 minutes per wash.
3. Permeabilization occurred with 0.2% Triton X-100 in PBS for 20 minutes.
4. Cells were incubated with control blocking solution for 1-2 hours.

Note: Two different blocking solutions have been used at different occasions. Both of them have been successful.

      i.   2% BSA, 5% goat serum and 0.1% Triton X-100 in PBS

     ii.   100% FBS (using FBS minimizes background noise when imaging)

5. Primary and secondary were prepared in blocking solution at the dilutions indicated. If using FBS for blocking, incubate primary and secondary in 50% FBS + 50% PBS. The appropriate dilutions are 1:1000 for primary and 1:2000 for secondary. If abcam primary antibodies are used, the dilutions used were 5 times less concentrated.
6. Primary antibody was incubated overnight at 4° C and secondary was incubated at room temperature for 1-2 hours.
7. Cells were washed 3 times with PBS for 5 minutes per wash after primary antibody incubation.
8. Cells were washed 3 times with PBS for 5 minutes per wash after secondary antibody incubation.
9. Cells were covered with aluminum foil and kept at 4°C.

A4: Immunofluorescence staining protocol for A10 cells

1. Cells were fixed with 3.7% formaldehyde prepared in PBS or 100% methanol and incubated at room temperature for 1 hour.
2. Cells were washed 3 times with PBS for 1 minute per wash.
3. Cells were permeabilized with 2mL of 0.2% NP40 in PBS and incubated for 5 minutes (NOT MORE!)

4. Cells were incubated with 4% BSA in 1X TBS for 30 minutes for blocking.

5. Primary antibody was prepared in 1% BSA in 1X TBS and incubated overnight at 4°C or for 2 hours at room temperature.

6. Cells were washed 3 times with 2mL of 1X TBS for 3 minutes per wash.

7. Secondary antibody was prepared in 1% BSA in 1X TBS and incubated for 1.5 hours at room temperature.

8. Cells were washed 3 times with 2mL of 1X TBS for 3 minutes per wash.

9. Cells were covered with aluminum foil and kept at 4°C.

A5: Immunofluorescence staining protocol for PC12 cells

1. Cells were fixed with 3.7% formaldehyde prepared in PBS and incubated at room temperature for 10 minutes.

2. Wash cells with MSM pipes buffer 3 times for 10 minutes each.

3. Cells were blocked in PBS containing 5% goat serum, 1% BSA and 50mM glycine for 30 minutes.

4. Primary antibody was prepared in 1% BSA in PBS and incubated overnight at 4°C or for 2 hours at room temperature.

5. Cells were washed 3 times with 2mL of 1X TBS for 3 minutes per wash.

6. Secondary antibody was prepared in 1% BSA in PBS and incubated for 1 hour at room temperature.

7. Cells were washed 3 times with 2mL of 1X TBS for 3 minutes per wash.

8. Cells were covered with aluminum foil and kept at 4°C.

MSM pipes buffer composition
    i.   PBS + 0.4% Triton X-100 (48mL of PBS + 192μL Triton X-100)